



**University of
Sheffield**

**Investigating the role of the protease
ADAMTS5 in ovarian cancer**

Shengnan Yuan

This thesis is submitted in partial fulfilment
of the requirements for the degree of
Doctor of Philosophy

The University of Sheffield
School of Biosciences
Faculty of Science

May 2024

Abstract

Ovarian cancer (OC) is the fifth most lethal gynaecologic malignancy in the UK. At the advanced stages (III and IV), there are peritoneal or distant metastases outside the peritoneal cavity, and the 5-year survival rate is less than 35%. Therefore, it is essential to identify the mechanisms controlling OC metastasis to prevent it. The extracellular matrix (ECM) is a dynamic structure which is remodelled under both normal and pathological conditions by modifying enzymes. Changes in the composition and structure of the ECM were previously detected in several types of tumours, including ovarian carcinoma. ADAMTS5 (a disintegrin and metalloproteinase domain with thrombospondin motifs 5) is a member of the ADAMTS family of proteases involved in ECM degradation. Previously, high ADAMTS5 expression was found to correlate with reduced overall survival in OC patients. Additionally, the expression of the ADAMTS5 substrate versican has also been shown to be upregulated in OC metastasis. However, the role of ADAMTS5 in OC progression remains unclear.

Here I showed that ADAMTS5 expression is promoted in OC cells over-expressing the small GTPase Rab25 grown on 3D matrices, through a NF- κ B dependent mechanism. We also found that ADAMTS5 inhibition and knockdown strongly reduced Rab25-dependent OC cell migration and invasion through 3D matrices. Furthermore, when in co-culture with cancer-associated fibroblasts, OC cells showed increased 3D invasion, which can be suppressed by ADAMTS5 downregulation. Altogether, this research investigated the upregulation mechanism of ADAMTS5 and demonstrated the tumour-promoting role of ADAMTS5 in OC, which could be considered a potential therapy target for OC metastasis.

Acknowledgement

I would like to thank my supervisor **Dr Elena Rainero** first for providing me the opportunity to work in her lab. Throughout my PhD, she had always supported me with her kindness, patience and confidence. She was the best supervisor I ever met. I've enjoyed the past four years that I spent in her lab. I would also like to thank my advisors, **Dr Kai Erdmann** and **Professor Carl Smythe** for their support during my PhD. Thank you, Kai, for always bringing great questions during our meetings, that was really helpful. I would also like to thank **Dr Nick van Hateren** and **Dr Darren Robinson** for their help and guidance in the LMF facility. Thanks to **Dr Anestis Tsakiridis** and **Dr Fay A Cooper** for their help and support with the qPCR assay. Thanks to **Dr Chun Guo** for his help with hypoxia assay.

Special thanks are given to all the members from **Kathryn Ayscough**, **Hellen Matthews** and **Elena Rainero** labs. Many thanks to **Shahd M Alhadid** and **Rachele Bacchetti** for being my best friends in Sheffield. Salute to the group of "The young ladies". Thanks to **Dr Mona Nazemi**, **Dr Keqian Nan**, **Bian Yanes**, and **Dr Montserrat Llanses Marínez** for being the big sisters and brother, who helped me greatly in the lab and life. Thanks to **Dr Victoria H Hart** for offering my antibody support. Thanks to **Zhe Bao**, for all the drama talk, and **Rachel H Lawson**, for all the cat talk. Thanks to **Haya Alomaim**, **Ifeoluwa F Oyelade** and **Isabella J Davis** for being great lab mates. Thanks to **Anthony J Hobber** for his help in the lab. I would also like to thank my friend **Yuening Li** for taking me out and getting me in touch with nature and animals regularly.

I want to extend my thanks to all my family, my parents **Hui Yuan** and **Li Chen**, and my little brother **Ruiqian Yuan**, for always loving me and supporting my dream. It was a bit of a hard time in the past years for our family and there were a lot of separations, but we finally made it! I also want to thank all members of Yuan's and Chen's families, I love you. I would like to specially thank my partner **Zihan Zhang** for always loving, trusting and supporting me despite the distance. You build up my confidence from pieces, without you being my sunshine my life would still be full of darkness.

Last but not least, I would like to thank my baby boy **Daimao** (top of the picture) for all the mental support over the past three years. Without him purring at my side I would not have made so far. I would also like to thank my neighbour **Xiaoxue Xu** and her baby boy **Zaizai** (bottom of the picture) for their visit and company every evening.



Declaration

I, Shengnan Yuan, declare that this thesis is the result of my own work with support from others that have been acknowledged, except those explicitly stated: the work presented in Figure 6.1 was done by J. Adams and the work presented in Figure 6.2 was done by Dr E. Rainero. I confirm that this thesis has not been submitted to the University of Sheffield or any other institutions previously. I confirm that where I have quoted from the work of others, the source is always given.

Shengnan Yuan

28/05/2024

Table of contents

Abstract	1
Acknowledgement	2
Declaration	4
Table of contents	5
List of figures	11
List of tables	14
Abbreviations	15
Chapter 1 – Introduction	19
1.1. Ovarian cancer	19
1.1.1. Epidemiology	19
1.1.2. Ovarian cancer subtypes and genetic features	19
1.1.3. Progression and metastasis.	22
1.1.4. Diagnosis and treatment.	25
1.2. The tumour microenvironment	27
1.2.1 Extracellular matrix	27
1.2.1.1 Collagens	28
1.2.1.2 Proteoglycan	30
1.2.1.3 Fibronectin	32
1.2.2 Extracellular matrix receptors	34
1.2.2.1 Integrins.....	34
1.2.2.2 Other receptors	37
1.2.3 Cancer-associated fibroblasts.....	38

1.3. ECM remodelling in cancer progression	39
1.3.1. Matrix metalloprotease (MMP)	39
1.3.2. A disintegrin and metalloprotease (ADAM)	42
1.3.3. A disintegrin and metalloprotease with thrombospondin motif (ADAMTS)	43
1.3.3.1 ADAMTS5 in cancer	46
1.4. Rab25 in cancer progression	49
1.4.1. Ras superfamily	49
1.4.2. Rab25 can function as both tumour promoter and suppressor.	51
1.5. Aims and objectives.....	52
Chapter 2 – Materials and Methods.....	54
2.1. Materials	54
2.1.1. Reagents and suppliers	54
2.1.2. Solutions	56
2.2. Methods.....	57
2.2.1. Cell culture	57
2.2.2. Plasmid transfection and maintenance	58
2.2.3. Cell-derived matrix generation	58
2.2.4. Conditioned media harvest.....	60
2.2.5. Western blotting.....	60
2.2.6. RT-qPCR.....	62
2.2.6.1. mRNA extraction	62
2.2.6.2. cDNA synthesis	62
2.2.6.3. qPCR	63

2.2.7. siRNA transfection	63
2.2.8. Cell proliferation assay	64
2.2.8.1. Cell proliferation assay with ADAMTS5 inhibitor	64
2.2.8.2. Co-culture cell proliferation assay	65
2.2.9. Random cell migration assay on CDM	67
2.2.9.1. Cell migration with small molecule inhibitors	67
2.2.9.2. Cell migration with conditioned media	67
2.2.10. 3D spheroid invasion assay.....	67
2.2.10.1. A2780-Rab25 spheroid invasion assay with ADAMTS5 inhibitor	67
2.2.10.2. Co-culture 3D spheroid invasion assay with ADAMTS5 inhibitor	69
2.2.10.3. Co-culture 3D spheroid invasion assay with ADAMTS5 or Rab25 KD.	71
2.2.10.4. EdU labelling of co-culture 3D spheroid.....	71
2.2.11. Hypoxia assays	71
2.2.12. Cell signalling inhibitor treatments	72
2.2.13. Immunofluorescence	72
2.2.14. Statistical analysis	73
Chapter 3 – Rab25 induces ADAMTS5 expression in ovarian cancer cells.	74
3.1. Introduction.....	74
3.2. Results.....	75
3.2.1. Characterisation of Rab25 expression in OC cell lines.....	75
3.2.2. Selection of A2780 cells line overexpressing Rab25.	77
3.2.3. Rab25 over-expression promoted ADAMTS5 expression in OC cell lines.	79

3.2.4. Rab25 KD reduced ADAMTS5 expression in OC cells endogenously overexpressing Rab25.	81
3.3. Discussion	83
Chapter 4 – Transcription factor NF-κB was required for Rab25-induced ADAMTS5 expression in OC cells.	87
4.1. Introduction	87
4.2. Results	92
4.2.1. HIF-1 inhibition reduced Rab25 and induced ADAMTS5 expression.	92
4.2.2. Hypoxia reduced Rab25 and ADAMTS5 expression.	93
4.2.3. NF- κ B inhibition reduced ADAMTS5 expression.	94
4.2.4. Rab25 induced NF- κ B nuclear translocation.	95
4.2.5. PI3K inhibition reduced ADAMTS5 expression.	98
4.2.6. Rab25 might regulate NF- κ B in an AKT-independent manner.	101
4.3. Discussion	101
Chapter 5 – Inhibition of ADAMTS5 showed limited effect on OC cell proliferation.	106
5.1. Introduction	106
5.2. Result	108
5.2.1. High concentration ADAMTS5 inhibitor affected OC cell proliferation.	108
5.2.2. Co-culture with CAFs promoted OVCAR3 cell proliferation.	110
5.2.3. TIFs failed to promote the proliferation of OVCAR3 cells.	112
5.2.4. Glucose and serum starvation increased the sensitivity of OC cells to ADAMTS5 inhibition.	114

5.3. Discussion	117
Chapter 6 – ADAMTS5 was required for OC cell migration and invasion.....	121
6.1. Introduction	121
6.2. Results.....	122
6.2.1. ADAMTS5 was required for Rab25-dependent pseudopod extension and directional migration in A2780 cells.....	122
6.2.2. Conditioned media derived from A2780-Rab25 enhanced the migration of A2780-DNA3 cells.....	125
6.2.3. ADAMTS5 inhibition prevents A2780-Rab25 CM-induced A2780-DNA3 cell directional migration.....	126
6.2.4. CM derived from ADAMTS5 KD A2780-Rab25 cells failed to promote the migration of A2780-DNA3 cells.	129
6.2.5. ADAMTS5 inhibition reduced the invasion of OC cells overexpressing Rab25 in 3D systems.	131
6.2.6. ADAMTS5 inhibition reduced the invasion of both CAFs and OC cells in a 3D co-culture model.....	133
6.2.7. ADAMTS5 inhibition did not affect the proliferation of OVCAR3 cells and CAFs in 3D.	135
6.2.8. ADAMTS5 inhibition did not affect the invasion of CAFs in monoculture..	137
6.2.9 Rab25 KD in OVCAR3 cells suppressed the invasion of both CAFs and OVCAR3 cells.	138
6.2.10 ADAMTS5 KD in OVCAR3 cells suppressed the invasion of OVCAR3 cells.	140

6.2.11. TIFs failed to promote the invasion of OVCAR3 cells in co-culture spheroids.....	142
6.3. Discussion	144
Chapter 7 – Discussion	147
7.1. Summary of key findings.....	147
7.2. Rab25 regulated ADAMTS5 expression through NF-κB-related signalling pathways.....	149
7.3. ADAMTS5 might promote OC cell migration and invasion via VCAN cleavage.	152
7.4. Conclusion and future directions.....	153
References	155

List of figures

Chapter 1 – Introduction

Figure 1.1. EOC subtypes are derived from different tissues.

Figure 1.2. Metastasis feature of OC

Figure 1.3. Standard structure of fibrillar collagen (collagen type I) molecule.

Figure 1.4. Structure of lecticans (hyalectans), including aggrecan, versican, neurocan and brevican.

Figure 1.5. A proposed mole of CD44, HA and VCAN mediating the ovarian cancer cell adhesion to the peritoneal cells.

Figure 1.6. Structure of fibronectin molecule.

Figure 1.7. The integrin sub-families.

Figure 1.8. Integrin endocytosis and recycling.

Figure 1.9. Structure of ADAMTS family.

Figure 1.10. High ADAMTS5 expression correlated with poor prognosis in OC patients.

Figure 1.11. Schematic of Ras GTPase activation cycle.

Chapter 2 – Materials and Methods

Figure 2.1. Generation of TIF and CAF CDMs.

Figure 2.2. Cell proliferation analysis by CME software in MetaXpress.

Figure 2.3. Generation of spheroids.

Figure 2.4. 3D spheroids invasion analysis.

Chapter 3 – Rab25 induces ADAMTS5 expression in OC cells

Figure 3.1. Rab25 protein levels in OC cell lines.

Figure 3.2. Rab25 gene expression in OC cell lines.

Figure 3.3. Rab25 localisation in OC cells.

Figure 3.4. Expression of Rab25 in A2780-Rab25 cell line before and after G418 selection.

Figure 3.5. Rab25 induced ADAMTS5 expression in the presence of CDM.

Figure 3.6. Different matrix organisation in TIF and CAF-CDMs.

Figure 3.7. ADAMTS5 expression was reduced upon Rab25 KD in OVCAR3 cells on both plastic and CDM.

Figure 3.8. Rab25 induces ADAMTS5 in ovarian cancer cells.

Chapter 4 – Rab25 induces ADAMTS5 expression through transcription factor NF- κ B in OC cells

Figure 4.1. Schematic of HIF-1 α and NF- κ B activation and function in regulating gene transcription.

Figure 4.2. Schematic of NF- κ B activation via PI3K/AKT/mTOR/ pathway.

Figure 4.3. HIF-1 inhibition with Echinomycin induced ADAMTS5 and reduced Rab25 expression in OC cells.

Figure 4.4. Hypoxia reduced both ADAMTS5 and Rab25 expression in OC cells.

Figure 4.5. NF- κ B inhibition reduced ADAMTS5 expression in OVCAR3 cells in a dose-dependent manner.

Figure 4.6. Rab25 overexpression induced the overall and nuclear level of NF- κ B.

Figure 4.7. Rab25 KD reduced the overall and nuclear level of NF- κ B.

Figure 4.8. PI3K inhibition reduced ADAMTS5 expression in OVCAR3 cells in a dose-dependent manner.

Figure 4.9. AKT phosphorylation was not affected by Rab25 KD.

Figure 4.10. Schematic of the role of Rab25 in inducing ADAMTS5 expression through NF- κ B.

Chapter 5 – Inhibition of ADAMTS5 shows limited effect on OC cell proliferation

Figure 5.1. High concentration ADAMTS5 inhibitor inhibited cell growth.

Figure 5.2. Proliferation of OVCAR3 cells was promoted by CAFs and inhibited by high concentrations of ADAMTS5 inhibitor.

Figure 5.3. TIFs failed to promote the proliferation of OVCAR3 cells.

Figure 5.4. ADAMTS5 inhibitor reduced the proliferation of A2780 cells under glucose or serum starvation.

Figure 5.5. ADAMTS5 inhibition reduced cell proliferation on plastic and CDM under glucose or serum starvation.

Chapter 6 – Inhibition of ADAMTS5 shows limited effect on OC cell proliferation.

Figure 6.1. ADAMTS5 pharmacological inhibition reduced pseudopod extension and directionality of A2780-Rab25 cells migrating on TIF-CDM.

Figure 6.2. ADAMTS5 KD in A2780-Rab25 reduced pseudopod extension and directionality of cells migrating on TIF-CDM.

Figure 6.3. CM derived from A2780-Rab25 cells enhanced pseudopod extension and directionality of A2780-DNA3 cells migrating on TIF-CDM.

Figure 6.4. ADAMTS5 inhibitor reduced the A2780-Rab25 CM-induced migration capacity of A2780-DNA3 cells on TIF-CDM.

Figure 6.5. CM derived from ADAMTS5 KD A2780-Rab25 cells failed to promote the migration of A2780-DNA3 cells on TIF-CDM.

Figure 6.6. ADAMTS5 inhibitor reduced the 3D invasion of A2780-Rab25 cells in a dose-dependent manner.

Figure 6.7. ADAMTS5 inhibitor reduced the 3D invasion of OVCAR3 cells and CAFs in co-culture.

Figure 6.8. ADAMTS5 inhibitor did not affect the proliferation of OVCAR3 cells in 3D.

Figure 6.9. ADAMTS5 inhibition did not affect the 3D invasion of CAF spheroids.

Figure 6.10. Rab25 KD in OVCAR3 cells reduced the 3D invasion of both OVCAR3 cells and CAFs in co-culture.

Figure 6.11. ADAMTS5 KD in OVCAR3 cells reduced the 3D invasion of OVCAR3 cells but not CAFs in co-culture.

Figure 6.12. TIFs suppressed the invasion of OVCAR3 cells.

Chapter 7 – General discussion

Figure 7.1. Schematic representation of the mechanisms of ADAMTS5 regulation and function.

Figure 7.2. Hypothesised mechanism of Rab25 mediated NF- κ B dependent ADAMTS5 upregulation and ADAMTS5 in promoting OC migration and invasion.

List of tables

Chapter 1 – Introduction

Table 1.1. FIGO 2014 staging for cancer of the ovary, fallopian tube, and peritoneum.

Table 1.2. MMP subgroups and substrates.

Table 1.3. ADAMTS subgroups and substrates.

Chapter 2 – Materials and Methods

Table 2.1. Reagents and suppliers.

Table 2.2. Recipes of solutions.

Table 2.3. Cell seeding numbers and solution volume for TIF and CAF-CDM generation.

Table 2.4. Western blotting antibody list.

Table 2.5. Time and temperature for cDNA synthesis.

Table 2.6. qPCR Primer list.

Table 2.7. Time and temperature for qPCR.

Table 2.8. Immunofluorescent antibody list.

Abbreviations

ADAM: a disintegrin and metalloprotease

ADAMTS: a disintegrin and metalloproteinase domain with thrombospondin motifs

AKT: protein kinase B

ARID1A: AT-rich interaction domain 1A

BM: basement membrane

BRAF: v-raf murine sarcoma viral oncogene homolog B1

BRCA: Breast Cancer gene

CA125: carbohydrate antigen 125

CAF: cancer-associated fibroblasts

CD44: cluster of differentiation 44

CDMs: cell-derived matrices

CLIC3: chloride intracellular channel 3

CM: conditioned media

COMP: cartilage oligomeric protein

DDRs: discoidin-domain receptors

ECM: extracellular matrix

EE: early endosome

EGFR: epidermal growth factor receptor

EMT: epithelial-to-mesenchymal transition

EOC: endothelial ovarian cancer

ER: endoplasmic reticulum

ERK: extracellular signal-regulated kinase

FACIT: fibril-associated collagens with interrupted triple-helices

FAK: focal adhesion kinase

FBS: foetal bovine serum

FDA: Food and Drug Administration

FGF2/7: fibroblast growth factor 2/7

FIGO: International Federation of Gynaecology and Obstetrics

GAG: glycosaminoglycan

GAPs: GTPase activating proteins

GEFs: guanine nucleotide exchange factors

GFs: growth factors

GPI: glycosyl-phosphatidyl-inositol

HA: hyaluronan

HB-EGF: heparin-binding EGF-like growth factor

HE4: human epididymis protein 4

HGF: hepatocyte growth factor

HGSOC: High-grade serous ovarian cancer

HIF: hypoxia-inducible factors

HRD: homologous repair deficiency

HUVEC: human umbilical vein endothelial cells

IBS: irritable bowel syndrome

IKK: inhibitor of nuclear factor kappa B kinase

IM: interstitial matrix

I κ B: inhibitor of nuclear factor kappa B

KD: knockdown

KRAS: Kirsten rat sarcoma viral oncogene homolog

LE: late endosomes

LGSOC: low-grade serous ovarian cancer

LOX: lysyl oxidase

LRR: leucine-rich repeats

MAPK: mitogen-activated protein kinase

miRNAs: micro-RNAs

MMP: matrix metalloproteinase

mTOR: mammalian target of rapamycin

mTORC: mammalian target of rapamycin complex

NEOC: non-endothelial ovarian cancer

NF- κ B: nuclear factor κ B

NHEJ: non-homologous end joining

NRAS: neuroblastoma rat sarcoma viral oncogene homolog

OC: ovarian cancer

PARP: poly ADP ribose polymerase

PHD: prolyl hydroxylase

PI3K: phosphoinositide 3-kinases

PIK3CA: the gene that encodes the p110 subunit of PI3K

PIP₂: phosphatidylinositol (4,5)-bisphosphate

PIP₃: phosphatidylinositol (3,4,5)-trisphosphate

PKD1: 3-phosphoinositide-dependent kinase 1

PTEN: phosphatase and tensin homolog

pVHL: von Hippel-Lindau tumour-suppressor protein

RCP: Rab-coupling protein

RGD: Arg-Gly-Asp

RHR: Rel homology region

ROMA: Risk of Ovarian Malignancy Algorithm

RT: room temperature

RTK: receptor tyrosine kinase

SLRP: small leucine-rich repeat proteoglycan

TCA: tricarboxylic acid

TCGA: The Cancer Genome Atlas

TF: transcription factor

TGF- β : transforming growth factor beta

TIFs: telomerase-immortalised human dermal fibroblasts

TIMP: tissue inhibitors of metalloproteinase

TMB: tumour mutation burden

TME: tumour microenvironment

TNF- α : tumour necrosis factor α

Treg: T regulatory

TSR: thrombospondin type I-like repeat

VCAN: versican

VEGFA: vascular endothelial growth factor A

vWF: von Willebrand factor

vWFCP: von Willebrand factor cleaving protease

α SMA: α -smooth muscle actin

Chapter 1 – Introduction

1.1. Ovarian cancer

1.1.1. Epidemiology

Ovarian cancer (OC) has been one of the top 5 lethal cancers among females worldwide in the past decade. In 2020, OC became the third most common gynaecological malignancy globally (Sung et al., 2021). The overall 5-year survival rate of patients is less than 35%, and the overall incidence rate of OC during a woman's lifetime is approximately 1.3% (Fotopoulou et al., 2017, Torre et al., 2018). Although there was a decreased overall occurrence and mortality rate among women all over the world, the incidence of OC among younger females was remarkably increased over the past decade (Huang et al., 2022b). One of the outstanding reasons that leads to patients' death is late-stage diagnosis. About 70% of OC patients were diagnosed at the advanced stage (Cho and Shih, 2009). In the early stages, the 5-year survival rate of OC patients is higher than 70%. However, in the advanced stages in the presence of peritoneal metastasis or distant metastasis outside of the peritoneal cavity, the 5-year survival rate is less than 30% (Bhatla and Jones, 2018).

The family history of breast cancer and OC is one of the main risk factors for OC, which is associated with the heritable mutation of Breast Cancer 1 (*BRCA1*) and 2 (*BRCA2*) genes. Other risk factors include ageing, nulliparity, hormone replacement therapy, menopause, overweight and smoking (Salehi et al., 2008, Huang et al., 2022b). There are also protective factors for OC, such as the usage of oral contraceptive pills, pregnancy and hysterectomy with tubal ligation (Fotopoulou et al., 2017).

1.1.2. Ovarian cancer subtypes and genetic features

OC can be classified into endothelial ovarian cancer (EOC), which accounts for 90% of the OC cases, and non-endothelial ovarian cancer (NEOC), which includes sex-cord stromal and germ cell tumours (Cho and Shih, 2009, Cheung et al., 2022). EOC can be further divided into four subtypes based on the histological features, which are serous, endometrioid, clear cell and mucinous carcinoma. These sub-types can then be classified into low-grade (Type I) and high-grade (Type II) based on the grading system established by the International Federation of Gynaecology and Obstetrics (FIGO) (Cho and Shih, 2009). As a vastly heterogeneous and complex malignancy, OC does not simply describe a

carcinoma that developed from ovarian tissues. Instead, it is a term for a series of diseases that are induced by distinct molecular and etiological factors localised at a similar anatomical location (Figure 1.1) (Vaughan et al., 2011). For example, most of the invasive mucinous OCs were identified as ovary metastasis from other primary cancers, including colon and gastric cancer. The occurrence of endometrioid and clear cell OC was found highly associated with endometriosis. High-grade serous ovarian cancer (HGSOC) is the most common and lethal subtype of OC, which accounts for 68% of overall OC cases and is responsible for 70%-80% of patients' deaths (Koshiyama et al., 2017, Bowtell et al., 2015). In addition to arising from ovarian surface epithelium, relatively high cases of HGSOC were derived from the secretory epithelial cells of the fallopian tubes (Vaughan et al., 2011, Bowtell et al., 2015).

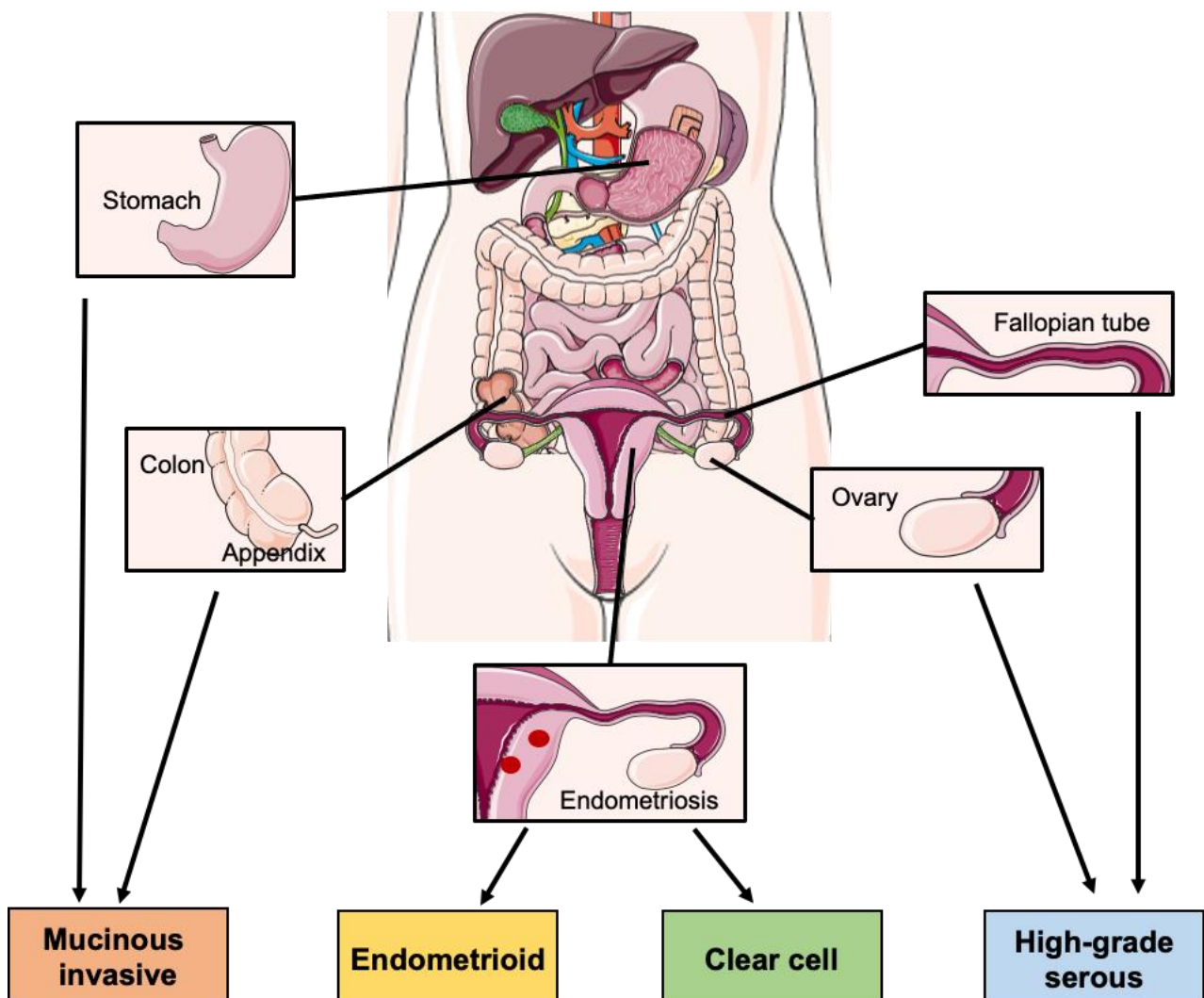


Figure 1.1. EOC subtypes are derived from different tissues. Most of the invasive mucinous were found to be metastases from other cancers, such as gastric and colon cancer, to the ovary. Endometriosis was found highly associated with the rise of endometrioid and clear cell carcinoma. HGSOC occurs in the ovary or

fallopian tube from the epithelial cells. The figure was adapted from (Vaughan et al., 2011) and made with items adapted from Servier Medical Art.

It is common knowledge that tumour development is a result of accumulated genetic changes, caused by the mutation of oncogenes and tumour suppressor genes. Apart from the different occurrence locations, the genetic and molecular features of OC subtypes were also varied. *TP53* is one of the most commonly mutated genes in HGSOC, which was identified in nearly 80% of the cases (Koshiyama et al., 2017). The mutation of *TP53* was found at the early stage of HGSOC and shown to contribute to the progression of the disease (Leitao et al., 2004). As a factor that regulates the cell cycle and mediates apoptosis upon non-repairable DNA damage, *TP53* mutation leads to genomic instability and mutation accumulation (Vousden and Lane, 2007). *BRCA1/2* is another common mutated oncogene in HGSOC. Although germline and somatic mutations of *BRCA1/2* were detected in only about 20% of the patients, they were found associated with over 90% of hereditary HGSOC cases, contributing to the higher family disease risk (Eoh et al., 2020, Koshiyama et al., 2017). Mutation of *BRCA1/2* is the leading cause of homologous recombination deficiency (HRD) in HGSOC (Bonadio et al., 2018). An overactivated phosphoinositide 3-kinase (PI3K)/protein kinase B (AKT)/mammalian target of rapamycin (mTOR) signalling pathway was also detected in approximately 70% of HGSOC patients, which resulted in dysregulated cell growth and apoptosis (Li et al., 2014). Activation of the PI3K pathway in OC is caused by the mutation of multiple signalling elements, such as mutation of *PIK3CA* (the gene that encodes the p110 subunit of PI3K), loss of phosphatase and tensin homolog (PTEN) and deregulation of AKT. In HGSOC, *PIK3CA*, *PTEN* and *AKT* mutation rates are lower compared to endometrioid and clear cell subtypes of EOC (Li et al., 2014). Alternatively, the overactivation of the PI3K signalling pathway in HGSOC is due to the altered gene amplification and DNA copy numbers (Cheaib et al., 2015). Additionally, the mutation rate of the mitogen-activated protein kinase (MAPK)/extracellular signal-regulated kinase (ERK) signalling pathway in HGSOC is relatively low compared to the low-grade serous ovarian cancer (LGSOC) (Cho and Shih, 2009). However, the dysregulation of this pathway caused by neuroblastoma rat sarcoma viral oncogene homolog (*NRAS*) mutation was also found to promote the progression of HGSOC (Chen et al., 2016b).

Unlike HGSOC, patients with LGSOC rarely have *TP53* and *BRCA1/2* mutations, while the upregulation of MAPK/ERK pathway was highlighted (Cho and Shih, 2009). Mutations of Kirsten rat

sarcoma viral oncogene homolog (*KRAS*) and v-raf murine sarcoma viral oncogene homolog B1 (*BRAF*) were identified in over 70% of the LGSOC patients, which are mainly responsible for the dysregulation of the MAPK pathway (Vaughan et al., 2011). Additionally, *NRAS* mutation was also found in LGSOC patients and resulted in the dysregulation of the MAPK pathway (Manning-Geist et al., 2022). The altered MAPK signalling pathway in LGSOC was found to promote cancer cell survival and micropapillary growth. It was recently found to also contribute to the stromal invasion of LGSOC (Hollis et al., 2023).

The rate of endometrioid and clear cell OC is higher among Asian women for unclear reasons (Torre et al., 2018). AT-rich interaction domain 1A (*ARID1A*) is the most frequently mutated tumour suppressor gene in clear cell and endometrioid OC, which was found associated with early-stage progression from endometriotic epithelium (Ayhan et al., 2012). Other most identified mutated genes in these two OC subtypes include *PIK3CA/PTEN*. *PIK3CA* mutation was detected in approximately 20% of clear cell and endometrioid OC cases, and *PTEN* deficiency was detected in 14-21% of endometrioid OC and 8% of clear cell OC (Cho and Shih, 2009). The mutation rate of *TP53*, *KRAS* and *BRAF* were detected in patients with clear cell and endometrioid OC, but the ratio is relatively low compared to other subtypes (Cho and Shih, 2009).

Due to the remarkably different gene mutation features in different OC subtypes, the oncogenesis, development and progression are also varied between these subtypes, leading to different targets for diagnosis and therapeutic methods. It is also important to distinguish the subtypes carefully during OC research.

1.1.3. Progression and metastasis.

The clinical staging of OC is based on the FIGO staging guidance, which was established in 1988 and most recently updated in 2014 (Table 1.1) (Prat, 2014). OC patients diagnosed at early stages (Stages I and II) show remarkably better survival than those diagnosed at advanced stages (Stages III and IV). When diagnosed at stages I and II, the 5-year overall survival rate of EOC patients are 90% and 70% respectively (Bhatla and Jones, 2018). However, when the tumour shows peritoneal metastasis at stage III or further metastasis outside of the peritoneal cavity at stage IV, the overall survival rate

is dramatically reduced to 39% and 17%. Unfortunately, most of the OC are diagnosed at the advanced stages, which made OC one of the most lethal cancers in the world (Cho and Shih, 2009).

Table 1.1 FIGO 2014 staging for cancer of the ovary, fallopian tube, and peritoneum.

Stage I	Tumour confined to ovaries
IA.	Tumour limited to one ovary, capsule intact, no tumour on ovary surface, negative peritoneal washings.
IB.	Tumour involves both ovaries, otherwise like IA.
IC.	Tumour limited to one or both ovaries.
IC1.	Surgical spill.
IC2.	Capsule rupture before surgery or tumour on the ovarian surface.
IC3.	Malignant cells in the ascites or peritoneal washings.
Stage II	Tumour in one or both ovaries with pelvic extension or primary peritoneal cancer
IIA.	Extension and/or implant to uterus and/or fallopian tubes.
IIB.	Extension to other pelvic intra-peritoneal tissues.
Stage III	Confirmed spread to extra-pelvic peritoneum and/or metastasis to the retroperitoneal lymph nodes
IIIA.	Positive retroperitoneal lymph nodes and/or microscopic metastasis beyond the pelvis.
IIIA1.	Positive retroperitoneal lymph nodes metastasis only.
IIIA2.	Microscopic, extrapelvic, peritoneal involvement with/without positive retroperitoneal lymph node.
IIIB.	Macroscopic, extrapelvic, peritoneal metastasis ≤ 2 cm \pm positive retroperitoneal lymph nodes. Includes extension to capsule of liver/spleen.
IIIC.	Macroscopic, extrapelvic, peritoneal metastasis > 2 cm \pm positive retroperitoneal lymph nodes. Includes extension to capsule of liver/spleen.
Stage IV	Distant metastasis out of peritoneal cavity
IVA.	Pleural effusion with positive cytology.
IVB.	Hepatic and/or splenic parenchymal metastasis, metastasis to extra-abdominal sites

The activation of tumour cell invasion and metastasis is an important hallmark of cancer, which reflects advanced-stage carcinomas with higher pathological grades (Hanahan and Weinberg, 2011). In OC, the most common way of metastasis is the passive dissemination of tumour cells via peritoneal fluid, which results in the development of a secondary tumour on the peritoneum and

the omentum (Figure 1.2) (Sorensen et al., 2009). However, increasing evidence indicates that metastasis through blood vessels is another critical mode of ovarian tumour spread (Lengyel, 2010, Zong and Nephew, 2019). In Sood's lab, a parabiosis mouse model was established to demonstrate the hematogenous metastasis of OC (Pradeep et al., 2014). Briefly, the skin of two female nude mice was surgically anastomosed to establish a common circulation, while the abdominal cavities of these paired mice were not connected. Then, the OC tumour cells were injected into the peritoneal cavity of one mouse (the host mouse). As a result, the tumour development and metastasis were observed in the other mouse (the guest mouse). Additionally, staining of the blood and lymphatic vessels from the connected skin tissue showed that the paired mice shared only hematogenous but not lymphatic systems. This indicated that apart from peritoneal dissemination, OC cells can also spread through the hematogenous system. Based on clinical observations, serous OC progresses quickly within the peritoneal cavity but rarely metastasizes outside of it until advanced stage IV (Redman et al., 2011, Lengyel, 2010). Before initiating the metastasis cascade, OC cells undergo an epithelial-to-mesenchymal transition (EMT), decreasing cell-to-cell and cell-to-matrix adhesion, and starting invasion. The single cancer cells or the spheroids then spread through ascites, arrive at the omentum and attach to the mesothelial layer through interaction with cell surface receptors, such as integrins and cluster of differentiation 44 (CD44) (Zong and Nephew, 2019). The cancer cells then further invade through the mesothelial layer and form secondary tumours. The angiogenesis process also happens to support secondary tumorigenesis and growth. Although it is relatively rare, especially at the early stages of metastasis, the OC cells can also invade or spread through the lymphatic system (Sundar et al., 2006).

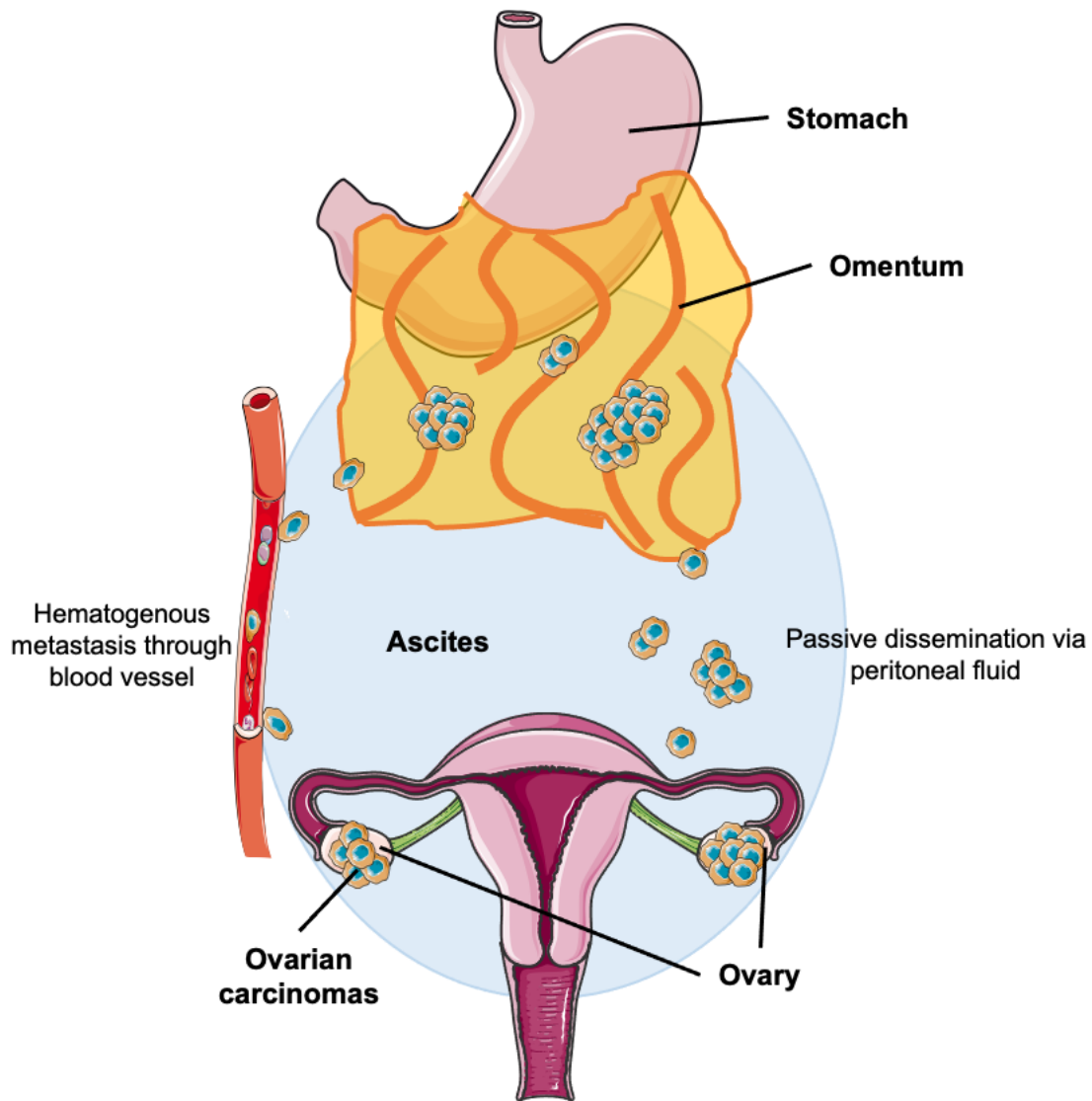


Figure 1.2. Metastasis feature of OC. The omentum is the primary metastasis site of OC. Passive dissemination through the peritoneal fluid is the main way of OC metastasis. OC cells can also invade the blood vessels and spread through the circulation system.

1.1.4. Diagnosis and treatment.

Late diagnosis is one of the leading causes of high OC mortality. Over 70% of the OC patients were diagnosed at stage III or stage IV and the metastasis is already present at the time of diagnosis (Cho and Shih, 2009). This is due to the lack of specific symptoms and reliable biomarkers for early diagnosis. OC symptoms such as pelvic or abdominal pain and persistent abdominal distension (bloating) are similar to the symptoms of irritable bowel syndrome (IBS) (Redman et al., 2011). Currently, there are no standardised screening tests for OC. Although biomarkers such as carbohydrate antigen 125 (CA125) and human epididymis protein 4 (HE4) have been widely used in

OC detection, there is still controversy about their sensitivity and specificity, especially in early-stage OC diagnosis (Zhang et al., 2021, Zhang et al., 2022b). Alternatively, the Risk of Ovarian Malignancy Algorithm (ROMA) assay combined the serum CA125 and HE4 levels and menopausal status via a logistic regression model was shown to have better accuracy in OC early-stage detection, and has been approved by the Food and Drug Administration (FDA) as a diagnosis method of OC (Zhang et al., 2022b). So far, CA125 is still the most frequently used biomarker for OC screening. Other biomarkers with higher accuracy and efficiency are still needed for the early detection of OC. Additionally, lavage of the uterine cavity can be used to collect the tumour cells shed from ovarian neoplasms and the tumour-specific mutations can be identified through next-generation sequencing in the collected cells (Maritschnegg et al., 2015). As a potential tool that can be used for OC diagnosis, this is now under investigation via a clinical trial (NCT02039388).

The gold-standard method for OC therapy requires cytoreductive surgery followed by platinum chemotherapy. The surgery aims to remove all visible macroscopic tumours, which have been proven to be associated with better survival (Fotopoulou et al., 2017). Platinum-based chemotherapy is then required to treat the residual cancer cells, especially for patients at stage II-IV. Chemotherapy agents such as Cisplatin and Carboplatin can form Cisplatin–DNA adducts in the nucleus of the cancer cells, which suppress DNA replication and transcription, arrest the cell cycle and induce apoptosis (Wang and Lippard, 2005). However, a high ratio of OC patients developed resistance to the chemotherapy, which brings challenges to OC therapy (Bowtell et al., 2015). Additionally, patients with *BRCA1/2* mutation could be treated with poly ADP ribose polymerase (PARP) inhibitors, such as Olaparib, Rucaparib and Niraparib, in combination with chemotherapy (Vetter and Hays, 2018). These inhibitors can prevent single-stranded DNA break repair and enhance error-prone non-homologous end joining (NHEJ) in HRD cells, which eventually leads to apoptosis (Patel et al., 2011).

Although disease screening and therapeutic methods have improved in the past 20 years, leading to a decreased overall mortality of OC patients in the world, late-stage diagnosis and therapy resistance are still remarkable challenges for OC. To solve these problems, research has been focusing on other factors that contribute to cancer development, including the surrounding environment of ovarian tumours.

1.2. The tumour microenvironment

Since Stephen Paget first proposed the “seed and soil” hypothesis that describes the crosstalk between cancer cells and the surrounding microenvironment, research has demonstrated the critical role of tumour microenvironment (TME) in promoting cancer cell growth, survival and metastasis (Fidler, 2003). The TME is composed of multiple cellular components, which include tumour cells and stromal cells. These cells are supported by the non-cellular component called extracellular matrix (ECM), a dynamic network continuously remodelled under normal and pathological conditions (Baghban et al., 2020). TME and the ECM suppress tumour development at the early stage of oncogenesis (Quail and Joyce, 2013). Cellular components such as fibroblasts and immune cells were also found to suppress the proliferation of tumour cells through cell-cell contact or by secreting growth-inhibiting factors (Zhuang et al., 2019). During cancer progression, tumour cells can alter the function of both ECM and TME-associated cells through complex signalling networks, which create a tumour-promoting microenvironment and assist cancer cell growth, migration and invasion (Quail and Joyce, 2013).

1.2.1 Extracellular matrix

ECM is the essential non-cellular component within all tissues and organs in the human body. It not only works as a scaffold that supports the adhesion of the cells but also regulates morphology, growth, differentiation and homeostasis by mediating a variety of intracellular signalling pathways (Huang et al., 2021). The basic composition of ECM includes water, proteins and polysaccharides. Although the main ECM components are similar between different tissues, the ECM-specific composition and topology are unique and are generated during tissue development (Frantz et al., 2010). Previous proteomic analyses combined with in silico prediction identified 278 genes that encoded ECM components, termed ‘core matrisome’ (Naba et al., 2012). These proteins include 43 collagens, 35 proteoglycans and 200 glycoproteins. Additionally, 1056 genes were found to encode proteins that are associated with ECM, defined as ‘associated matrisome’. These include ECM regulators, such as ECM modifying enzymes, secreted factors, such as growth factors (GFs), and ECM-affiliated proteins that share similar biological or structural functions with ECM proteins. The ECM can be classified into basement membrane (BM) and interstitial matrix (IM) (Cox, 2021). The

BM is rich in laminin and collagen IV, and separates the endothelial and epithelial layers of the tissues from the IM. The IM mainly contains fibrillar collagens, glycoproteins and proteoglycans (Nissen et al., 2019). During metastasis, tumour cells first breach the BM, and then invade the IM by secreting proteases and degrading ECM components. Additionally, cell-ECM adhesion relying on the ECM receptors on the cell surface, such as integrins and syndecans, is also essential for multiple biological progress, including cell migration and invasion (Frantz et al., 2010). During OC peritoneal metastasis, OC cells interact and invade through the mesothelium, which is formed by a monolayer of mesothelial cells attached to a BM (Yeung et al., 2015). The adhesion ability of spheroids derived from the ascites of patients with advanced ovarian carcinoma was previously characterised. Ascites spheroids were found to adhere to the mesothelial cell monolayers, which is mediated by the interaction between $\beta 1$ integrin and ECM components such as fibronectin (Burlison et al., 2004). After attaching to the mesothelial cells, OC cells were found to induce fibronectin expression and secretion by the mesothelial cells through transforming growth factor beta 1 (TGF- $\beta 1$) secretion, which promoted further invasion and proliferation of OC cells (Kenny et al., 2014).

1.2.1.1 Collagens

Collagens are the most abundant ECM components which constitute approximately 30% of the total protein mass in the human body (Frantz et al., 2010). To date, 28 different types of collagen chains have been identified. All collagens are homo- or heterotrimers of α chains, and over 40 different α chains with varying sizes from 662 to 3152 amino acids have been identified in the human body. Each of the α chains contains numerous Gly-X-Y repeats. Although X and Y could be any amino acids, proline and 4-hydroxyproline are the most frequently found amino acids for X and Y respectively (Figure 1.3) (Mouw et al., 2014). The collagen superfamily can be divided into fibril-forming collagens (e.g. type I, II, III), fibril-associated collagens with interrupted triple-helices (FACIT) (e.g. type IX), network-forming collagens (e.g. type IV) and other types (e.g. type XV, XXV) based on structural differences (Ricard-Blum, 2011). In comparison to the fibril-forming collagens which contain one complete triple-helix (Gly-X-Y) domain, FACITs contain multiple triple-helix domains, which are interrupted by non-collagenous domains. To form the collagen fibril, procollagen molecules are first assembled with the α chains in the endoplasmic reticulum (ER), followed by modification and packaging into vesicles in the Golgi apparatus (Mouw et al., 2014). The procollagens are cleaved by modifying enzymes such as matrix metalloproteinases (MMPs), which

form collagen molecules and are secreted extracellularly. Collagen molecules are then cross-linked by lysyl oxidase (LOX) and a stabilised supramolecular collagen structure is generated. The interaction of FACITs at the surface of the collagen fibril can also stabilise the collagen structure. Additionally, the BM is rich in network-forming collagens such as type IV, while the major collagen types in IM are fibril-forming collagens such as type I and II (Ricard-Blum, 2011).

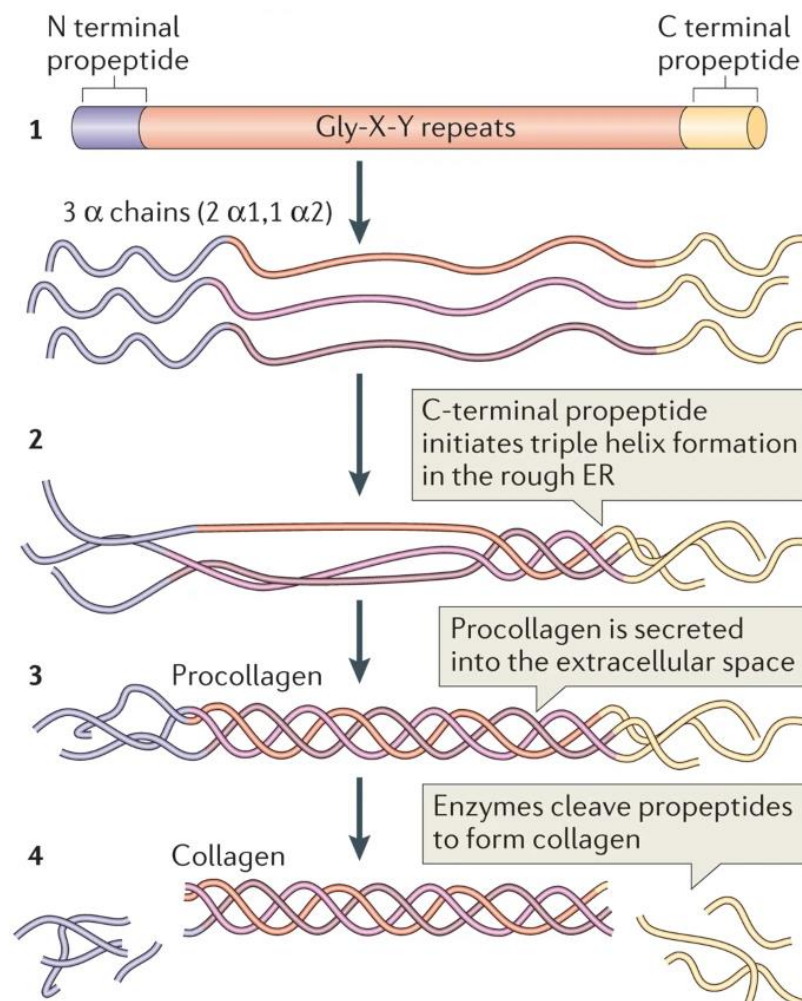


Figure 1.3. Standard structure of fibrillar collagen (collagen type I) molecule. Fibrillar collagen is a triple helix molecule formed by three α chains. The procollagen is generated in the ER and packed in the Golgi apparatus for secretion. Then, the procollagen was cleaved at both N and C-terminal by modifying enzymes to form collagen. Figure from (Mouw et al., 2014)

During cancer development, altered collagen deposition, modification and degradation are some of the most common observations compared to the healthy tissues (Cox, 2021). Collagen type I is a main fibrillar collagen that was found to be upregulated during the progression of multiple cancer types, including pancreatic, gastric and breast cancer (Shi et al., 2022). Collagen I was found to promote proliferation, adhesion and motility of pancreatic cancer cells (Panc1) (Armstrong et al.,

2004, Lu et al., 2014). Similarly, stromal cell-derived collagen I promoted the proliferation and adhesion of invasive breast cancer cell lines MDA-MB-231 and MCF7 (Kim et al., 2014). In OC, dysregulated collagen I architecture was identified in the tissues of patients with all four tested subtypes, HGSOC, LGSOC, clear cell and endometrioid carcinoma (Sarwar et al., 2022). Collagen I with increased thickness and reduced abundance was identified in OC tissue samples in comparison to the normal tissue of the patients (Sarwar et al., 2022). In vitro, collagen I derived from fibroblasts promoted the migration and invasion of OC cells (Li et al., 2020). Elevated collagen I was also identified in the ascites of the EOC patients, which suggested the role of collagen I in OC peritoneal metastasis (Li et al., 2020).

1.2.1.2 Proteoglycan

Proteoglycans are another primary ECM component, important in supporting the hydration of the ECM (Yanagishita, 1993). Based on the location, the proteoglycans can be classified into four groups, intracellular, cell surface, pericellular and extracellular proteoglycans (Iozzo and Schaefer, 2015). Currently, only one type of intracellular proteoglycan has been identified in the human body, serglycin. Transmembrane proteoglycans can function as receptors on the cell surface such as syndecans (described in [section 1.2.2.2](#)). Most of the proteoglycans are located extracellularly, these can be further divided into two types, lecticans (also known as hyalectans) and small leucine-rich repeat proteoglycans (SLRPs) (Mouw et al., 2014). There are four distinct proteoglycans included in the lectican class, aggrecan, versican (VCAN), neurocan and brevican, which are encoded by distinct genes but share similar structures ([Figure 1.4](#)) (Iozzo and Schaefer, 2015). Each of the lectican contains a core protein with an N-terminal hyaluronan (HA) binding domain, a central glycosaminoglycan (GAG) domain that binds to the GAG chains such as chondroitin sulphate, and a C-terminal lectin binding domain (Iozzo and Schaefer, 2015, Mouw et al., 2014). SLRP is the largest family of proteoglycans, encoded by 18 distinct genes. The core protein of SLRP contains multiple leucine-rich repeats (LRR). SLRPs can be classified into five classes. Class I-III, also called canonical SLRPs, contain GAG chains that bind to the core protein, while class IV and V, also called non-canonical SLRPs, have no GAG side chains (Iozzo and Schaefer, 2015). Proteoglycans crosslinked with hyaluronic acid and collagen fibril form the basic structure of the ECM. Other components such as laminin and fibronectin further reinforce the network, enhancing the connection between ECM and cells (Mouw et al., 2014).

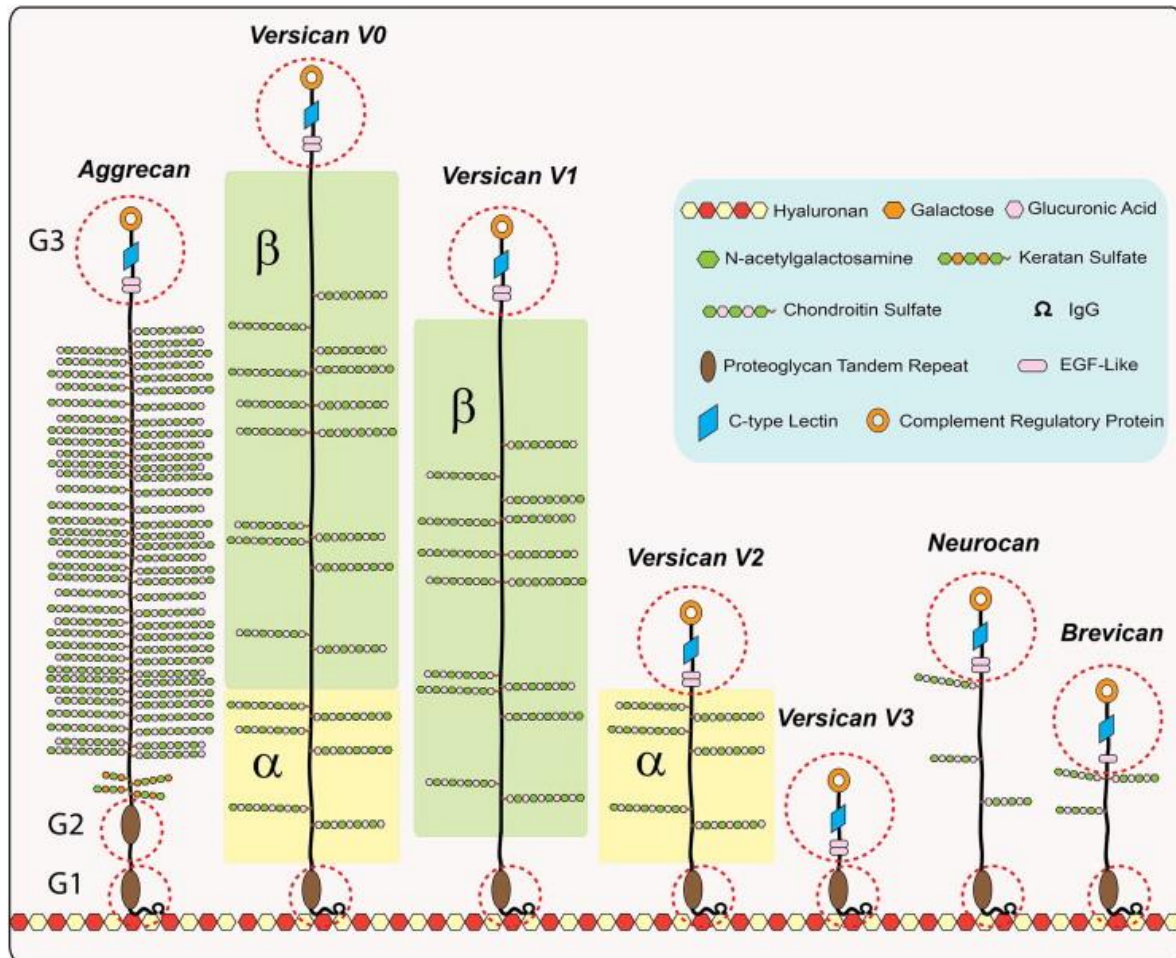


Figure 1.4. Structure of lecticans (hyalectans), including aggrecan, versican, neurocan and brevican. The full-length VCAN (V0) and the splice isoforms of V1, which contains only the GAG- β domain, V2, which contains only the GAG- α domain, and V3, which has no GAG domain. The dotted circles indicate the domains that are shared with the other hyalectans (G1–G3). Figure from (Iozzo and Schaefer, 2015)

Altered proteoglycan expression and composition were found to promote the peritoneal metastasis of OC. OC patients with higher VCAN and HA levels showed poor prognosis outcomes. Previous studies showed that intact VCAN can promote ovarian cancer metastasis, as VCAN was shown to increase ovarian cancer cell migration and invasion potential (Ghosh et al., 2010, Ween et al., 2011). Furthermore, a higher VCAN expression was detected in malignant EOC cells compared with benign and borderline tumour cells, which are less invasive and proliferative than malignant cells (Lima et al., 2016). The tumour samples were classified into malignant, borderline and benign tumours based on the morphological criteria. Similarly, upregulated VCAN expression level was found significantly associated with the invasion and occupation of malignant cells at the omentum metastatic site of HGSOC patients (Pearce et al., 2018). Apart from local invasion, VCAN is also essential during cancer

cell peritoneal fluid dissemination and tumorigenesis on the peritoneum. Ween and colleagues reported a HA/VCAN pericellular matrix in migrating ovarian cancer cells, which protects ovarian cancer cells during metastasis in the peritoneal cavity and increases their adhesion to peritoneal cells by interacting with surface receptor CD44 (Figure 1.5) (2011).

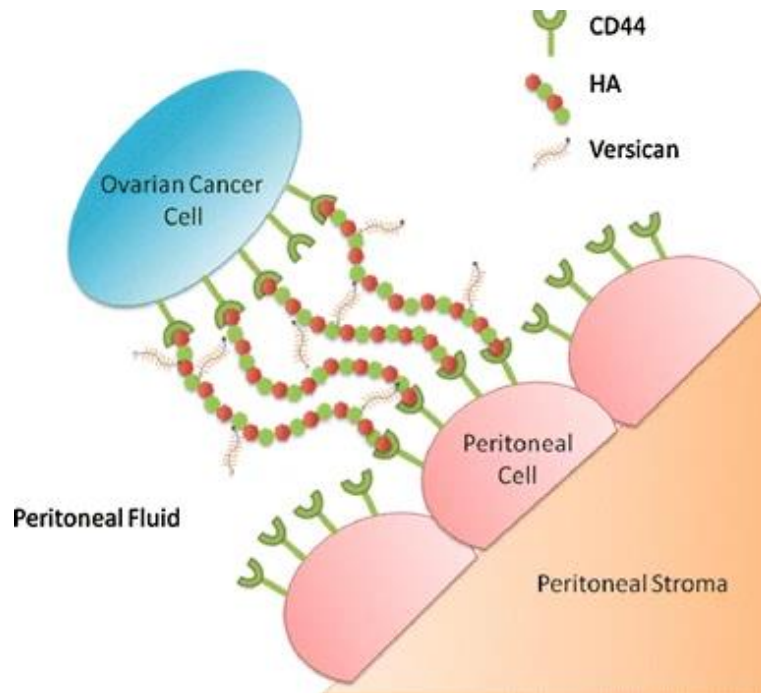


Figure 1.5. A proposed mole of CD44, HA and VCAN mediating the ovarian cancer cell adhesion to the peritoneal cells. Stabilized HA/VCAN pericellular matrix around the ovarian cancer cells contributes to peritoneal metastasis by increasing the motility and adhesion ability of cancer cells to the peritoneal cells through interaction with CD44 cell surface receptor. Figure from (Ween et al., 2011)

1.2.1.3 Fibronectin

Fibronectin is a secreted glycoprotein that is critical in cell-ECM adhesion and cell migration. It is a dimeric molecule, and each monomer contains three types of homologous repeats, including 12 type I, 2 type II and 17 type III repeats (Hynes and Yamada, 1982, Mouw et al., 2014). The formation of fibronectin dimer relies on the antiparallel disulphide bonds at the C-terminal of the molecules, and it is further folded via the ionic interactions between the type III repeats (Figure 1.6). The assembly of fibronectin dimers into the fibril structure is a cell-mediated process initiated by binding to cell-surface ECM receptors (Pankov et al., 2000). Integrin $\alpha 5 \beta 1$ is the primary receptor for fibronectin, binding to the Arg-Gly-Asp (RGD) domain (Huveneers et al., 2008). Additionally, syndecan 4 is another ECM receptor that contributes to the assembly of fibronectin. Co-operative

binding of integrin $\alpha 5\beta 1$ and syndecan 4 to fibronectin supports focal adhesion formation and migration of the cells (Morgan et al., 2007).

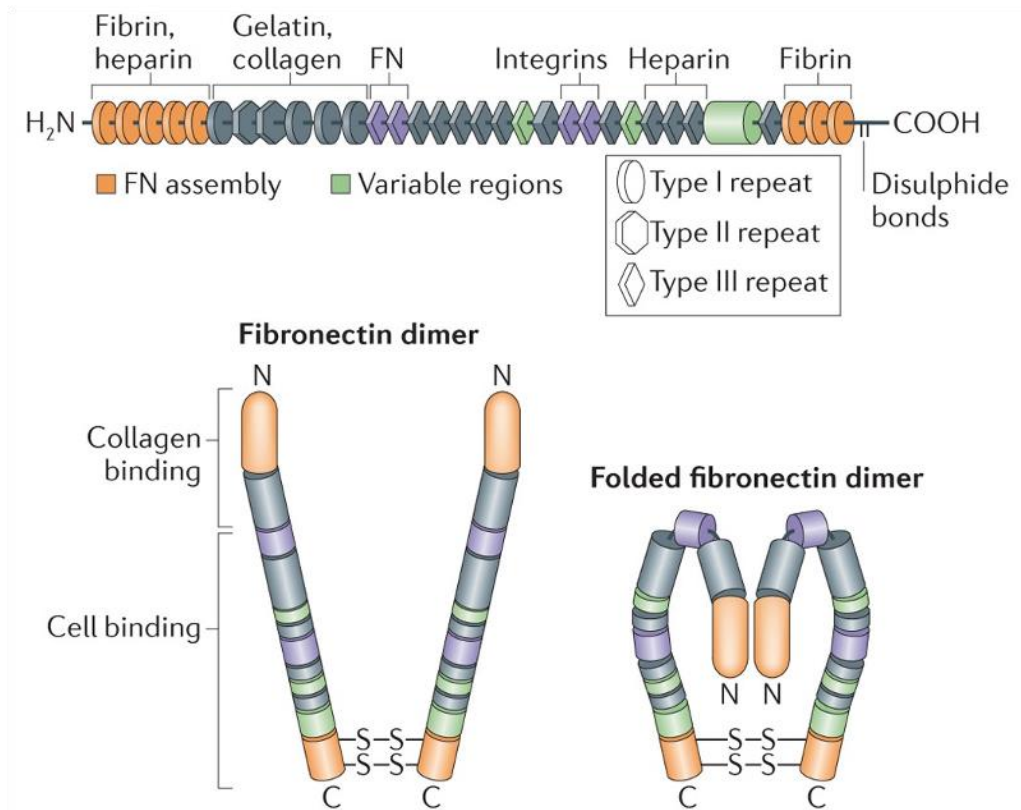


Figure 1.6. Structure of fibronectin molecule. A fibronectin monomer is formed by type I, II and III homologues repeats. Fibronectin dimers form antiparallel disulphide bonds at the C-terminal of the molecules, and they are further folded via the ionic interactions between the type III repeats. Figure form (Mouw et al., 2014).

In OC, patients with higher fibronectin levels in the tumour stroma showed significantly shorter overall survival (Kujawa et al., 2020). Fibronectin was also widely identified in the malignant ascites from OC patients (Carduner et al., 2013). *In vitro*, fibronectin is essential for integrin $\alpha 5\beta 1$ dependent migration and invasion of OC cells (Caswell et al., 2007). It was found to promote the migration and invasion of A2780 and OVCAR3 cells, by activating focal adhesion kinase (FAK)-PI3K/AKT signalling pathway (Yousif, 2014). Furthermore, fibronectin produced by mesothelial cells was found to promote early OC metastasis to the omentum (Kenny et al., 2014). On one hand, OC cells were found to induce fibronectin gene expression and secretion of human mesothelial cells by producing TGF- $\beta 1$. On the other hand, the proliferation and invasion ability of OC cells on mesothelial cells with fibronectin KD was significantly reduced compared to the mesothelial cells expressing fibronectin. In an *in vivo* model, mice with fibronectin deficiency showed significantly

reduced omentum metastasis after being injected with OC cells. These indicated the important role of fibronectin in promoting mesothelial cell invasion and OC metastasis (Kenny et al., 2014).

1.2.2 Extracellular matrix receptors

1.2.2.1 Integrins

Since the integrin family was first described by Hynes (1987), they became the main and most well-understood cell surface receptors that mediate cell-ECM adhesion (Hynes, 2002). Integrins are heterodimers formed by one α and one β subunit. In mammalian cells, 18 α subunits and 8 β subunits have been identified, which form 24 distinct integrin dimers. Both α and β subunits are transmembrane glycoproteins which contain a large (>1600 amino acids) extracellular domain and a small (20-50 amino acids) cytoplasmic domain (Hynes, 1987, Hynes, 2002). Integrins are generally in an inactive conformation at the cell surface and the extracellular domain of the α and β subunits are non-covalently linked. When interacting with ECM components such as collagens, fibronectin and laminin through the binding pocket, integrins switch to an active conformation (Kinbara et al., 2003). Based on ECM ligand-binding properties, integrins can be classified into four sub-families, collagen receptors, laminin receptors, RGD receptors and leukocyte-specific receptors (Figure 1.7) (Hynes, 2002). The majority of integrins contain the β 1 subunit and the β 2 subunit is only involved in leukocyte-specific receptors. The α V subunit can form RGD receptors with β 3, β 5, β 6 or β 8 subunits. Apart from being activated by extracellular signals (“outside-in” signalling), integrin can also be activated through “inside-out” signalling (Hynes, 2002). Proteins such as talin and kindlin can bind to the tail of β integrin upon intracellular stimulation, which alters the conformation of the integrin dimer resulting in a higher affinity for ECM ligands (Moreno-Layseca et al., 2019). The inside-out signalling pathways were found to mediate cell migration, invasion and ECM degradation (Pang et al., 2023).

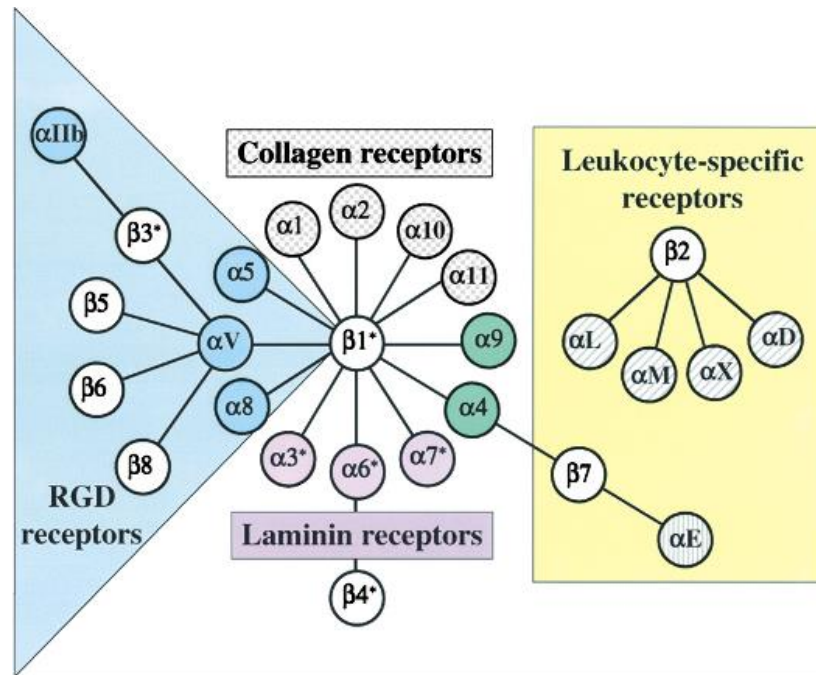


Figure 1.7. The integrin sub-families. Integrin heterodimers are formed by α and β subunits. 18 α and 8 β subunits can form 24 distinct integrin heterodimers in the human body. Integrins can be classified into four sub-families, RGD receptors (blue), Collagen receptors (grey hatching), Leukocyte-specific receptors (yellow) and laminin receptors (Purple). Figure from (Hynes, 2002)

During tumorigenesis, integrins were found to regulate multiple cancer-promoting biological progress, such as cell proliferation, adhesion, migration and metabolism by activating multiple downstream pathways, including MAPK/ERK, PI3K/AKT and nuclear factor κ B (NF- κ B) signalling pathways (Cox, 2021, Pang et al., 2023).

Integrins are constitutively trafficking in the cells. This dynamic trafficking is mediated by multiple Rab family members, a subfamily of Ras small GTPases (details see [section 1.4](#)). Integrins can be endocytosed via multiple pathways and be delivered to Rab5-positive early endosomes (EEs). For degradation purposes, EEs mature into late endosomes (LEs) and their content is degraded after fusion with lysosomes. Most of the integrins are recycled back to the plasma membrane following internalisation. Two main pathways are involved in this process, the Rab4-dependent short loop and the Rab11-dependent long loop ([Figure 1.8](#)). The trafficking of integrin between the cell surface and intracellular pools is precisely regulated to maintain the biological functions in the organism, while the dysregulation of these processes was observed in cancers. For example, altered integrin $\alpha 5\beta 1$ expression and trafficking were found to promote the development of multiple cancers (Hou et al., 2020). In OC, Rab25 was found to directly interact with $\beta 1$ integrin and regulate the recycling of

integrin $\alpha 5 \beta 1$ from the LE at the pseudopod tips of OC cells, which promoted migration and invasion in the presence of fibronectin. Interestingly, Rab25 did not affect cell migration on plastic (Caswell et al., 2007).

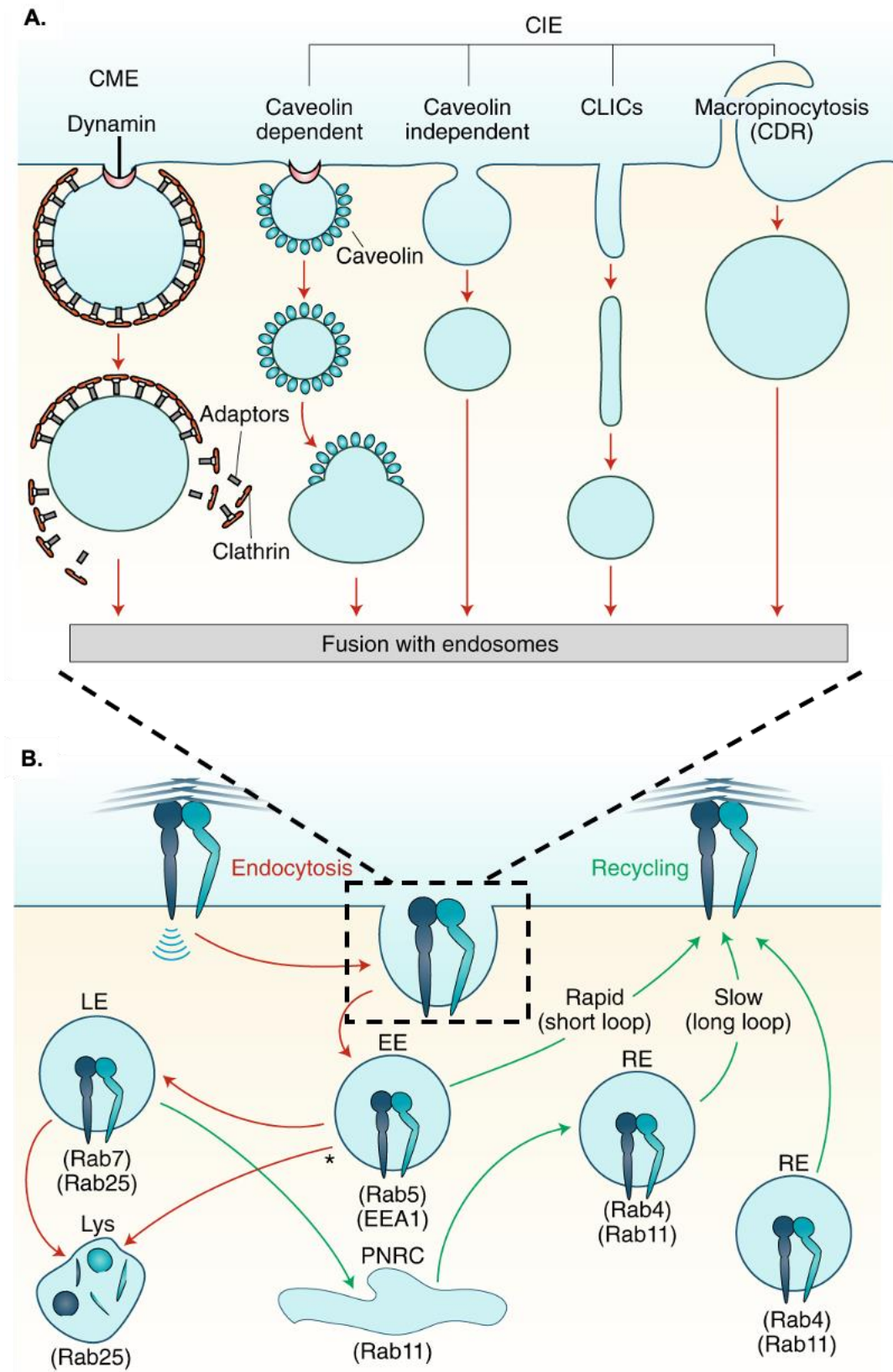


Figure 1.8. Integrin endocytosis and recycling. Cell membrane integrins can be internalised through multiple mechanisms (A.). After being delivered to Rab5-positive EEs, integrins are recycled (green arrows) back to the plasma membrane through Rab4-dependent short loop, or Rab11-dependent long loop. The maturation of EEs to LEs leads to the degradation of integrins by fusing with lysosomes. Alternatively, active integrins can be recycled from the lysosomes back to the plasma membrane and a Rab25- and CLIC3-dependent manner Figure from (Moreno-Layseca et al., 2019)

1.2.2.2 Other receptors

Apart from integrins, other receptors that can bind to the ECM include CD44, syndecans, discoidin-domain receptors (DDR) and uPARAP/Endo180. CD44 mainly interacts with HA. Other ligands of CD44 include osteopontin, collagens and fibronectin (Goodison et al., 1999). The roles of CD44 in normal tissues include hyaluronic metabolism regulation, immune response induction and cytokine release mediation (Senbanjo and Chellaiah, 2017). On the other hand, CD44 also activates pro-tumourigenic signalling pathways and contributes to cell survival, proliferation, angiogenesis and metastasis in breast, prostate and OC (McFarlane et al., 2015, Desai et al., 2007, Martincuks et al., 2020).

Syndecans are a family of transmembrane proteoglycans that contain four members (syndecan 1-4) (Salmivirta and Jalkanen, 1995). Based on the structure similarity, they can be further classified into two subfamilies. Syndecans 1 and 3 contain GAG binding sites at both sides of the central ectodomain while syndecans 2 and 4 only have GAG chain binding at the N-terminal side of the ectodomain. Syndecans can interact with ECM components such as fibronectin through the GAG chains and further mediate cell-cell or cell-ECM interactions (Afratis et al., 2017). Additionally, the expression of syndecans is distinct between tissue and cell types. Syndecan 1 is mainly expressed in epithelial and plasma cells. As the loss of syndecan 1 on the surface of myeloma cells contributed to the proliferation and dissemination, which is also associated with poor patients' survival, it was suggested as a prognostic biomarker for myeloma (Aref et al., 2003). Syndecan 2 is expressed in mesenchymal cells, such as fibroblast and smooth muscle cells (Afratis et al., 2017). Upregulated syndecan 2 was also identified in mesenchymal breast cancer cells and the knockdown (KD) of syndecan 2 reduced cell migration and enhanced focal adhesion formation (Lim and Couchman, 2014). The expression of syndecan 3 is mainly found in neural and developing musculoskeletal tissues (Afratis et al., 2017). Interestingly, overexpression of syndecan 3 was also identified in OC and pancreatic cancer, which was associated with poor patient prognosis (Hillemeier et al., 2022,

Yao et al., 2017). Syndecan 4 is ubiquitously expressed in the human body, and mainly regulates cell adhesion (Afratis et al., 2017). The overexpression of syndecan 4 promotes cell proliferation and metastasis of breast cancer (Leblanc et al., 2018). Remarkably, syndecans were found to interact and cooperate with other cell membrane receptors including integrins. Syndecan 1 can activate integrin $\alpha\beta3$ and $\alpha\beta5$ in an inside-out signalling manner, which has been shown to promote tumour angiogenesis (Beauvais and Rapraeger, 2010, Beauvais et al., 2009). Similarly, syndecan 4 crosstalk with integrin $\alpha5\beta1$ was found to activate PKC α during focal adhesion formation and cell migration (Mostafavi-Pour et al., 2003).

1.2.3 Cancer-associated fibroblasts

Stromal cells are another important component of TME that promotes cancer development, and include normal and cancer-associated fibroblasts (CAFs), immune cells and endothelial cells (Baghban et al., 2020). Normal fibroblasts are the major producers of ECM in tissues. During the wound healing process, fibroblasts are activated into myofibroblasts by multiple signalling molecules, such as ECM components, cytokines and GFs (Younesi et al., 2024). The main marker of activated myofibroblasts is the expression of α -smooth muscle actin (α SMA) under stimulation with TGF- β , which contributes to the changes in cell morphology, increased cell proliferation and migration and altered ECM remodelling. The term CAF broadly describes the activated fibroblasts in the tumour stroma, which are mediated by cancer cell-derived cytokines and GFs. For example, TGF- β secreted by cancer cells was found to mediate the activation of CAFs by upregulating the expression of α SMA in normal fibroblasts, which is similar to the activation of myofibroblasts. This type of CAF is also called myCAF (Sahai et al., 2020). Other types of CAFs were also identified in the tumour stroma, including inflammatory CAFs (iCAFs) and antigen-presenting CAFs (apCAFs) (Yang et al., 2023). iCAFs are mainly induced by IL-1 α and TNF- α and show higher expression levels of IL-6. Additionally, CAF heterogeneity was identified in the TME, which indicated the existence of CAFs with distinct precursor cells (Yang et al., 2023). Apart from normal fibroblast, CAFs were also found derived from bone marrow mesenchymal stem cells, endothelial cells, epithelial cells and adipocytes (Zhang et al., 2022a).

CAFs can promote cancer progression from multiple aspects. CAF-derived GFs, such as hepatocyte growth factor (HGF), were found to promote the proliferation of multiple types of cancer cells, including OC (Wu et al., 2021, Deying et al., 2017). CAFs can also secrete multiple pro-angiogenesis factors including fibroblast growth factor 2/7 (FGF2/7) and vascular endothelial growth factor A (VEGFA) to promote neo-angiogenesis (Wang et al., 2019a). Additionally, CAFs are also involved in tumour metastasis. In vitro, squamous cell carcinoma cells showed enhanced invasion into collagen and matrigel when in co-culture with CAFs (Gaggioli et al., 2007). Exosomes derived from omentum CAFs were also found to promote the invasion of OC cells (Han et al., 2023). Research shows that CAFs promote cancer cell local invasion by secreting ECM-modifying enzymes such as MMP (Kalluri, 2016). CAF-secreted matrices can also promote the invasion of cancer cells. For example, VCAN derived from ovarian CAFs was found to promote the invasion ability of OC cells into matrigel (Yeung et al., 2013). Contrarily, the role of CAFs in suppressing tumorigenesis has also been observed. For instance, the immunosuppressive role of apCAFs by recruiting T regulatory (Treg) cells was identified in breast cancer and pancreatic cancer (Costa et al., 2018, Huang et al., 2022a). Additionally, apCAFs were involved in the anti-tumour immune activity of T-cell in lung cancer (Kerdidani et al., 2022).

1.3. ECM remodelling in cancer progression

ECM is a dynamic structure that is under continuous remodelling in both normal and pathological conditions (Frantz et al., 2010). During the progression of multiple types of cancer, altered ECM remodelling was observed in TME, which further contributed to the proliferation, migration and invasion of cancer cells (Winkler et al., 2020). The ECM remodelling in TME is mediated by not only cancer cells but also stroma cells such as fibroblasts. Altered production of ECM-modifying enzymes by tumour cells and CAFs is one of the main causes of ECM remodelling dysregulation (Winkler et al., 2020). Metalloprotease is a group of main ECM modifying and degrading enzymes, which include matrix metalloprotease (MMP), a disintegrin and metalloprotease (ADAM), a disintegrin and metalloprotease with thrombospondin motif (ADAMTS) (Bonnans et al., 2014). During cancer development, altered expression and regulation of multiple types of metalloproteases have been identified, including OC.

1.3.1. Matrix metalloprotease (MMP)

MMPs are calcium-dependent zinc-containing endopeptidases metalloproteinases that are widely involved in the development and physiologic events, such as maintaining tissue morphology (Vu and Werb, 2000). In mammals, 24 types of MMPs have been identified. They can be classified into eight subgroups based on the structure, function and cellular localisation: collagenases, gelatinases, stromelysins, matrilysins, transmembrane type I and type II, glycosyl-phosphatidyl-inositol (GPI) anchored and other MMPs (Niland and Eble, 2020, Moliere et al., 2023). Apart from transmembrane type I, II and GPI-anchored MMPs that are located at the cell membrane, other MMPs are secreted extracellularly. As a family of proteases that remodel the ECM, MMPs from different subgroups can specifically cleave multiple ECM components, including collagens, gelatin, fibronectin and laminin (Table 1.2) (Snoek-van Beurden and Von den Hoff, 2005). MMPs are produced as pro-protein and are activated through the cleavage of the pro-domain. Furin cleavage is one of the main activation processes of MMPs, including cell surface MMPs and extracellular MMP11, 21 and 28 before secretion (Ra and Parks, 2007). Alternatively, MMPs without furin cleavage sites are activated extracellularly through non-furin proteolytic mechanisms. These pro-MMPs were found to be cleaved by other activated MMPs. As an example, pro-MMP2 is activated at the cell surface by MT1-MMP (MMP14). The function of MMPs in ECM degradation is balanced by the tissue inhibitors of metalloproteinases (TIMPs), which include four members (TIMP1-4). TIMPs are secreted proteins, that exist as soluble forms (TIMP1, 2 and 4) or bound to the ECM (TIMP3) (Cabral-Pacheco et al., 2020). Although different TIMPs can inhibit the same type of MMP, the inhibition affinity is distinct. Additionally, TIMPs were also found to mediate the activation of several MMPs. For example, TIMP2 was found to contribute to the activation of pro-MMP2 by MT1-MMP (Hernandez-Barrantes et al., 2001).

Table 1.2 MMP subgroups and substrates.

Subgroup	Name	MMP member	Substrates
Collagenases	Collagenase-1	MMP1	Col I, II, III, VII, VIII, X, gelatin
	Collagenase-2	MMP8	Col I, II, III, VII, VIII, X, gelatin, aggrecan
	Collagenase-3	MMP13	Col I, II, III, IV, IX, X, XIV, gelatin
	Collagenase-4	MMP18	Col I, II, III, gelatin
Gelatinases	Gelatinase A	MMP2	Gelatin, Col I, II, III, IV, VII, X
	Gelatinase B	MMP9	Gelatin, Col IV, V
Stromelysins	Stromelysin 1	MMP3	Col II, IV, IX, X, XI, gelatin
	Stromelysin 2	MMP10	Col IV, laminin, fibronectin, elastin
	Stromelysin 3	MMP11	Col IV, laminin, fibronectin, aggrecan
Matrilysins	Matrilysin 1	MMP7	Fibronectin, laminin, Col IV, gelatin
	Matrilysin 2	MMP26	Fibrinogen, fibronectin, gelatin
Transmembrane type I	MT1-MMP	MMP14	Gelatin, fibronectin, laminin
	MT2-MMP	MMP15	Gelatin, fibronectin, laminin
	MT3-MMP	MMP16	Gelatin, fibronectin, laminin
	MT5-MMP	MMP24	Gelatin, fibronectin, laminin
Transmembrane type II	CA-MMP	MMP23	Gelatin, casein, fibronectin
GPI-anchored MMPs	MT4-MMP	MMP17	Fibrinogen, fibrin
	MT6-MMP	MMP25	Gelatin
Other MMPs	Metalloelastase	MMP12	Elastin, fibronectin, Col IV
	RASI-1	MMP19	Aggrecan, elastin, fibrillin, Col IV, gelatin
	Enamelysin	MMP20	Aggrecan
		MMP21	Aggrecan
		MMP27	Gelatin, casein
	Epilysin	MMP28	Casein

During tumorigenesis, MMPs are not only secreted by cancer cells but also produced by stromal cells such as fibroblasts (Moliere et al., 2023). Dysregulation of MMPs has been observed in the TME of multiple cancer types. Remarkably, both tumour-promoting and suppressing roles of MMPs have been reported previously. The cancer-promoting function of MMPs was reported at multiple stages of tumorigenesis. In the early stages, MMPs can degrade BM components and allow the invasion of cancer cells (Cathcart et al., 2015). Increased expression of MMP2 and MMP9 was identified in colorectal tumour samples, resulting in the disruption of type IV collagen (Zeng et al., 1999). Similarly, the expression levels of inactivated pro-MMP9, pro-MMP2 and activated MMP2 are significantly higher in malignant ovarian tumour samples in comparison to benign samples, which suggests a role of MMP2 and MMP9 in promoting metastasis (Schmalfeldt et al., 2001). MT1-MMP is involved in the activation of MMP2 and MMP9 (Ra and Parks, 2007, Nyante et al., 2019). OC cells overexpressing MT1-MMP showed increased collagen-dependent proliferation and performed better in multicellular aggregate formation (Moss et al., 2009). Additionally, the overexpression of MT1-MMP was also found to enhance VEGF production, which promotes angiogenesis, in breast

cancer and glioblastoma (Sounni et al., 2004, Deryugina et al., 2002). Contrarily, anti-tumour MMPs such as MMP8 and MMP12 were also identified (Konstantinopoulos et al., 2008). In breast cancer cells, both KD of MMP8 in non-metastatic cells (NM-2C5) and overexpression of MMP8 in metastatic cells (M-4A4) showed altered metastatic behaviour in vivo (Montel et al., 2004). Mice injected with MMP8 KD NM-2C5 cells showed increased lung metastasis in comparison to the control, while M-4A4 with MMP8 overexpression showed reduced lung metastasis. Although their critical role in cancer progression suggested MMPs as potential targets for cancer therapy, multiple clinical trials with MMP inhibitors were terminated due to the remarkable side effects. Since MMPs are also highly involved in the normal functions of ECM remodelling and substrates of MMPs are variable, novel inhibition approaches and targeted drug delivery systems are under investigation to minimise the side effects (Cathcart et al., 2015).

1.3.2. A disintegrin and metalloprotease (ADAM)

The ADAMs are another group of zinc-dependent metalloproteinases that share similar functions with MMPs in ECM remodelling. However, unlike MMPs which contain both extracellular and cell membrane-located members, in mammalian cells, all 21 ADAM family members are transmembrane proteases (Edwards et al., 2008). Interestingly, half of the ADAMs identified in humans lack catalytic zinc activation sites and remain in an inactivated form without proteolytic functions (e.g. ADAM2, 7, 11, 18, 22, 23, 27, 29 and 33). Other family members are activated through zinc activation and pro-domain cleavage by furin (Giebler and Zigrino, 2016). ADAM8, 10 and 17 can also be activated through a furin-independent autocatalytic mechanism which does not involve the cleavage of the pro-domains (Mierke, 2023). The cysteine-rich domain of ADAM12 was found to interact with syndecan 4, which further engages with integrin β 1 and mediates cell spreading and stress fibre formation (Thodeti et al., 2003). Furthermore, ADAMs can also regulate the function of the epidermal growth factor receptor (EGFR) by processing of the ligands, such as TGF- α , tumour necrosis factor α (TNF- α) and heparin-binding EGF-like growth factor (HB-EGF), in a catalytic activity-dependent manner (Blobel, 2005).

A recent pan-cancer analysis investigated the expression of ADAMs across 33 types of cancer using multiple datasets integrating bulk RNA-seq, tumour mutation burden (TMB), and clinicopathological

parameters in The Cancer Genome Atlas (TCGA) (Ma and Yu, 2023). As a result, enhanced gene expression of multiple ADAMs was identified in numerous tested cancers, among which the significantly upregulated ADAM8 was identified in 16 out of 18 tested cancers. Contrarily, a significant pan-cancer downregulation of ADAM33 was also identified. Compared to the ADAMs lacking catalytic activity, the functions of enzymatically active ADAMs in cancer progression are better characterised, as previously reviewed (Mullooly et al., 2016). For instance, breast cancer MDA-MB-231 cells showed better trans-endothelial migration compared to ADAM8 KD cells in vitro (Conrad et al., 2018). The expression of MMP9 in MDA-MB-231 cells was correlated with ADAM8 expression, which suggests that ADAM8/MMP crosstalk may promote breast cancer metastasis. Moreover, the blocking of β 1 integrin also suppressed the transmigration of MDA-MB-231 cells. This work did not provide any insight into how β 1 integrin, MMP9 and ADAM8 could mechanistically control each other. ADAM8 was also found to promote the migration and invasion of pancreatic cancer cells, which could be suppressed by the ADAM8-specific inhibitor BK-1361 (Schlomann et al., 2015). Currently, several ADAM-targeting inhibitors are under clinical trials and showed little musculoskeletal side effects compared to MMP targeting therapy (Mullooly et al., 2016). However, there are still knowledge gaps in the mechanisms of ADAMs in cancer so further investigations are still required.

1.3.3. A disintegrin and metalloprotease with thrombospondin motif (ADAMTS)

ADAMTSs are metalloproteases which contain a disintegrin domain and thrombospondin motifs. There are 19 *ADAMTS* genes named from 1 to 20 in mammalian genomes due to the exclusion of *ADAMTS11* (Kelwick et al., 2015). Similar to their relative metalloproteinases, MMPs and ADAMs, ADAMTSs are members of the metzincin protease superfamily that modify the structure and function of the ECM. Unlike MT-MMP and ADAM which contain transmembrane modules, ADAMTSs are secreted extracellular proteinases. The 19 human ADAMTS proteins are classified into four main groups based on their structure and functions (Figure 1.9 and Table 1.3). The proteoglycanase group, including ADAMTS1, 4, 5, 8, 9, 15 and 20, can cleave hyaluronans including aggrecan, brevican, neurocan and VCAN (Stanton et al., 2011). Additionally, ADAMTS1 was found to cleave syndecan-4 at the N-terminal ectodomain (Rodriguez-Manzaneque et al., 2009). ADAMTS5 and to a lesser extent ADAMTS4 can also degrade the glycoprotein fibulin-2 (Fontanil et al., 2017). Under the same

conditions, ADAMTS1 was not involved in fibulin-2 degradation. ADAMTS2, 3 and 14 belong to the procollagenase N-peptidase group, which specifically cleaves the fibrillar procollagens (Kelwick et al., 2015). Recently, ADAMTS3 was also found to cleave the Pro²⁴⁶⁶ - Leu²⁴⁶⁷ peptide bond at the C-terminal of fibronectin (Gibson et al., 2023). ADAMTS13 is a special family member of von Willebrand factor (vWF) cleaving protease (vWFPCP), which processes large vWF precursors to optimal size glycoprotein for blood coagulation (Fujikawa et al., 2001, Kelwick et al., 2015). ADAMTS7 and 12 were recognised as cartilage oligomeric protein (COMP) proteases. ADAMTS12 was also found to cleave neurocan in the mouse brain tissue, which could be involved in repairing the central nervous system (Fontanil et al., 2019). ADAMTS10 has been found to cleave fibrillin-1 (Kutz et al., 2011) and fibronectin has been identified as a substrate for ADAMTS16 and 18 recently (Schnellmann et al., 2018, Ataca et al., 2020), while the substrate and function of ADAMTS6, 17 and 19 still remain unclear (Kelwick et al., 2015). The activation of ADAMTS catalytic activity is also varied across the family members. The majority of ADAMTSs are activated by furin through cleavage of the pro-domain, while others, such as ADAMTS7 and 13, can cleave specific substrates with the pro-domain intact (Rose et al., 2021, Stanton et al., 2011).



Figure 1.9. Structure of ADAMTS family. Schematic of the 19 family members of ADAMTS, grouped based on the structure and function. The ADAMTSs share similar N-terminal domain organisations and some members have unique C-terminal domains (Bacchetti et al., 2024).

Table 1.3 ADAMTS subgroups and substrates.

Subgroup	ADAMTS member	Substrates
Proteoglycanase	ADAMTS1	Aggrecan, versican, syndecan 4, gelatin
	ADAMTS4	Aggrecan, versican, brevican, neurocan, fibulin-2
	ADAMTS5	Aggrecan, versican, brevican, neurocan, fibulin-2
	ADAMTS8	Aggrecan
	ADAMT15	Aggrecan, versican
	ADAMTS9	Aggrecan, versican
	ADAMTS20	Versican
Propeptidase	ADAMTS2	Procollagens type I, II, III, V
	ADAMTS3	Procollagens type II, fibronectin
	ADAMTS14	Procollagen type I
vWFCP	ADAMTS13	vWF
COMP proteinases	ADAMTS7	COMP
	ADAMTS12	COMP, neurocan
Others	ADAMTS6	Unknown
	ADAMTS10	Fibrillin-1
	ADAMTS16	Fibronectin
	ADAMTS18	Fibronectin
	ADAMTS17	Unknown
	ADAMTS19	Unknown

Since ADAMTSs show a narrow substrate specificity, they are considered a potentially safe target for drug development (Tortorella et al., 2009). However, the detailed molecular mechanism of how ADAMTSs are involved in different diseases remains unclear, especially for cancers. The altered expression of ADAMTSs has been identified in multiple types of cancer. A pan-cancer analysis showed that in comparison to the healthy tissue, the expression levels of different ADAMTS family members are either upregulated or downregulated. For instance, in pancreatic cancer, different ADAMTS family members have been shown to be upregulated (Bacchetti et al., 2024). Interestingly, both pro-and anti-tumour roles of the same ADAMTS members were identified in distinct cancers. As an example, ADAMTS1 was found to promote tumour growth and metastasis in pancreatic and lung cancer (Masui et al., 2001, Liu et al., 2006). Contrarily, the anti-angiogenic role of ADAMTS1 has been reported in breast cancer (Martino-Echarri et al., 2013). As a secreted protease located in the TME, ADAMTSs were found to mediate cancer progression through ECM remodelling (Bacchetti et al., 2024). ADAMTSs are produced by both cancer cells and stromal cells. Downregulated

ADAMTS1, 5 and 9 together with upregulated natural inhibitor TIMP3 were observed in the prostate tumour stroma, which resulted in the accumulation of VCAN and could further enhance metastasis (Cross et al., 2005). In breast cancer, deficiency of myoepithelial cell-derived ADAMTS3 led to the accumulation of fibronectin, which promoted cancer cell 3D invasion in an integrin $\alpha 5\beta 1$ dependent manner (Gibson et al., 2023). Alternatively, ADAMTSs can also regulate cancer progression by mediating multiple cell signalling pathways including Wnt/ β -catenin, TGF- β , MEK/ERK, PI3K/AKT and NF- κ B (Bacchetti et al., 2024). For instance, overexpression of ADAMTS6 in breast cancer cell lines suppressed the activation of EGFR and ERK, which further suppressed cell migration and invasion (Xie et al., 2016). Reduced activation of EGFR/AKT was also observed in lung cancer cells overexpressing ADAMTS18 (Zhang et al., 2019).

1.3.3.1 ADAMTS5 in cancer

As a set of proteins translated by paired genes on human chromosome 21q21, ADAMTS5 shares homologous structure and similar functions with ADAMTS1 and ADAMTS4, which are also considered a potential target for cancer diagnosis and therapy (Kelwick et al., 2015, Santamaria, 2020). Similar to ADAMTS1, the dual function of ADAMTS5 was also identified in different cancer types.

In melanoma (Kumar et al., 2012) and gastric carcinoma (Huang et al., 2019), ADAMTS5 suppresses tumour progression by inhibiting angiogenesis. Decreased expression of ADAMTS5 was detected in these cancer cell lines caused by the hypermethylation of its promoter. In addition, decreased cell adhesion and increased cell invasion and metastasis were detected in cancer cell lines with reduced ADAMTS5 expression. Moreover, ADAMTS5 was shown to affect angiogenesis via different molecular mechanisms in different cancer types. According to Kumar et al. (2012), the ADAMTS5 thrombospondin type I-like repeat (TSR) domain can interact and downregulate VEGF expression, which inhibits tumour angiogenesis. However, research done by Huang et al. (2019) in gastric cancer cell lines indicates that the anti-angiogenesis effect of ADAMTS5 is not mediated by the VEGF signalling pathway, but through inhibiting ETS1, a transcription factor which contributes to neo-angiogenesis. Nevertheless, increased expression of ADAMTS5 was shown to improve cancer cell invasion and migration ability in other types of cancers, including glioblastomas (Held-Feindt et al., 2006), non-small cell lung cancer (Gu et al., 2016), and head and neck cancer (Demircan et al., 2009).

However, the detailed mechanism of how ADAMTS5 promotes migration and invasion in these types of cancer is still unclear. In breast cancer, ADAMTS5 promote cancer cell invasion via cleavage of fibulin-2, which can be suppressed by ADAMTS12 both in vitro and in vivo (Fontanil et al., 2017, Fontanil et al., 2014).

Remarkably, opposing roles of ADAMTS5 were reported in colorectal and hepatocellular carcinoma. On the one hand, the anti-angiogenic role of ADAMTS5 was observed in hepatocellular carcinoma, the downregulation of which resulted in poor patient prognosis (Li et al., 2015a). Similarly, the silencing of ADAMTS5 was shown to be related to a poor survival rate in colorectal cancer patients (Li et al., 2018). Hypermethylated ADAMTS5 promoter was identified in colorectal cancer cell lines, which increased the angiogenesis, cell invasion and migration (Li et al., 2018). On the other hand, upregulated ADAMTS5 expression was found in hepatocellular tumour samples compared to normal or adjacent peritumoral tissues (Zhu et al., 2021). Patients with high ADAMTS5 expression were shown to have a poorer overall survival rate. A higher expression level of ADAMTS5 was detected in colorectal cancer patients in stage III-IV than in 0-II. Since the patients with higher ADAMTS5 expression levels also had increased lymphatic invasion, ADAMTS5 is considered a potential marker for colorectal cancer cell lymphatic metastasis (Haraguchi et al., 2017).

In OC, significantly increased ADAMTS5 expression was detected in malignant tumours compared to borderline and benign tumours, which suggested a potential role of ADAMTS5 in OC metastasis (Lima et al., 2016). Furthermore, OC patients with higher ADAMTS5 expression showed reduced overall survival ([Figure 1.10. Data from \(Gyorffy et al., 2012\)](#)). However, the role of ADAMTS5 in OC progression are still unclear.

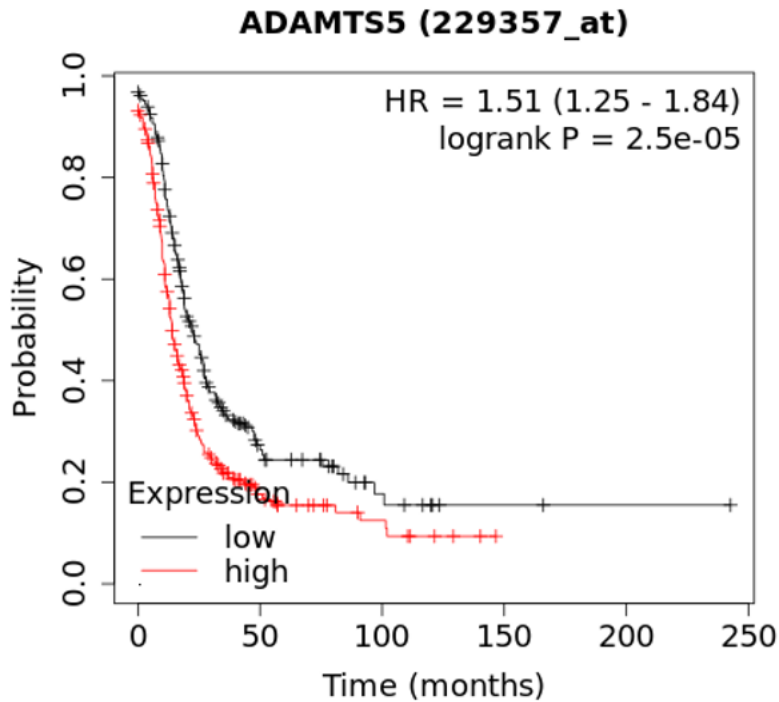


Figure 1.10. High ADAMTS5 expression correlated with poor prognosis in OC patients. Patients were stratified between high (red) and low (black) ADAMTS5 mRNA levels. Data from www.kmplot.com/ovar. This dataset was generated based on microarray data from 1287 ovarian cancer patients (Gyorffy et al., 2012).

As a substrate of ADAMTS5, altered expression of VCAN and its cleaved soluble fragment were also detected in cancers (Timms and Maurice, 2020, Papadas and Asimakopoulos, 2020). VCAN, or V1 in particular, can be cleaved at the Glu⁴⁴¹-Ala⁴⁴² site by ADAMTS1, 4, 5, 9, 15 and 20 (Table 1.3). Cleavage of VCAN generates a G1-DPEAAE fragment, known as versikine (Longpre et al., 2009). Research showed that upon TGF- β 2 stimulation, an increase of both VCAN and ADAMTSs cleaved versikine fragments was identified in glioma cancer cells. Furthermore, blocking the ADAMTS cleavage site of VCAN reduced the migration of glioma cancer cells, suggesting the potential role of versikine in glioma tumour progression (Arslan et al., 2007). Similar to ADAMTS5, which shows a dual function in cancer progression, the tumour-suppressive role of VCAN and versikine was also reported. In lung cancer, high versikine deposition (>100 μ g/mL) was found to suppress cancer cell migration, while a lower deposition (<50 μ g/mL) increased cell migration and invasion ability (Paris et al., 2006, Maingonnat et al., 2003). Similarly, ADAMTS15 was found to suppress prostate tumour progression through VCAN cleavage (Binder et al., 2020). Additionally, VCAN can also interact with cell surface receptors and alter cancer cell adhesion, proliferation and migration. For instance, VCAN can interact with β 1 integrin in glioma cells, which enhances glioma cell adhesion and inhibits apoptosis (Wu et al., 2002). VCAN can also interact with CD44 through its chondroitin sulphate

chains (Kawashima et al., 2000). Evidence shows that this interaction may stabilize HA-CD44 binding, trigger downstream c-Src signalling pathways, and further enhance cell migration (Bourguignon et al., 2001). In OC, a higher *VCAN* expression level was detected in malignant EOC tumours compared with benign and borderline tumours (Lima et al., 2016). Higher *VCAN* expression was also found associated with omentum metastasis in HGSOE (Pearce et al., 2018). Furthermore, *VCAN* was found to promote OC cell invasion and metastasis (Yeung et al., 2013, Ween et al., 2011), as described in [section 1.2.1.2](#). However, the role of versikine in ovarian cancer metastasis remains unclear.

1.4. Rab25 in cancer progression

1.4.1. Ras superfamily

Rab25 is a small Ras-GTPase (guanosine triphosphatases) that belongs to the RAS superfamily (Colicelli, 2004). The Ras superfamily contains over 170 related proteins and can be subclassified into five families, Ras, Rho, Rab, Arf and G α -family. These proteins mediate a wide range of biological processes in human cells and those belonging to distinct subfamilies have different roles. For example, Ras family members are known for regulating gene expression and cell proliferation through MAPK and PI3K signalling pathways. Members of the Rho family regulate cytoskeleton dynamics, which therefore mediate cell migration. The Arf and Rab families are widely involved in vesicle-associated processes such as endocytosis and cell surface receptor recycling (Bos et al., 2007). All family members share a common biological activity of binding GTP, which leads to a conformational change and the activation of the GTPase. Hydrolysis of GTP to GDP alternatively leads to the inactivation of the GTPase. Under normal conditions, the GTPases cycle between activation and inactivation, and the GDP/GTP exchanges are balanced by guanine nucleotide exchange factors (GEFs) and GTPase activating proteins (GAPs) ([Figure 1.11](#)) (Colicelli, 2004, Moore et al., 2020). GEFs mediate the GDP release and GTP exchange of inactivated RAS proteins, while GAPs induce GTP hydrolysis of activated RAS proteins. To ensure the specificity of signalling transductions, different types of GEFs and GAPs selectively mediate the activation of small Ras-GTPases from different subfamilies, as previously reviewed by Bos et al. (2007).

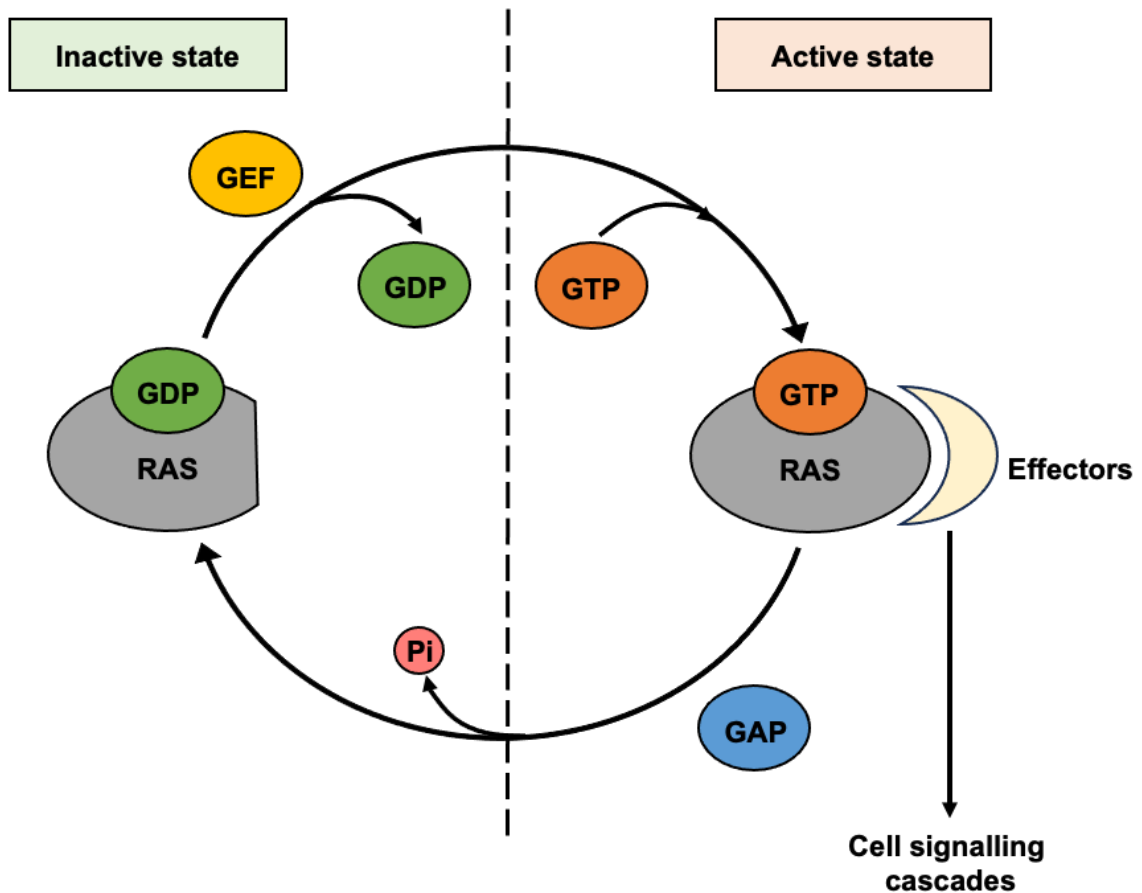


Figure 1.11. Schematic of Ras GTPase activation cycle. Ras proteins switch between inactivated GDP-bound form and activated GTP-bound form. GEFs regulate the dissociation of GDP and binding of GTP, which activates Ras proteins, while GAPs promote GTP hydrolysis, which inactivates Ras proteins. Activated Ras proteins can interact with multiple downstream effectors, which further activate several signalling cascades. Figure adapted from (Moore et al., 2020)

Rab proteins are Ras-related proteins that constitute the largest subfamily of the Ras superfamily, containing 71 members (Colicelli, 2004). The family members are distributed in different intracellular compartments. The detailed distribution and the role of Rab family proteins in cell membrane trafficking has been summarised by (Zerial and McBride, 2001). For example, integrin endocytosis and recycling are mediated by Rab proteins including Rab5, Rab4, Rab11 and Rab25, which has been previously described in [section 1.2.2.1](#) (Moreno-Layseca et al., 2019). Rab25 together with the two closest homologues (Rab11a and Rab11b) constitute the Rab11 family, which specifically mediates the transport and recycling of endosomes to the plasma membrane (Casanova et al., 1999). Additionally, Rab25 expression is restricted to epithelial cells (Wang et al., 2017).

1.4.2. Rab25 can function as both tumour promoter and suppressor.

Rab25 was identified as either a tumour suppressor gene or an oncogene in different cancers (Wang et al., 2017). Interestingly, a unique glutamine-to-leucine substitution was identified at the GTP-binding domain consensus sequence in Rab25, which is commonly observed in oncogenic mutants of Ras proteins and results in a constitutively activated and GTP-bound conformation (Agarwal et al., 2009). Overexpressed Rab25 was identified in liver cancer tissues (He et al., 2002), and high expression level was correlated with poor overall survival of prostate cancer patients (Hu et al., 2017). In breast, renal, gastric and prostate cancer, Rab25 expression correlated with tumour growth, metastasis, cancer cell migration and invasion (Cheng et al., 2004, Li et al., 2015b, Cao et al., 2013, Hu et al., 2017). Increased Rab25 expression was correlated with lymphatic metastasis in breast cancer patients (Yin et al., 2012). Rab25 was shown to promote EMT and enhance the invasiveness of breast cancer cells, which can be inhibited by micro-RNAs (miRNA) including miR-185 and miR-577 (Shahabi et al., 2021, Yin et al., 2018). In non-small-cell lung cancer, Rab25 KD reduced erlotinib resistance both in vitro and in vivo. Furthermore, Rab25 and integrin β 1 mediated the activation of AKT in non-small-cell lung cancer cells, which promoted cell proliferation through the Wnt/ β -catenin signalling pathway (Wang et al., 2019b).

Rab25 expression level in the tumour samples remains the same in OC patients at early stages (I and II) compared to normal samples, while a significantly increased Rab25 mRNA level was identified at the advanced stages (stage III and IV) (Cheng et al., 2004). High Rab25 expression was also found to be associated with poor overall survival of OC patients. Moreover, altered Rab25 expression was found to contribute to OC cell growth and metastasis (Cheng et al., 2004). OC cells overexpressing Rab25 showed better survival under stress, while decreased Rab25 levels led to reduced OC cell proliferation and increased apoptosis (Cheng et al., 2004, Liu et al., 2012). Rab25 was also found to promote OC cell migration and invasion. At the pseudopodia tip of OC cells, Rab25 vesicles were found to recycle the integrin α 5 β 1 from the late endosomes or lysosomes and deliver them to the plasma membrane, which promoted the pseudopodia extension, directional migration and 3D matrices invasion of OC cells (Caswell et al., 2007, Dozynkiewicz et al., 2012). In an in vivo model, OC cells stably transfected with Rab25 generated significantly larger tumours when injected into nude mice. Furthermore, metastatic colonies in the lung of nude mice injected with Rab25

overexpressing cells were larger and in a higher number (Jeong et al., 2018). This research indicates that Rab25 is contributing to the tumorigenesis of the OC. Additionally, Rab25 was found responsible for platinum-based chemotherapy resistance in OC, both in vitro (Fan et al., 2015) and in vivo (Gomez-Roman et al., 2015).

A tumour-suppressing role of Rab25 was observed in colon, head and neck and squamous cell carcinoma (Goldenring and Nam, 2011, Seven et al., 2015, Tong et al., 2012, Clausen et al., 2016), where Rab25 expression was shown to suppress metastasis and tumour cell invasiveness. In colon cancer, Rab25 was found to suppress EMT, migration and invasion of HCT-116 cells by inactivating the EGFR/Ras/Snail signalling pathway (Cho et al., 2024). The expression of junction protein claudin-7 was upregulated in Rab25 overexpressed HCT-116 cells, which is responsible for the downregulated EGFR and KRAS activation. In a mouse model, loss of Rab25 expression leads to increased formation of intestinal polyps and colonic tumours compared to the wild type (Nam et al., 2010). Rab25 promoter was found hypermethylated in esophageal squamous cell carcinoma tissue samples and cell lines, which resulted in the downregulation of Rab25 (Tong et al., 2012). Furthermore, the overexpression of Rab25 in an esophageal squamous cell carcinoma cell line (EC109-Rab25) resulted in significantly decreased migration and invasion ability. Conditioned media (CM) derived from EC109-Rab25 also suppressed the tube-forming ability of human umbilical vein endothelial cells (HUVEC), indicating the anti-angiogenesis role of Rab25 in esophageal squamous cell carcinoma. In vivo, tumours generated by Rab25 overexpressing cells are also significantly smaller than the ones generated by Rab25 deficient cells. Since the levels of phosphorylated FAK, c-Raf, MEK1/2 and ERK were significantly reduced in EC109 cells overexpressing Rab25, Rab25 may suppress tumour progression through inhibiting FAK/MAPK/ERK pathway, while the involvement of integrin in this process has not been investigated.

1.5. Aims and objectives

Currently, metastasis is the leading cause of OC patient death, due to late diagnosis and therapy resistance (Cho and Shih, 2009, Bhatla and Jones, 2018). Therefore, the identification of new diagnosis markers and therapeutic targets is critical to improving patient survival and prognosis in OC. Altered ECM composition and remodelling have been identified in OC stroma, which was found

to promote tumour progression and metastasis (Cho et al., 2015). Significantly increased expression of ADAMTS5 was previously observed in malignant OC tumour samples and was correlated with poor patient survival (Held-Feindt et al., 2006). Additionally, preliminary data from our lab showed that ADAMTS5 is required for OC cell migration in 3D matrices (data not shown). These results indicated that ADAMTS5 may play a critical role in promoting OC metastasis. Interestingly, previous research by the Norman's lab identified upregulated ADAMTS5 expression in OC cells overexpressing Rab25 (Dożynkiewicz, 2011). Therefore, the current study focused on elucidating the role of ADAMTS5 in OC cell invasion and how this protease is regulated by Rab25.

Here I hypothesise that overexpression of Rab25 in OC cells induces upregulation of ADAMTS5, which in turn promotes OC cell migration in the presence of ECM. The main aims of this project were to:

- Investigate the role of Rab25 in regulating ADAMTS5 expression in OC cell lines in the presence of ECM.
- Investigate the molecular mechanism through which Rab25 control ADAMTS5 expression.
- Characterise the role of ADAMTS5 in OC cell proliferation.
- Characterise the role of ADAMTS5 in Rab25-dependent OC cell migration and invasion in 3D systems.

Chapter 2 – Materials and Methods

2.1. Materials

2.1.1. Reagents and suppliers

Table 2.1 Reagents and suppliers

Reagents	Supplier
0.22µm syringe filter	Gilson
0.45µm syringe filter	Gilson
10cm petri dishes	Greiner bio-one
12-well tissue culture plates	Greiner bio-one
15mm glass-bottom dishes	NEST
35mm glass-bottom dishes	Ibidi
5X siRNA buffer	Horizon Discovery by Perkin Elmer
6-well tissue culture plates	Greiner bio-one
96-well glass-bottom plates	Greiner bio-one
96-well plastic bottom plates	FALCON
Alexa Fluor™ 555 Phalloidin	Invitrogen
Alexa Fluor™ 647 Phalloidin	Invitrogen
Ambion™ Nuclease-Free Water	Invitrogen
Amicon Ultra® - 4 Centrifugal filters 10k	Milipore
Ammonium hydroxide (NH ₄ OH)	Sigma
Cell tracker™ Red CMTPX	Invitrogen
Click-iT™ EdU Alexa Fluor™ 555 Imaging Kit	Invitrogen
Collagen type I	Ibidi
Color Prestained Protein Standard Broad Range	BioLabs
DharmaFect 1 Reagent	Dharmacon
Deoxyribonuclease I /DN25 (DNase I)	Sigma

Dimethyl sulfoxide (DMSO)	Fisher Scientific
DRAQ5™	Rocher
Dulbecco's Modified Eagle Medium (DMEM), high glucose, pyruvate	Gibco
Fibronectin bovine plasma	Sigma-Aldrich
Foetal bovine serum (FBS)	Gilson
Gelatin	Sigma
Geltrex™ Reduced Growth Factor Basement Membrane Matrix without phenol red	Gibco
Glutaraldehyde solution	Sigma Aldrich
Glycine	Sigma
High-Capacity cDNA Reverse Transcription Kit	Appliedbiosystems
Hoechst 33342	Invitrogen
Human Plasma-Like Medium (HPLM)	Gibco
Invitrogen™ Lipofectamine™ 2000 Transfection Reagent	Thermofisher
L-ascorbic acid	Sigma
Lipofectamine® 2000 Transfection Kit	Invitrogen
Magnesium chloride	Sigma-Aldrich
Methylcellulose	Sigma
Microplate PCR 384 well	Alphalaboratories
NHS-fluorescein	Thermofisher
Penicillin/streptomycin (Pen/Strep)	Gibco
Phosphate buffer saline, containing calcium and magnesium (PBS++)	Gibco and Sigma
PVDF membrane	IMMOBILON-FL
QiaShredder	QIAGEN
qPCRBIO SyGreen Blue Mix Lo-ROX	PCRBIO SYSTEMS
QuantiNova® SYBR® Green PCR Kit	QIAGEN
Rnase-free water	Cleaver scientific and Horizon Discovery

RNeasy Mini Kit (50)	QIAGEN
RPMI-1640, L-Glutamine	Gibco
Sodium chloride	Sigma-Aldrich
Sodium deoxycholate	Sigma-Aldrich
Soluble collagen I	Bio Engineering
T75 flask	Thermofisher
Tris(hydroxymethyl)aminomethane (Tris)	Sigma-Aldrich
Triton X-100	Sigma
Trypan Blue stain 0.4%	Gibco by life technologies
Tween-20	Sigma
VECTASHIELD Antifade Mounting Medium with DAPI	VECTOR laboratories

2.1.2. Solutions

Table 2.2 Recipes of solutions

Solutions	Recipes
Triton extraction buffer	20mM NH ₄ OH, 0.5% (v/v) Triton X-100 in PBS with Ca ²⁺ and Mg ²⁺
PLA2 extraction buffer	50mM Tris-HCl pH 8, 150mM NaCl, 1mM MgCl ₂ , 1mM CaCl ₂ , 0.5% sodium deoxycholate and 20 unit/ml PLA2 in dH ₂ O
SDS lysis buffer	50mM Tris pH7 and 1% SDS in dH ₂ O
EdU staining	1x Click-iT, 4mM CuSO ₄ , 0.25% (v/v) Alexa Flour azide and 1x Reaction buffer additive in dH ₂ O
Loading buffer	Protein sample, 1mM DTT, 1x NuPAGE
Running buffer	25mM Tris, 192mM Glycine and 1% SDS in dH ₂ O
1xTBST	10mM Tris-HCl pH7.4, 150mM NaCl, 0.1% (v/v) Tween-20 in dH ₂ O
Towbin transfer buffer	25mM Tris, 192mM glycine and 20% methanol (v/v) in dH ₂ O, pH 8.3
cDNA synthesis mix	mRNA sample, 1xRT buffer, 1xdNTP Mix, 1xRT Random Primers and 0.5% (v/v) Multiscribe Reverse Transcriptase in nuclease-free water
SYBR Green RT-qPCR mix	cDNA template sample, 1xSYBR Green PCR Master Mix and 1x QuantiTect Primer Assay in nuclease-free water

2.2. Methods

2.2.1. Cell culture

The ovarian cancer cell lines A2780, OVCAR3, and omental cancer-associated fibroblast (CAFs) were cultured in RPMI-1640 medium supplemented with 10% (v/v) foetal bovine serum (FBS) and 1% (v/v) penicillin/streptomycin (Pen/Strep), which is referred to as RPMI-1640 complete medium hereafter. The A2780 cells expressing empty pc3 vector (A2780-DNA3) or overexpressing Rab25 (A2780-Rab25) were a gift from Prof Jim Norman's lab (Cancer Research UK Scotland Institute), the OVCAR3 cells from Prof Patrick Caswell's lab (The University of Manchester) and the hTERT immortalized omental CAFs from Prof Sara Zanivan's lab (Cancer Research UK Scotland Institute, Glasgow). The ovarian cancer cell line SKOV3 and telomerase-immortalised human dermal fibroblasts (TIFs) were cultured in high glucose Dulbecco's modified Eagle medium (DMEM) supplemented with 10% (v/v) FBS and 1% (v/v) Pen/Strep. All cell lines were maintained at 37°C in 5% CO₂ and split when 90% confluent. To split the cells, after the media was removed, the cells were washed once with phosphate buffer saline (PBS), and then incubated with 0.25% (w/v) trypsin-EDTA for up to 5 minutes at 37°C in 5% CO₂. Detached cells were then transferred into new 10cm tissue culture dishes with complete medium.

For long term storage, all cell lines were frozen down and cryopreserved. When the cells reached 80-90% confluency in a 10cm dish, the cells were trypsinised and resuspended in complete media. Then, the cell solution was centrifuged at 1000rpm for 5 minutes. After removing the supernatant, the cell pellets were resuspended in 500µL of a solution containing 50% normal media and 50% FBS and transferred into a cryo-vial. 500µL of a solution containing 80% FBS and 20% DMSO was further added drop by drop, and the solution was mixed gently. The vials were first kept in Biocision™ CoolCell™ LX freezing container at -80°C for a few days and then stored in liquid nitrogen. To recover the cells from cryopreservation, the cryo-vial was defrosted in the water bath. For cancer cell lines and TIFs, the cell suspension was transferred into a 10cm culture dish with complete media directly. For CAFs, the cell suspension was mixed with complete media, centrifuged at 1000rpm for 5 minutes, and the cell pellet was resuspended in 10mL complete media and transferred into a 10cm tissue culture dish.

2.2.2. Plasmid transfection and maintenance

A2780-DNA3 and Rab25 cells were generated in Dr Gordon Mill's lab, as described in (Cheng et al., 2004) To maintain the overexpression of Rab25, both cell lines were treated with 0.4mg/mL G418 for a week every 10 passages.

To generate stable OVCAR3 cells expressing nuclear GFP, 5×10^5 cell/well was seeded in a 6-well plate one day before transfection and cultured in 2mL complete medium without Pen/Strep. 2.5µg of the pCAG-H2B-GFP plasmid (Addgene #184777) and 5µL of Invitrogen™ Lipofectamine™ 2000 Transfection Reagent were suspended in 250µL Opti-MEM media respectively and incubated at room temperature (RT) for 5 minutes. Then the solutions were mixed and incubated at RT for 20 min. The 500µL solution was then added on top of the OVCAR3 cells and incubated at 37°C and 5% CO₂ for 6 hours. After that, the cells were washed twice with PBS and cultured with complete media without Pen/Strep overnight. Following 72 hours, the cell was selected with 50ng/mL Puromycin (1mg/mL stock concentration). To maintain the expression of GFP, the cells were cultured with complete media containing 25ng/mL Puromycin for 3 days every 2 passages.

2.2.3. Cell-derived matrix generation

The process of generating cell-derived matrices (CDMs) was previously described by (Kaukonen et al., 2016) and summarised in [Figure 2.1](#). The CDMs were generated in 10cm dishes, 6-well, 12-well and 96-well plates. The plates or dishes were firstly coated with 0.2% (v/v) gelatin in PBS for 1 hour at 37°C, followed by two washes with PBS. Then the plates were crosslinked by 1% (v/v) sterile glutaraldehyde in PBS for 30 minutes at RT, followed by two washes with PBS. After that, the glutaraldehyde was quenched with 1M sterile glycine in dH₂O for 20 minutes at RT, followed by two washes with PBS. Complete medium was thereafter used for equilibration for 30 minutes at 37°C. TIFs and CAFs were then seeded on top of the coated plates according to [Table 2.3](#). After an overnight incubation at 37°C in 5% CO₂, the media was changed to complete media containing 50µg/mL ascorbic acid and was refreshed every other day.

TIFs were kept in DMEM complete media with ascorbic acid for 9 days to secrete CDM. After then, the cells were washed once with PBS containing Ca²⁺ and Mg²⁺ (PBS⁺⁺) and then treated with triton

extraction buffer (20mM NH₄OH and 0.5% (v/v) Triton X-100 in PBS⁺⁺) at RT for up to 5 minutes until all cells were removed. After two PBS⁺⁺ washes, 10µg/mL DNase I in PBS⁺⁺ was added on top of extracted CDM and incubated at 37°C for 1 hour. The CDM was then washed twice with PBS⁺⁺, stored at 4°C in PBS⁺⁺ and used within a month.

CAFs were kept in Human Plasma-Like Medium (HPLM, Gibco) with ascorbic acid for 11 days since the CAFs secrete less ECM compared to TIFs. Then, the cells were washed once with PBS⁺⁺ and then treated with PLA2 extraction buffer (50mM Tris-HCl pH 8, 150mM NaCl, 1mM MgCl₂, 1mM CaCl₂, 0.5% sodium deoxycholate and 20 unit/ml PLA2) at 37°C for 1 hour. After two washes with PBS⁺⁺, 10µg/mL DNase I in PBS⁺⁺ was added on top of extracted CDM and incubated under 37°C overnight. The CDM was then washed twice with PBS⁺⁺ and stored at 4°C in PBS⁺⁺ and was used within two weeks. Since the CAF-CDM is less stable compared to TIF-CDM, PLA2 as a gentler extraction buffer was used.

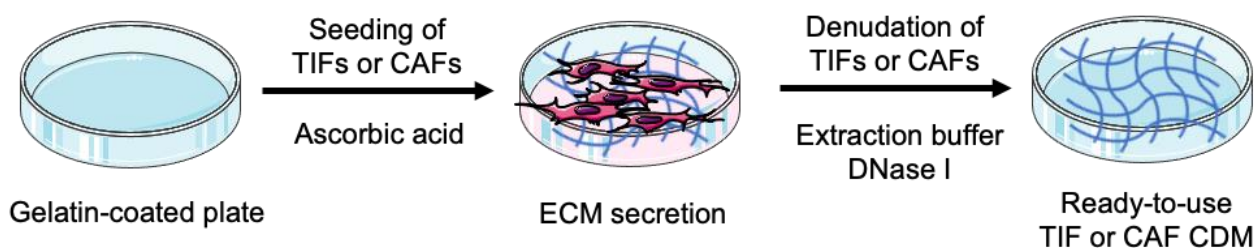


Figure 2.1. Generation of TIF and CAF CDMs. TIFs or CAFs were seeded on top of gelatin-coated plates/dishes to secrete ECM in the culture media supplemented with 50µg/mL ascorbic acid for 9 to 11 days. The CDMs were then denudated with extraction buffer and treated with DNase I, and the ready-to-use CDMs were stored at 4°C in PBS⁺⁺.

Table 2.3 Cell seeding numbers and solution volume for TIF and CAF-CDM generation.

TIF-CDM		
Plate/Dish type	Cell seeding numbers	Solution volume
6-well plate	4x10 ⁵ cells/well	2mL
12-well plate	2.5x10 ⁵ cells/well	1mL
96-well plate	6x10 ³ cells/well	100µL
10cm dishes	3x10 ⁶ cells/well	5mL

CAF-CDM		
Plate/Dish type	Cell seeding numbers	Solution volume
6-well plate	6×10^5 cells/well	2mL

2.2.4. Conditioned media harvest

5×10^5 A2780-DNA3 and Rab25 cells/well were seeded in 6 well plates or 3×10^6 cells in 10cm tissue culture dishes and cultured at 37°C in 5% CO₂ for 72 hours. Then, the culture media, hereafter referred to as CM, was transferred into falcon tubes and subjected to a 3-step centrifugation protocol at 4°C. The CM was spun at 300g for 10 minutes, 2,000g for 10 minutes, and 10,000g for 30 minutes (Gupta et al., 2012). The supernatant was transferred into new falcon tubes and stored at 4°C up to a week. These CMs were used for the cell migration experiments (see section 2.2.9.2)

To analyse CM proteins by western blotting, 5×10^5 A2780-DNA3 and Rab25 cells were seeded and cultured at 37°C in 5% CO₂ for 4 hours, followed by two PBS washes. As the serum will disrupt the concentrating process and result in background on the blot, the culture media was changed into serum-free media after the cells attached. The cells were cultured for 3 Days. After the 3-step centrifugation protocol described above, the CM was further concentrated using Amicon Ultra® - 4 Centrifugal filters (3,000 or 10,000 MWCO PES). The filter tube was centrifuged at 4,000g until the CM in the top tube reaches target volume.

2.2.5. Western blotting

A2780-DNA3, Rab25, OVCAR3, OVCAR4 and SKOV3 cells were seeded in 6-well plates for western blotting. The seeding number was altered based on the culture time before the sample harvesting. For 24 hours culture, 5×10^5 cells per/well were seeded. For 72 hours culture, 2×10^5 per/well were seeded. For cells seeded on plastic, the cells were washed twice with ice cold PBS and 100µL of the SDS-lysis buffer (50mM Tris PH7, 1% SDS in dH₂O) was added on top. For cells seeded on TIF-CDM, the cells lysate was harvested with Triton extraction buffer (see section 2.2.3). The cell lysate was then spun down through QiaShredder columns at full speed for 5 min. For all protein samples, 4x

NuPAGE buffer containing 1mM DTT was mixed with the samples and boiled at 70°C for 5 minutes. 20 to 25µL of the samples and 1µL of the protein ladder (BioLabs) were loaded into a Bio-Red 4-15% Mini-PROTEAN precast polyacrylamide gel and run at 100V for 75 minutes in 1x running buffer (25mM Tris, 192mM glycine and 1% SDS in dH₂O), followed by transfer into a FL-PVDF membrane at 100V for 75 minutes in Towbin transfer buffer (25mM Tris, 192mM glycine and 20% methanol (v/v) in dH₂O, pH 8.3). The membranes were then blocked with 5% (w/v) Skimmed milk in 1xTBST (50mM Tris HCl, 150mM NaCl and 0.5% (w/v) Tween 20 in dH₂O) for 1 hour at RT. After that, the membranes were incubated overnight with target primary antibody (Table 2.4) together with GAPDH (1:1000 diluted in 5% (w/v) bovine serum albumin (BSA) in 1xTBST) as housekeeping gene at 4°C. After three washes for 10 minutes in TBST, the membranes were incubated for 1 hour at RT with secondary anti-mouse IgG LICOR IR Dye 800 (1:30,000) and anti-rabbit IgG LICOR IR Dye 680 (1:20,000) in TBST containing 0.01% (w/v) SDS, followed by another three washes with TBST and one in dH₂O. The Membranes were then imaged in a LICOR Odyssey Sa system. Image Studio Lite software was used to acquire and quantify the intensity of the protein bands. Intensity of the target protein was normalized to GAPDH, and the results from different biological replicates were then normalized to the control groups.

Table 2.4 Western blotting antibody list.

Primary antibodies	Supplier	Dilution
ADAMTS5	abcam (ab41037)	1:250
Rab25	Proteintech (13189-1-AP)	1:600
AKT	Cell Signalling (#4691)	1:1,000
p-AKT (Ser473)	Cell Signalling (#4075)	1:1,000
GAPDH	Santa Cruz Biotechnology (SC-47724)	1:1,000
Secondary antibodies		
Secondary antibodies	Supplier	Dilution ration
IR Dye 680LT anti-Rabbit antibody	LICOR Biosciences	1:20,000
IR Dye 800LT anti-Mouse antibody	LICOR Biosciences	1:30,000

2.2.6. RT-qPCR

2.2.6.1. mRNA extraction

5x10⁵ A2780-DNA3, Rab25, OVCAR3 and SKOV3 cells were seeded in 6-plates and cultured overnight. For cells seeded on plastic, the cells were trypsinized, collected in a falcon tube and spun down at full speed for 5 min. For cells seeded on CDM, cells were incubated with 400µL complete media containing Collagenase (0.25mg/mL) and Hyaluronidase (0.05mg/mL) at 37°C for 1 hour, and the cell suspension were then spun down at full speed for 5 min. After one wash with PBS, the cell pellets were snap-frozen in dry ice and stored at -80°C. mRNA was extracted from the cell pellets using RNeasy® Mini kit (Qiagen) following the manufacturer's protocol. Briefly, the cell pellets were lysed by 350µL Buffer RLT containing 1% (v/v) β-mercaptoethanol and spun down through QiaShredder columns at full speed for 2 min. Then, 350µL of 70% ethanol was added to the flowthrough and transferred to RNeasy spin columns, which were centrifuged at 8,000g for 30 sec. The flowthrough was discarded, and the columns were further washed once with 700µL Buffer RW1 and twice with 500µL Buffer RPE. Finally, the mRNA sample was eluted with 30µL RNase-free water.

2.2.6.2. cDNA synthesis

cDNA was synthesized using High-Capacity cDNA Reverse Transcription Kit (Fisher). Briefly, mRNA solution concentration was measured by Nanodrop LITE Spectrophotometer (Thermo Scientific) and 1µg of mRNA per sample was used to synthesise cDNA. A 20µL solution containing 1x RT buffer, 1x dNTP mix, 1x RT Random Primers and 1µL of MultiScribe Reverse Transcriptase and mRNA was placed in a 0.2mL PCR tube. The -RT control was prepped with the mRNA sample with the highest concentration. Instead of MultiScribe Reverse Transcriptase, 1µL of RNase-free water was added into the -RT control. The samples were run on a thermocycler followed by the settings in [Table 2.5](#). The synthesized cDNA samples were stored at -80°C.

Table 2.5 Time and temperature for cDNA synthesis

	Step 1	Step 2	Step 3	Step 4
Temperature (°C)	25	37	85	4
Time (min)	10	120	5	∞

2.2.6.3. qPCR

For qPCR loading, master mix containing 1x QuantiNova SYBR® Green PCR Kit (Qiagen) master mix and 1x QuantiTect® Primer Assay for target genes (Table 2.6) was prepped in RNase-free water. 7µL of loading master mix together with 3µL of diluted cDNA solution (1:100 dilution, 5ng/µL final conc.) were loaded into a 384-well plate. For each experiment, the -RT and blank water controls were tested for all target genes. Quantstudio 12K flex real-time PCR system was used to analyse the samples. The machine was set as shown in Table 2.7 and ran for 40 cycles. The melting curve was generated after the cycles to verify the purity of amplified genes. Expression levels of the target genes were calculated using $2^{-\Delta\Delta Ct}$ method ($2^{-(\Delta Ct_{\text{Target gene}} - \Delta Ct_{\text{Housekeeping gene}})}$) with GAPDH as the housekeeping gene. Three technical replicates were tested for each sample and the results from different biological replicates were normalised to the control groups.

Table 2.6 qPCR Primer list.

Primer	Assay name	Stock concentration
ADAMTS5	Hs_ADAMTS5_1_SG	10x
Rab25	Hs_RAB25_1_SG	10x
GAPDH	Hs_GAPDH_1_SG	10x

Table 2.7 Time and temperature for qPCR.

	Hold Stage	PCR Stage		Melt Curve Stage		
Temperature (°C)	95	95	60	95	60	95
Time (min:sec)	2:00	00:10	00:30	00:15	1:00	00:15

2.2.7. siRNA transfection

ADAMTS5 (L-005775-00-0005) and Rab25 (L-010366-00-0005) ON-TARGETplus SMARTpool siRNAs (Dharmacon, Horizon discovery) were resuspended in RNase-free 1x siRNA Buffer to obtain a 20µM final concentration. 5×10^5 A2780 and OVCAR3 cells per well were seeded in 6-well plates. After overnight culture at 37°C, cells reached 70-80% confluency. For each well, 2µL Dharmafect I was mixed with 198µL FBS free medium and incubated for 5 minutes at RT. Then, 2.5µL siRNA (20µM)

and 197.5µL FBS free medium were added to the Dharmafect solution and incubated for 20 min at RT. After that, the cells were washed twice with PBS and the 400µL solution was placed on top of the cells and topped up to 2mL with complete medium without antibiotic. After a 24 h incubation, the cells were washed twice with PBS and 2mL complete medium without antibiotic was added to culture the cells. siGENOME non-targeting control siRNA #4 was used as a non-targeting control. To assess the knockdown efficiency, western blot and RT-qPCR were performed as described in [section 2.2.5 and 2.2.6](#).

2.2.8. Cell proliferation assay

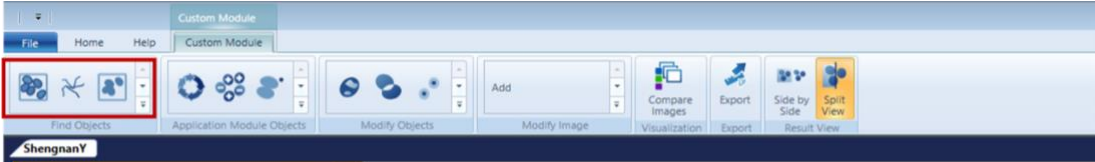
2.2.8.1. Cell proliferation assay with ADAMTS5 inhibitor

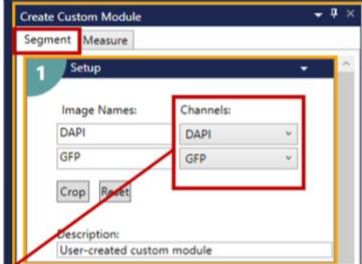
Matrigel was diluted in ice-cold PBS to obtain a 3mg/mL solution and 15µL/well of a 96 well plate were spread to fully cover the wells. After polymerisation at 37°C for 4 hours, PBS was added on top of the matrigel. The plates were kept at 37°C overnight and used the following day. For TIF-CDM generation, see [section 2.2.3](#). 600 A2780-DNA3 and Rab25 cells were seeded on plastic, 3mg/mL matrigel or TIF-CDM in 96-well plates. After a 4 h incubation to allow cell attachment, cells were washed twice with PBS and complete or starvation (5mM glucose, 1mM glutamine or 5% FBS) culture media containing DMSO or 5µM of ADAMTS5 inhibitor was added. For each condition, three wells were seeded as technical replicates. Three plates were prepped for each experiment and fixed at day 2, day 4 and day 6 with 40µL 4% (w/v) paraformaldehyde (PFA) for 15 min at RT. Cells seeded on plastic and matrigel were stained with DRAQ5 (Rocher, 1:1000 in PBS) for 1 hour at RT, followed by two washes with PBS. The plates were left in the last wash on a rocker for an extra 30 min to minimise the background signal. 140µL/well PBS was added, the plates were imaged with a LICOR Odyssey Sa system (700nm channel) and the intensity for each well was measured with Image Studio Lite software.

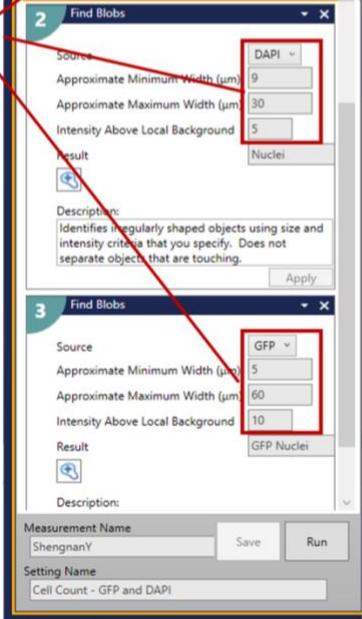
To reduce the background noise and increase the accuracy of cell counting, cells seeded on CDM were stained with Hoechst 33342 (1:1000) during PFA fixation, followed by two PBS washes. The plates were left in the last wash on a rocker for extra 30 min, and 140µL PBS was added at the end. The cells were imaged by ImageXpress microscope with 2x objective DAPI channel and further counted by MetaXpress and Costum Module Editor (CME) software ([Figure 2.2](#)).

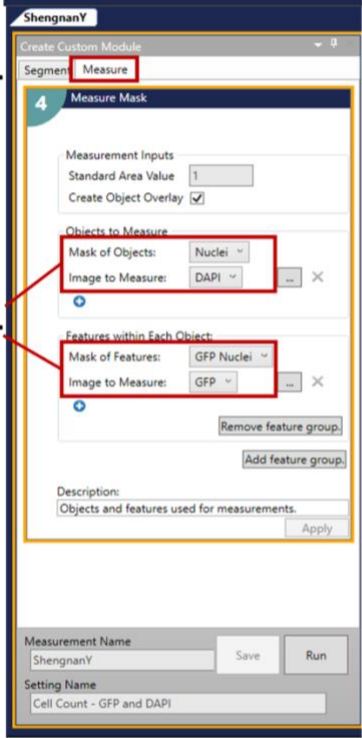
2.2.8.2. Co-culture cell proliferation assay

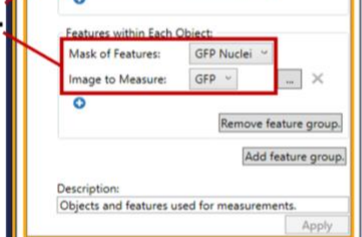
4,000 GFP-OVCAR3 and 2,000 CAF cells/well were seeded in 96-well plates for CAF-OVCAR3 co-culture proliferation assay. Meanwhile, 6,000 GFP-OVCAR3 or CAF cells/well were seeded as a monoculture. For the TIF-OVCAR3 co-culture proliferation assay, 3,000 GFP-OVCAR3 and 1,500 TIF cells/well were seeded in 96-well plates, since TIFs proliferate faster than CAFs. 4,500 GFP-OVCAR3 or TIF cells/well were seeded as a monoculture. After a 24h incubation, cells were washed twice with PBS and complete culture media containing DMSO, 5 or 10 μ M of ADAMTS5 inhibitor was added. Two plates were prepped for each experiment and stained with Hoechst 33342 (1:2000 in media) for 15 minutes at 37°C on day4 and day8. After two PBS washes, the cells were left in PBS and imaged live by an ImageXpress microscope (10x objective) in both DAPI and GFP channels. OVCAR3 cells show both DAPI and GFP fluorescence while CAF cells show only DAPI fluorescence. Images were analysed by CME software ([Figure 2.2](#)).

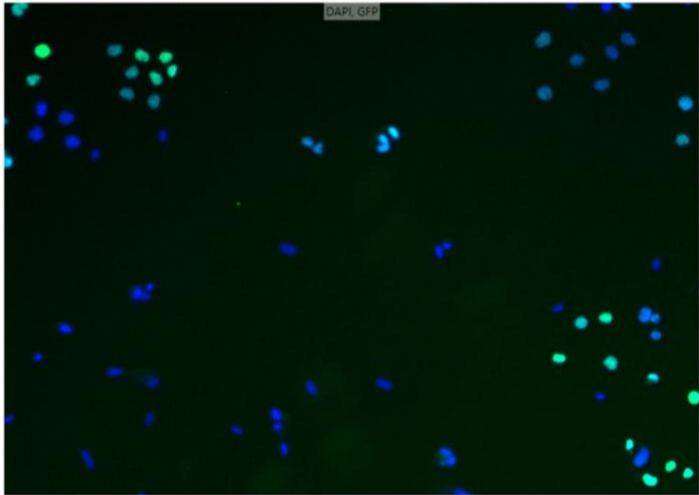
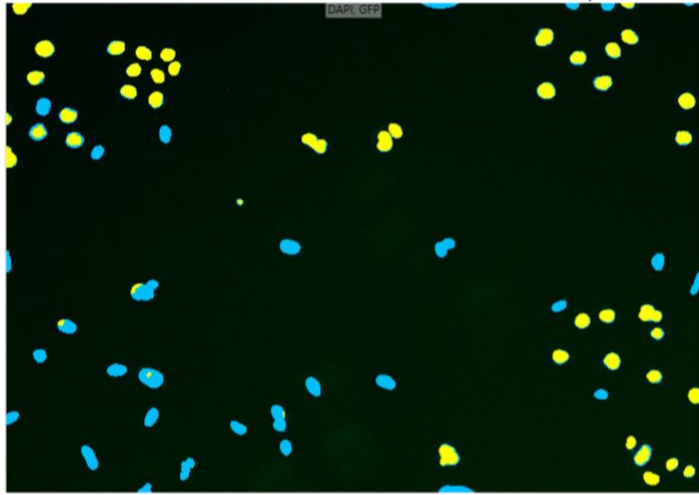
1. 

2. 



3. 

4. 

5. 

Mask Legend

Layer	Color	Mask Name
1		Nuclei
2		GFP Nuclei

Data Table

Row ID	ObjectID	Cell count-Nuclei	GFP Nuc
1	1	1	1
2	2	1	0
3	3	1	0
4	4	1	0
5	5	1	1
6	6	1	0
7	7	1	1
8	8	1	1
9	9	1	1
10	10	1	1
11	11	1	1
12	12	1	1

Figure 2.2. Cell proliferation analysis by CME software in MetaXpress. To automatically count the number of cells with DAPI and/or GFP fluorescence, analysis was performed with CME software as follows. Find object tool was selected (1.) to detect the cells. For both DAPI and GFP signal, “Find Blobs” option was selected. In the segment option (2.), target channels were selected (3.), and the parameters were defined to obtain the best mask result of the signal. 4. To measure the count of the nuclei and GFP nuclei, 5. The “Main objective” and the “Mask of Features” were defined separately. By applying this measurement to each mask identified, the number of objects was summarized.

2.2.9. Random cell migration assay on CDM

2.2.9.1. Cell migration with small molecule inhibitors

TIF-CDM was generated in 12-well plates as described in [section 2.2.3](#). 5×10^4 A2780 cells/well were seeded and cultured at 37°C in 5% CO₂. After a 4h incubation, DMSO control or 5µM ADAMTS5 inhibitor were added into the culture media.

Cells were imaged live with a Nikon widefield live-cell system (Nikon Ti eclipse with Oko-lab environmental control chamber) with a Plan Apo 10X objective (NA 0.75). For each well, 5 positions were randomly selected for imaging. Images were acquired every 10 minutes for 16 hours (97 images in total were obtained for each position). Cell migration was manually tracked using Fiji ImageJ plugin Manual Tracking (Schindelin et al., 2012, Cordelières, 2005), and the velocity and directionality of the migrating cells were calculated with the chemotaxis tool plugin in Fiji Image J (<https://ibidi.com/chemotaxis-analysis/171-chemotaxis-and-migration-tool.html>). The distance between nuclei and the tip of the pseudopod in the direction of cell migration, defined as pseudopod extension length, was measured in ImageJ with the “Straight” tool.

2.2.9.2. Cell migration with conditioned media

CM derived from A2780-DNA3 or Rab25 cells were harvested as described in [section 2.2.4](#). 5×10^4 A2780-DNA3 cells were seeded on TIF-CDM-coated 12-well plates in complete medium mixed with CM (1:1). Where indicated, the inhibitors were added after 4 hours after seeding the cells. Cells were imaged and analysed as described above (see [section 2.2.9.1](#)).

2.2.10. 3D spheroid invasion assay

2.2.10.1. A2780-Rab25 spheroid invasion assay with ADAMTS5 inhibitor

Spheroids were generated using the hanging drop method as previously described by Bayarmagnai et al. (2019) [Figure 2.3](#). Briefly, 5×10^5 A2780-Rab25 cells were seeded in 6-well plate for 24 hours and labelled with Cell trackerTM Red CMTPX (1:3000 in FBS-free media) at 37°C for 1 hour. Afterwards, 1×10^5 of labelled cells were suspended in 2mL of complete culture medium containing 20µg/mL soluble collagen I (BioEngineering) and 4.8mg/mL Methyl Cellulose (MTC, Sigma-Aldrich). 20µL drops of this cell solution (containing 1×10^3 A2780-Rab25 cells) were then added to the lid of 10cm tissue culture dishes. The lid was then flipped, so that the cell suspension is hanged to form spheroids. 8mL of PBS was added to the culture dishes to prevent evaporation. After 48 hours of incubation at 37°C, spheroids were gently washed off from the lid with 800µL of ice-cold complete media and washed twice with 800µL of ice-cold complete media. Individual spheroids were then embedded into 45µL of ECM mixtures containing 3mg/mL collagen I (Ibidi), 3mg/mL Geltrex (Gibco) and 25µg/mL Fibronectin (Sigma-Aldrich) and placed on a 35mm glass bottom dish, with each dish containing three spheroids as technical replicates. To keep the spheroid in the middle of the ECM during matrix polymerisation, the dishes were first incubated at 37°C upright for 2 minutes, flipped upside down and incubated for another 2 minutes. After 5 up and down flips (10 minutes in total), the dishes were kept upside down and cultured at 37°C for another 20 to 25 minutes until the matrices polymerised. Then, 1.5mL of complete media containing DMSO, 5 or 10µM ADAMTS5 inhibitor was added to the dishes drop by drop. A2780-Rab25 spheroids were imaged live with Nikon A1 confocal microscope, CFI Plan Fluor 10x objective (NA 0.3) at day 0, day 1 and day 2. Cell invasion was quantified with Fiji Image J ([Figure 2.4](#)). Images were thresholded, and the areas of the spheroid cores and the total area were measured. The invasion area was then calculated by total area - core area, and the invasion area was normalized to the core area. Results from different biological replicates were normalised to the DMSO control groups at 24h.

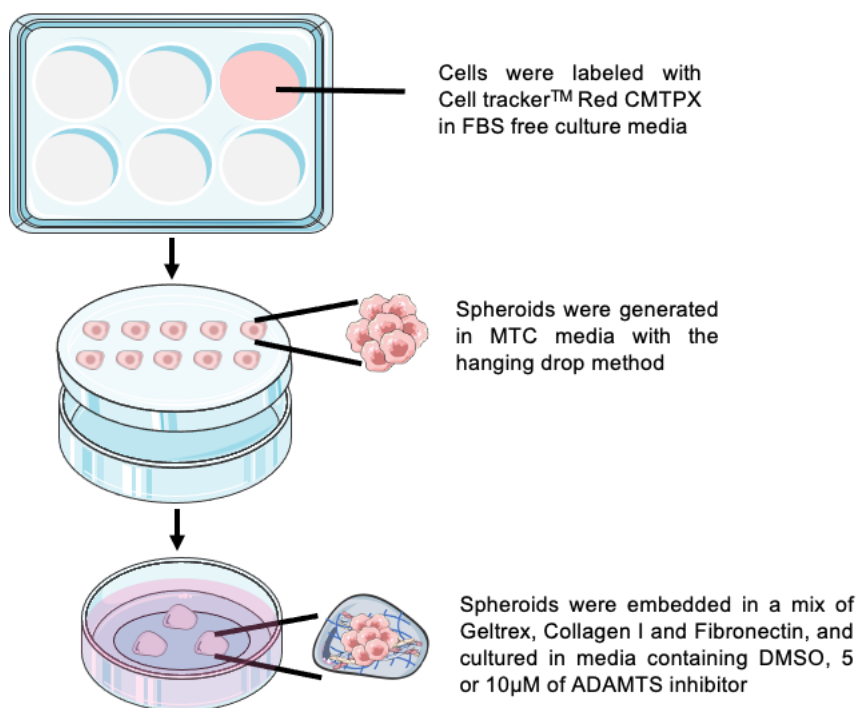


Figure 2.3. Generation of spheroids. Cells were labelled with Cell tracker™ Red and suspended in media containing 4.8mg/mL MTC and 20µg/mL soluble collagen I. Spheroids were generated with the hanging drop method on the lid of a 10 cm dish. The spheroids were then embedded in ECM mixtures containing Geltrex, Collagen I and Fibronectin, and incubated with culture media containing DMSO, 5 or 10µM of ADAMTS5 inhibitor.

2.2.10.2. Co-culture 3D spheroid invasion assay with ADAMTS5 inhibitor

To generate OVCAR3-GFP and CAF/TIF co-culture spheroids, 5×10^5 CAF/TIF cells were seeded in 6-well plates for 24 hours and then labelled with Cell tracker™ Red CMTPIX for 1 hour. 1.4×10^5 of OVCAR3-GFP and 0.7×10^5 of CAF/TIF cells were suspended in 2mL culture medium containing 20µg/mL soluble collagen and 4.8mg/mL MTC and spheroids with 2.1×10^3 cells in total were generated as described above. After a 24h incubation, the co-culture spheroids were harvested and embedded as above (section 2.2.10.1). 1.5mL of complete media containing DMSO, 5 or 10µM ADAMTS5 inhibitor was added to the dishes. Co-culture spheroids were imaged on day 0, day 4, day 6 and day 8 after embedding. Fresh media with inhibitor was replaced on day 4. The invasion of both OVCAR3 and CAF/TIF was quantified (Figure 2.4). Results from different biological replicates were normalised to the DMSO control groups on day 2.

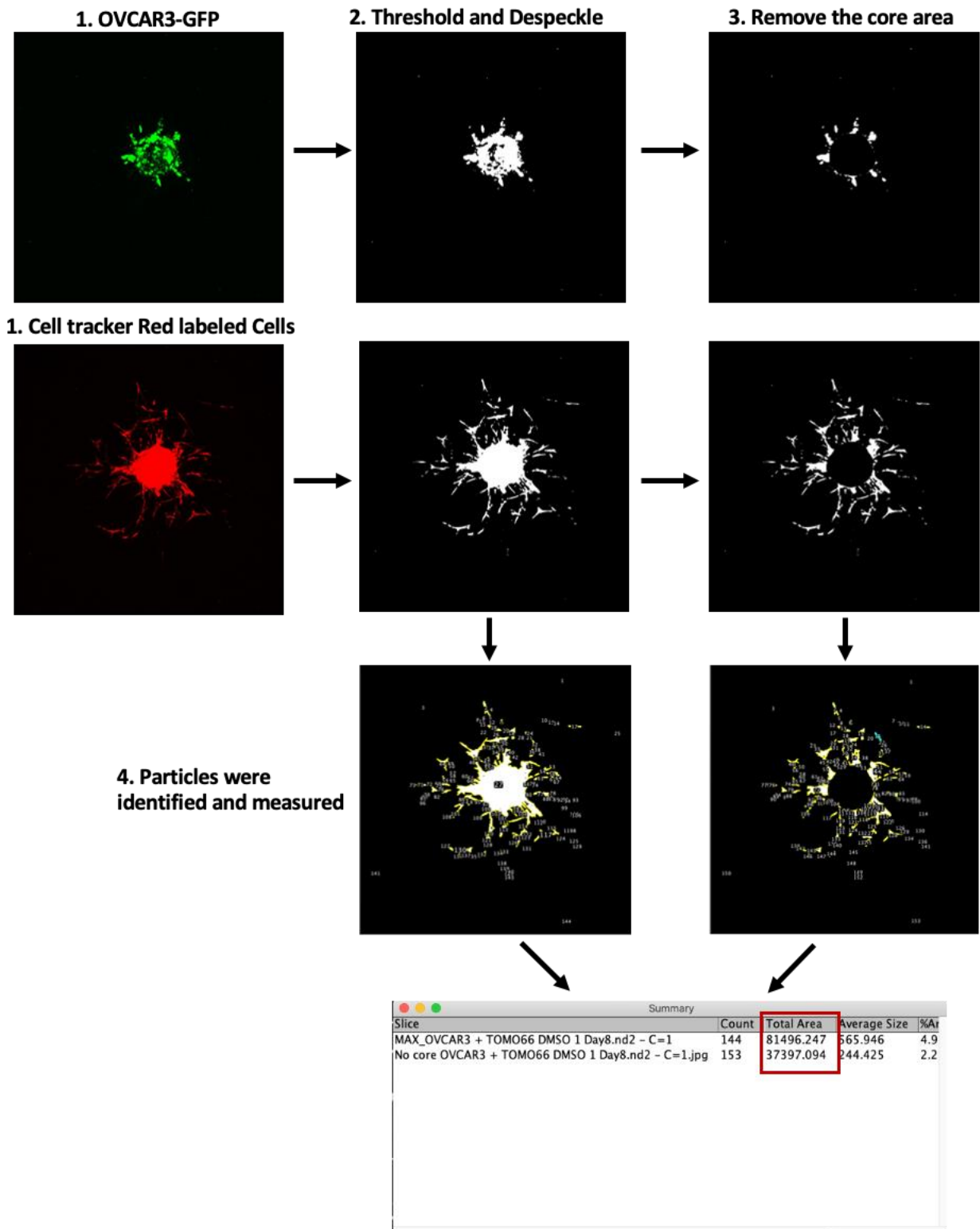


Figure 2.4. 3D spheroids invasion analysis. 1. Cells labelled with cell tracker red (A2780-Rab25 and CAFs/TIFs) were imaged in the TRITC channel (562nm sapphire laser) and OVCAR3-GFP cells were imaged in the FITC channel (488nm sapphire laser) with a Nikon A1 confocal microscope. 2. Each channel was thresholded individually and the Despeckle function was used to remove the background noise. 3. The core area was manually identified and subtracted, to obtain the invasion area of the spheroids. 4. The particles from both total area and invasion area were analysed and the “Total area” value were recorded.

2.2.10.3. Co-culture 3D spheroid invasion assay with ADAMTS5 or Rab25 KD.

OVCAR3-GFP cells were transfected with non-targeting (NT), ADAMTS5 or Rab25 targeting siRNA as described in [section 2.2.7](#). 24 hours after the transfection, the cells were washed twice with PBS and trypsinised. Co-culture spheroids were generated with 1.4×10^5 of transfected OVCAR3-GFP cells and 0.7×10^5 of Cell tracker™ Red labelled CAF cells, as described in [section 2.2.10.2](#), and embedded as described in [section 2.2.10.1](#). 1.5mL of complete culture media was added in the dishes. Spheroids were imaged at day 0, day 4, day 6 and day 8, and fresh media was replaced on day 4. The invasion of both OVCAR3 and CAF cells was quantified ([Figure 2.4](#)). Results from different biological replicates were normalised to the NT control groups on day 2.

2.2.10.4. EdU labelling of co-culture 3D spheroid.

Co-culture spheroid was generated with OVCAR3-GFP, and unlabelled CAF cells and embedded as described above ([section 2.2.10.2](#)). After 6 days, 1.5µL of 10mM EdU solution was spiked into the media to make a final concentration of 10µM. After 2 days of labelling (8 days after embedding), the spheroids were fixed and stained with 4% PFA containing Hoechst 33342 (1:500) at 37°C for 20min. After gently washing twice with PBS, the spheroids were permeabilized with 500µL IF wash buffer (46mM NaN₃, 0.1% (w/v) BSA, 0.2% (v/v) Triton-X 100 and 0.04% (v/v) Tween-20 in 1xPBS) for 2 hours at RT on a rocker, followed by two washes with PBS. The spheroids were stained with Click-iT EdU Imaging Kits (Invitrogen) at 4°C overnight, followed by two washes with PBS. The spheroids were then imaged live with a Nikon A1 confocal microscope, CFI Plan Fluor 10x objective (NA 0.3) and the area of each channel were measured. The percentage of EdU (%EdU) was calculated by the area of EdU signal divided by the area of DAPI and GFP signal.

2.2.11. Hypoxia assays

5×10^5 A2780, OVCAR3 and SKOV3 cells/well were seeded in 6-well plates and incubated overnight at 37°C in 5% CO₂. The hypoxia chamber was set at 37°C in 5% CO₂ and 1% O₂ level. To degas the media, T75 tissue culture flasks containing 5mL of complete culture medium were placed in the hypoxia chamber with the lids loosen for 24h. The culture media of the cells was then replaced with degassed media and incubated in the hypoxia chamber for 24 hours. Cells cultured with normal fresh media and incubated in the standard incubator (20% O₂) were set as normoxia controls. Cells

lysates were collected for western blotting as described in [section 2.2.5](#), or mRNA was extracted for RT-qPCR as described in [section 2.2.6](#).

2.2.12. Cell signalling inhibitor treatments

Echinomycin (ECH) is a small molecule inhibitor that specifically inhibits HIF-1 DNA binding activity and the IC_{50} of ECH in cancer stem cells is 29.4nM (Kong et al., 2005, Wang et al., 2011). 5×10^5 OVCAR3 and SKOV3 cells/well were seeded in 6-well plates and incubated at 37°C in 5% CO₂ overnight. Then, DMSO or ECH (MedChemExpress) were spiked in the culture medium to obtain a final ECH concentration of 5, 10 or 25nM and incubated for 24 hours. Cells were collected for western blotting as described in [section 2.2.5](#), or for RT-qPCR as described in [section 2.2.6](#).

LY294002 is a widely used inhibitor for the PI3K/AKT pathway and the IC_{50} s obtained from in vitro lipid kinase assay for PI3K α , PI3K β and PI3K δ are 0.5, 0.973 and 0.57 μ M respectively (Gharbi et al., 2007, Chaussade et al., 2007). BAY 11-7082 is an NF- κ B inhibitor, which can suppress the phosphorylation of I κ B α and reduce the translocation of the p65 subunit (Mabuchi et al., 2004). 5×10^5 OVCAR3 cells were seeded in 6-well plates. After an overnight incubation at 37°C in 5% CO₂, cells were treated with DMSO, 2.5, 5 or 10 μ M of the LY294002 (MedChemExpress) or BAY 11-7082 (Selleckchem) for 24 hours. Cells were collected for RT-qPCR as described in [section 2.2.6](#).

2.2.13. Immunofluorescence

35mm glass bottom dishes (12mm glass diameter) were coated with 0.1mg/mL Geltrex for a better attachment of cells on the glass surface. 100 μ L Geltrex solution in PBS was added to the dishes and incubated at 37°C for 1h. 2×10^5 cells were seeded, incubated at 37°C overnight and fixed with 4% PFA in PBS for 15 min at RT. After two washes with PBS, the cells were permeabilized with 0.25% (v/v) Triton X-100 in PBS for 5 min, followed by two washes with PBS. Cells were blocked with 1% (w/v) BSA in PBS for 1h. Then, the cells were incubated with primary antibodies (1:100 in 1% BSA/PBS, [Table 2.8](#)) for 1h at RT. After three PBS washes, secondary antibodies (1:1000 in 1% BSA/PBS, [Table 2.8](#)) were added for a 45 min incubation. The cells were then incubated with Phalloidin Alexa Fluor 555 (1:400 in PBS) or Alexa Fluor 647 (1:300 in PBS) for 10 minutes to label the actin cytoskeleton. Finally, the cells were washed twice with PBS, once with dH₂O and 2 drops

of Vectashield mounting agent containing DAPI were added on top. The samples were stored at 4°C. Images were taken with a Nikon A1 confocal microscope, CFI Plan Apochromat VX 60X oil immersion objective and analysed with Fiji Image J. The integrated density was measured and divided by the cell area. Results from biological replicates were normalised to the control groups.

Table 2.8 Immunofluorescent antibody list.

Primary antibodies	Supplier	Dilution ration
NF-κB p65	Proteintech (10745-1-AP)	1:100
Rab25	Proteintech (18139-1-AP)	1:100
Secondary antibodies	Supplier	Dilution ration
Alexa Fluor® 488 goat anti-rabbit IgG (H+L)	Invitrogen (A11034)	1:1,000
Alexa Fluor® 555 donkey anti-rabbit IgG (H+L)	Life technologies (A31572)	1:1,000

2.2.14. Statistical analysis

Experimental data from biological repeats were normalised to the control population for each individual experiment. Data were analysed and presented in GraphPad Prism software (Version 9.1.0). For experiments containing two data sets, unpaired non-parametric t-tests were used (Mann-Whitney test). For experiments containing multiple data sets, one-way ANOVA with multiple comparisons correction was performed. For those containing two variables, two-way ANOVA with multiple comparisons was used. Differences were considered statistically significant when $p < 0.05$. SuperPlots were generated to present the scattered plot as described in (Lord et al., 2020). Datapoints from the same experiment were presented in the same colour, while the different biological replicates were in distinct colours. The mean value of each biological replicate is plotted in larger dots.

Chapter 3 – Rab25 induces ADAMTS5 expression in ovarian cancer cells.

3.1. Introduction.

Previous research in OC highlighted the role of Rab25 in promoting tumour development and metastasis, which further leads to poor prognosis (Cheng et al., 2004). In *in vitro* OC studies, A2780, SKOV3 and OVCAR3 are the top 3 most frequently used cell lines (Domcke et al., 2013). A2780 is a cell line established from an ovarian endometrioid adenocarcinoma sample of a patient who did not receive any treatment, while both SKOV3 and OVCAR3 cells were derived from the ascitic fluid of the OC patients with ovarian serous cystadenocarcinoma and HGSOC, respectively (Hernandez et al., 2016). The gene mutation features of these cell lines have been previously characterised. Briefly, both A2780 and SKOV3 cells contain PIK3CA mutation. PTEN mutation was found in A2780 cells, while TP53 mutation was identified in OVCAR3 cells. BRCA1/2 mutation was not found in any of these three cell lines (Domcke et al., 2013). Among these cell lines, the expression of Rab25 was also measured in previous studies. Through western blotting, Rab25 expression was not detected in A2780 (Cheng et al., 2004) and SKOV3 cells (Temel et al., 2020). The OVCAR3 cell line was found to endogenously overexpress Rab25 (Temel et al., 2020). Since upregulated Rab25 promotes OC tumour development, which is linked to therapy resistance and results in poor prognosis, it is valuable to further characterise the molecular mechanisms mediating these processes as they could lead to the identification of novel therapeutic targets.

In OC tumours, increased stiffness and altered remodelling of the ECM were recognized (Cho et al., 2015). Therefore, the role of ECM has been drawing attention during OC research. To identify the molecular mechanisms through which Rab25 promotes OC cell invasion in 3D matrices, ECM-induced changes in gene expression were analysed in the presence and absence of Rab25 overexpression previously. The microarray assay was done in Norman's lab to identify genes with altered expression levels in Rab25 overexpressing cells with and without the presence of CDM. In comparison to the commercially available ECM compartments such as collagen, matrigel and fibronectin, CDM represent a better *in vivo* microenvironment, which is now frequently used in TME-related studies (Rubi-Sans et al., 2021). The A2780 cells stably expressing a control empty vector (A2780-DNA3) or a vector containing Rab25 (A2780-Rab25) were cultured on either plastic or CDM for 16h and the mRNA was extracted from the cells. Biotinylated cDNA was then synthesised

for microarray hydration. Through multiway ANOVA analysis of the obtained data, significantly up or down-regulated genes in A2780-Rab25 cells were identified.

Among the upregulated genes, a 3.8-fold-change of ADAMTS5 expression was identified in A2780-Rab25 cells seeded on CDM, compared to a 1.2-fold-change when cells were plated on plastic (Dożynkiewicz, 2011). This indicates that Rab25 may promote the expression of ADAMTS5 in OC, and this process could be mediated by the presence of ECM. Interestingly, ADAMTS5 may also promote the development of OC. A significantly increased ADAMTS5 expression was detected in malignant tumour samples compared to borderline and benign tumour samples from OC patients (Lima et al., 2016). However, the regulator and downstream effectors remain unclear for ADAMTS5 in OC.

In this chapter, the role of Rab25 in regulating ADAMTS5 expression was investigated. Rab25 expression level was first characterised in multiple OC cell lines to select the best research model and two paired models were selected. The A2780-DNA3 and A2780-Rab25 cell lines were generated in Dr Gordon Mill's lab, as described in (Cheng et al., 2004). The OVCAR3 cell line was identified as endogenously overexpressing Rab25. As a result, the overexpression of Rab25 resulted in significantly higher ADAMTS5 at both mRNA and protein levels, indicating that Rab25 induces ADAMTS5 expression.

3.2. Results

3.2.1. Characterisation of Rab25 expression in OC cell lines.

The protein level of Rab25 was measured through western blotting in A2780-DNA3, A2780-Rab25, OVCAR3, OVCAR4 and SKOV3 cells. Cells were seeded in 6-well plates and the proteins were harvested after a 24h incubation. Clear Rab25 bands were identified in A2780-Rab25 and OVCAR3 cells, but not in A2780-DNA3, SKOV3 and OVCAR4 cells (Figure 3.1). The molecular weight of Rab25 bands detected in A2780-Rab25 cells is larger than OVCAR3 cells, which is probably because the Rab25 overexpressed in A2780 cells is tagged.

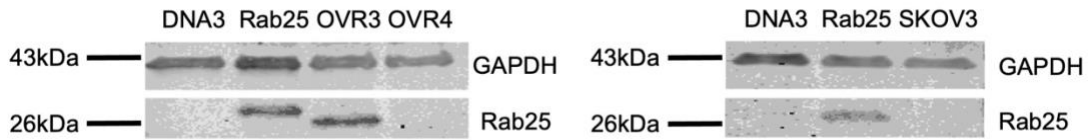


Figure 3.1. Rab25 protein levels in OC cell lines. A2780-DNA3, A2780-Rab25, OVCAR3, OVCAR4 and SKOV3 cells were seeded on plastic. After a 24h incubation, the proteins were harvested and the Rab25 protein level was measured by western blotting. GAPDH was used as a loading control. Membranes were imaged with the Licor Odyssey Sa system, and the band intensity was quantified by Image Studio Lite software. N=1 independent experiment.

To confirm *Rab25* expression at the mRNA level, A2780-DNA3, A2780-Rab25, OVCAR3 and SKOV3 cells were seeded in 6-well plates and incubated for 24h, and then the mRNA was extracted and quantified by SYBR-green based qPCR (Figure 3.2). The ΔC_t values of *Rab25* and the housekeeping gene *GAPDH* were obtained, and gene expression was calculated using the $2^{-\Delta\Delta C_t}$ method ($2^{-(\Delta C_t \text{ Rab25} - \Delta C_t \text{ GAPDH})}$). *Rab25* was undetectable in A2780-DNA3 and SKOV3 cells, which is consistent with the western blotting results. In comparison to OVCAR3 cells, which endogenously overexpress Rab25, *Rab25* mRNA level in A2780-Rab25 cells was more variable between different biological replicates.

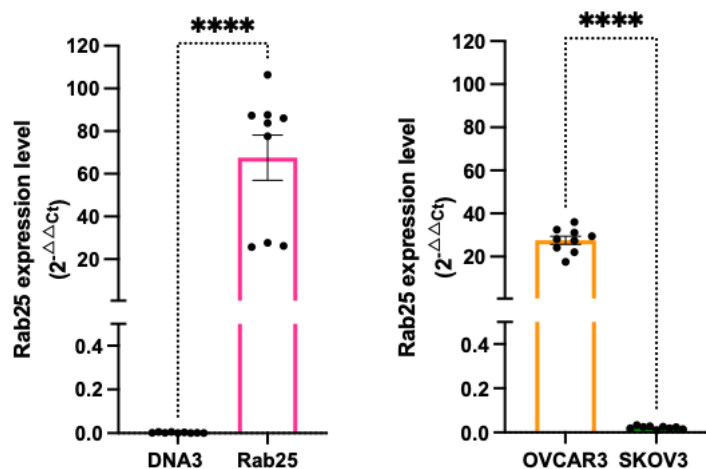


Figure 3.2. Rab25 gene expression in OC cell lines. A2780-DNA3, A2780-Rab25, OVCAR3 and SKOV3 cells were seeded on plastic. After a 24h incubation, the mRNA was extracted from the cells. Rab25 mRNA levels were measured by SYBR-green based qPCR. GAPDH was used as the control housekeeping gene and Rab25 expression level was plotted as $2^{-\Delta\Delta C_t}$. Data are presented as mean \pm SEM. N=3 independent experiments. **** $p < 0.0001$, Mann-Whitney test.

Immunofluorescence staining was performed to assess the localisation of Rab25 in A2780-DNA3, A2780-Rab25 and OVCAR3 cells. The cells were seeded on glass-bottom confocal dishes for 24h and stained for the actin cytoskeleton, nuclei and Rab25 (Figure 3.3). Consistent with the qPCR and WB

results, the Rab25 signal was not detected in A2780-DNA3 cells. In both A2780-Rab25 and OVCAR3 cells, Rab25 showed a perinuclear recycling compartment localisation, visible as a bright green spot near the nucleus. The integrated density of the Rab25 signal in OVCAR3 cells was significantly higher than in A2780-Rab25 cells, while this trend was not observed in the western blotting and qPCR results. However, this could be due to the expression loss of Rab25 in A2780-Rab25 cells, as discussed below.

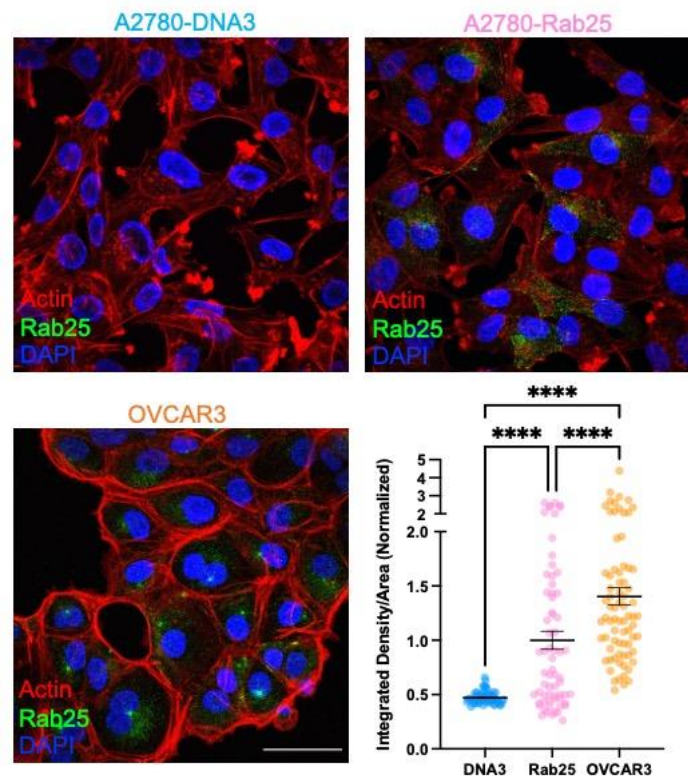


Figure 3.3. Rab25 localisation in OC cells. A2780-DNA3, A2780-Rab25 and OVCAR3 cells were seeded on glass-bottom confocal dishes for 24h, fixed and stained for actin (red), Rab25 (green) and nuclei (blue). Samples were imaged with a Nikon A1 confocal microscope, CFI Plan ApoChromat VX 60X oil immersion objective and the integrated density was calculated and normalised to the area with image J. Z-stacked images were maximum-projected. Graphs show the mean \pm SEM. Scale bar: 50 μ m. **** $p < 0.0001$, Kruskal-Wallis test, N=1, 64 A2780-DNA3, 66 A2780-Rab25 and 75 OVCAR3 cells.

Altogether, we demonstrated that OVCAR3 endogenously overexpress Rab25, while this GTPase was not detected in SKOV3 and OVCAR4. For the following experiments, A2780-DNA3 and Rab25 cells were used as paired cell lines, OVCAR3 cells were selected as Rab25 endogenously overexpressing cells and SKOV3 cells were selected as an additional Rab25-negative cell line.

3.2.2. Selection of A2780 cells line overexpressing Rab25.

During the Rab25 immunofluorescence staining, a remarkable loss of Rab25 expression in A2780-Rab25 cells was observed. As shown in [Figure 3.4A](#), Rab25 could be detected in a small fraction of A2780-Rab25 cells, while most of them show similar expression levels as in A2780-DNA3 cells. Since the cells were generated with plasmids containing the Neomycin resistance gene (neo), the cells expressing transfected vectors are resistant to G418, an aminoglycoside antibiotic. The selection concentration and the time were first optimized (data not shown). Based on this, A2780-DNA3 and A2780-Rab25 cells were cultured in media with 0.4mg/mL G418 for two passages, and the immunofluorescence staining was performed again to test the selection result. As shown in [Figure 3.4B](#), a significantly overexpressed Rab25 was detected in A2780-Rab25 cells compared to DNA3 cells after selection. Throughout this project, A2780 cells were selected with 0.4mg/mL G418 every 10 passages.

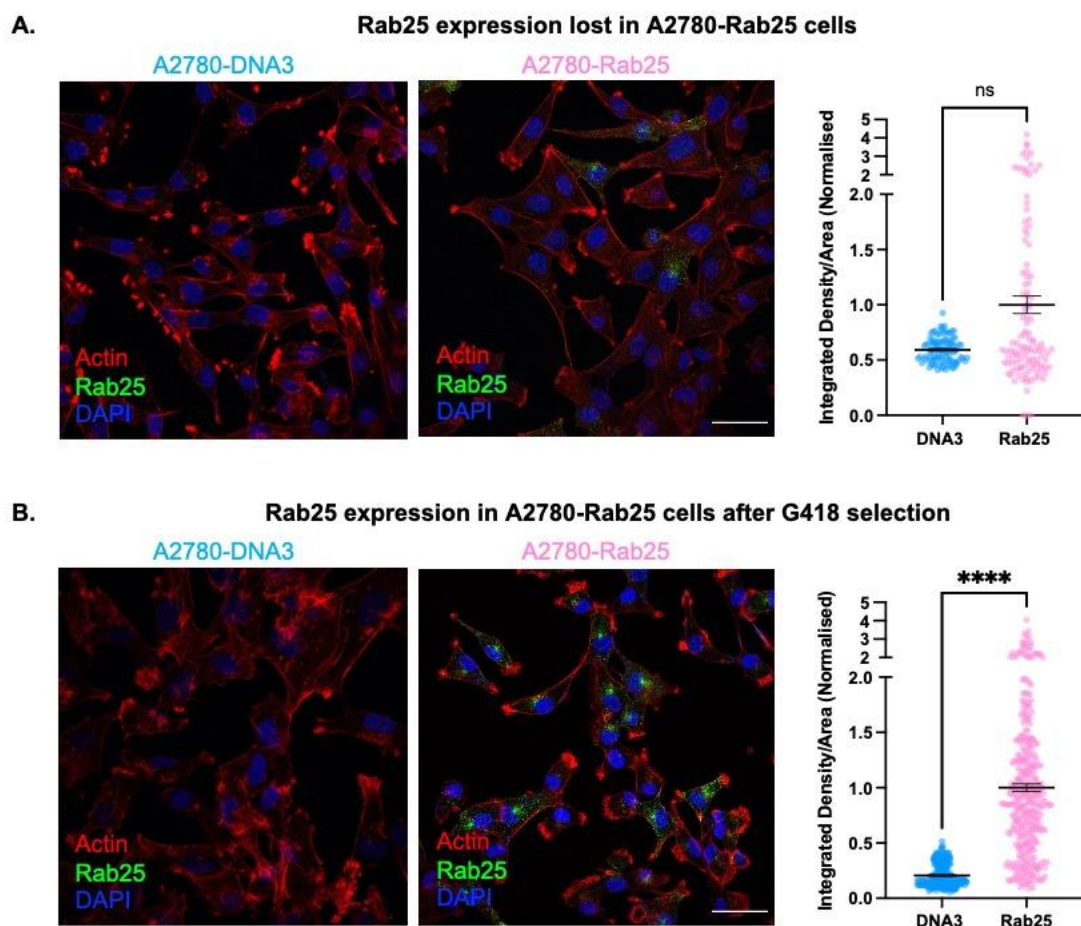


Figure 3.4. Expression of Rab25 in A2780-Rab25 cell line before and after G418 selection. A2780-DNA3 and A2780-Rab25 cells were seeded on glass-bottom confocal dishes for 24h before (A) or after G418 selection (B), fixed and stained for actin (red), Rab25 (green) and nuclei (blue). Samples were imaged with a Nikon A1 confocal microscope, CFI Plan Apochromat VX 40X oil immersion objective and the integrated density was

calculated and normalised to the cell area with image J. **A.** N=1. **B.** N=3. Graphs show the mean \pm SEM. Scale bar: 50 μ m.*** p<0.0001, Mann-Whitney test.

3.2.3. Rab25 over-expression promoted ADAMTS5 expression in OC cell lines.

Previous experiments investigating altered gene expression associated with Rab25 overexpression in OC cells showed a matrix-dependent ADAMTS5 expression upregulation in A2780-Rab25 cells compared to A2780-DNA3 cells (Norman lab, unpublished data). To validate and further investigate this, A2780-DNA3 and A2780-Rab25 cells were seeded on plastic or TIF-CDM and ADAMTS5 expression was measured at both protein and mRNA levels. Since ADAMTS5 is a secreted protease, both cell lysate and CM were harvested and tested by western blotting as shown in [Figure 3.5A](#). The cells were seeded in 6-well plates for 4h, either on plastic or on CDM, the media was replaced with serum-free media and incubated for 3 days. The CM was concentrated using Amicon Ultra[®] - 4 Centrifugal filter tubes (3,000 or 10,000 MWCO PES). The cell lysate was harvested with triton-based extraction buffer to avoid solubilising the CDM.

The western blotting data quantified and plotted here represent ADAMTS5 level in the CM only, as the ADAMTS5 level in the cell lysate was variable on both plastic and CDM. The result shows that when cells are seeded on plastic, ADAMTS5 expression level in A2780-Rab25 cells was similar to A2780-DNA3 cells. However, when cells were seeded on TIF-CDM, ADAMTS5 level was significantly increased in Rab25-overexpressing cells in comparison to DNA3 control cells ([Figure 3.5B](#)). This result indicates that Rab25 could promote ADAMTS5 expression and/or secretion in the media. To assess whether Rab25 regulated ADAMTS5 expression at the transcriptional level, SYBR-green based qPCR was performed. Similar to the western blotting result, there was no difference between the *ADAMTS5* mRNA levels in A2780-DNA3 and A2780-Rab25 cells when seeded on plastic, while on TIF-CDM a significantly increased *ADAMTS5* mRNA level was observed in Rab25-overexpressing cells ([Figure 3.5C](#)). As shown before, the expression level of Rab25 was strongly increased in A2780-Rab25 compared to A2780-DNA3 cells and was not affected by the presence of the CDM. Additionally, an increased but no significant Rab25 expression level was identified in A2780-Rab25 cells when placed on CDM. This result indicates that the Rab25 can induce ADAMTS5 expression in A2780 cells while the presence of CDM is required.

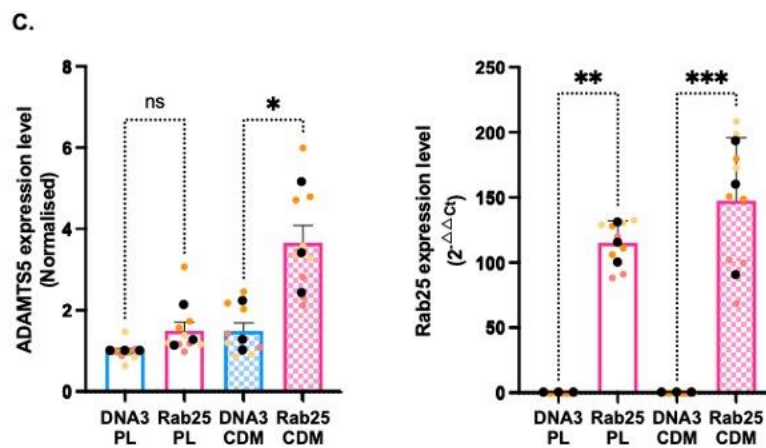
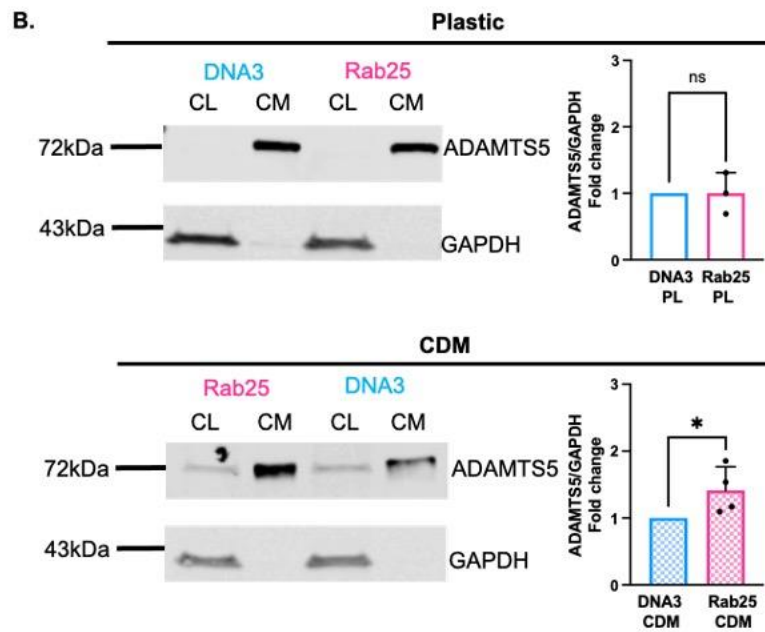
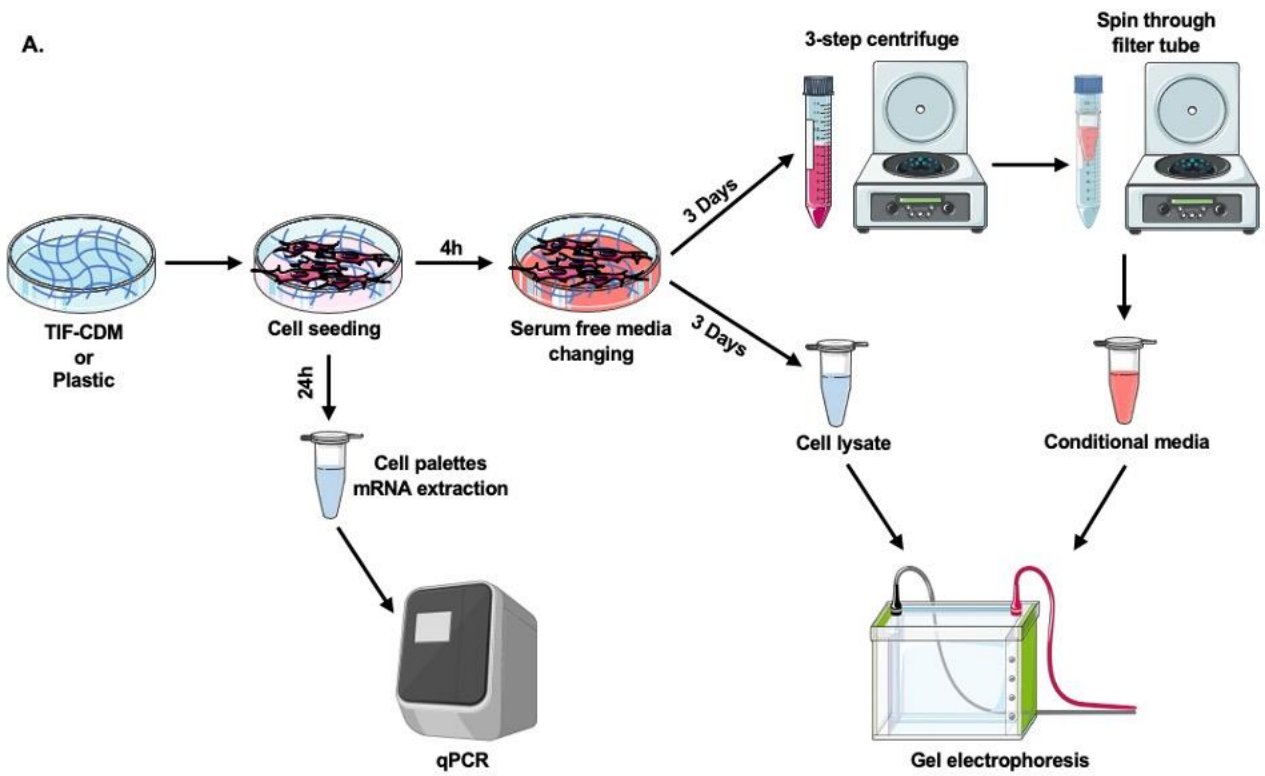


Figure 3.5. Rab25 induced ADAMTS5 expression in the presence of CDM. **A.** Schematic of the experimental plan, made with items adapted from Servier Medical Art **B.** A2780-DNA3 and A2780-Rab25 cells were plated on plastic (N=3 independent experiments) or TIF-CDM (N=4 independent experiments) for 3 days. Both cell lysate and concentrated conditioned media were extracted and tested by western blotting. Membranes were stained for ADAMTS5 and GAPDH, imaged with a Licor Odyssey Sa system, and the band intensity was quantified by Image Studio Lite software. ADAMTS5 signal was normalised to the GAPDH loading control, and the fold change of expression in A2780-Rab25 cells in comparison to DNA3 cells was plotted. Data are presented as mean \pm SEM. * $p=0.0286$, Mann-Whitney test. CL: cell lysate, CM: conditioned media, PL: plastic. **C.** A2780-DNA3 and A2780-Rab25 cells were seeded on plastic or TIF-CDM for 24h, mRNA was extracted and quantified by SYBR-green based qPCR. *GAPDH* was used as the control housekeeping gene and the data was normalised to the DNA3 plastic group (*ADAMTS5*) or plotted in $2^{-\Delta\Delta C_t}$ (Rab25). Data are presented as mean \pm SEM. N=3 independent experiments, the black dots represent the mean of individual experiments. * $p=0.0226$, ** $p=0.0054$, *** $p=0.0005$, Kruskal-Wallis test.

3.2.4. Rab25 KD reduced ADAMTS5 expression in OC cells endogenously overexpressing Rab25.

To further validate the induction of ADAMTS5 in Rab25 overexpressing cells, Rab25 KD was performed in OVCAR3 cells, endogenously overexpresses Rab25 (Figure 3.1-3.3), and the ADAMTS5 expression level was tested by SYBR-green based qPCR. However, when seeded on TIF-CDM, the morphology of OVCAR3 cells changed dramatically and cell survival was strongly decreased (not shown). Therefore, hTERT immortalized omental CAFs were used to generate CDM. TIF- and CAF-CDM were generated as described in section 2.2.3 on glass-bottom confocal dishes, stained with 10mg/mL NHS-fluorescein and imaged with a Nikon A1 confocal microscope, CFI Plan Apochromat VX 60X oil immersion objective. As shown in Figure 3.6, TIF- and CAF-CDMs showed different matrix architecture, with thinner and more aligned fibres in TIF-CDM and thicker and more random-oriented fibres in CAF CDM.

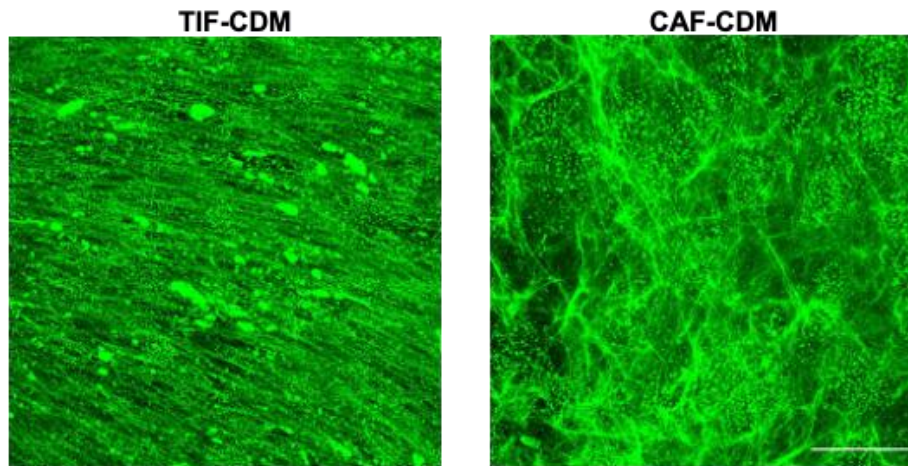


Figure 3.6. Different matrix organisation in TIF and CAF-CDMs. TIF and CAF-CDM were generated on glass-bottom dishes, stained with 10mg/mL NHS-fluorescein and imaged with a Nikon A1 confocal microscope, CFI Plan Achromat VX 60X oil immersion objective. Z-stacked images were maximum-projected. Scale bar: 50 μ m N=1.

To investigate whether Rab25 KD affected ADAMTS5 expression, OVCAR3 cells were seeded on plastic and transfected with a non-targeting control or Rab25-targeting siRNA for 24h. Then, the cells were reseeded on either plastic or CAF-CDM in antibiotic-free media for 24h, the mRNA was extracted, and SYBR-green based qPCR was performed (Figure 3.7A). The expression level of both *ADAMTS5* and *Rab25* was quantified. As a result, a significantly reduced ADAMTS5 expression level was observed in OVCAR3 upon Rab25 KD on both plastic and CAF-CDM (Figure 3.7B). *Rab25* mRNA quantification showed an 80% reduction upon KD. This demonstrates that Rab25 regulates ADAMTS5 expression in OC cells.

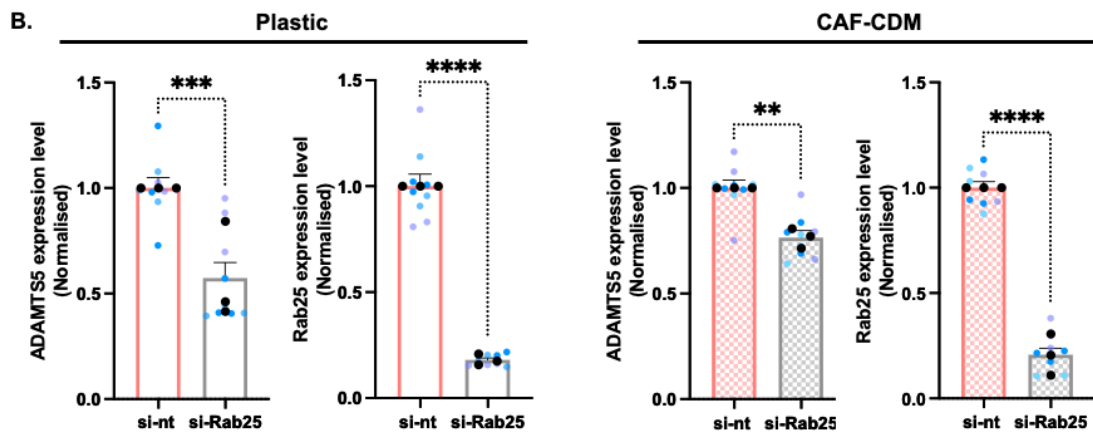
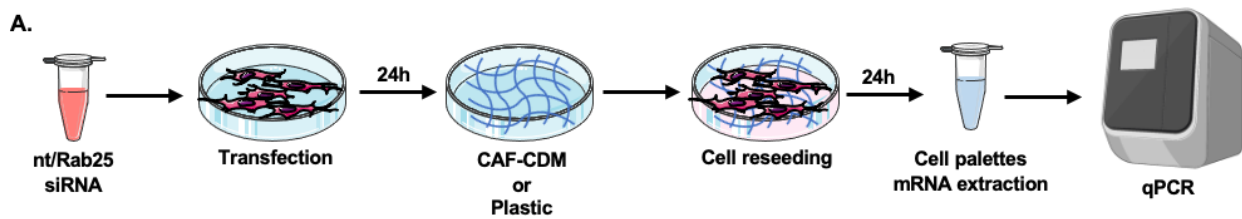


Figure 3.7. ADAMTS5 expression was reduced upon Rab25 KD in OVCAR3 cells on both plastic and CDM. A. Schematic of the experimental plan, made with items adapted from Servier Medical Art. **B.** OVCAR3 cells were transfected with a non-targeting control (si-nt) or Rab25-targeting siRNA (si-Rab25) for 24h and reseeded on plastic or CAF-CDM for 24h. ADAMTS5 and Rab25 mRNA levels were measured by SYBR-green based qPCR. GAPDH was used as the control housekeeping gene and the data was normalised to si-nt control. Data are presented as mean \pm SEM. N=3 independent experiments, the black dots represent the mean of individual experiments. ** $p=0.0012$, *** $p=0.0003$, **** $p<0.0001$, Mann-Whitney test.

3.3. Discussion

In this chapter, I presented the expression level of Rab25 in different OC cell lines and the role of Rab25 in promoting ADAMTS5 expression in these cells (Figure 3.8). The overexpression of Rab25 was observed in patients and has been found to contribute to the aggressiveness of OC (Cheng et al., 2004). However, the overexpression of Rab25 in OC cell lines is controversial. Immunoblot results by Temel and colleagues showed overexpressed Rab25 in OVCAR3 and OVCAR4 cells (2020), while here, Rab25 expression was only detected in OVCAR3 but not in OVCAR4 cells. In agreement with my result, Rab25 expression was not detected in SKOV3 cells by Temel et al. (2020). However, Rab25 was detected in SKOV3 cells by Fan et al (2015). The difference in Rab25 expression could be due to the different sources of the cells. SKOV3 cells used by Fan et al. (2015) were purchased from Shanghai Institute of Cell Biology, Chinese Academy of Sciences (Shanghai, China), while the SKOV3 cells in our lab were from ATCC and maintained at a low passage number. A2780-DNA3, A2780-

Rab25 and OVCAR3 cells which obtained from other labs were STR-profiled. Therefore, for Rab25-related research in OC, it is important to confirm the expression level in different cell lines.

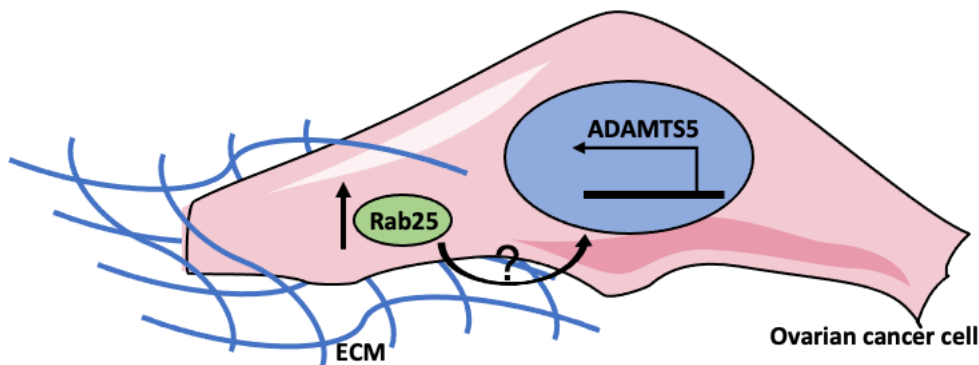


Figure 3.8. Rab25 induces ADAMTS5 in ovarian cancer cells. In the presence of ECM, Rab25 overexpression induces ADAMTS5 expression in OC cells. Image made with items adapted from Servier Medical Art.

The aim of this chapter was to characterise the role of Rab25 in regulating ADAMTS5 expression. Since ADAMTS5 is a secreted protease, ADAMTS5 protein was mainly detected in the CM rather than in the cell lysate. Although intracellular ADAMTS5 was also observed on the representative blot, the appearance of the band is variable and not reproducible, therefore, was not quantified. The CM was analysed through western blotting as previously described in (Gupta et al., 2012). Serum-free media was changed after 4h of cell seeding to reduce the background on the blot. For secretome-related studies, serum-free media was generally recommended to avoid contamination from FBS proteins, especially when targeting low abundant secreted proteins (Shin et al., 2015). However, previous research identified differences in mesenchymal stem cell-secreted proteins cultured in serum-free and serum-containing media (Shin et al., 2019). Reduced secretion of ECM-modifying enzymes such as MMP14 was observed in serum-free media compared to serum-containing media. Since secreted ADAMTS5 was not identified in this research, it is unclear if ADAMTS5 secretion could be affected by serum starvation. Although serum-free media may change the secretion of ADAMTS5, it was still used in this project since we failed to obtain a clear band of ADAMTS5 in serum-containing media (data not shown).

Our data showed that in A2780 cells overexpressing Rab25, upregulated ADAMTS5 expression was only identified in the presence of TIF-CDM. This result is consistent with what has been previously observed in Norman's lab. Including ADAMTS5, the expression of other 17 genes such as chloride

intracellular channel 3 (CLIC3) was found in a Rab25- and matrix-dependent manner (Dozynkiewicz, 2011). When plated on plastic, CLIC3 expression in A2780-Rab25 cells is 6-fold higher in comparison with A2780-DNA3 cells, while an over 20-fold expression change was observed when cells were plated on CDM (Dozynkiewicz et al., 2012). Alternatively, OVCAR3 cells with Rab25 KD show reduced ADAMTS5 expression on both plastic and CAF-CDM, indicating that the depletion of Rab25 resulted in the downregulation of ADAMTS5 even without CDM.

Compared to CAF-CDM, TIF-CDM failed to support the survival and the morphology maintenance of the OVCAR3 cell line. This may be caused by the difference between their structural features and cell signalling regulation. The difference between CDM derived from normal fibroblast, TIF and CAF isolated from patients with head and neck squamous cell carcinoma has been previously characterised (Kaukonen et al., 2016). Architecturally, both normal fibroblast- and TIF-CDM consist of more aligned and uniform fibres, in agreement with what I observed (Figure 3.6). Furthermore, normal fibroblast and TIF-CDM were found to inhibit breast cancer cell proliferation through down-regulating histone demethylase JMJD1A, and this growth restriction was not observed on CAF-CDM (Kaukonen et al., 2016). Therefore, TIF-CDM may similarly inhibit the growth of OVCAR3. However, it is unclear why this inhibition has only been observed in OVCAR3 but not A2780 cells.

Gene expression could be affected by multiple factors, including the altered epigenetic modification and dysregulated transcriptional signalling pathways (Gibney and Nolan, 2010). Here, I showed that Rab25 promotes ADAMTS5 expression, in a matrix-dependent manner in A2780 cells, while this might not be the case in OVCAR3 cells. This could be due to differences in integrin expression between A2780 and OVCAR3 cells (unpublished data, Rainero lab) Given that the recycling of integrin $\alpha 5\beta 1$ from the LE to the plasmid membrane regulated by Rab25 was found to promote OC cell invasion and migration (Huveneers et al., 2008, Caswell et al., 2007), it is tempting to speculate that Rab25 may induce gene expression, including ADAMTS5, through the regulation of integrin recycling and trafficking. Additionally, several evidence suggested the potential interaction between integrins and EGFR, which can activate downstream transcriptional signalling pathways. As an example, Rab-coupling protein (RCP) promoted the physical association and the coordinate recycling of integrin $\alpha 5\beta 1$ and EGFR1, which enhanced the EGF-induced EGFR1 autophosphorylation and AKT activation (Caswell et al., 2008).

To summarise, our research found that the expression of ADAMTS5 was induced upon Rab25 overexpression, while Rab25 down-regulation reduced ADAMTS5 expression OC cells. The changes in expression were detected at both protein and mRNA levels indicating a transcription-related mechanism. The following chapter will investigate downstream signalling pathways regulated by Rab25 which might regulate ADAMTS5 gene expression.

Chapter 4 – Transcription factor NF- κ B was required for Rab25-induced ADAMTS5 expression in OC cells.

4.1. Introduction

Transcription factors (TFs) are proteins that directly mediate DNA transcription by binding to specific DNA sequences and guiding gene transcription. This regulation by TFs is necessary for multiple crucial biological functions such as tissue-specific gene expression, cell differentiation and gene activation in response to stimulations (Latchman, 1997). The prototypical structure of TFs includes DNA-binding domains and effector domains (Lambert et al., 2018). The DNA-binding domains of the TFs can scan through the genome and recognise the DNA binding sequences. These domains show a higher binding affinity for these specific binding sites than for other sequences (Geertz et al., 2012). It was also shown that TFs can recruit other TFs or co-activators through protein-protein interactions to recognize the DNA-binding site (Reiter et al., 2017). Meanwhile, the DNA-binding sites for TFs on the genome are not always accessible. For example, the binding site could be packed in the nucleosomes or be epigenetically modified. In this case, TFs can recruit histone and chromatin-modifying enzymes to expose the DNA-binding site and initiate the transcription (Frietze and Farnham, 2011). Apart from DNA-binding properties, TFs can also recognize genome sites with epigenomic marks, such as DNA with methylation or histone modifications (Frietze and Farnham, 2011). After reaching the specific site on the genome, the effector domain of the TFs can then recruit co-factors and regulate the transcription process. Fundamentally, it can recruit RNA polymerase II (pol II) and other essential co-activators for transcription initiation and elongation (Eberhardy and Farnham, 2002).

A great number of inactivated TFs are located intracellularly in the cytoplasm. Signals from the extracellular environment can activate receptors on the cell surface through ligand-binding, which further activates downstream kinases to stimulate the latent TFs. The activated TFs then bind to a transport protein, importin, and enter the nucleus through the nuclear pores. During cancer progression, altered TF levels are caused by the dysregulation of these signalling proteins or mutations in TF coding genes. This can lead to the upregulation of oncogenes and/or the downregulation of tumour suppressors, which has been widely identified in breast, prostate, colorectal, lung and other types of cancer (Lee and Young, 2013). Currently, research about

targeting the TFs of oncogenes for cancer therapy is ongoing and several small-molecule inhibitors that can inhibit the specific DNA binding activities of TFs are in clinical trials (Bushweller, 2019).

In EOC, a list of altered TFs was found to be shared between different histological subtypes (Nameki et al., 2021). *TP53* is one of the most commonly mutated tumour suppressor genes in cancer. In EOC, the top 2 most common *TP53* mutations are at positions R273 and R248, the frequency of which are 8.13% and 6.02% respectively (Cho and Shih, 2009). The p53 protein encoded by *TP53* with these two mutations does not change the overall protein conformation but affects the DNA binding ability and further contributes to oncogenesis. Indeed, *TP53* mutation was found to promote the transcription of chemoresistance genes (Brachova et al., 2013). Other TFs in EOC are expressed in an histotype-specific manner, which may explain the histological diversity among different EOC subtypes (Nameki et al., 2021). Although TFs are known to mediate oncogenesis in OC, most studies about TFs in OC remain pre-clinical.

Hypoxia-inducible factors (HIFs) are a family of TFs that regulate cell signalling in response to oxygen level, including HIF-1 α , HIF-1 β and HIF-2. In normoxia, prolyl hydroxylases (PHDs) activated by oxygen, ferrous iron and 2-oxoglutarate can hydroxylate HIF-1 α . Then, the von Hippel-Lindau tumour-suppressor protein (pVHL), a component of an E3 ubiquitin ligase complex, can interact with hydroxylated HIF-1 α and lead to ubiquitination and degradation of HIF-1 α in the cytoplasm (Figure 4.1). During oncogenesis, hypoxia conditions in the tumour microenvironment inhibit the PHDs. HIF-1 α therefore remains stable and can be translocated into the nucleus, where it forms a complex with HIF-1 β and p300/CBP and then binds to the promoter of target genes. Activation of these genes can contribute to proliferation, apoptosis and angiogenesis (Harris, 2002). Similar to most types of cancer, the microenvironment of OC solid tumour is hypoxic. Additionally, the oxygen pressure and oxygen content in the ascites of OC patients are also lower compared to blood gas values, which promote metastasis (Kim et al., 2006). Furthermore, high HIF-1 α expression results in poor prognosis outcomes for OC patients, leading to resistance to chemotherapy and immunotherapy (Wang et al., 2021, Klemba et al., 2020). Since HIF-1 α is a TF that regulates multiple signalling pathways that promote OC cancer progression, metastasis and therapy resistance, it is a rational therapeutic target for OC. Indeed, several HIF-1 α inhibitors are in clinical trials (Wang et al., 2021).

However, the efficacy of these inhibitors is still limited, so further studies are required to determine whether HIF-1 α inhibitors are a successful option for OC treatment.

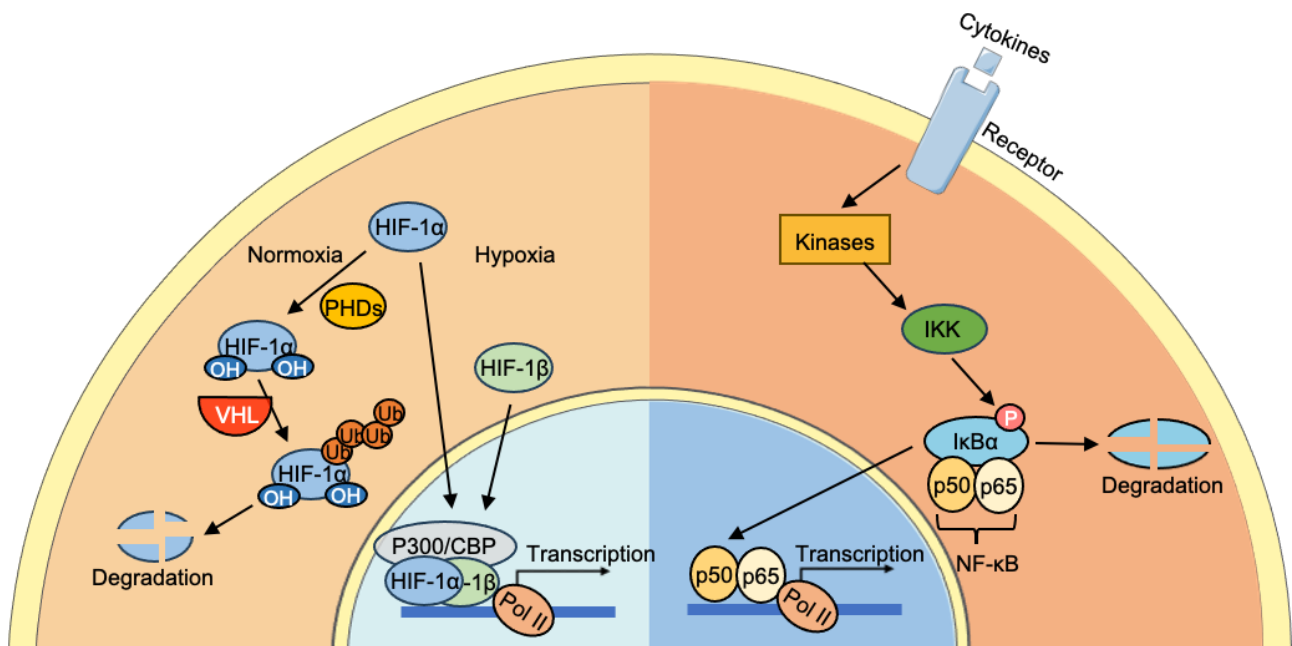


Figure 4.1. Schematic of HIF-1 α and NF- κ B activation and function in regulating gene transcription. Oxygen level mediates HIF-1 α function through PHDs. In normoxia, HIF-1 α is hydroxylated by PHDs and ubiquitinated by VHL, which leads to degradation. Under hypoxic conditions, HIF-1 α remains stable and is translocated into the nucleus, forming the dimer with HIF-1 β , recruiting the co-factor p300/CBP and pol II to initiate the transcription of target genes. NF- κ B signalling pathway is activated by cytokines (e.g. TNF- α , IL-1, IL-6) through binding to the corresponding receptors. The activated downstream kinases then activate IKK, which further phosphorylates the I κ B α . This results in the degradation of I κ B α and the release of NF- κ B subunits (e.g. p50/p65). NF- κ B is then translocated into the nucleus, recruiting pol II and initiating the transcription of target genes. Image made with items adapted from Servier Medical Art.

NF- κ B is a family of TFs well-known for regulating inflammation immune responses. NF- κ B proteins that contain a Rel homology region (RHR) are encoded by five genes in mammalian cells, which are NF- κ B1 (p50 and precursor p105), NF- κ B2 (p52 and precursor p105), RelA (p65), RelB and c-Rel (Karin and Ben-Neriah, 2000). The RHR of NF- κ B is responsible for DNA binding and protein-protein interactions, such as dimerisation and inhibitory protein binding. Inactivated NF- κ B is localised in the cytoplasm and inhibited by binding to the inhibitor of nuclear factor kappa B (I κ B) proteins. When the receptors are activated by extracellular cytokines, the downstream I κ B kinase (IKK) is activated. I κ B proteins are then phosphorylated by IKK and targeted for degradation. The NF- κ B subunits are released from I κ B, translocated into the nucleus and mediate gene transcription (Figure

4.1). Tumour-promoting inflammation is a hallmark of cancer (Hanahan and Weinberg, 2011), which was widely found induced by NF- κ B (Hoesel and Schmid, 2013). Furthermore, NF- κ B can also activate the expression of oncogenes and regulate cell signalling pathways to contribute to cancer cell proliferation and invasiveness (Dolcet et al., 2005). In OC, elevated NF- κ B (p65 and p50) protein levels were identified in borderline and malignant compared to the benign tumour samples (Giopanou et al., 2014). NF- κ B was found to contribute to the evasion of apoptosis signal induced by TNF- α (Xiao et al., 2003), while inhibition of NF- κ B with small molecule inhibitors increased the sensitivity of OC cells to cisplatin treatment, both in vitro and in vivo (Mabuchi et al., 2004).

The activation of NF- κ B is mediated by multiple signalling pathways in cancers, including PI3K/AKT/mTOR (Ghoneum and Said, 2019), which is one of the most commonly activated pathways in OC (Bast et al., 2009). Receptor tyrosine kinases (RTKs) activated by cytokines (e.g. IL-1 and TNF- α) or GFs (e.g. EGFR) can activate PI3K (Reddy et al., 1997, Sizemore et al., 1999, Koul et al., 2001, Guo and Donner, 1996, Li et al., 2016), which mediates the conversion of phosphatidylinositol (4,5)-bisphosphate (PIP₂) to phosphatidylinositol (3,4,5)-trisphosphate PIP₃. This process is reversible through dephosphorylation by PTEN. The PI3K can activate the AKT in cooperation with PIP₃, which activates the mammalian target of rapamycin complex 2 (mTORC2) and 3-phosphoinositide-dependent kinase 1 (PKD1) and further phosphorylate AKT at Ser473 and Thr308 correspondingly. Phosphorylated AKT can then mediate the release and translocation of the NF- κ B by activating IKKs (Bai et al., 2009). Additionally, mTORC1 activated by AKT was also found to activate NF- κ B through interactions with IKK (Dan et al., 2008, Li et al., 2016) (Figure 4.2).

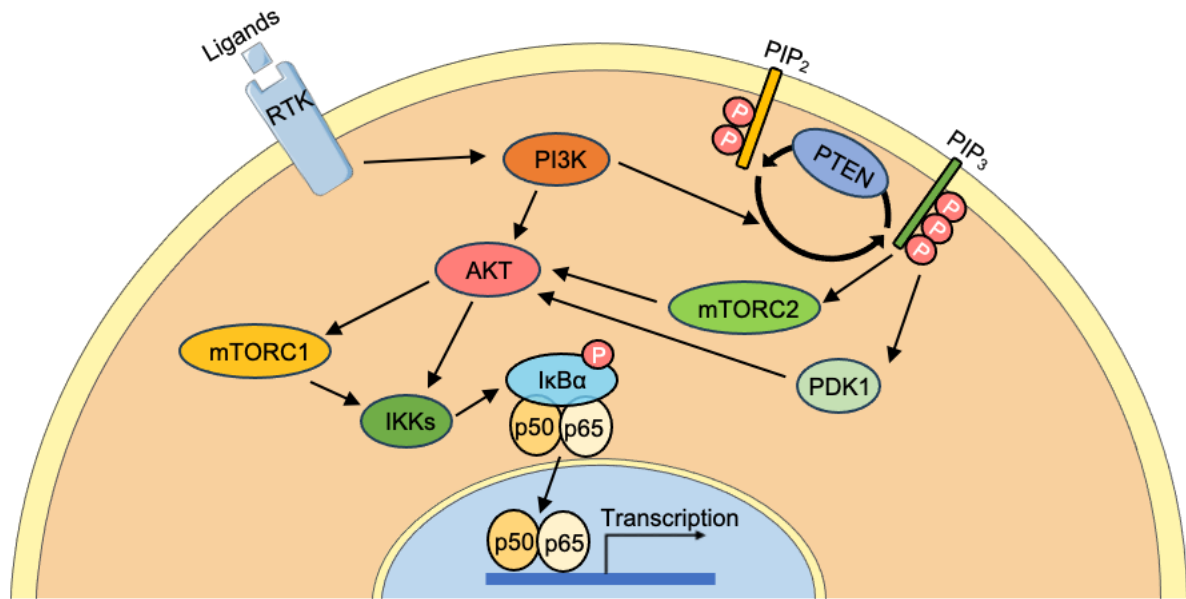


Figure 4.2. Schematic of NF-κB activation via PI3K/AKT/mTOR/ pathway. RTK activated by cytokines and GFs activate PI3K, which catalyses the conversion of PIP₂ to PIP₃. PIP₃ then activates AKT through phosphorylation by mTORC2 and PDK1. Activated AKT further mediates the activation of NF-κB through activating IKK, directly or indirectly via mTORC1 activation. Adapted from (Ghoneum and Said, 2019). Image made with items adapted from Servier Medical Art

In the previous chapter, I showed that Rab25 regulated the expression of ADAMTS5 in OC cell lines. Here I investigated the downstream transcription factors involved in this pathway. Interestingly, several TFs were identified to induce ADAMTS5 expression in osteoarthritis development (Kobayashi et al., 2013). Bioinformatic analysis using the TFSEARCH website identified binding motifs of HIF, NF-κB, C/EBP, STAT, SOX, RUNX, OCT and SP-1 on the proximal promoter of ADAMTS5. Vectors containing these putative TFs were transfected into mouse chondrogenic cells that expressed human ADAMTS5 promoter constructed with a luciferase reporter. As a result, cells with transfected TFs showed different levels of luciferase signal, which indicates ADAMTS5 promoter activation level. Among all TFs tested, an NF-κB family member, RelA(p65), showed the strongest activation ability. The interaction of RelA(p65) with ADAMTS5 promoter was further confirmed through chromatin immunoprecipitation (ChIP) assay. Additionally, the siRNA-mediated knockdown of RelA(p65) resulted in a significantly reduced ADAMTS5 expression. Furthermore, in primary chondrocytes derived from mesenchymal cell-specific RelA(p65) knock-out mice, ADAMTS5 expression was significantly reduced and the release of cleaved proteoglycan fragments in the culture media was decreased, indicating that loss of RelA(p65) function reduced the expression of ADAMTS5, resulting in loss of aggrecanase activity (Kobayashi et al., 2013). Although RelA(p65) was

found to activate ADAMTS5 expression, the role of Rab25 in regulating RelA(p65) or other NF- κ B family members is unclear. HIF-1 α can also interact with ADAMTS5 promoter and activate its expression. Meanwhile, Rab25 was found to promote HIF-1 α protein translation in OC cell lines, which contributed to Rab25-dependent aggressive phenotype of OC both in vitro and in vivo (Gomez-Roman et al., 2016).

In this chapter, I showed that NF- κ B inhibition resulted in the reduction of ADAMTS5 expression. Furthermore, Rab25 overexpression promoted the expression and nuclear translocation of NF- κ B in OC cell lines, while Rab25 knock-down reduced these. On the other hand, HIF-1 and hypoxia negatively regulated the expression of ADAMTS5, in a Rab25-independent manner. This data suggested that Rab25 induced ADAMTS5 expression through NF- κ B.

4.2. Results

4.2.1. HIF-1 inhibition reduced Rab25 and induced ADAMTS5 expression.

It was reported that Rab25 enhanced the translation of HIF-1 α protein in OC cells (Gomez-Roman et al., 2016), and HIF-1 α was found to bind to ADAMTS5 promoter and induce its expression (Kobayashi et al., 2013). Therefore, we hypothesised that Rab25 might promote ADAMTS5 expression by regulating HIF1 α -dependent transcription. To investigate this, OC cells were treated with a small molecule inhibitor targeting HIF-1 and the expression of ADAMTS5 was assessed. Echinomycin is a strong inhibitor of HIF-1 through competitive binding to the DNA-binding sequence of HIF-1 on the genome, without affecting the binding of other TFs such as NF- κ B (Kong et al., 2005). OVCAR3 cells, which endogenously over-express Rab25, and SKOV3 cells, which do not express Rab25, were used. Cells were treated with DMSO or Echinomycin up to a concentration of 25nM for 24h, as any higher concentration led to noticeable cell death (not shown). Surprisingly, a dose-dependent increase in ADAMTS5 expression levels was identified in both OVCAR3 and SKOV3 cells, up to 10nM Echinomycin, while 25nM reduced ADAMTS5 expression but not significantly ([Figure 4.3A](#)). Furthermore, the inhibition of HIF-1 also led to a decrease in Rab25 expression in OVCAR3 cells ([Figure 4.3B](#)). Altogether, these data indicated that inhibition of HIF-1 activity induced ADAMTS5 expression in a Rab25-independent manner, while it also reduced the expression of Rab25 in OC cells.

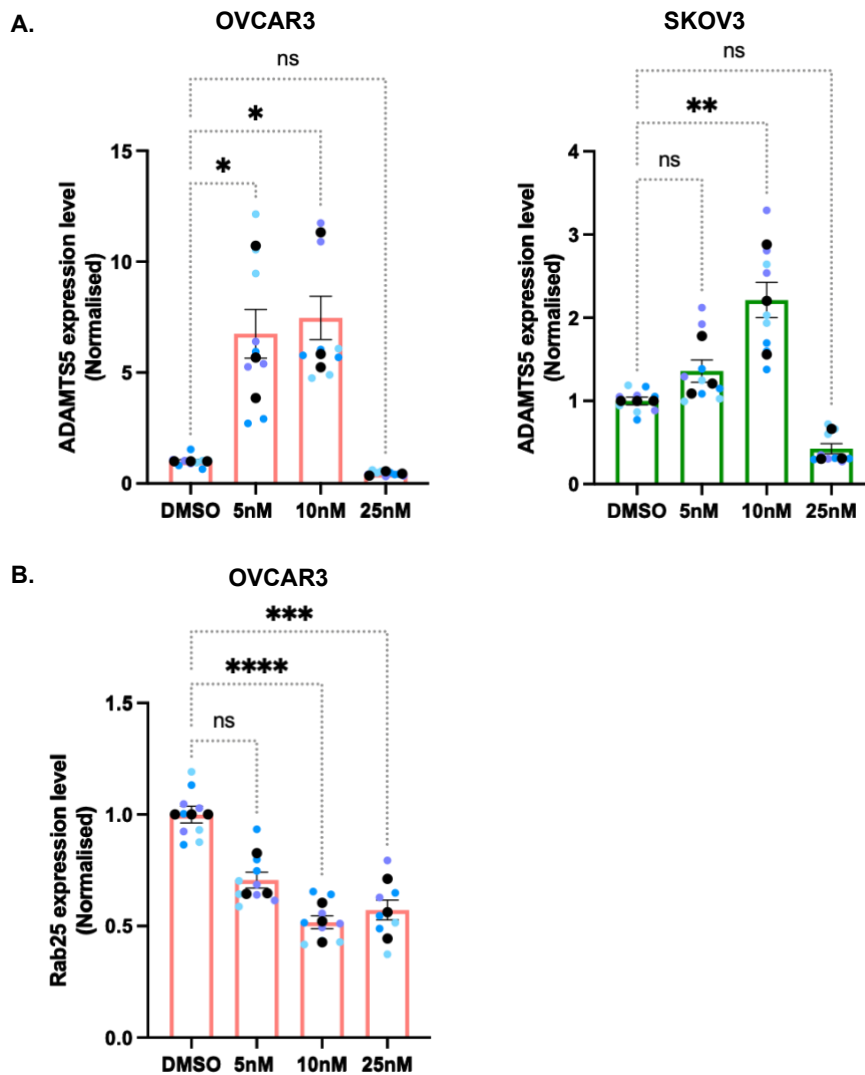


Figure 4.3. HIF-1 inhibition with Echinomycin induced ADAMTS5 and reduced Rab25 expression in OC cells. OVCAR3 and SKOV3 cells were seeded on plastic and treated with DMSO, 5, 10 or 25nM Echinomycin for 24h, the mRNA was extracted and ADAMTS5 (A) and Rab25 (B) expression was tested by SYBR-green based qPCR. GAPDH was used as the control housekeeping gene and the data were normalised to DMSO control. Data are presented as mean \pm SEM. N=3 independent experiments, the black dots represent the mean of individual experiments. * $p < 0.05$, ** $p = 0.0056$, *** $p = 0.0004$, **** $p < 0.0001$, Kruskal-Wallis test.

4.2.2. Hypoxia reduced Rab25 and ADAMTS5 expression.

To further elucidate the role of HIF-1 in regulating ADAMTS5 and Rab25 expression, OVCAR3, SKOV3, A2780-DNA3 and A2780-Rab25 cells were seeded on plastic overnight and then cultured in normoxia (20% O₂) or hypoxia (1% O₂) conditions for 24h. The induction of HIF-1 α upregulation by hypoxia was confirmed through western blotting (data not shown). ADAMTS5 and Rab25 expression levels in OVCAR3, SKOV3 and A2780 cells were assessed by qPCR. The mRNA level of ADAMTS5 in

all four cell lines, with and without Rab25 overexpression, was significantly reduced under hypoxic conditions (Figure 4.4A), which is consistent with the HIF-1 inhibition result (Figure 4.3A). However, Rab25 expression level was also reduced in OVCAR3 cells kept under hypoxia (Figure 4.4B), which contrasts with the HIF-1 pharmacological inhibitor result (Figure 4.3B). These results suggest that HIF-1 is inhibiting ADAMTS5 expression, but the role of HIF-1 in regulating Rab25 expression remains unclear.

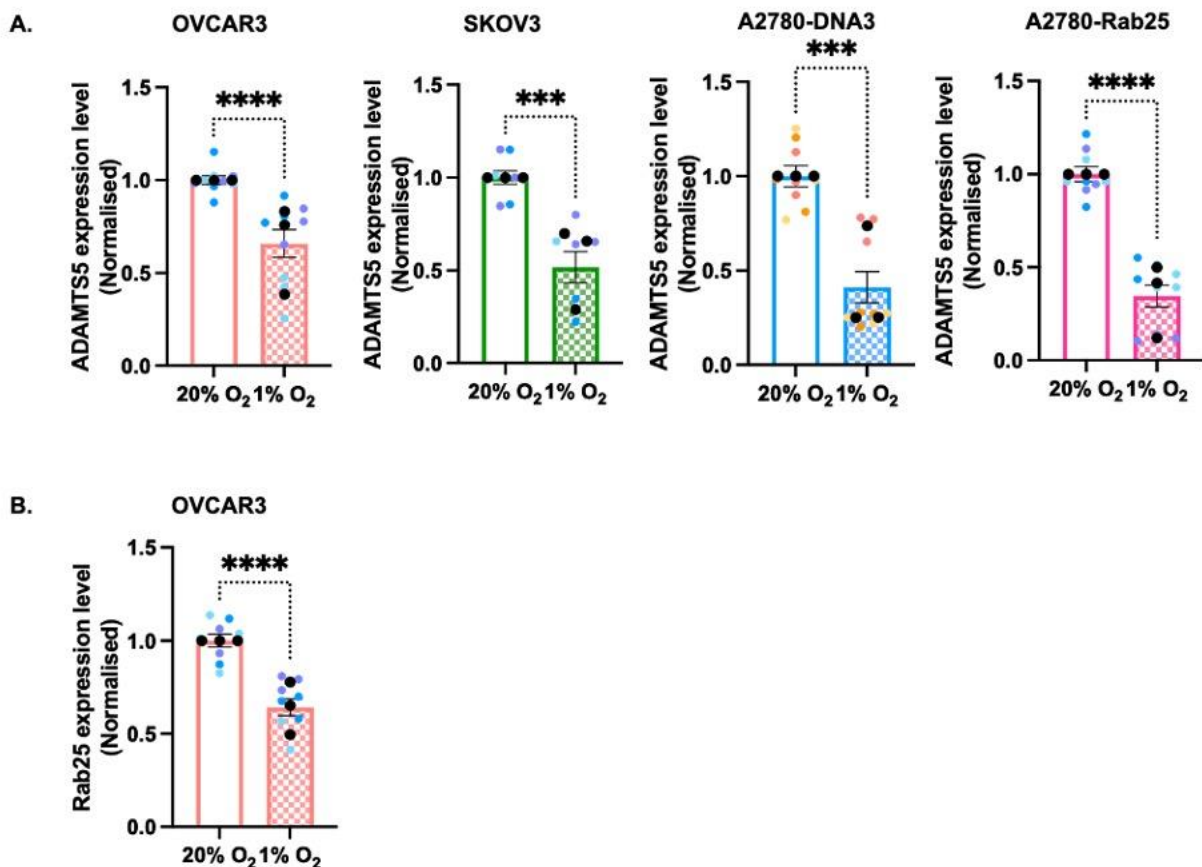


Figure 4.4. Hypoxia reduced both ADAMTS5 and Rab25 expression in OC cells. OVCAR3, SKOV3, A2780-DNA3 and Rab25 cells were seeded and incubated under Normoxia (20% O₂) or Hypoxia (1% O₂) for 24h. **A.** ADAMTS5 and **B.** Rab25 mRNA levels were measured by SYBR-green based qPCR. GAPDH was used as the control housekeeping gene and the data was normalised to 20% O₂ groups. Data are presented as mean \pm SEM. N=3 independent experiments, the black dots represent the mean of individual experiments. *** p<0.001, **** p<0.0001, Mann-Whitney test.

4.2.3. NF- κ B inhibition reduced ADAMTS5 expression.

Previous research by Kobayashi et al. (2013) showed that the NF- κ B family member RelA(p65) promoted ADAMTS5 expression in mouse and human chondrogenic cells. To investigate whether this was also the case in OC, cells were treated with an NF- κ B inhibitor, BAY 11-7082, and the

expression of ADAMTS5 was assessed by qPCR. BAY 11-7082 is a small molecule inhibitor that targets the IKK, reducing the phosphorylation of I κ B α and further inhibiting the release, nuclear translocation and DNA-binding of NF- κ B (Pierce et al., 1997). Previous experiments done in OC cell lines Caov-3 and A2780 identified significantly reduced phosphor-I κ B α levels upon the treatment of 5 μ M BAY 11-7082 (Mabuchi et al., 2004). OVCAR3 cells were seeded on plastic overnight and then treated with DMSO or BAY 11-7082 up to 10 μ M for 24h, while a higher concentration led to noticeable cell death (data not shown). As a result, ADAMTS5 expression level was reduced in a dose-dependent manner with BAY 11-7082 treatment, and the reduction was statistically significant for 5 and 10 μ M inhibitor (Figure 4.5A). The expression of Rab25 was not significantly affected by the inhibitor treatment (Figure 4.5B). This result indicates that NF- κ B regulated ADAMTS5 expression, suggesting that NF- κ B could be a potential signalling pathway involved in Rab25-dependent ADAMTS5 expression.

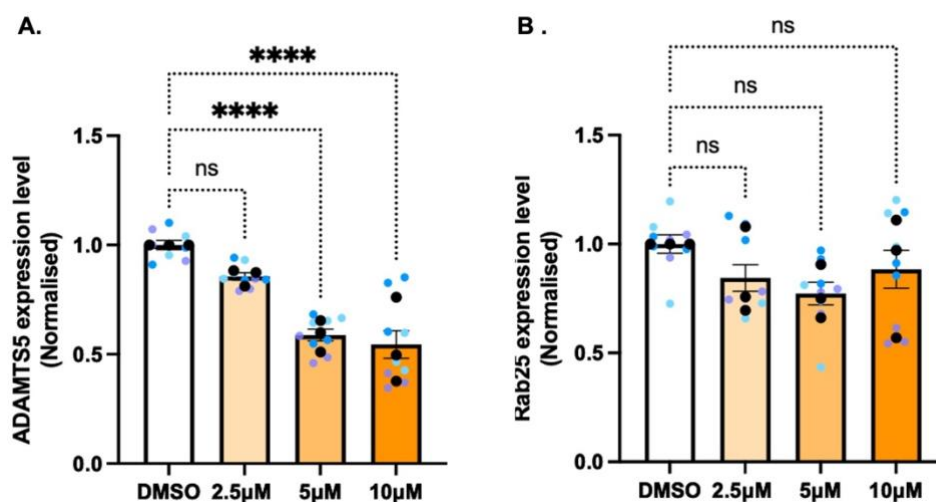


Figure 4.5. NF- κ B inhibition reduced ADAMTS5 expression in OVCAR3 cells in a dose-dependent manner. OVCAR3 cells were seeded and treated with DMSO, 2.5, 5 or 10 μ M of BAY 11-7082 for 24h. ADAMTS5 (A) and Rab25 (B) mRNA levels were measured by SYBR-green based qPCR. GAPDH was used as the control housekeeping gene and the data was normalised to DMSO control. Data are presented as mean \pm SEM. N=3 independent experiments, the black dots represent the mean of individual experiments. **** $p < 0.0001$, Kruskal-Wallis test.

4.2.4. Rab25 induced NF- κ B nuclear translocation.

Unlike HIF-1 α which was previously found regulated by Rab25 (Gomez-Roman et al., 2015), there is no evidence showing that the expression and translocation of NF- κ B were correlated with Rab25 expression. To investigate the role of Rab25 in regulating NF- κ B activation, the nuclear translocation

level of NF- κ B subunit p65 was measured using immunofluorescence, which is a well-established readout of NF- κ B activation (Meier-Soelch et al., 2021). A2780-DNA3 and A2780-Rab25 were seeded on glass-bottom confocal dishes overnight and the cells were stained for the actin cytoskeleton, nuclei and p65 (Figure 4.6A). The intensity of the NF- κ B signals in both the whole cell and the nucleus only were quantified as described in section 2.2.13. For the total integrated density was then divided by the cell area and the nucleus integrated density was divided by the nuclear area. In comparison to A2780-DNA3 cells, A2780-Rab25 cells showed higher overall and nuclear expression of NF- κ B (Figure 4.6B, C). To confirm this result, Rab25 KD was performed in OVCAR3 cells, and cells were fixed and stained for p65 (Figure 4.7A). In agreement with Rab25 overexpression results, Rab25 KD resulted in significantly lower NF- κ B expression and nuclear translocation (Figure 4.7B, C). Overall, this result indicated that Rab25 promoted NF- κ B activity in OC cells, which was not reported before.

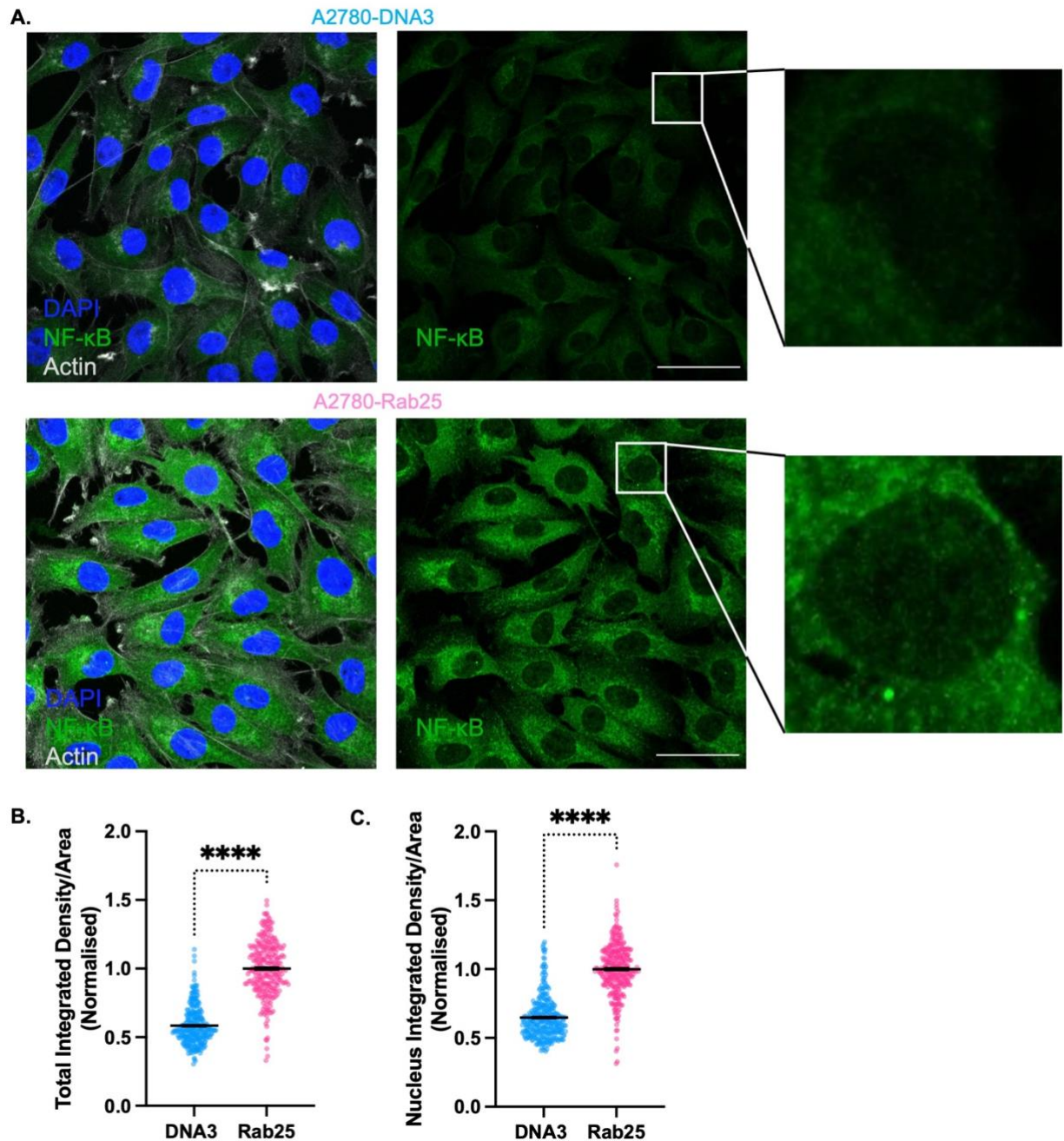


Figure 4.6. Rab25 overexpression induced the overall and nuclear level of NF-κB. **A.** A2780-DNA3 and A2780-Rab25 cells were seeded on glass bottom confocal dishes for 24h, fixed, stained for actin (grey), NF-κB (green) and nuclei (blue), and imaged with a Nikon A1 confocal microscope, CFI Plan Apochromat VX 60X oil immersion objective. NF-κB integrated density for the whole cell (**B.**) and the nucleus (**C.**) was calculated with image J and normalised to the area. Z-stacked images were maximum-projected. Scale bar: 50μm. Data are presented as mean ± SEM. N=3 independent experiments. **** $p < 0.0001$, Mann-Whitney test.

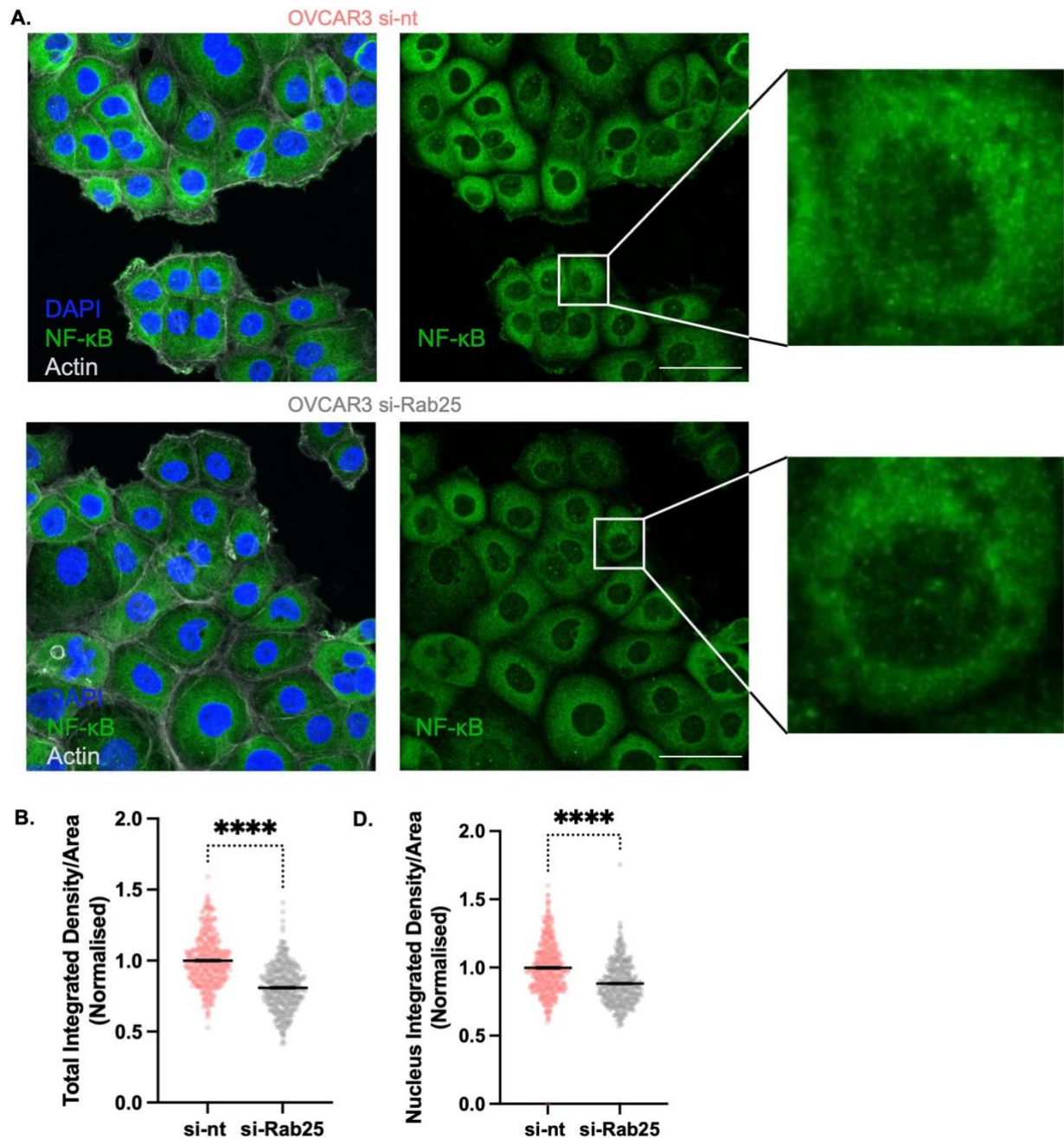


Figure 4.7. Rab25 KD reduced the overall and nuclear level of NF- κ B. **A.** OVCAR3 cells were transfected with non-targeting (si-nt) or Rab25 targeting si-RNA (si-Rab25) for 24h, reseeded on glass bottom dishes for 24h, fixed, stained for actin (grey), NF- κ B (green) and nuclei (blue), and imaged with a Nikon A1 confocal microscope, CFI Plan Apochromat VX 60X oil immersion objective. NF- κ B integrated density for the whole cell (**B.**) and the nucleus (**C.**) was calculated with image J and normalised to the area. Z-stacked images were maximum-projected. Scale bar: 50 μ m. Data are presented as mean \pm SEM. N=3 independent experiments. **** $p < 0.0001$, Mann-Whitney test.

4.2.5. PI3K inhibition reduced *ADAMTS5* expression.

Since NF- κ B was found activated via PI3K/AKT/mTOR pathway in multiple cancer types, including OC (Ghoneum and Said, 2019), here I investigated the role of PI3K/AKT signalling in *ADAMTS5*

expression. OVCAR3 cells were treated with the PI3K inhibitor LY294002 and the expression of ADAMTS5 and Rab25 was measured by qPCR. The effectiveness of the inhibitor treatment was confirmed by assessing AKT phosphorylation (Ser473) by western blotting. As expected, after a 24h treatment with LY294002, a dose-dependent inhibition of AKT phosphorylation was observed in OVCAR3 cells, with an undetectable phosphor-AKT band at 10 μ M LY294002 (Figure 4.8A). The expression of *ADAMTS5* was also reduced in a dose-dependent manner (Figure 4.8B), while the expression of *Rab25* was not affected (Figure 4.8C). This result is consistent with what has been observed with NF- κ B inhibition, which suggested that Rab25 could regulate ADAMTS5 expression through the PI3K/AKT/NF- κ B pathway.

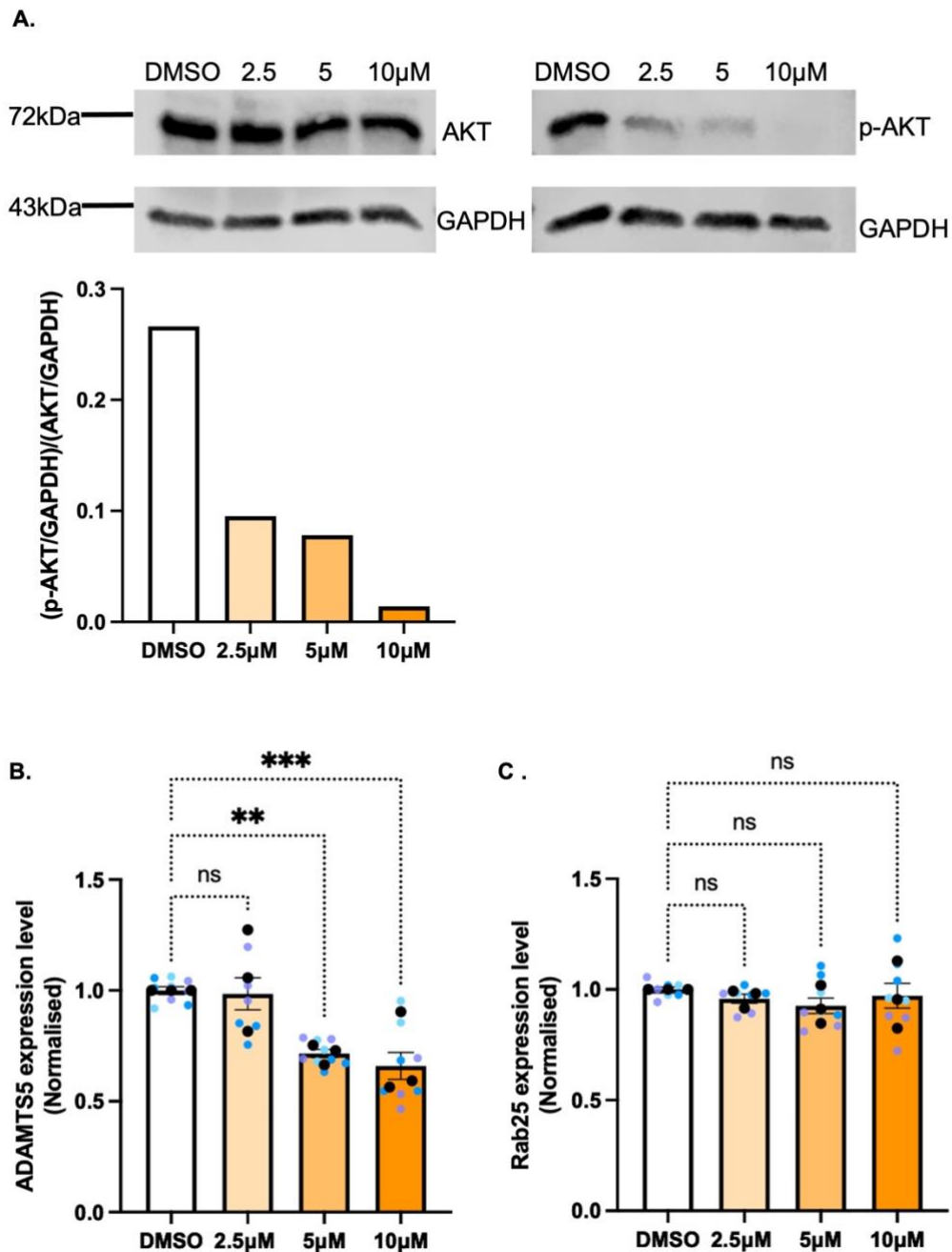


Figure 4.8. PI3K inhibition reduced ADAMTS5 expression in OVCAR3 cells in a dose-dependent manner. A. OVCAR3 cells were seeded overnight and treated with DMSO, 2.5, 5 or 10µM LY294002 for 24h. Cell lysates were analysed by western blotting. Membranes were stained for AKT, p-AKT, and GAPDH and imaged with a Licor Odyssey Sa system. The band intensity was quantified by Image Studio Lite software. AKT and p-AKT signal was normalised to the GAPDH loading control and the ratio of normalised p-AKT/AKT was calculated and plotted. N=1. **B, C.** Cells were treated as in (A), ADAMTS5 (B) and Rab25 (C) mRNA levels were measured by SYBR-green-based qPCR. GAPDH was used as the control housekeeping gene and the data were normalised to DMSO control. Data are presented as mean \pm SEM. N=3 independent experiments, the black dots represent the mean of individual experiments. **p=0.0021, ***p=0.0008, Kruskal-Wallis test.

4.2.6. Rab25 might regulate NF- κ B in an AKT-independent manner.

Previous research found that Rab25 is responsible for the activation of the PI3K/AKT signalling pathway, which resulted in chemotherapy resistance in OC (Fan et al., 2015). To investigate whether Rab25 controls NF- κ B through the PI3K pathway, the activity of AKT in response to Rab25 knockdown was assessed in OC cells. OVCAR3 cells were seeded overnight and transfected with non-targeting or Rab25 targeting siRNA and the protein levels of AKT and p-AKT (Ser473) were measured by western blotting. Surprisingly, p-AKT levels were not changed upon Rab25 KD in OVCAR3 cells (Figure 4.9). This result indicates that in our model, the expression of Rab25 did not affect the activation of AKT and therefore Rab25 did not control NF- κ B via AKT signalling.

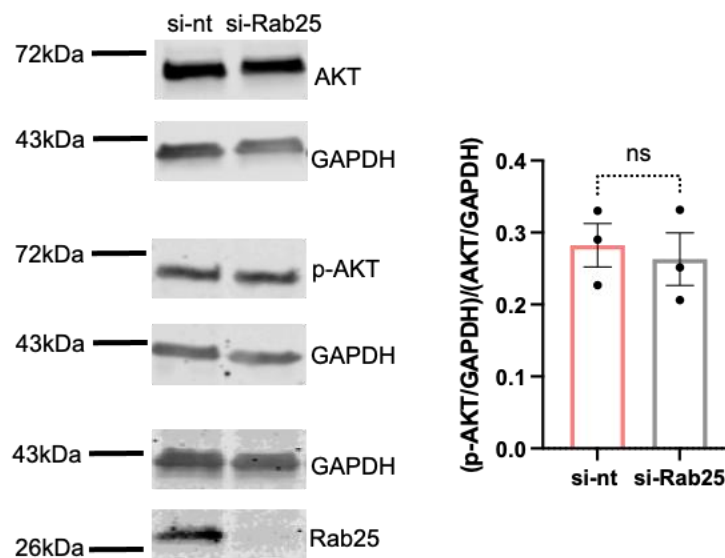


Figure 4.9. AKT phosphorylation was not affected by Rab25 KD. OVCAR3 cells were seeded and transfected with non-targeting siRNA (si-nt) or Rab25 targeting siRNA (si-Rab25) for 24h and cultured in complete media for 3 days. Cell lysates were collected on day 4 after transfection and analysed by western blotting. Membranes were stained for AKT, phospho-AKT (p-AKT), Rab25 and GAPDH, imaged with a Licor Odyssey Sa system, and the band intensity was quantified by Image Studio Lite software. AKT and p-AKT signal was normalised to the GAPDH loading control and the ratio of normalised p-AKT/ACT was calculated and plotted. Data are presented as mean \pm SEM. N=3 independent experiments. Mann-Whitney test.

4.3. Discussion

In this chapter, I investigated the mechanism through which Rab25 regulates ADAMTS5 expression in OC cells. Both HIF-1 α and NF- κ B RelA(p65) subunit were previously found to interact with the proximal promoter of ADAMTS5. Remarkably, the level of ADAMTS5 promoter activated by HIF-1 α was significantly higher than the control but was about 50-fold lower than the level activated by

RelA(p65) (Kobayashi et al., 2013). Interestingly, HIF-1 α was found to be regulated by Rab25 (Gomez-Roman et al., 2016). Here, my result suggested that HIF-1 α suppressed ADAMTS5 expression in OC cells, which contrasts with previous finding in chondrocytes (Kobayashi et al., 2013), suggesting that HIF-1 α might control ADAMTS5 expression in a context-dependent manner. The inhibition of HIF-1 with Echinomycin at low concentrations (5 or 10nM) upregulated the expression of ADAMTS5, and ADAMTS5 was downregulated under hypoxia. When treated with 25nM of Echinomycin, the reduction of ADMATS5 could be caused by off-target toxicity, as higher concentration led to noticeable cell death. Although it is not clear how HIF-1 might inhibit the expression of ADAMTS5, this process is likely Rab25-independent as a similar result was obtained with Rab25 non-expressing cells.

The expression of Rab25 in OVCAR3 cells was also reduced when treated with the HIF-1 inhibitor. However, a contradictory result was obtained under hypoxic conditions as the Rab25 expression level was downregulated. Additionally, stabilised HIF-1 α was not detected in Rab25 overexpressing OC cells under normoxia (data not shown), which is contrary to Gomez-Roman et al. (2016). It is also surprising that Rab25 as an oncogene that mediates OC development was found downregulated under hypoxia. It is not clear if the expression of any upstream regulating proteins of Rab25 and ADAMTS5 was altered under hypoxic conditions, which could be a research direction in the future.

Results show that the expression of ADAMTS5 was reduced when inhibiting the activity of NF- κ B with BAY 11-7082 in OC cells, which is consistent with the work done by (Kobayashi et al., 2013), showing that NF- κ B activated the expression of ADAMTS5 in chondrogenic cells. The NF- κ B family includes seven proteins encoded by five genes (Karin and Ben-Neriah, 2000), which function as hetero- or homodimers in activating transcription in mammalian cells. Since the dimers formed by different subunits show different binding and transcriptional activities, it is important to clarify different family members when investigating NF- κ B (Saccani et al., 2003). In the previous work by Kobayashi et al. (2013), vectors containing all NF- κ B family members were tested and RelA(p65) showed the highest activity in promoting ADAMTS5 expression. Moreover, co-transfection of RelA(p65) and NF- κ B1 strongly enhanced the activation of ADAMTS5 compared to RelA(p65) alone. *NF κ B1* encodes for p50 and the precursor p105. Upon stimulations, p105 is processed to be degraded and p50 is activated (Concetti and Wilson, 2018). Therefore, it is likely the NF- κ B

heterodimer p50/p65 induced the expression of ADAMTS5. Another possibility is that ADAMTS5 was activated by the homodimer of RelA(p65). However, in comparison with p50/p65, p65/p65 homodimers are unstable and less abundant in mammalian cells (Florio et al., 2022). Since the inhibitor used in this research, BAY 11-7082, is targeting IKK and inhibiting the phosphorylation of $\text{I}\kappa\text{B}\alpha$, it is not specifically blocking the activity of the p50/p65 dimer.

In addition to direct binding to the ADAMTS5 promoter, NF- κ B may also promote the expression of ADAMTS5 by regulating cytokine expression, such as IL-1, IL-6 and IL-8 (Hoesel and Schmid, 2013). In osteoarthritis, IL-1 β and IL-6 were found to induce the expression of ADAMTS5 through activating other TFs (Jiang et al., 2021). IL-1 β induces ADAMTS5 expression through AP-1, which reduces the expression of ADAMTS5 suppressor, miR-30a, in human chondrocytes (Ji et al., 2016). IL-6 stimulation of mouse chondrocytes induced ADAMTS5 expression through the activation of STAT3 (Latourte et al., 2017). In OC, a high IL-6 level was identified in malignant patient samples, which promoted metastasis and resulted in a poor prognosis (Coward et al., 2011, Browning et al., 2018). It would be interesting to further investigate the role of IL-1 and IL-6 in ADAMTS5 expression in OC and other cancer types.

The altered expression of Rab25 is also positively associated with the total and nuclear expression of the NF- κ B, which indicates that Rab25 may induce ADAMTS5 expression through the activation of NF- κ B in OC. Remarkably, the antibody used for the IF staining of NF- κ B (Figure 4.5) targeted the p65 subunit, so the level of other subunits was not checked. Since the total expression level of NF- κ B in the cytoplasm also increased significantly in OC cells overexpressing Rab25, it is hard to distinguish if Rab25 enhanced the translocation of NF- κ B or Rab25 increased the overall expression of NF- κ B, which led to the increased level of the subunits in the nucleus. Additionally, in combination with immunofluorescent staining and further characterisation of the activation of NF- κ B, the expression level of NF- κ B target genes such as *CXCL8* could be measured in the future experiment (Meier-Soelch et al., 2021).

The inhibition of PI3K with LY294002 indicated that the expression of ADAMTS5 is also regulated by the PI3K pathway, which was previously found to be mediated by Rab25 and led to cisplatin resistance in OC cells (Fan et al., 2015, Ding et al., 2017). Here, my result suggested that the

phosphorylation of AKT at Ser473 residues, which is mediated by the mTORC2 (Ghoneum and Said, 2019), was not affected by Rab25 KD in OVCAR3 cells. The correlation between Rab25 expression and AKT activation is controversial. In OC cells, Rainero et al. (2015) identified similar p-AKT-Ser473 levels in A2780-DNA3 and A2780-Rab25 cells. On the other hand, Rab25 KD reduced the phosphorylation of PI3K and AKT (Ser473) without affecting the total expression level in human glioblastoma multiforme cells (Ding et al., 2017). Remarkably, research by Fan et al. (2015) identified a higher p-AKT-Thr308 level in OC cells overexpressing Rab25, which was not checked in this research due to the limitation of time and antibody and could be tested in further research. Additionally, Fan et al. found that inhibiting the PI3K pathway with LY294002 also reduces the expression of Rab25, which was not observed in our result (Figure 4.8C). This discrepancy could be caused by the selection of cell lines. In Fan's research (2015), SKOV3 cells were used as Rab25 overexpressing cells in comparison with ES-2 cells which express lower levels of Rab25, while the expression of Rab25 was not detected in SKOV3 cells in our lab, which has been discussed in the previous chapter. Altogether, these results suggested that Rab25 may regulate NF- κ B through the PI3K signalling pathway and further mediate the expression of ADAMTS5. However, the intermediate regulators are still unclear.

As shown in Figure 4.2, NF- κ B can also be activated by mTORC1, which can be downstream of the PI3K/AKT pathway. In PTEN-null-prostate cancer cells, protein-protein interactions between mTORC1 and IKKs were identified through immunoprecipitation, together with increased phosphorylation of IKKs (Dan et al., 2008). In head and neck cancer cells, EGFR-mediated PI3K/AKT/mTOR pathway was also found to enhance the phosphorylation of IKKs and the activation of NF- κ B (Li et al., 2016). Additionally, the inhibitor specifically targeting mTORC1, Rapamycin, was found to reduce the activities of both IKKs and NF- κ B (Li et al., 2016, Dan et al., 2008). Since the PI3K inhibitor, LY294002 can also bind to and inhibit mTORC1 directly (Gharbi et al., 2007), the reduction of ADAMTS5 expression in OC cells with LY294002 treatment could be mediated by mTORC1 instead of PI3K. Furthermore, mTORC1 could be activated via several AKT-independent ways. For example, the activation of the mTORC1 pathway is highly dependent on the accessibility of nutrients, such as amino acids and glucose (Memmott and Dennis, 2009). Interestingly, OC cells overexpressing Rab25 show increased mTORC1 activation (Rainero et al., 2015). Enhanced recruitment of mTOR to the late endosome was also observed in A2780-Rab25 cells, which is integral for amino acid-mediated

mTORC1 activation (Efeyan et al., 2012). Therefore, Rab25 could mediate ADAMTS5 expression via NF- κ B activated by mTORC1. Further research could characterise the role of mTORC1 in regulating ADAMTS5.

In summary, in this chapter I reported that Rab25 induced ADAMTS5 expression in OC cells through NF- κ B, which could be activated via PI3K and mTOR pathways, while HIF-1 α negatively regulated the expression of ADAMTS5 (Figure 4.10).

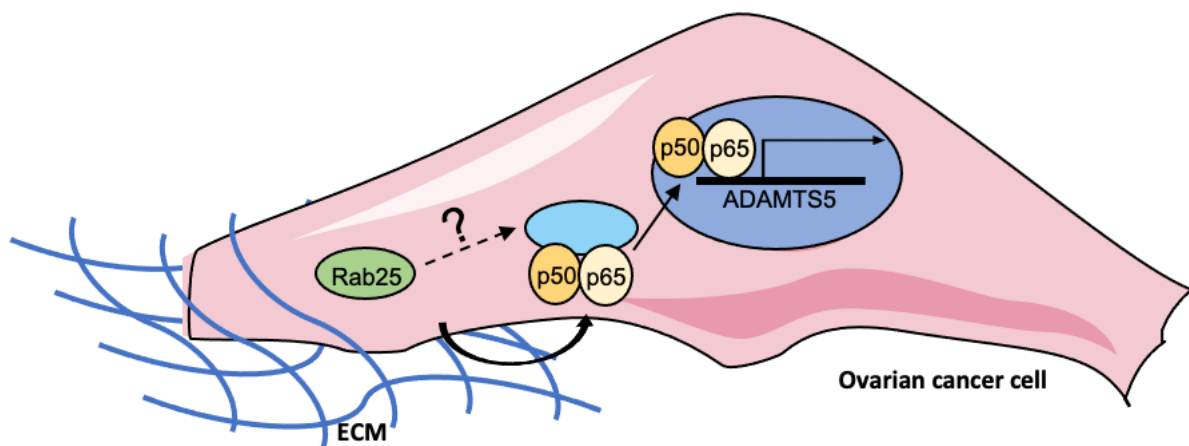


Figure 4.10. Schematic of the role of Rab25 in inducing ADAMTS5 expression through NF- κ B. Rab25 can promote the activation and translocation of NF- κ B, which in turn increases the expression of ADAMTS5. NF- κ B activation could be mediated by PI3K/mTOR signalling. Dashed arrows indicate indirect activation. Image made with items adapted from Servier Medical Art.

Chapter 5 – Inhibition of ADAMTS5 showed limited effect on OC cell proliferation.

5.1. Introduction

The ability to proliferate continuously is one of the most fundamental features of cancer cells. Unlike normal cells, which regulate cell growth signalling pathways strictly by producing and releasing GFs upon stimulation, proliferative signalling pathways in cancer cells are deregulated, which is one of the outstanding hallmarks of cancer (Hanahan and Weinberg, 2011). Cancer cells obtain the capacity to proliferate continuously in multiple ways. They can either generate GFs by themselves, or stimulate the surrounding cells in the TME, such as CAFs, to release GFs to support their proliferation (Cheng et al., 2008, Bhowmick et al., 2004). Additionally, altered numbers and structures of GF receptors were identified on cancer cell membrane, which also elevates the activation of cell growth signalling pathways (Hanahan and Weinberg, 2011).

CAFs were found to promote cancer cell growth by secreting multiple types of GFs, including TGF- β , FGF2/7, VEGF and HGF (Wu et al., 2021). CAFs isolated from OC tumour stroma release a significantly higher level of HGF compared to normal fibroblasts, and CAF-derived HGF was found to promote the proliferation of OC cell lines SKOV3 and HO-8910 via upregulating the c-Met/PI3K/AKT signalling pathway. CAFs can also promote OC cell proliferation by secreting microRNAs, such as miRNA-29c-3p and miRNA-98-5p (Han et al., 2023, Guo et al., 2019). Cytokines secreted by CAFs, including IL-6, COX-2 and CXCL-1, were also found to support the growth of OC via activating NF- κ B mediated gene expression (Erez et al., 2013). Furthermore, CAFs can promote the proliferation of cancer cells by secreting and remodelling ECM around cancer cells. Upregulated MMP9 secretion by CAFs was found in co-culture with breast cancer cells, which promoted tumour proliferation, angiogenesis and metastasis (Stuelten et al., 2005, Suh et al., 2018). Additionally, CAFs were found to promote drug resistance of OC cells. CAF-derived miRNA-98-5p was found to promote Cisplatin resistance of OC cells both in vitro and in vivo (Guo et al., 2019). When plated on CAF-CDM, OC cells show a higher resistance to paclitaxel-induced apoptosis than on plastic (Deying et al., 2017). Considering the critical role of CAFs in supporting cancer cell growth, targeting CAFs and the factors mediating their crosstalk with cancer cells are considered for cancer treatment (Wu et al., 2021).

To support the continuous proliferation, the metabolism of the cancer cells is altered to obtain sufficient energy in a nutrient-poor TME. In normal cells, glucose metabolism is highly dependent on the oxygen level. Under aerobic conditions, pyruvate is generated from glucose via glycolysis and then enters the mitochondria and produces ATP through the tricarboxylic acid (TCA) cycle. Alternatively, under hypoxic conditions pyruvate undergoes an anaerobic glycolysis, is converted into lactate and produces less amount of ATP (Warburg et al., 1927). However, cancer cells were found to favour glycolysis regardless of the presence of oxygen, which is termed aerobic glycolysis. Although this metabolic way allows cancer cells to produce ATP faster, the amount of ATP per glucose generated is about 18-fold lower than the TCA cycle (Pfeiffer et al., 2001). To compensate for this difference, upregulated glucose uptake was observed in cancer cells (Murakami et al., 1992). GFs are also essential in mediating nutrient consumption to support the growth of cancer cells in a nutrient-poor environment (Thompson and Bielska, 2019). Indeed, the PI3K/AKT/mTOR pathway activated by GFs was found to enhance glucose uptake by promoting the activation of glucose transporter GLUT1 and preventing the recycling and internalization of GLUT1 mediated by Rab11a (Wieman et al., 2007).

Apart from altered metabolism, cancer cells can also internalise and break down ECM as a nutrient source to adapt to the nutrient-poor environment. Breast cancer cells were found to internalise matrix protein laminin through binding with integrin $\beta 4$ under nutrient restrictions, which further enhanced mTORC1 signalling and rescued cell survival (Muranen et al., 2017). Similarly, previous research in our lab demonstrated that the ECM supported breast cancer cell growth under nutrient deficiency. The presence of collagen I, matrigel and CAF-CDM partially rescued the growth of invasive breast cancer cells under glutamine and amino acid starvation through ECM internalisation and degradation, which further enhanced the phenylalanine and tyrosine metabolism (Nazemi et al., 2024).

Preliminary results obtained by Dr E. Rainero showed that in OC cells with ADAMTS5 KD, a significantly reduced ECM internalisation was observed, which suggested ADAMTS5 was required for ECM uptake. Therefore, ECM remodelling by ADAMTS5 might also contribute to ECM-dependent cell growth. In this chapter, I characterised the effect of ADAMTS5 inhibition on OC cell proliferation and showed that ADAMTS5 pharmacological inhibition only affected OC cell growth at high

concentrations, in the presence and absence of ECM. CAFs, but not TIFs, were found to promote the growth of OC cells, which also reduced the sensitivity of OC cells to the ADAMTS5 inhibitor. When in glucose and serum deficiency, OC cells treated with ADAMTS5 inhibitor showed worse proliferation, and the presence of ECM failed to rescue the proliferation of OC cells under ADAMTS5 inhibition.

5.2. Result

5.2.1. High concentration ADAMTS5 inhibitor affected OC cell proliferation.

The effect of ADAMTS5 inhibitor on OC cell proliferation was tested in A2780-DNA3 and A2780-Rab25 cells. Since it was known that ECM supports the growth of cancer cells (Bonnans et al., 2014), A2780-DNA3 and A2780-Rab25 cells were seeded on either plastic or dishes coated with matrigel. The cells were treated with DMSO or different concentrations of ADAMTS5 inhibitor and cell proliferation was measured by DRAQ5 nuclear staining on day 2, day 4 and day 6 (see section 2.2.8.1). The experimental design is shown in [Figure 5.1A](#).

As a result, the inhibition of ADAMTS5 did not affect the proliferation of both A2780-DNA3 and A2780-Rab25 cells at concentrations up to 5 μ M on matrigel. A significant reduction in cell growth was only observed in A2780-Rab25 but not A2780-DNA3 cells when cells were plated on plastic and treated with 5 μ M ADAMTS5 inhibitor. However, in the presence of 10 μ M inhibitor, a significantly reduced proliferation was identified in both A2780-DNA3 and Rab25 cells both on plastic and matrigel ([Figure 5.1B i, ii, iii, iv](#)). Notably, when seeded on matrigel, A2780-DNA3, but not A2780-Rab25, cells showed reduced proliferation on day 6 compared to plastic ([Figure 5.1B iii, iv](#)). These results suggested ADAMTS5 might control cell proliferation in a Rab25-dependent manner.

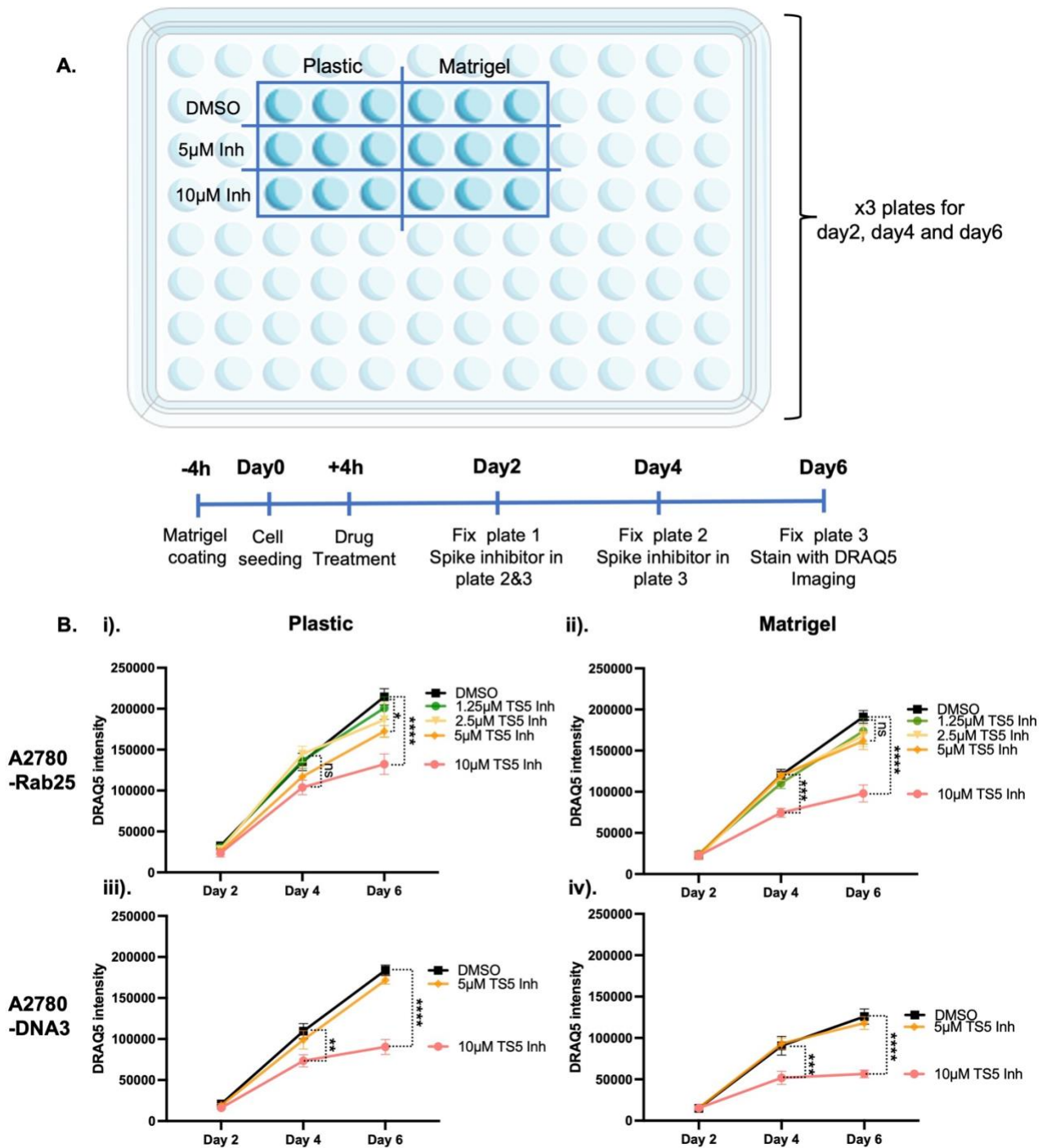


Figure 5.1. High concentration ADAMTS5 inhibitor inhibited cell growth. **A.** Schematic of experimental design. 96-well plates were coated with 3mg/mL matrigel and incubated at 37°C for polymerisation for 4h. 600 A2780-DNA3 and A2780-Rab25 cells per well were seeded and cultured for up to 6 days in the presence of DMSO, 1.25, 2.5, 5 or 10µM of ADAMTS5 inhibitor. The inhibitor was added after 4h of seeding and was supplied every two days. Cells were fixed on day 2, day 4 and day 6 and stained with DRAQ5. Cells were imaged with a Licor Odyssey Sa system, and the intensity of each well was quantified by Image Studio Lite software. **B.** Data are presented as mean \pm SEM. N=3 independent experiments. * $p=0.0363$, ** $p=0.0015$, *** $p<0.001$, **** $p<0.0001$, two-way ANOVA, Tukey's multiple comparisons test.

5.2.2. Co-culture with CAFs promoted OVCAR3 cell proliferation.

Considering that CAFs promote the growth and drug resistance of the OC cells (Deying et al., 2017, Guo et al., 2019, Han et al., 2023), co-culture proliferation assays were performed to further investigate the effect of ADAMTS5 inhibition on OC cell growth. The proliferation ability of OVCAR3 and CAFs alone or in co-culture was tested in the presence of DMSO or ADAMTS5 inhibitor. To distinguish between the two cell lines, OVCAR3 cells expressing nuclear GFP (generated as described in [section 2.2.2](#)) were combined with unlabelled CAFs and both cell lines were stained with Hoechst and imaged live. During imaging, OVCAR3 cells show both Hoechst and GFP fluorescence while CAFs only show Hoechst fluorescence. To minimize the effect on the proliferation caused by the different cell numbers, the total seeding number of the cells in each well was kept constant. The total seeding number and the ratio of OVCAR3/CAFs were optimized to reach the best cell growth (data not shown). For OVCAR3 cells and CAFs cultured alone, 6,000 cells per well were seeded. For co-culture, 4,000 OVCAR3 cells and 2,000 CAFs per well were seeded. The schematic of the experimental design is shown in [Figure 5.2A](#).

Consistent with the results obtained with A2780 cells ([Figure 5.1B i, iii](#)), the proliferation of OVCAR3 was significantly reduced by ADAMTS5 inhibitor at 10 μ M but not at 5 μ M ([Figure 5.2B i](#)). When co-cultured with CAFs, OVCAR3 cells showed an overall higher growth rate at day 8 compared to the monoculture ([Figure 5.2B ii](#)), which indicates that CAFs promoted the proliferation of OVCAR3 cells. The inhibition of ADAMTS5 reduced the proliferation of co-cultured OVCAR3 cells, to a similar extent than in OVCAR3 alone. Furthermore, CAF proliferation was not affected by ADAMTS5 inhibition when cultured alone ([Figure 5.2B iii](#)), while the co-culture with OVCAR3 increased the sensitivity of CAFs to 10 μ M ADAMTS5 inhibitor and led to a small but significant reduction of cell growth ([Figure 5.2B iv](#)). Notably, the reduction of CAF proliferation under co-culture when treated with ADAMTS5 inhibitor is mild in comparison to the proliferation reduction of OVCAR3 cells. Altogether, these results showed that when treated with ADAMTS5 inhibitor at a high concentration, the proliferation of OVCAR3 cells was also reduced. When in contact with CAFs, OVCAR3 cells showed better growth compared to the monoculture, with and without ADAMTS5 inhibition.

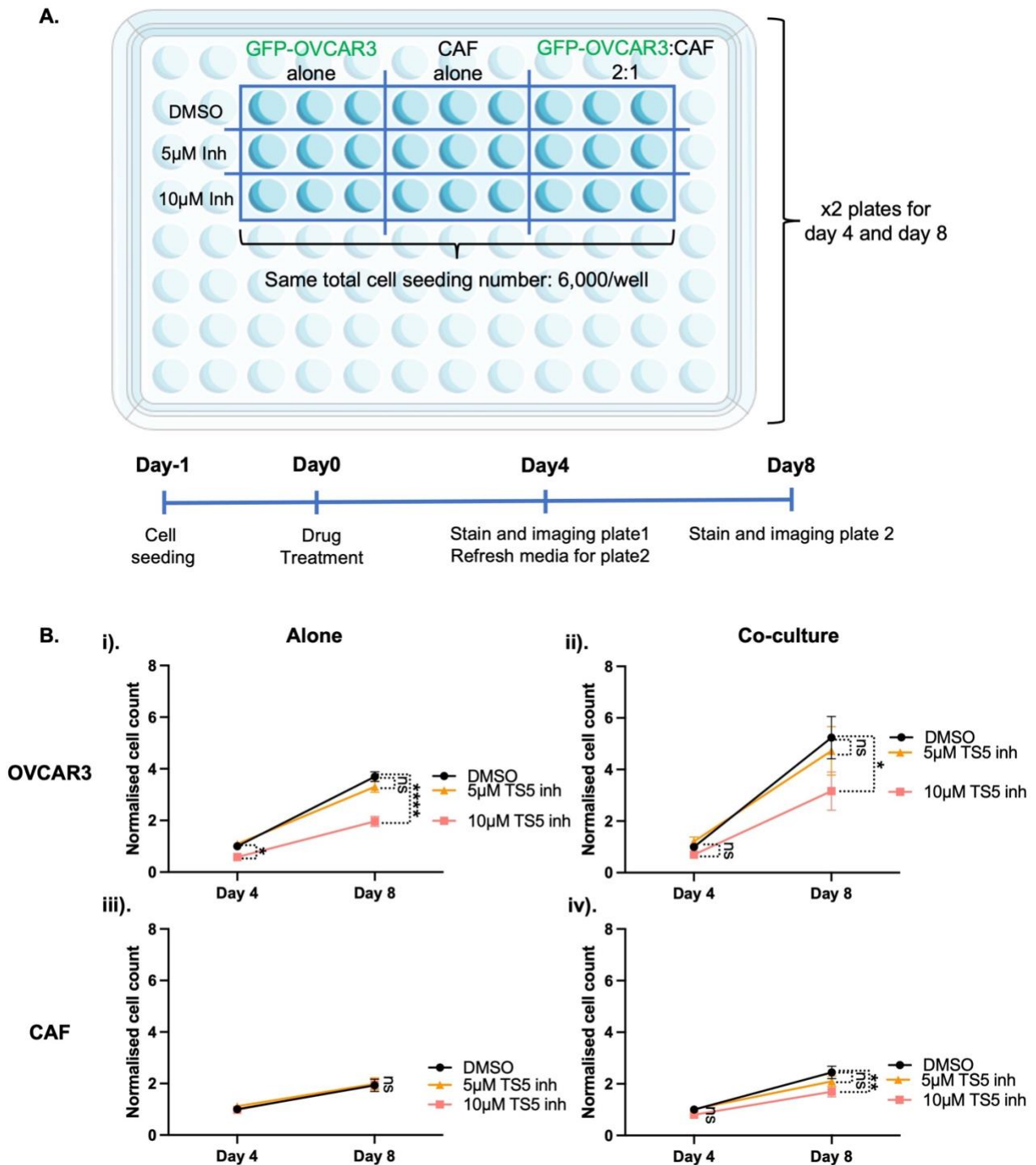


Figure 5.2. Proliferation of OVCAR3 cells was promoted by CAFs and inhibited by high concentrations of ADAMTS5 inhibitor. **A.** Schematic of the experimental design. 6,000 GFP-OVCAR3 and CAF cells were seeded alone, or 4,000 GFP-OVCAR3 together with 2,000 CAF cells were seeded on 96-well glass bottom plates and allowed to attach overnight. Then, DMSO, 5 or 10µM of ADAMTS5 inhibitor was added to the cells and refreshed on day 4. On day 4 and day 8, cells were live stained with Hoechst nuclear staining for 15 min and then imaged with ImageXpress micro and analysed by MetaXpress software as described in section 2.2.8.2. **B.** For OVCAR3 (**i**) and CAF cells (**iii**) cultured alone, the cell counts were obtained based on the Hoechst signal. For co-culture (**ii**, **iv**), the cell counts of OVCAR3 cells were obtained based on the GFP signal and CAF cells were obtained by Hoechst minus GFP. Data are normalised to DMSO day 4 as the control group and presented as mean \pm SEM. N=3 independent experiments. * $p < 0.05$, ** $p = 0.0047$, **** $p < 0.0001$, two-way ANOVA, Tukey's multiple comparisons test.

5.2.3. TIFs failed to promote the proliferation of OVCAR3 cells.

Unlike CAFs that enhance the growth of cancer cells, normal fibroblast-derived matrix showed limited promotion or even inhibition of cancer cell proliferation (Kaukonen et al., 2016, Nazemi et al., 2024). Here, I further performed the co-culture proliferation assay with OVCAR3 cells and TIFs. Again, GFP-OVCAR3 cells and TIFs were cultured alone or together in the presence of DMSO or ADAMTS5 inhibitor (Figure 5.3A). When 6,000 TIFs per well were seeded, the cells were over-confluent at day 8, which affected both cell proliferation and data analysis (not shown). Therefore, the total cell seeding number was reduced to 4,500 for monoculture, and for cells in co-culture, 3,000 OVCAR3 cells and 1,500 TIFs per well were seeded.

A similar inhibition of OVCAR3 cell proliferation in the presence of 10 μ M ADAMTS5 inhibitor was observed, indicating that the reduction of total cell seeding number did not affect OVCAR3 proliferation or the sensitivity to ADAMTS5 inhibitor (Figure 5.3B i). When co-cultured with TIFs, OVCAR3 shows reduced overall proliferation (Figure 5.3B ii), which is the opposite compared to the co-culture with CAFs (Figure 5.2B ii). When treated with 5 μ M ADAMTS5 inhibitor in co-culture with TIFs, the proliferation of OVCAR3 on day 8 was significantly reduced compared to DMSO control, which was not observed when cultured alone (Figure 5.3B i) or in co-culture with CAFs (Figure 5.2B ii). This result suggests that OVCAR3 showed increased sensitivity to ADAMTS5 inhibition when co-cultured with TIFs. Surprisingly, the proliferation of TIFs was suppressed by both 5 and 10 μ M of ADAMTS5 inhibitor (Figure 5.3B iii). Additionally, the co-culture with OVCAR3 promoted the proliferation of TIFs compared to the monoculture, while this promotion was suppressed with ADAMTS5 inhibition (Figure 5.3B iv).

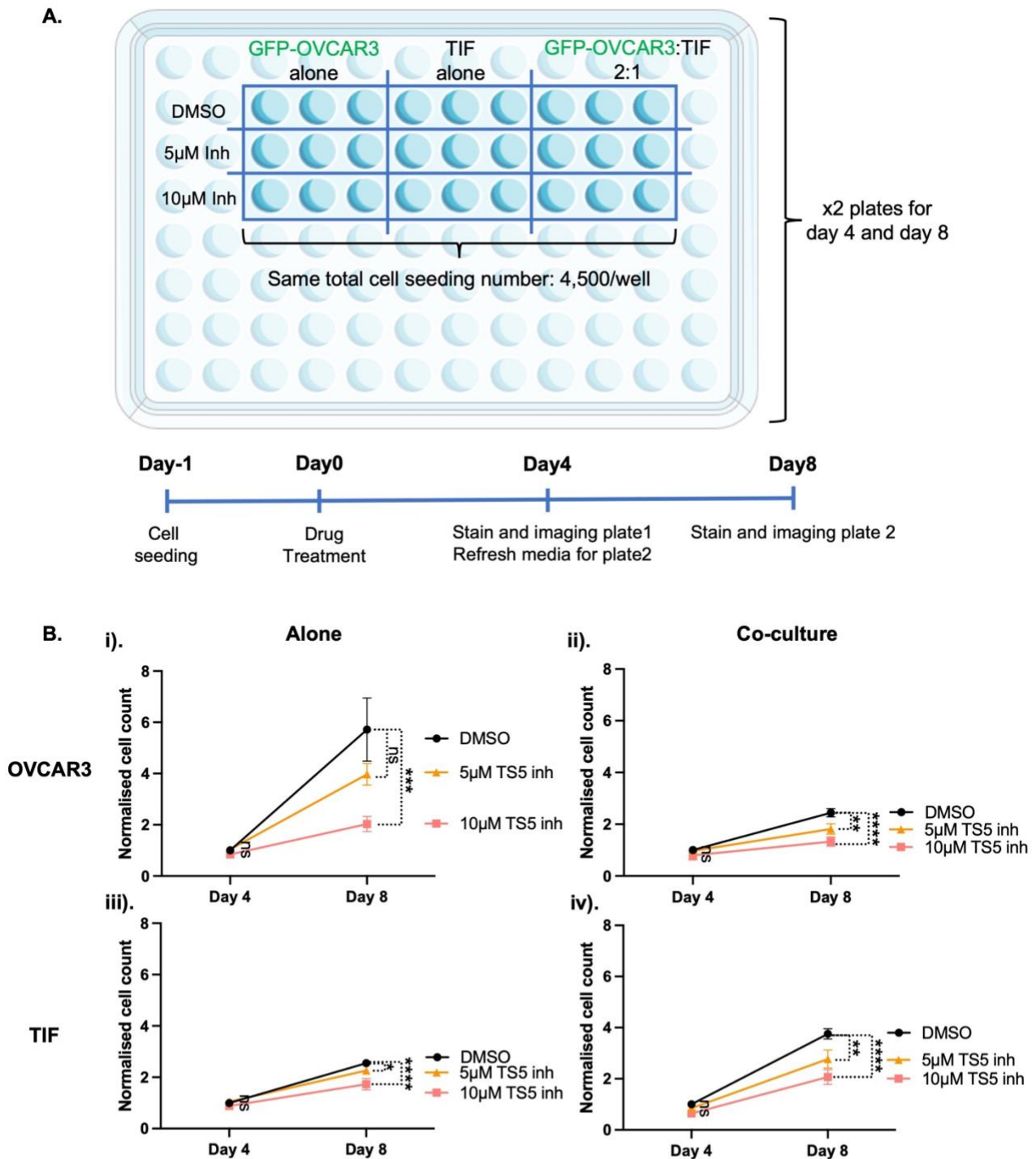


Figure 5.3. ADAMTS5 inhibitor concentration optimization. **A.** Schematic of experiment design. 4,500 GFP-OVCAR3 and TIF cells were seeded alone, and 3,000 GFP-OVCAR3 together with 1,500 TIF cells were seeded for co-culture on 96-well glass bottom dishes and allowed to attach overnight. Then, DMSO, 5 or 10µM of ADAMTS5 inhibitor was added to the cells and refreshed on day 4. On day 4 and day 8, cells were live-stained with Hoechst nuclear staining for 15 min and then imaged with ImageXpress micro and analysed by MetaXpress software as described in section 2.2.8.2. **B.** For OVCAR3 and TIF cells cultured alone, the cell counts were obtained based on the DAPI signal. For co-culture, the cell counts of OVCAR3 cells were obtained based on the GFP signal and TIF cells were obtained by DAPI minus GFP. Data are normalised to DMSO day 4 as the control group and presented as mean \pm SEM. N=2 independent experiments. * $p < 0.05$, ** $p < 0.005$, *** $p < 0.001$, **** $p < 0.0001$, two-way ANOVA, Tukey's multiple comparisons test.

Figure 5.3. TIFs failed to promote the proliferation of OVCAR3 cells. **A.** Schematic of the experimental design. 4,500 GFP-OVCAR3 and TIF cells were seeded alone, or 3,000 GFP-OVCAR3 together with 1,500 TIF cells were seeded in 96-well glass bottom plates and allowed to attach overnight. Then, DMSO, 5 or 10µM of ADAMTS5

inhibitor was added to the cells and refreshed on day 4. On day 4 and day 8, cells were live stained with Hoechst nuclear staining for 15 min and then imaged with ImageXpress micro and analysed by MetaXpress software as described in section 2.2.8.2. **B.** For OVCAR3 cells **(i)** and TIFs **(iii)** cultured alone, the cell counts were obtained based on the Hoechst signal. For co-culture **(ii, iv)**, the cell counts of OVCAR3 cells were obtained based on the GFP signal and TIF cells were obtained by Hoechst minus GFP. Data are normalised to DMSO day 4 as the control group and presented as mean \pm SEM. N=2 independent experiments. *p=0.025, **p<0.005, ***p=0.0001, **** p<0.0001, two-way ANOVA, Tukey's multiple comparisons test.

5.2.4. Glucose and serum starvation increased the sensitivity of OC cells to ADAMTS5 inhibition.

Similar to other cancer types, OC cells were found to obtain energy via aerobic glycolysis, resulting low-glucose concentrations in the TME (Lin et al., 2022). Furthermore, a significantly lower glucose level was also identified in ascites from malignant OC patients in comparison to the ascites from cirrhosis patients (Shender et al., 2014). Since cancer cells were found to internalise ECM to support cell growth under nutrient starvation (Muranen et al., 2017, Nazemi et al., 2024), and ADAMTS5 was found to be required for ECM uptake (data not shown), here I wanted to investigate the effects of ADAMTS5 inhibition on OC cell proliferation under glucose, serum or glutamine starvation, with and without ECM. The growth of A2780-DNA3 and A2780-Rab25 cells under starvation was first optimised. Media with glucose or glutamine deprivation, 2.5mM glucose or 0.5mM glutamine (25% of the complete media) led to complete cell death on plastic (data not shown). Therefore, media containing 1mM glutamine, 5mM glucose and 5% serum (50% of the complete media) was used for starvation conditions. A2780-DNA3 and A2780-Rab25 cells were seeded on plastic or matrigel and allowed to attach. Then, the cells were cultured in starvation media containing DMSO or 5 μ M of the ADAMTS5 inhibitor and the proliferation was measured on day 2, day 4 and day 6. The experimental plan is shown in [Figure 5.4A](#).

When plated on matrigel, the proliferation of A2780-DNA3 but not A2780-Rab25 was reduced in comparison to cells grown on plastic, as previously shown in [Figure 5.1B](#). A2780-Rab25 cells on plastic showed a significant reduction in proliferation when treated with ADAMTS5 inhibitor compared to DMSO control ([Figure 5.4B i](#)). The proliferation of A2780-DNA3 cells on plastic and matrigel and the A2780-Rab25 cells on matrigel was not affected by 5 μ M ADAMTS5 inhibitor in full media, consistent with my previous observations ([Figure 5.1B](#)). Under glucose starvation, ADAMTS5 inhibition significantly reduced the proliferation of both A2780-DNA3 and Rab25 cells, both on

plastic and matrigel (Figure 5.4B iii, iv). Under serum starvation, both of the cell lines showed a significantly reduced proliferation when treated with ADAMTS5 inhibitor on plastic, while on matrigel A2780-Rab25 grew more than A2780-DNA3 cells and this increase in proliferation was completely blunted by ADAMTS5 inhibition (Figure 5.4B v, vi). These results suggested that ADAMTS5 could play a role in controlling cell proliferation under limiting nutrient conditions.

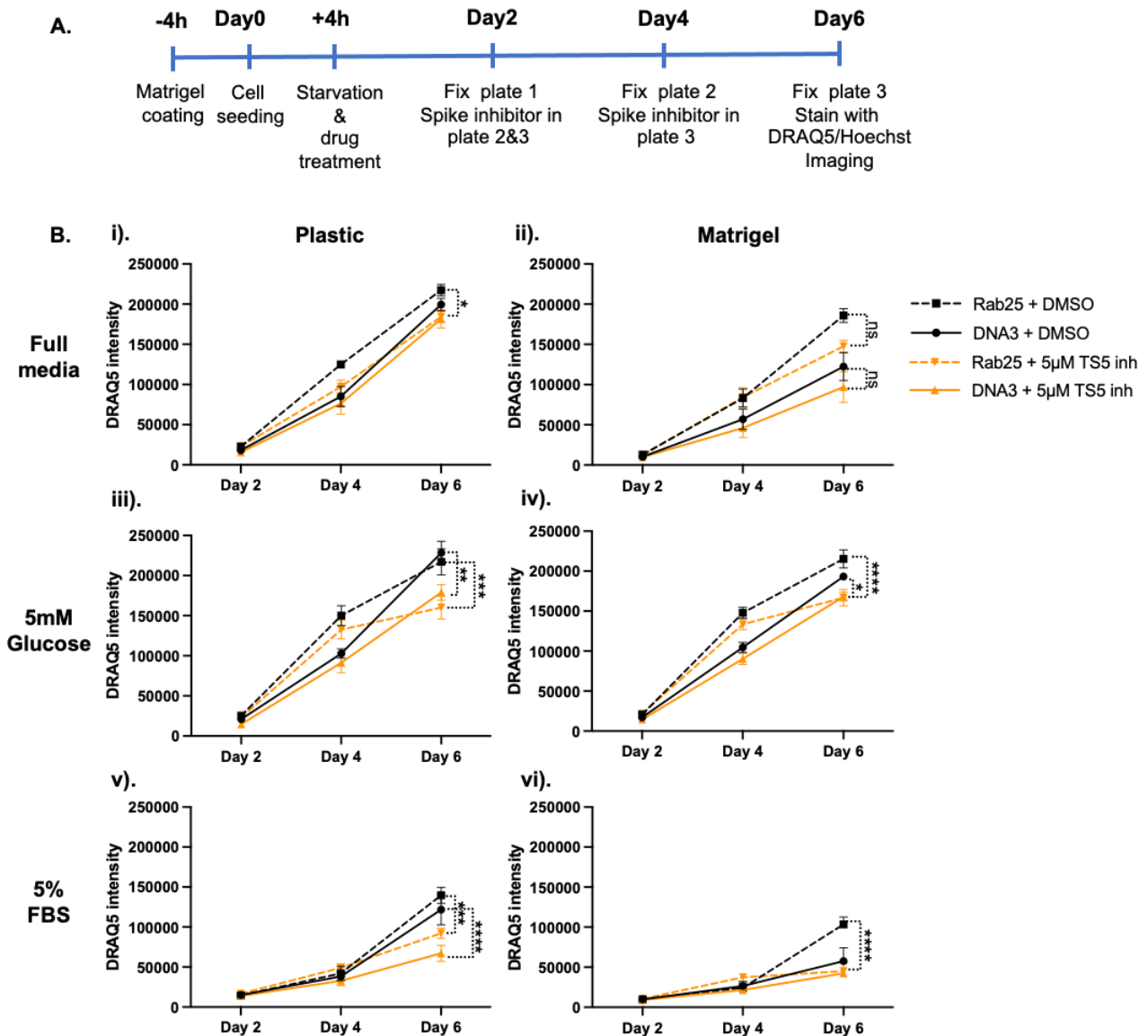


Figure 5.4. ADAMTS5 inhibitor reduced the proliferation of A2780 cells under glucose or serum starvation. **A.** Schematic of the experimental design. 96-well plates were coated with 3mg/mL matrigel and incubated at 37°C for polymerisation for 4h. 600 A2780-DNA3 and A2780-Rab25 cells per well were seeded on plastic or matrigel, allowed to attach for 4h and treated with complete or starvation media (media containing 5mM glucose or 5% FBS) in the presence of DMSO or 5µM of ADAMTS5 inhibitor (TS5 inh). The inhibitor was supplied every two days. Cells were fixed on day 2, day 4 and day 6 and stained with DRAQ5. The cells were then imaged with a Licor Odyssey Sa system, and the intensity of each well was quantified by Image Studio Lite software. **B.** Data are presented as mean \pm SEM. N=3 independent experiments. * p <0.05, ** p =0.0058, *** p <0.001, **** p <0.0001, two-way ANOVA, Tukey's multiple comparisons test.

To further validate these results, A2780 cells were seeded on plastic or TIF-CDM (generated as described in [section 2.2.3](#)) under the same starvation conditions and treated with DMSO or 5 μ M ADAMTS5 inhibitor. The nucleus was stained with Hoechst and the cell count was obtained with ImageXpress on day 2, day 4 and day 6 ([see section 2.2.8.1](#)), which is more sensitive compared to the measurement of DRAQ5 intensity.

When plated on TIF-CDM, the proliferation of both A2780-DNA3 and A2780-Rab25 was reduced in comparison to cells grown on plastic, which is consistent with results from Kaukonen et al. (2016) and suggest that TIF-CDM suppresses the growth of OC cells. Surprisingly, significantly reduced A2780-DNA3 and Rab25 cell counts were obtained on both plastic and TIF-CDM when treated with 5 μ M ADAMTS5 inhibitor ([Figure 5.5B i, ii](#)), which was not obtained with DRAQ5 staining ([Figure 5.4B i, ii](#)). Under glucose starvation, ADAMTS5 inhibition significantly reduced the proliferation of both cell lines on either plastic or TIF-CDM ([Figure 5.5B iii, iv](#)). Under serum starvation, both cell lines showed a significantly reduced proliferation when treated with ADAMTS5 inhibitor on plastic, while on TIF-CDM A2780-Rab25 grew more than A2780-DNA3 cells and this increase in proliferation was completely blunted by ADAMTS5 inhibition ([Figure 5.5B v, vi](#)), which is consistent with [Figure 5.4B v, vi](#). Altogether, these results indicated that the inhibition of ADAMTS5 showed some effect on cell growth, which is more apparent under glucose and serum starvation.

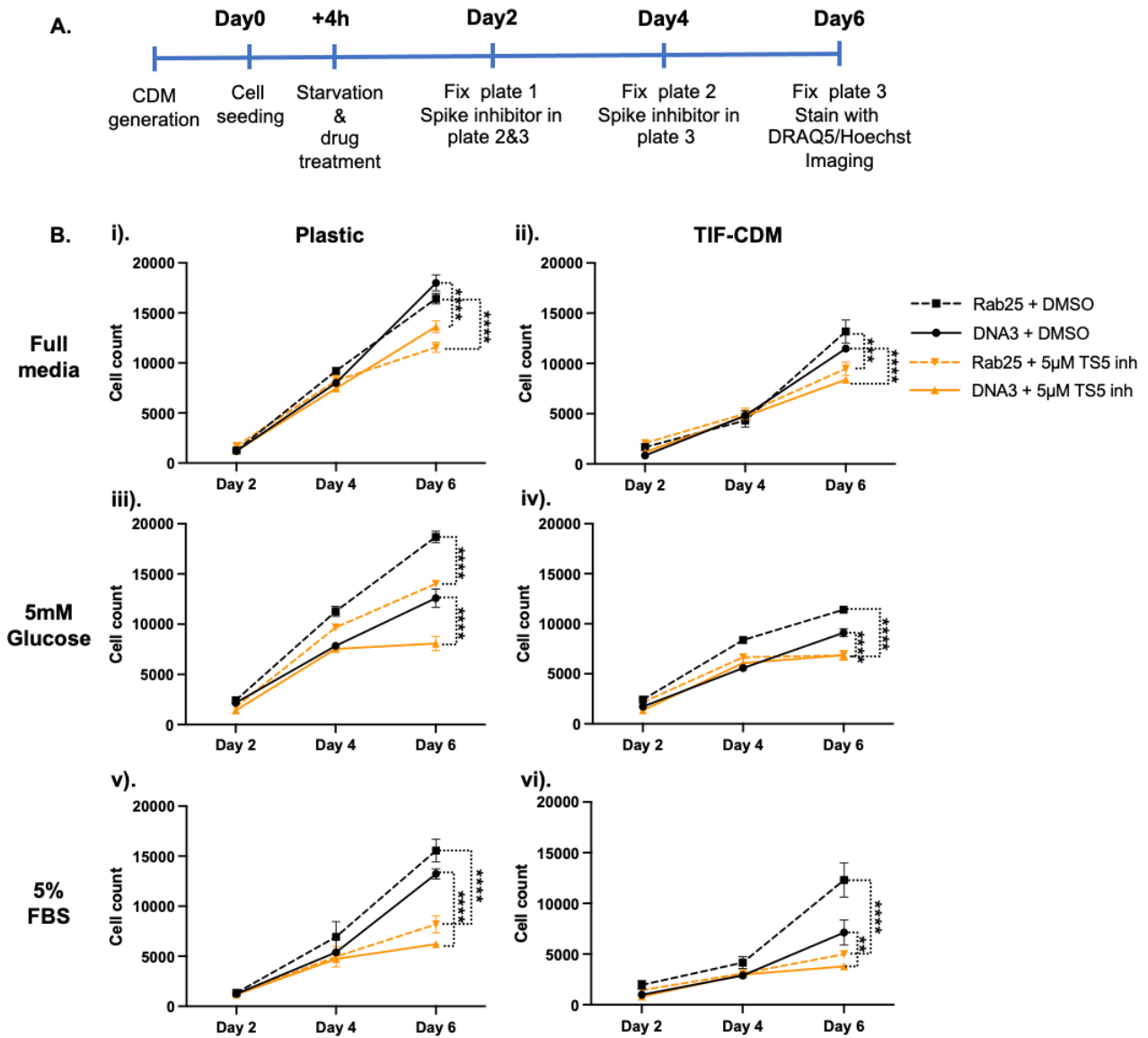


Figure 5.5. ADAMTS5 inhibition reduced cell proliferation on plastic and CDM under glucose or serum starvation. **A.** Schematic of the experimental design. TIF-CDM was generated in 96-well plates as described in section 2.2.3. 600 A2780-DNA3 and A2780-Rab25 cells per well were seeded on plastic or CDM. After cultured for 4h and allowed to attach, the cells were treated with complete or starvation media (media containing 50% glucose or 50% FBS) together with DMSO 5 or 10 μ M of ADAMTS5 inhibitor. The inhibitor was supplied every other two days. Cells were fixed on day 2, day 4 and day 6 and stained with Hoechst nuclear staining, imaged with ImageXpress micro and analysed by MetaXpress software as described in section 2.2.8.1. **B.** Data are presented as mean \pm SEM. N=2 independent experiments. ** p <0.005, *** p <0.001, **** p <0.0001, two-way ANOVA, Tukey's multiple comparisons test.

5.3. Discussion

In this chapter, I characterised the effect of ADAMTS5 pharmacological inhibition on OC cell proliferation. As a result, the proliferation of OC cell lines A2780-DNA3 and A2780-Rab25 started to be affected in the presence of 5 μ M ADAMTS5 inhibitor and a significantly reduced proliferation was observed in all three cell lines, including OVCAR3, when treated with ADAMTS5 inhibitor at a

concentration of 10 μ M. The ADAMTS5 inhibitor (114810) used in this project is 5-((1H-pyrazol-4-yl)methylene)-2-thioxothiazolidin-4-one, which inhibits the aggrecanase activity of ADAMTS5 specifically. It was developed from a high throughput screening and characterized by Gilbert et al. (2007). In comparison to ADAMTS4, another well-known aggrecanase, inhibitor 114810 shows >40-fold selectivity when targeting ADAMTS5 (IC₅₀=1.1 μ M, compared to IC₅₀ =44 μ M For ADAMTS4). Therefore, it is unlikely that a concentration at 10 μ M suppressed the cell proliferation by inhibiting other ADAMTSs. Noticeably, the inhibition of ADAMTS5 showed a small but significant reduction of TIF proliferation with both 5 and 10 μ M of the inhibitor, which brought concern about the cell toxicity of the ADAMTS5 inhibitor. Since the role of ADAMTS5 in cancer has only been investigated in the past decade, there is no clinical trial assessing ADAMTS5 inhibition for cancer treatment yet. However, as a main aggrecanase that leads to the destruction of cartilage ECM, ADAMTS5 has been considered a therapeutic target for osteoarthritis and several ADAMTS5 inhibitors are undergoing pre-clinical or clinical trials (Jiang et al., 2021). GLPG1972 is an ADAMTS5 inhibitor that is currently under phase II clinical trial, the safety of which has been approved previously (Schnitzer et al., 2023, van der Aar et al., 2022, Brebion et al., 2021). Therefore, there is potential to target ADAMTS5 for cancer therapy. Further characterisation of ADAMTS5 and the effect on the proliferation and apoptosis of OC cells and normal cells would be useful.

CAFs were previously found to promote the growth and drug resistance of OC cells (Deying et al., 2017, Guo et al., 2019). Consistent with this, OVCAR3 cells in co-culture with CAFs show increased proliferation compared to cultured alone. Remarkably, the inhibition of ADAMTS5 at high concentration reduces the OVCAR3 proliferation with and without the presence of CAFs, indicating that CAFs failed to improve the resistance of OVCAR3 cells to ADAMTS5 inhibitor. Interestingly, CAFs in co-culture with OVCAR3 cells also showed higher sensitivity to ADAMTS5 inhibition compared to cultured alone. This result needs to be further verified due to technique limitations: since the GFP expressing rate of OVCAR3 cells is not 100%, but 80%-90%, the OVCAR3 cells that do not express GFP would be identified as CAFs in our system. Although these cells that have been counted as CAFs only take a small ratio among the total cell number, it is possible that this could affect the statistical analysis. It would be essential to repeat these experiments with fluorescently labelled CAFs. Additionally, a previous study showed that OC cells (SKOV3) can also promote the proliferation of CAFs, by the secretion of exosomes (Ding et al., 2023). However, our result showed that co-culture

with OVCAR3 did not alter the growth rate of CAFs, suggesting that this effect could be cell line specific.

The proliferation of OVCAR3 was suppressed when in co-culture with TIFs. Indeed, the tumour-suppressing role of TIFs has been widely reported, which has been summarised by (Delinassios and Hoffman, 2022). Since OC was not included in the list, here, my data validated the suppressing role of normal fibroblasts in OC. Considering that normal fibroblast-derived matrix was found to suppress breast cancer cell proliferation (Kaukonen et al., 2016), TIFs could suppress OVCAR3 proliferation via unfavourable matrix secretion. This hypothesis is also supported by the observed result in [Chapter 3](#) that TIF-CDM failed to support the biological function of OVCAR3. It would be interesting to further investigate the matrix components derived by TIFs that suppressed the growth of OC cells. Additionally, it is also important to validate these results with normal ovarian fibroblasts since the TIFs used here are from the skin (Polanska et al., 2011).

Matrigel is a commercial ECM that is used in cell culture as a basement membrane substrate, which was found to support the growth of breast cancer cells (Benton et al., 2011). However, reduced proliferation of A2780-DNA3 cells was observed when seeded on matrigel compared to plastic control. This could be caused by the different stiffness of the cell attachment surface. In comparison to matrigel, breast tumour cells placed on stiffer hydrogel showed enhanced proliferation (Northcutt et al., 2023). ECM stiffness was found to affect cancer cell growth through the YAP/TAZ pathway. Reduced ECM stiffness sensed via focal adhesion leads to reduced nuclear translocation of YAP and TAZ, which downregulate the expression of target genes that support cancer cell growth (Cai et al., 2021). Additionally, the activation of YAP was found to be mediated by integrin $\alpha 5\beta 1$ in Ewing sarcoma cells (He et al., 2019). Since Rab25 regulates the trafficking of $\alpha 5\beta 1$ integrin to the plasma membrane (Caswell et al., 2007), this may explain why only the proliferation of A2780-DNA3, but not A2780-Rab25 cells, was affected by the stiffness of the growing surface.

When under glucose or serum starvation, OC cells with ADAMTS5 inhibition showed significantly reduced proliferation compared to the DMSO control on both plastic and ECM, indicating that ADAMTS5 could play a role in controlling metabolism reprogramming under nutrient starvation. Additionally, glutamine starvation had a dramatic effect on the proliferation of both A2780-DNA3

and Rab25 cells when plated on plastic, while when plated on matrigel, the proliferation of both cell lines was rescued. However, there was no significant impact of ADAMTS5 inhibition on cell proliferation under glutamine starvation (data not shown). Previous work from our lab showed that the growth of breast cancer cells can be partially rescued by the presence of ECM under glucose and glutamine but not serum starvation conditions (Nazemi, 2021). Moreover, ECM uptake is required for ECM-dependent cell growth under glutamine starvation (Nazemi et al., 2024). Interestingly, previous data obtained by Dr Rainero showed ADAMTS5 KD significantly reduced TIF-CDM internalisation of A2780-Rab25 cells (data not shown), which suggested that ADAMTS5 inhibition may suppress OC cell growth through inhibiting ECM internalisation under starvation conditions.

Altogether, this chapter showed that inhibition of ADAMTS5 mostly affected cell proliferation under nutrient deficiency, with limited effect in complete media. It is essential to validate this result with ADAMTS5 KD experiments. Further apoptosis and viability experiments would be helpful to better characterise the outcome of ADAMTS5 inhibition on OC cell proliferation.

Chapter 6 – ADAMTS5 was required for OC cell migration and invasion.

6.1. Introduction

Activated invasion and metastasis are an important hallmarks of cancer, which is also the leading cause of patients' death (Hanahan and Weinberg, 2011). Metastasis is the process whereby cancer cells detach from the primary site, move to a separate location, and form a secondary tumour. The process of invasion and metastasis includes multiple steps, termed invasion-metastasis cascade (Talmadge and Fidler, 2010). The omentum is the most common metastasis site of OC and most of the tumour cells are carried by the peritoneal fluid and spread through passive dissemination (Sorensen et al., 2009). Although OC cells rarely spread through the lymphatic system, they were found to invade the blood vessels and metastasise through the hematogenous system (Sundar et al., 2006, Pradeep et al., 2014).

During tumour metastasis, proteases-mediated ECM degradation and remodelling contribute to the invasion and migration of the tumour cells. These proteases were found secreted by both cancer cells and CAFs (Winkler et al., 2020). In OC, cleavage of ECM components by proteases is essential for the invasion of tumour cells (Cho et al., 2015). Previous research demonstrated that MMP2 contribute to the OC cell omentum and peritoneum attachment through the cleavage of vitronectin and fibronectin, which initiates the early metastasis of OC cells (Kenny et al., 2008). Consistently, exosomes derived from omentum CAFs were found to promote the metastasis of SKOV3 cells both in vitro and in vivo (Han et al., 2023). Furthermore, CAF-secreted matrices can also promote the invasion of OC cells. Previous research identified an upregulated VCAN level in the CM of ovarian CAFs and TGF- β stimulated normal fibroblasts. Secreted VCAN was then found to promote the matrigel invasion ability of OC cells (Yeung et al., 2013). CAFs can also promote early peritoneal metastasis by recruiting the ascites HGSOC cells and forming heterotypic CAF-tumour spheroids. When treated with Imatinib, which inhibits the viability of CAFs, the formation of heterotypic spheroids was disrupted and reduced peritoneal metastasis was observed in mice (Gao et al., 2019).

Considering the critical role of the TME during tumour progression, study models that represent a better biological function of the extracellular microenvironment are preferred for cancer research. In comparison to in vitro 2D models, 3D models generated from stable cell lines or primary cells

isolated from patients performed better in mimicking the TME and representing cell-cell and cell-microenvironment interactions (Atat et al., 2022, Jubelin et al., 2022). There are two main types of 3D culture systems, liquid-based and scaffold-based 3D tumour models. The liquid-based 3D models rely on the low attachment coating, gravity or fluid movement to prevent the cells attaching to the culture vessels, resulting in the formation of spheroids through cell-cell interactions instead of monolayers on the surface. Commercially available matrices such as matrigel and collagens can be used to establish scaffold-based 3D models. Tumour cell spheroids generated from the liquid-based models can be further embedded into the scaffold models, which can be used to study the cell-ECM interactions (Jubelin et al., 2022). Currently, these models are used to characterise the invasion and migration ability of the tumour cells (Atat et al., 2022).

Previously, increased expression of ADAMTS5 has been shown to promote the metastasis of glioblastoma (Held-Feindt et al., 2006), non-small cell lung cancer (Gu et al., 2016) and head and neck cancer (Demircan et al., 2009). Although upregulated expression of ADAMTS5 was identified in borderline and malignant ovarian tumour samples compared to the benign samples (Lima et al., 2016), the role of ADAMTS5 in promoting OC cell invasion and migration remains unclear. In this chapter, I demonstrated the role of ADAMTS5 in promoting OC cell migration and invasion, in 2D and 3D models.

6.2. Results

6.2.1. ADAMTS5 was required for Rab25-dependent pseudopod extension and directional migration in A2780 cells.

Previous research showed that overexpression of Rab25 induced pseudopod elongation in A2780 cells (Caswell et al., 2007). To investigate the role of ADAMTS5 in this process, the random migration assay of A2780-DNA3 and A2780-Rab25 cells on TIF-CDM in the presence or absence of ADAMTS5 inhibition was performed by Jamie Adams, a former master student in our lab. To assess the migration capacity of the cells, pseudopod extension, migration directionality and velocity of the cells were measured. In comparison to A2780-DNA3 cells, A2780-Rab25 cells show significantly increased pseudopod length and directionality, but not migration velocity (Figure 6.1). This result confirmed that the overexpression of Rab25 promoted the migration ability of A2780 cells. In the

presence of the ADAMTS5 inhibitor, significantly reduced pseudopodia length and directionality of A2780-Rab25 cells were observed, while the migration of A2780-DNA3 cells was not affected by ADAMTS5 inhibition, indicating that the catalytic activity of ADAMTS5 was required for Rab25-induced directional cell migration (Figure 6.1A, B). The migration velocity of both cell lines was also not affected by ADAMTS5 inhibition (Figure 6.1C). These results indicated that Rab25 promoted the migration of A2780 cells in an ADAMTS5-dependent manner.

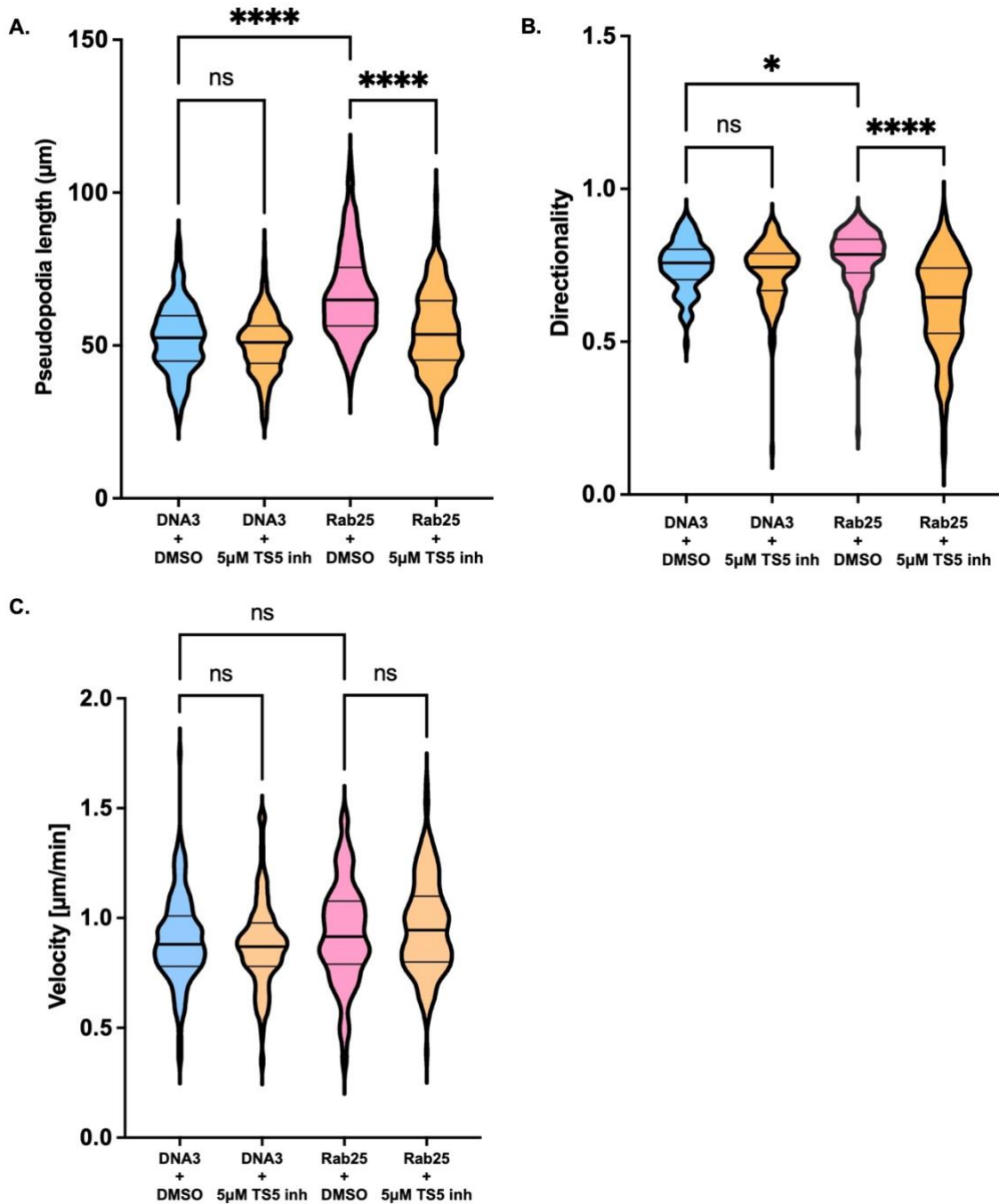


Figure 6.1. ADAMTS5 pharmacological inhibition reduced pseudopod extension and directionality of A2780-Rab25 cells migrating on TIF-CDM. TIF-CDM were generated in 12-well plates as described in section 2.2.3. A2780-DNA3 and A2780-Rab25 cells were seeded and allowed to attach for 4h, then DMSO or 5µM of

ADAMTS5 inhibitor was supplied before imaging. Cells were imaged live with a Nikon widefield live-cell system (Nikon Ti eclipse with Oko-lab environmental control chamber) with a Plan Apo 10X objective (NA 0.75) for 16h, and the pseudopod length (μm) (A.), directionality (B.) and average velocity [$\mu\text{m}/\text{min}$] (C.) were measured in ImageJ as described in section 2.2.9.1. N=3 independent experiments. Violin plot with median and quartiles. * $p=0.0155$, **** $p<0.0001$, Kruskal-Wallis test. These experiments were performed by J. Adams.

To confirm the role of ADAMTS5 in mediating OC cell migration, ADAMTS5 was KD in A2780-Rab25 cells and migration assays on TIF-CDM were performed by Dr Elena Rainero. Consistent with ADAMTS5 pharmacological inhibition, A2780-Rab25 cells with ADAMTS5 KD showed significantly reduced pseudopod length and directionality, while the average velocity was not affected (Figure 6.2). ADAMTS5 qPCR demonstrated $\sim 80\%$ reduction in mRNA expression upon siRNA transfection (Figure 6.2D). Altogether, these results indicated that ADAMTS5 is required for the Rab25-dependent migration of OC cells.

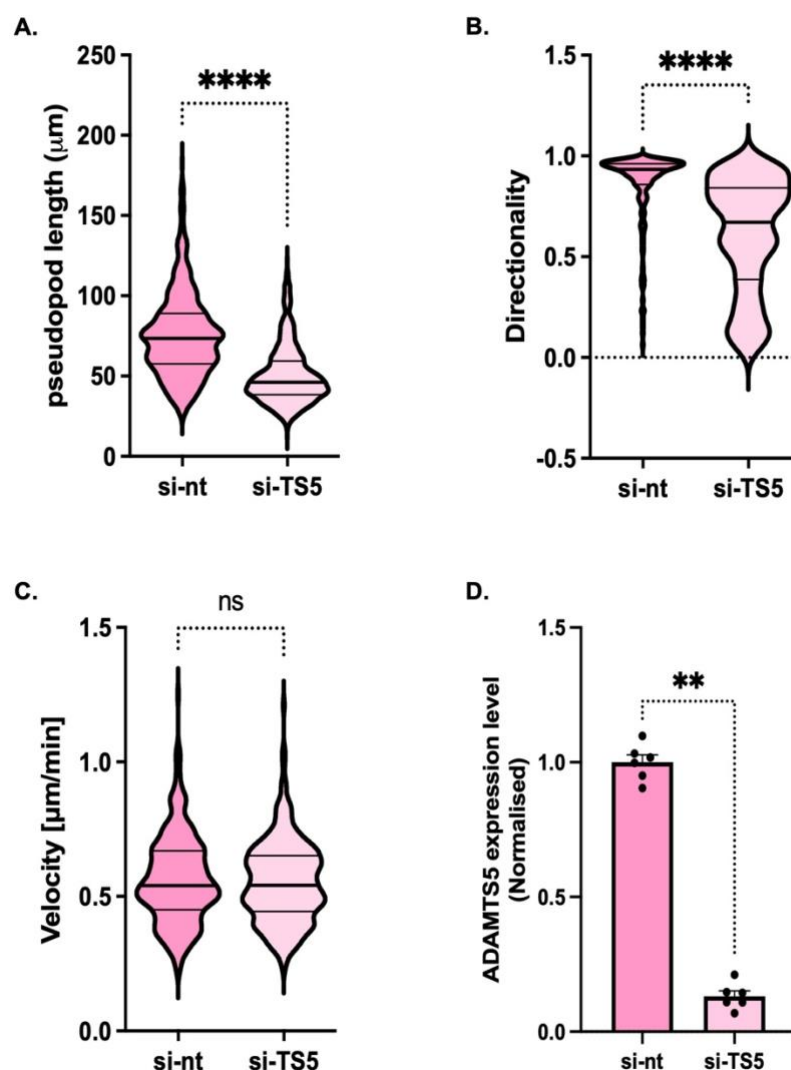


Figure 6.2. ADAMTS5 KD in A2780-Rab25 reduced pseudopod extension and directionality of cells migrating on TIF-CDM. TIF-CDM were generated in 12-well plates as described in section 2.2.3. A2780-Rab25 cells were transfected with non-targeting (si-nt) or ADAMTS5 targeting si-RNA (si-TS5) and seeded on TIF-CDM for 4h. Cells were imaged live with a Nikon widefield live-cell system (Nikon Ti eclipse with Oko-lab environmental control chamber) with a Plan Apo 10X objective (NA 0.75) for 16h, and the pseudopod length (μm) (**A.**), directionality (**B.**) and velocity [$\mu\text{m}/\text{min}$] (**C.**) were measured in ImageJ as described in section 2.2.9.1. N=3 independent experiments. Violin plot with median and quartiles. **** $p < 0.0001$, Mann-Whitney test. **D.** A2780-Rab25 cells were transfected as in A, mRNA was extracted 24hr after transfection and ADAMTS5 and GAPDH levels were measured by SYBR-green based qPCR. GAPDH was used as the control housekeeping gene and the data was normalised to si-nt. Data are presented as mean \pm SEM. N=2 independent experiments. ** $p = 0.0022$ Mann-Whitney test. The experiments in A-C were performed by E. Rainero.

6.2.2. Conditioned media derived from A2780-Rab25 enhanced the migration of A2780-DNA3 cells.

In Chapter 3, I have shown that Rab25 promoted the expression of ADAMTS5, and a significantly higher ADAMTS5 protein level was detected in the CM derived from A2780-Rab25 cells compared to A2780-DNA3. If Rab25 promotes cell migration by stimulating the secretion of ADAMTS5, we hypothesised that CM from Rab25-expressing cells would promote A2780 cell migration. To investigate this, A2780-DNA3 cells were treated with CM derived from either A2780-DNA3 or A2780-Rab25 cells (see section 2.2.4) and their migration capacity on CDM was measured (Figure 6.3A). In comparison to cells treated with A2780-DNA3 CM, A2780-DNA3 cells treated with A2780-Rab25 CM showed significantly elongated pseudopods (Figure 6.3B black arrowheads, D). The spider plots present the cell migration paths, and cells with low migration directionality (< 0.5) are marked in red (Figure 6.3C). These results show that A2780-Rab25 CM significantly increased the directional migration of A2780-DNA3 cells (Figure 6.3DE). Additionally, the velocity of the A2780-DNA3 cells was not affected by the CM from A2780-Rab25 cells (Figure 6.3F), which is consistent with previous results (Figure 6.1C).

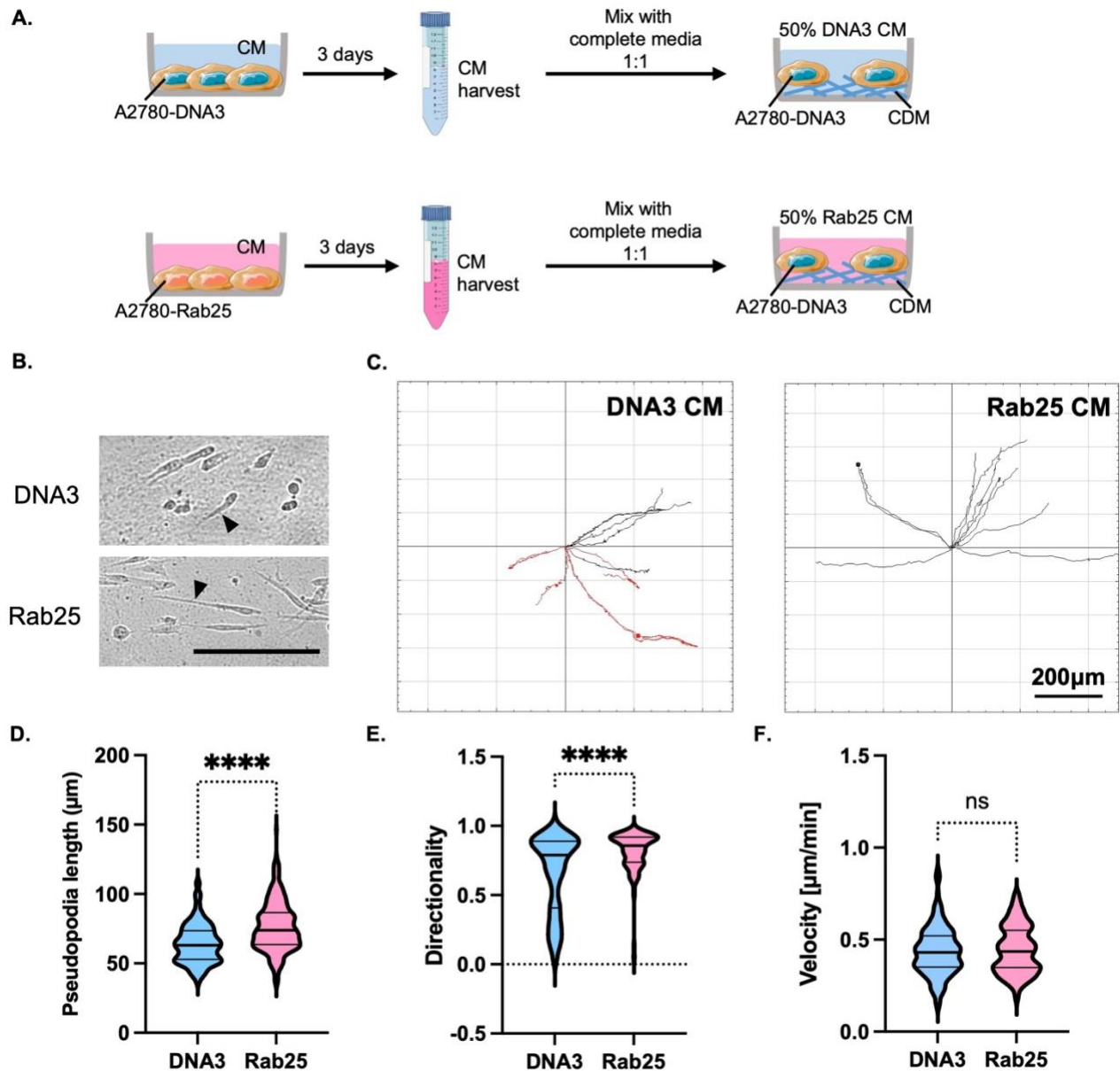


Figure 6.3. CM derived from A2780-Rab25 cells enhanced pseudopod extension and directionality of A2780-DNA3 cells migrating on TIF-CDM. **A.** Schematic of the experimental plan. A2780-DNA3 and A2780-Rab25 cells were seeded on plastic for 3 days and the CM was harvested as described in section 2.2.4. A2780-DNA3 cells were seeded on TIF-CDM in complete media with A2780-DNA3 or Rab25 CM (1:1) for 4h. Cells were imaged live with a Nikon widefield live-cell system (Nikon Ti eclipse with Oko-lab environmental control chamber) with a Plan Apo 10X objective (NA 0.75) for 16h and the images were analysed as described in section 2.2.9. **B.** Black arrowheads point to the elongated pseudopods. Scale bar: 200µm. **C.** Representative spider plots generated by ImageJ show the migration path of the cells, with the colour indicating the directionality, >0.5 in black, <0.5 in red. The pseudopod length (µm) (**D.**), directionality (**E.**) and velocity [µm/min] (**F.**) of cell migration were measured in ImageJ as described in section 2.2.9.1. N=3 independent experiments. Violin plot with median and quartiles. **** p<0.0001, Mann-Whitney test.

6.2.3. ADAMTS5 inhibition prevents A2780-Rab25 CM-induced A2780-DNA3 cell directional migration.

The CM derived from A2780-Rab25 cells could contain a variety of factors stimulating A2780-DNA3 cell migration. Previously, Rab25 was found to promote CLIC3 expression in A2780 cells and secreted CLIC3 was found to promote the migration of WT A2780 and MDA-MB-231 cells (Hernandez-Fernaud et al., 2017, Dozynkiewicz et al., 2012). To further confirm that Rab25 promotes OC cell migration through ADAMTS5, DMSO or 5 μ M ADAMTS5 inhibitor was supplied with A2780-Rab25 CM and the migration capacity of A2780-DNA3 cells on TIF-CDM was quantified (Figure 6.4A). As a result, ADAMTS5 inhibition significantly reduced the pseudopod extension of A2780-DNA3 cells induced by A2780-Rab25 CM compared to the DMSO control (Figure 6.4B, D). Similarly, the ADAMTS5 inhibitor significantly reduced the directional migration of A2780-DNA3 cells treated with A2780-Rab25 CM (Figure 6.4C, E). Interestingly, ADAMTS5 inhibition also reduced the migration velocity of A2780-DNA3 cells in the presence of A2780-Rab25 CM (Figure 6.4C, F), which was not identified in either A2780-DNA or A2780-Rab25 cells directly (Figure 6.1C). These results showed that ADAMTS5 inhibition suppressed the migration of A2780-DNA3 cells, which was promoted by A2780-Rab25 CM.

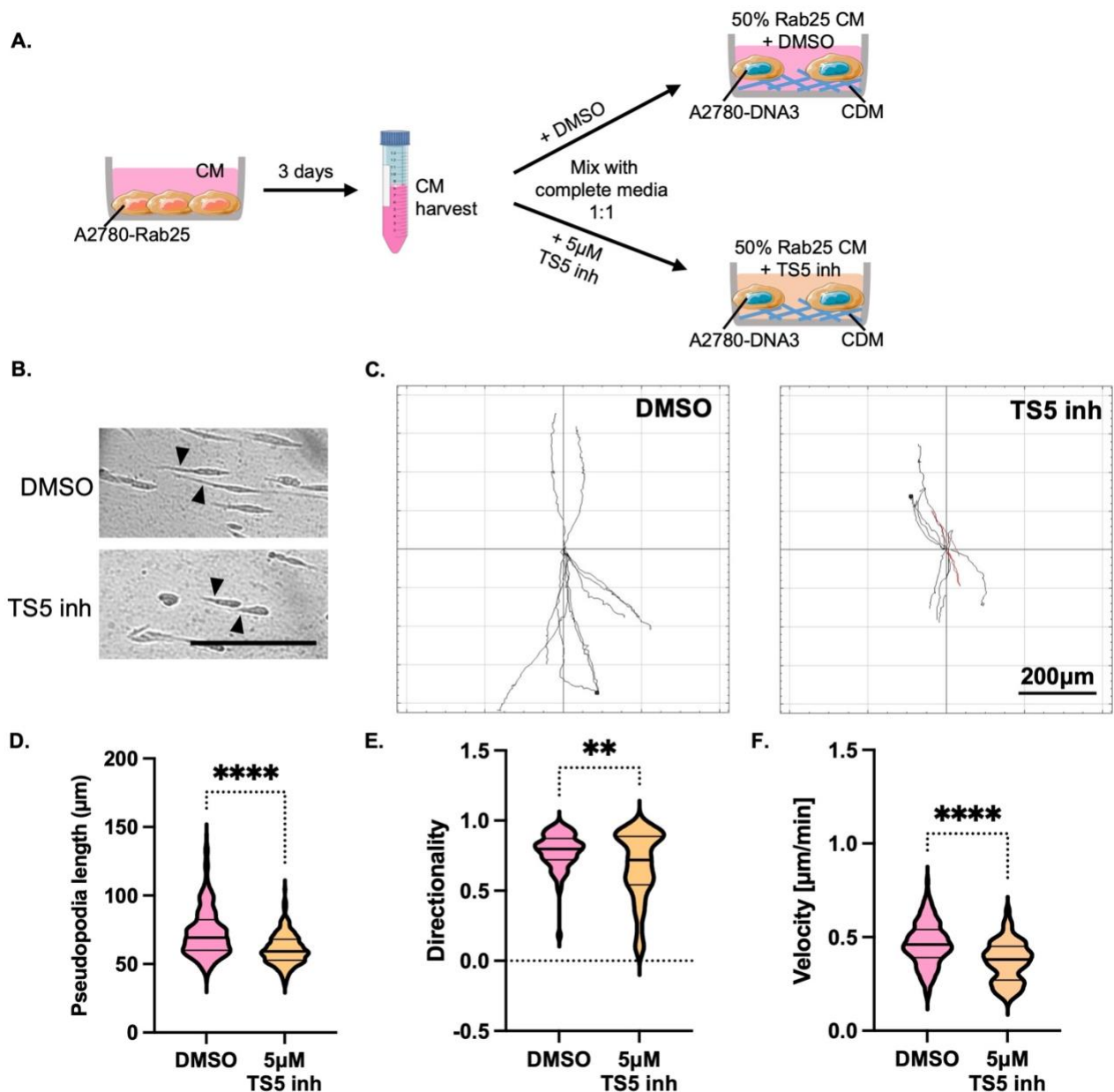


Figure 6.4. ADAMTS5 inhibitor reduced the A2780-Rab25 CM-induced migration capacity of A2780-DNA3 cells on TIF-CDM. **A.** Schematic of the experimental design. A2780-Rab25 cells were seeded on plastic for 3 days and the CM was harvested as described in section 2.2.4. A2780-DNA3 cells were seeded on TIF-CDM in complete media with A2780-Rab25 CM (1:1) for 4h. DMSO or 5µM of ADAMTS5 inhibitor was supplied before imaging. Cells were imaged live with a Nikon widefield live-cell system (Nikon Ti eclipse with Oko-lab environmental control chamber) with a Plan Apo 10X objective (NA 0.75) for 16h and the images were analysed as described in section 2.2.9. **B.** Black arrowheads point to the elongated pseudopods. Scale bar: 200µm. **C.** Representative spider plots generated by ImageJ show the migration paths of the cells. The colour indicates the directionality, >0.5 in black, <0.5 in red. The pseudopod length (µm) (**D.**), directionality (**E.**) and average velocity [µm/min] (**F.**) of cell migration were measured in ImageJ as described in section 2.2.9.1. N=3 independent experiments. Violin plot with median and quartiles. ** p=0.0018 **** p<0.0001, Mann-Whitney test.

6.2.4. CM derived from ADAMTS5 KD A2780-Rab25 cells failed to promote the migration of A2780-DNA3 cells.

To confirm the role of secreted ADAMTS5 in promoting OC cell migration, A2780-Rab25 cells were transfected with non-targeting or ADAMTS5 targeting siRNA and the CM were harvested. Then, the migration of A2780-DNA3 treated with the CM from either control or ADAMTS5 KD A2780-Rab25 cell CM was measured (Figure 6.5A). Consistent with the ADAMTS5 inhibitor results (Figure 6.4), A2780-DNA3 cells treated with CM derived from ADAMTS5 KD A2780-Rab25 cells showed a significantly reduced pseudopod length (Figure 6.5B, D), directionality (Figure 6.5C, E) and velocity (Figure 6.5C, F) compared to control siRNA CM. Altogether, these results demonstrate that secreted ADAMTS5 is sufficient to promote pseudopod extension and directional migration in OC cells.

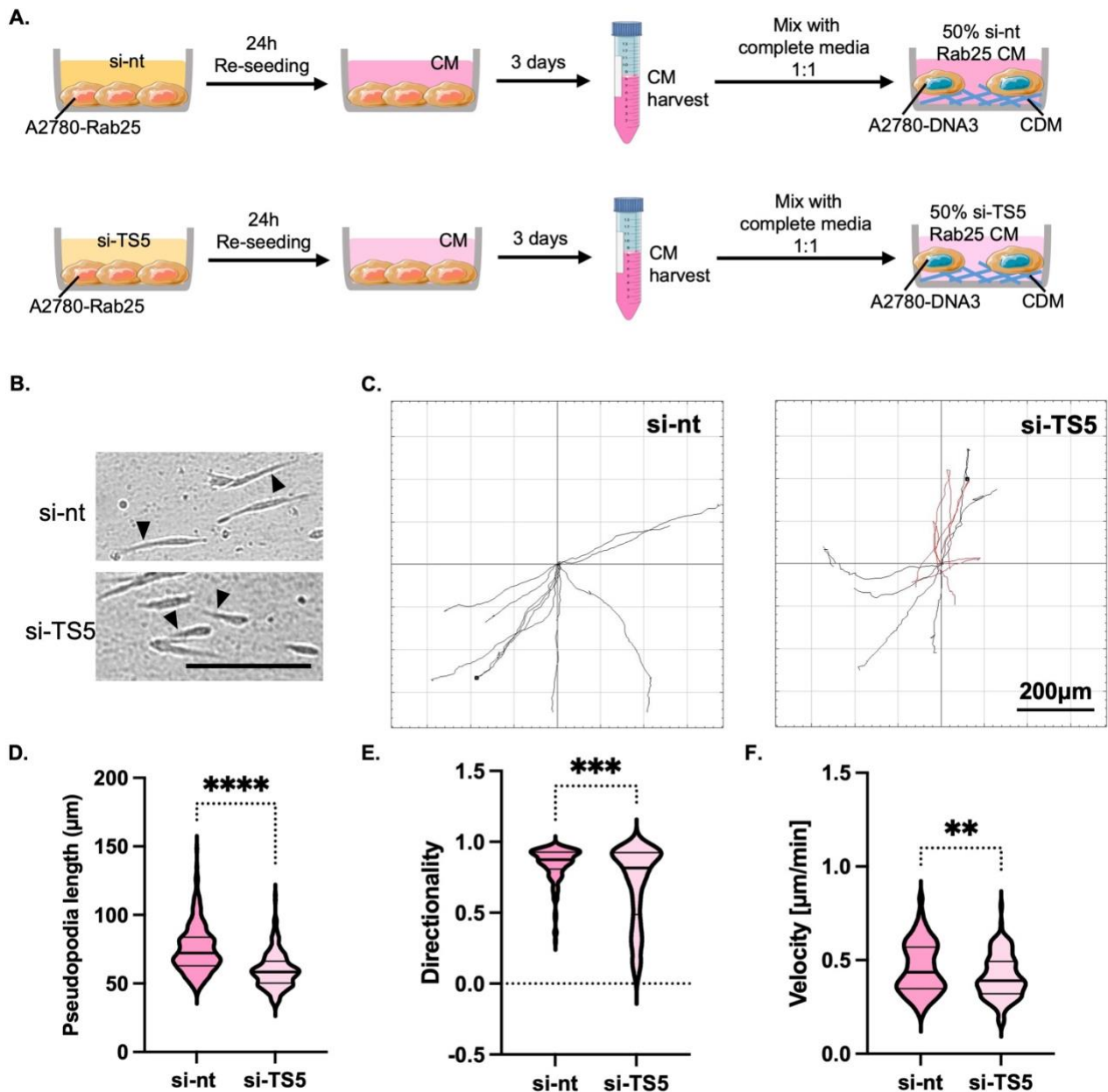


Figure 6.5. CM derived from ADAMTS5 KD A2780-Rab25 cells failed to promote the migration of A2780-DNA3 cells on TIF-CDM. **A.** Schematic of the experimental design. A2780-Rab25 cells were transfected with non-targeting (si-nt) or ADAMTS5 targeting si-RNA (si-TS5) for 24h and re-seeded on plastic for 3 days. The CM was harvested as described in section 2.2.4. A2780-DNA3 cells were seeded on TIF-CDM in complete media with control or ADAMTS5 KD A2780-Rab25 CM 1:1 for 4h. Cells were imaged live with a Nikon widefield live-cell system (Nikon Ti eclipse with Oko-lab environmental control chamber) with a Plan Apo 10X objective (NA 0.75) for 16h and the images were analysed as described in section 2.2.9. **B.** Black arrowheads point to the elongated pseudopods. Scale bar: 200 μ m. **C.** Representative spider plots generated by ImageJ show the migration paths of the cells, with the colour indicating the directionality, >0.5 in black, <0.5 in red. The pseudopod length (μ m) (**D.**), directionality (**E.**) and velocity [μ m/min] (**F.**) of cell migration were measured in ImageJ as described in section 2.2.9.1. N=3 independent experiments. Violin plot with median and quartiles. ** $p=0.0057$, *** $p=0.0002$, **** $p<0.0001$, Mann-Whitney test.

6.2.5. ADAMTS5 inhibition reduced the invasion of OC cells overexpressing Rab25 in 3D systems.

Previous research showed that Rab25 promoted the invasion of OC cells into matrigel and collagen I in a fibronectin-dependent manner (Caswell et al., 2007). As ADAMTS5 is required for Rab25-dependent migration of A2780 cells, here, I hypothesised that ADAMTS5 could similarly be required for the invasion of Rab25-expressing OC cells. 3D spheroid invasion assays were performed to assess the invasion capacity of A2780-Rab25 cells in the presence of DMSO control or ADAMTS5 pharmacological inhibitor. Cells were labelled with Cell tracker™ Red CMTPX and spheroids were then generated with the hanging drop method and embedded into a matrix mix containing 3mg/mL geltrex, 3mg/mL collagen I and 25µg/mL fibronectin (see section 2.2.10.1). The concentration of geltrex and collagen I was optimised to support the spheroids to avoid sinking to the bottom of the dishes (data not shown). Since fibronectin was required for Rab25-dependent invasion of OC cells (Caswell et al., 2007), the same concentration of fibronectin was introduced in our 3D model. Spheroids were cultured in complete media containing DMSO, 5 or 10µM of ADAMTS5 inhibitor and cells were imaged live on day 0, 1 and 2 after embedding (Figure 6.6A).

Invading protrusions from the spheroids were observed after being embedded into the matrix. The area of protrusions outside the spheroid core was calculated and marked as 'invasion area'. In comparison to the DMSO control, A2780-Rab25 spheroids treated with ADAMTS5 inhibitor showed a dose-dependent reduction of the invasion area. After cultured for 1 day, the cells showed a small and non-statistically significant reduction of the invasion capacity in the presence of both concentrations of ADAMS5 inhibitor. After 2 days, the invasion area of A2780-Rab25 spheroids treated with 5µM of ADAMTS5 inhibitor was reduced, but this difference was not statistically significant, while the spheroids treated with 10µM of ADAMTS5 inhibitor showed a significant reduction of the invasion ability (Figure 6.6B). These results indicate that ADAMTS5 catalytic activity is required for the invasion of Rab25-expressing OC cells.

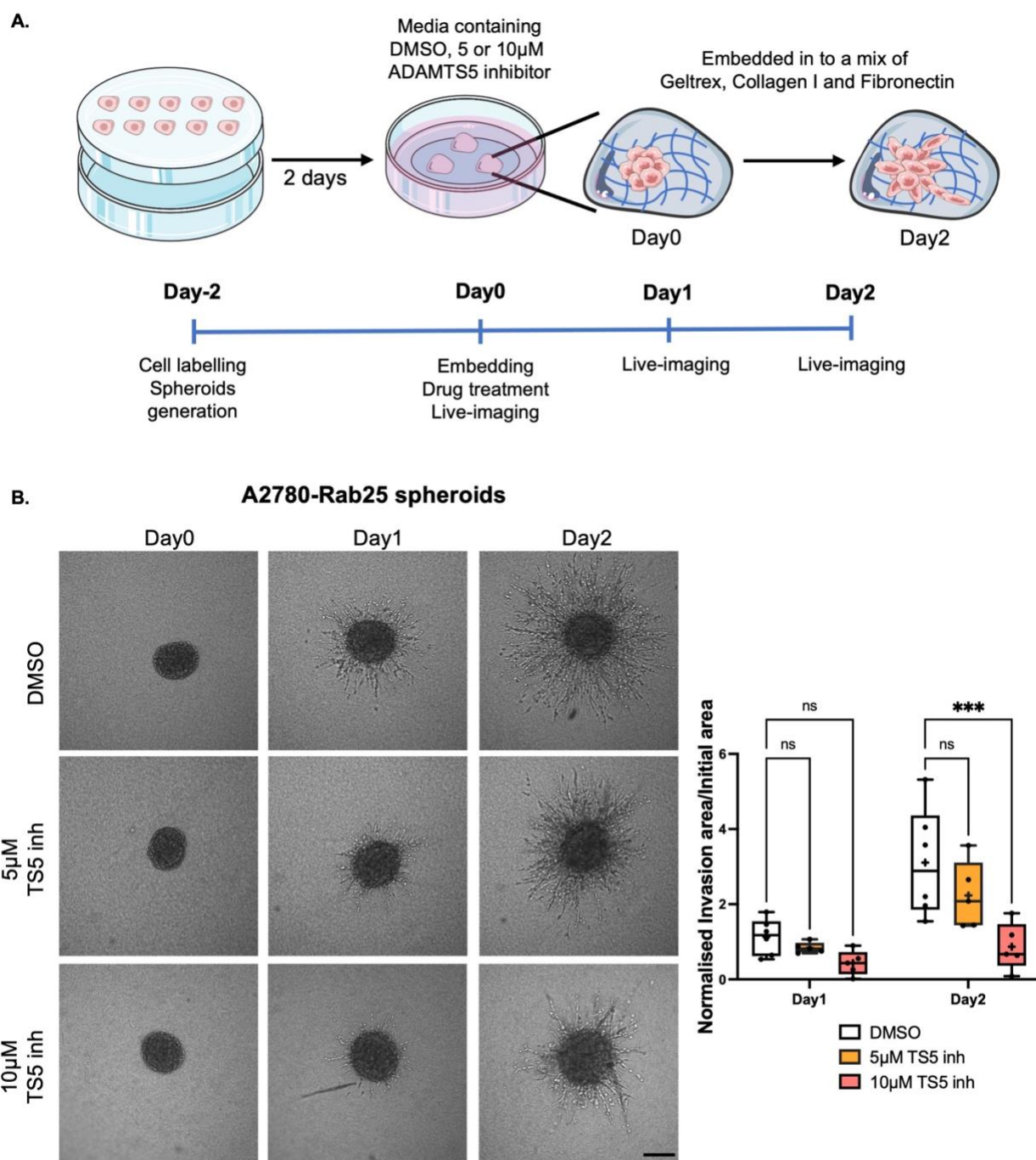


Figure 6.6. ADAMTS5 inhibitor reduced the 3D invasion of A2780-Rab25 cells in a dose-dependent manner.

A. Schematic of 3D invasion assay. A2780-Rab25 cells were labelled with Cell tracker™ Red CMTPX and spheroids were generated, embedded in a matrix mix (3mg/mL of geltrex, 3mg/mL of collagen I and 25μg/mL of fibronectin) and cultured in media in the presence of DMSO, 5 or 10μM of ADAMTS5 inhibitor. The spheroids were imaged live with a Nikon A1 confocal microscope, CFI Plan Fluor 10x objective (NA 0.3) on day 0, 1 and 2, and analysed in ImageJ as described in section 2.2.11. **B.** The invasion area was calculated by the total area - the initial area (day 0) and the ratio of invasion area/initial area of each spheroid was obtained. The ratio was then normalised to the DMSO control on day 1 and plotted. Scale bar: 200μm. N=3 independent experiments. Box and whisker plots represent Min to Max, + represents the mean. *** p=0.0002 two-way ANOVA, Dunnett's multiple comparisons test.

6.2.6. ADAMTS5 inhibition reduced the invasion of both CAFs and OC cells in a 3D co-culture model.

CAFs were found to form heterotypic spheroid during OC metastasis and promote the invasion of OC cells both through secreting proteases and ECM components (Gao et al., 2019, Cho et al., 2015, Yeung et al., 2013). To better mimic the TME of the OC and investigate the role of CAFs in ADAMTS5-mediated OC cell invasion, a co-culture spheroid model was established with CAFs and OVCAR3 cells, which endogenously overexpress Rab25. The ratio of CAFs/OVCAR3 cells was consistent with the proliferation assays in Chapter 5. To distinguish the cells during imaging, OVCAR3 cells expressing nuclear GFP were used and CAFs were labelled with Cell tracker™ Red CMTPX. The spheroids were generated by the hanging drop method, embedded in a mix of ECM components (3mg/mL geltrex, 3mg/mL collagen I and 25µg/mL fibronectin) and maintained in media containing DMSO, 5 or 10µM of ADAMTS5 inhibitor for up to 8 days. Inhibitor/DMSO-containing media was refreshed on day 4 to avoid nutrient deficiency. Images were taken on day 0, 4, 6 and 8 (Figure 6.7A).

Consistent with the observations in A2780-Rab25 spheroids (Figure 6.6B), the invasion of OVCAR3 cells in co-culture spheroids was significantly impaired by the ADAMTS5 inhibitor in a dose-dependent manner. CAFs (in red) were observed at the tips of invading protrusions from the spheroids, which were followed by the OVCAR3 cells with GFP-labelled nuclei. The invasion areas of both CAFs and OVCAR3 cells were quantified. A significantly reduced cell invasion started to be observed on day 6 in the presence of 10µM of ADAMTS5 inhibitor. On day 8, the invasion of OVCAR3 cells was inhibited by both 5 and 10µM of ADAMTS5 inhibitor. On the other hand, the invasion capacity of CAFs in co-culture spheroids was also repressed by ADAMTS5 inhibitor on day 6 and day 8 (Figure 6.7B). These results confirmed the important role of ADAMTS5 in promoting OC invasion, which affects both cancer cells and CAFs.

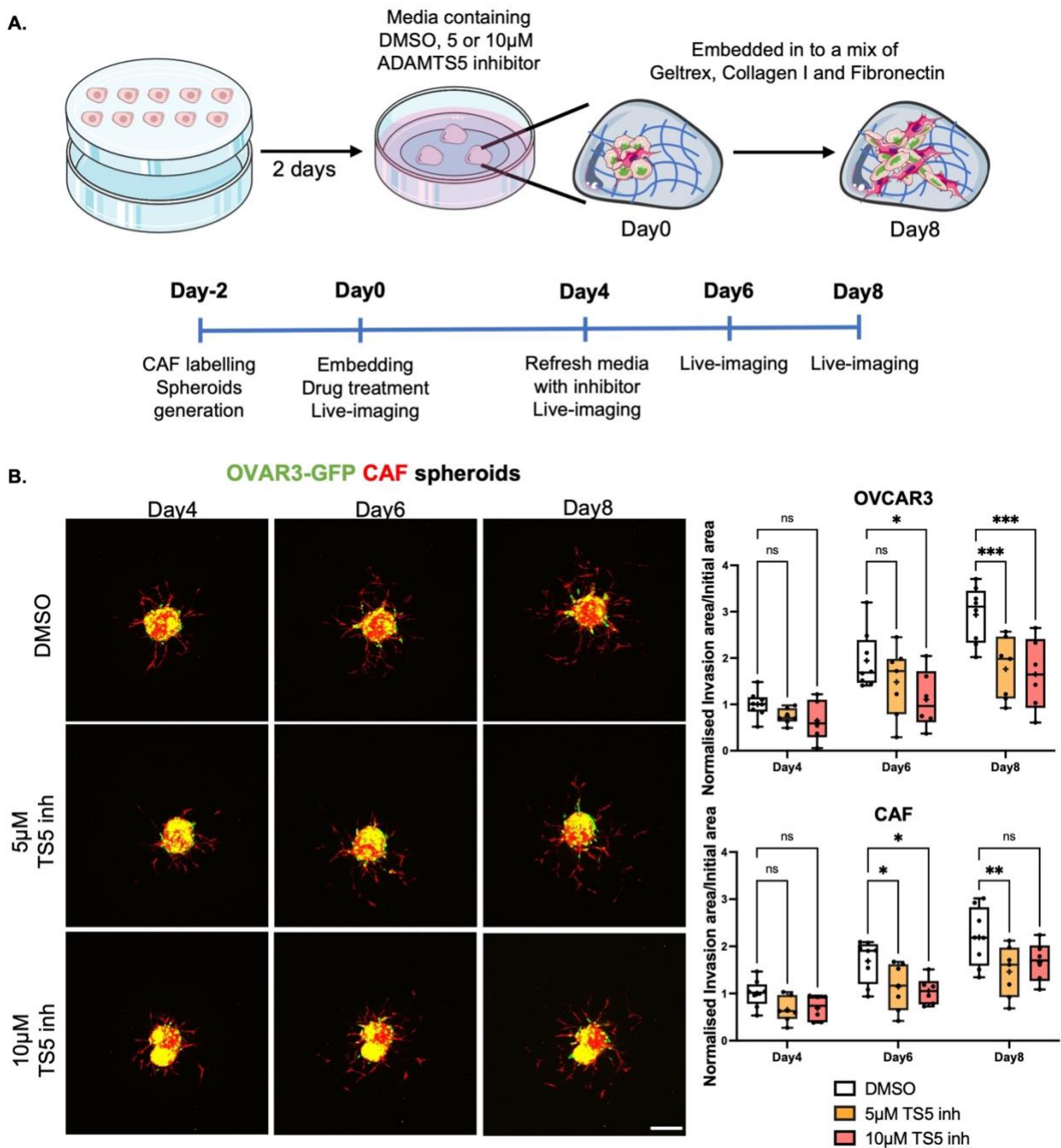


Figure 6.7. ADAMTS5 inhibitor reduced the 3D invasion of OVCAR3 cells and CAFs in co-culture. **A.** Schematic of co-culture 3D invasion assay. OVCAR3 cells stably expressing nuclear GFP (H2B-GFP) were generated and CAFs were labelled with Cell tracker™ Red CMTPIX. The co-culture spheroids were generated with OVCAR3:CAF=2:1, embedded in a matrix mix (3mg/mL of geltrex, 3mg/mL of collagen I and 25 μ g/mL of fibronectin) and cultured in media with DMSO, 5 or 10 μ M of ADAMTS5 inhibitor. Fresh media with inhibitor/DMSO was replaced on day 4. The spheroids were imaged live with a Nikon A1 confocal microscope, CFI Plan Fluor 10x objective (NA 0.3) on day 0, 4, 6 and 8, and analysed in ImageJ as described in section 2.2.11. **B.** The invasion area was calculated by the total area - the initial area (day 0) and the ratio of invasion area/initial area of each spheroid was obtained. This ratio was then normalised to the DMSO control on day 4 and plotted. Scale bar: 200 μ m. N=3 independent experiments. Box and whisker plots represent Min to Max, + represents the mean value. *p<0.05, **p<0.005, *** p<0.001, two-way ANOVA, Dunnett's multiple comparisons test.

6.2.7. ADAMTS5 inhibition did not affect the proliferation of OVCAR3 cells and CAFs in 3D.

In the previous chapter, I showed that 10 μ M of ADAMTS5 inhibitor suppressed the proliferation of OC cells in 2D. To assess whether ADAMTS5 inhibitor at high concentration reduced the invasion ability of OC cells by affecting the proliferation in 3D, cell growth in co-culture spheroids was measured by an EdU incorporation assay. Briefly, co-culture spheroid generated with OVCAR3-GFP cells and non-labelled CAFs were embedded and cultured up to day 8 in media containing DMSO or 10 μ M of ADAMTS5 inhibitor. Media was refreshed on day 4. On day 6, the EdU solution was spiked into the culture media and the spheroids were fixed with 4% PFA on day 8. The spheroids were then stained with Hoechst 33342 and EdU detection kit as described in [section 2.2.10.4](#) and imaged ([Figure 6.8A](#)).

Consistently with the previous results, a reduced invasion was observed in spheroids treated with ADAMTS5 inhibitor. The Hoechst stains the nucleus of both CAFs and OVCAR3 cells while the GFP indicates the nucleus of OVCAR3 cells. The EdU staining was only detected in the nucleus of OVCAR3 cells but not in CAFs in both DMSO and ADAMTS5 treated spheroids, which indicated the low proliferation rate of CAFs in 3D. The area of the EdU signal was normalised to the area of Hoechst and GFP, which represents the total cell proliferation rate and OVCAR3 cell proliferation rate, respectively. As a result, the proliferation of OVCAR3 cells was not affected by ADAMTS5 inhibition in 3D ([Figure 6.8B](#)), which is the opposite of the observations in 2D.

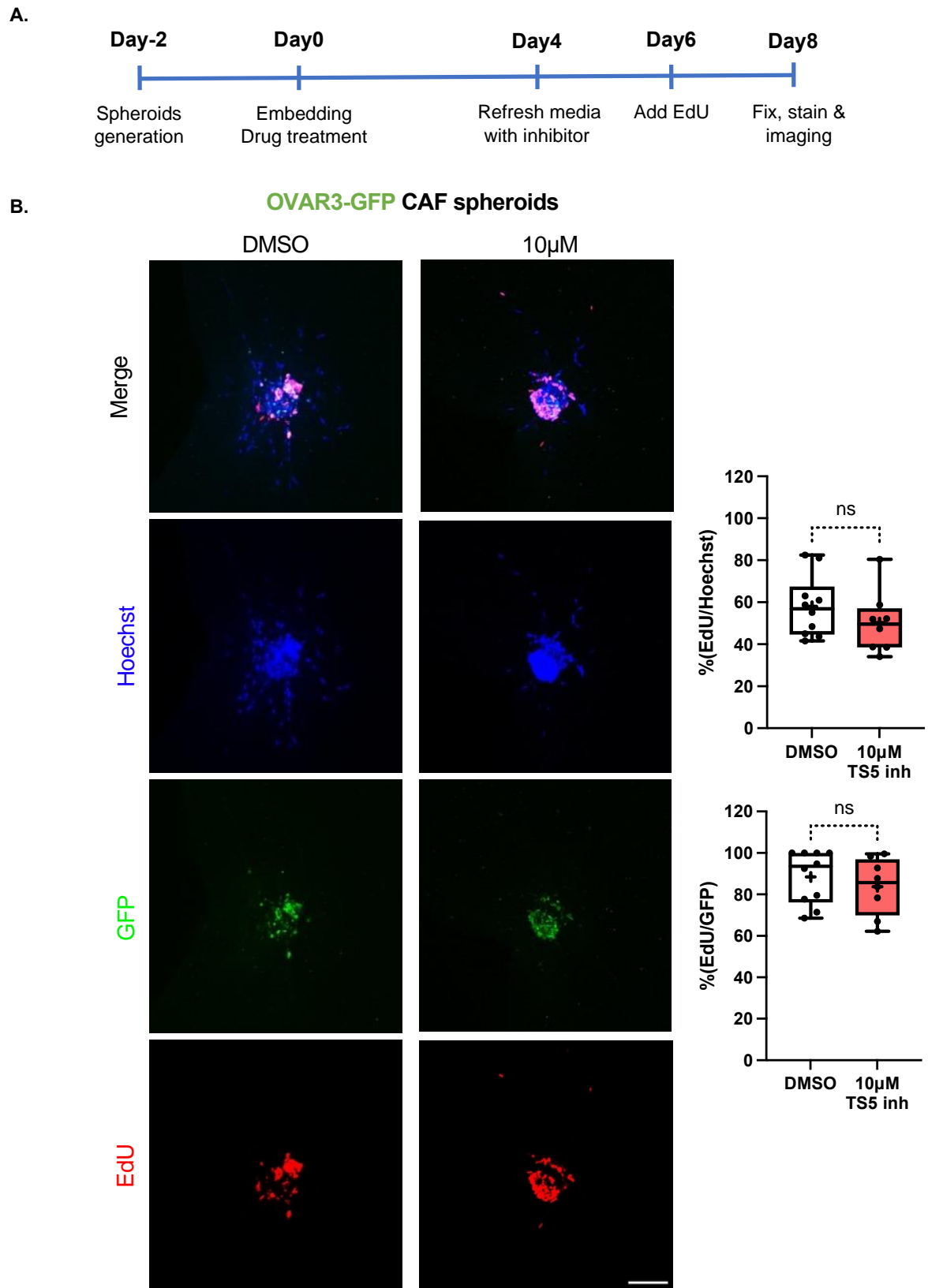


Figure 6.8. ADAMT5 inhibitor did not affect the proliferation of OVCAR3 cells in 3D. **A.** Co-culture spheroids were generated with OVCAR3-GFP (H2B-GFP) cells and non-labelled CAFs (2:1), embedded in a matrix mix (3mg/mL of geltrex, 3mg/mL of collagen I and 25 μ g/mL of fibronectin) and cultured in media with DMSO or 10 μ M of ADAMT5 inhibitor. Fresh media with inhibitor/DMSO was replaced on day 4. EdU was added at day 6. The spheroids were fixed on day 8, stained with EdU detection reagent and Hoechst 33342 and imaged with a Nikon A1 confocal microscope, CFI Plan Fluor 10x objective (NA 0.3) as described in section

2.2.11.4. **B.** The total area of each staining was measured in ImageJ and the percentage of EdU against Hoechst and GFP was calculated and plotted. Scale bar: 200 μ m. N=3 independent experiments. Box and whisker plots represent Min to Max, + represents the mean value, Mann-Whitney test.

6.2.8. ADAMTS5 inhibition did not affect the invasion of CAFs in monoculture.

In our co-culture spheroid model, CAFs showed a better invasion ability than OVCAR3 cells, which seems to lead to the invasion of OVCAR3 cells. Since the inhibition of ADAMTS5 in 3D reduced the invasion of both OVCAR3 cells and CAFs in co-culture spheroids (Figure 6.7B), there is the possibility that ADAMTS5 inhibitor only suppressed the invasion ability of CAFs, which in turn inhibited the invasion of OVCAR3 cells indirectly. To investigate this, CAF mono-culture spheroids were generated and treated with 10 μ M of ADAMTS5 inhibitor. Interestingly, the invasion of CAFs was not affected by ADAMTS5 inhibition in monoculture (Figure 6.9). This result suggested that ADAMTS5 inhibition only suppressed the invasion of CAFs when co-cultured with OVCAR3 cells.

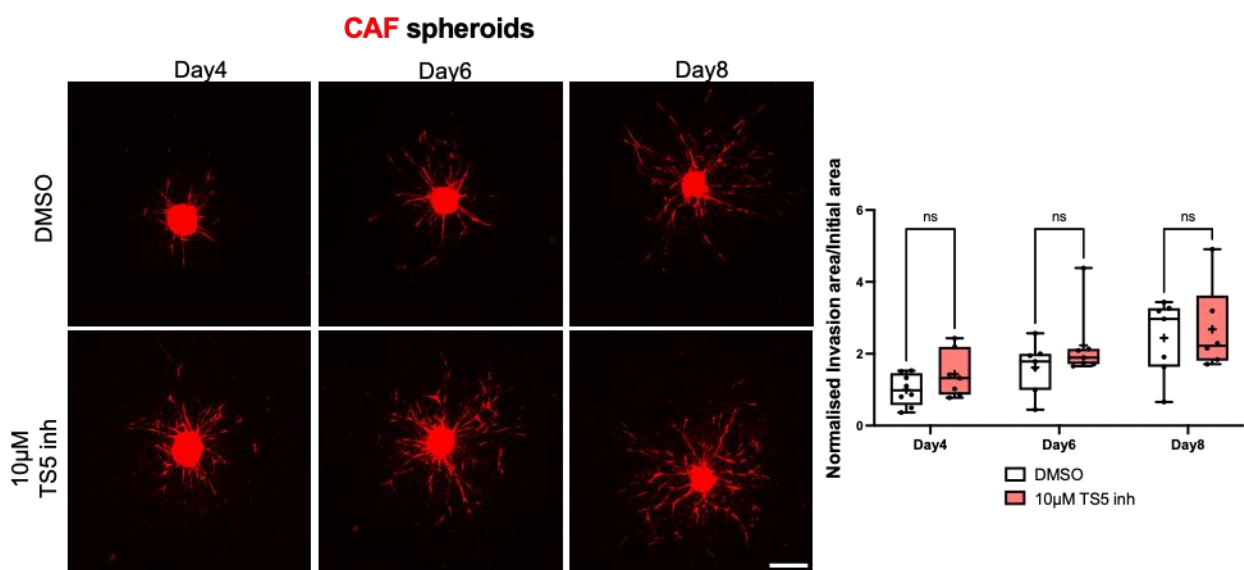


Figure 6.9. ADAMTS5 inhibition did not affect the 3D invasion of CAF spheroids. CAFs were labelled with Cell tracker™ Red CMTPX. CAF spheroids were generated, embedded, and cultured in media with DMSO or 10 μ M of ADAMTS5 inhibitor. Fresh media with inhibitor was replaced on day 4. Spheroids were imaged live with a Nikon A1 confocal microscope, CFI Plan Fluor 10x objective (NA 0.3) on day 0, 4, 6 and 8, and analysed in ImageJ as described in section 2.2.11. The invasion area of the spheroid was calculated by the total area - the initial area. The invasion area/initial area was normalised to the DMSO control on day 4 and plotted. Scale bar: 200 μ m. N=3 independent experiments. Box and whisker plots represent Min to Max, + represents the mean value. Two-way ANOVA, Dunnett's multiple comparisons test.

6.2.9 Rab25 KD in OVCAR3 cells suppressed the invasion of both CAFs and OVCAR3 cells.

Previous research by Caswell et al. (2007) demonstrated that Rab25 promoted A2780 cell invasion. Here, I validated this result in our 3D co-culture spheroid model. OVCAR3-GFP cells were transfected with non-targeting or Rab25 targeting siRNA for 24h, and co-culture spheroids were generated with transfected OVCAR3-GFP cells and CAFs labelled with Cell tracker™ Red CMTPX. The spheroids were cultured for up to 8 days and the images were taken on day 0, 4, 6 and 8 (Figure 6.10A). CAFs (in red) were observed at the tips of invading protrusions from the spheroids followed by the OVCAR3 cells with GFP-labelled nuclei when OVCAR3 cells were transfected with the non-targeting siRNA. As a result, Rab25 KD in OVCAR3 cells, a significantly reduced invasion was observed in both OVCAR3 cells and CAFs (Figure 6.10B). This confirmed Rab25 is required for the invasion of OC cells. Furthermore, Rab25 KD in OVCAR3 cells also affected the invasion of CAFs, which suggested the potential role of Rab25 in mediating the crosstalk between OC cells and CAFs. The KD efficiency of Rab25 in OVCAR3 cells on day 4, 6 and 8 was confirmed by western blotting (Figure 6.10C).

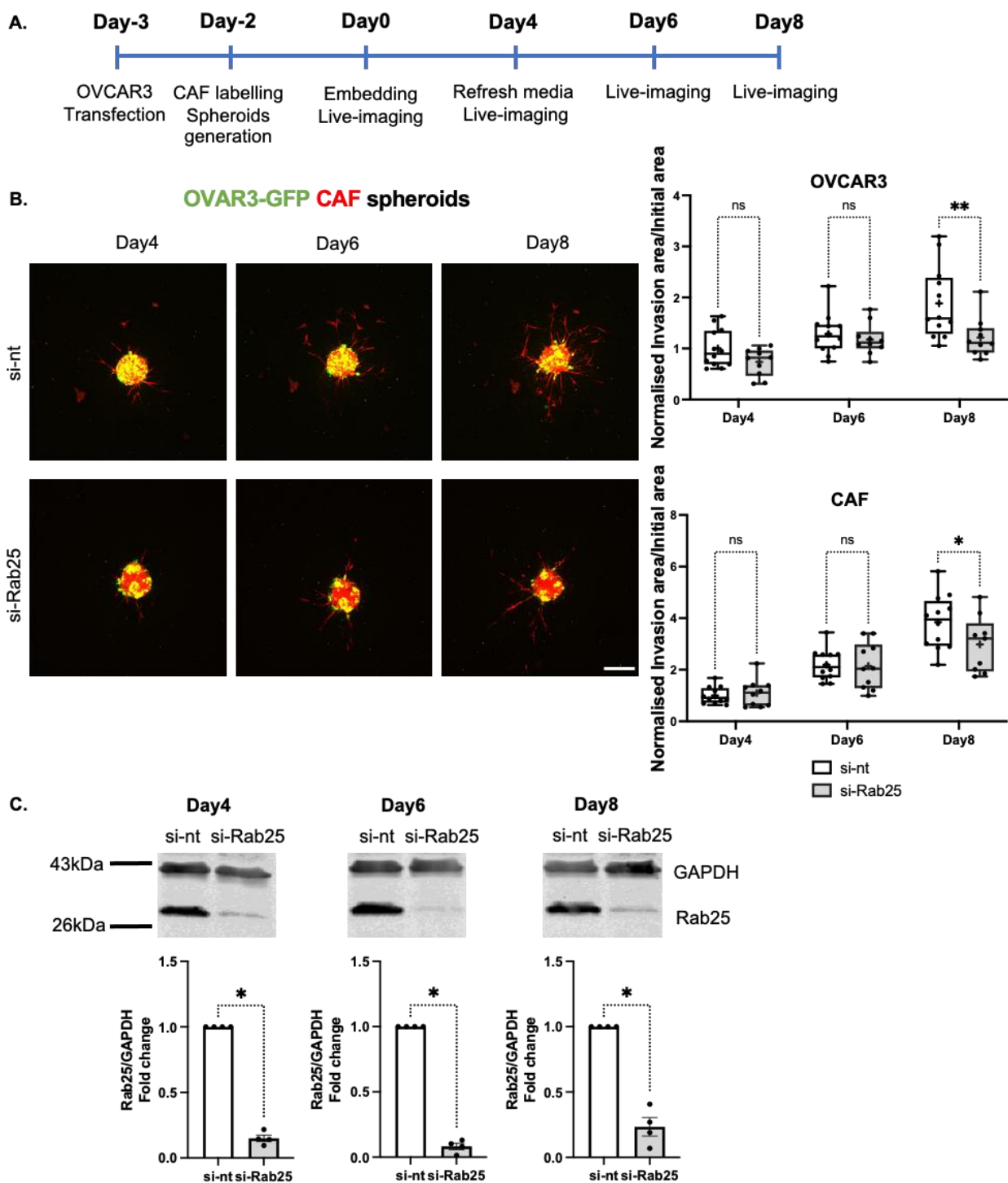


Figure 6.10. Rab25 KD in OVCAR3 cells reduced the 3D invasion of both OVCAR3 cells and CAFs in co-culture. **A.** Schematic of co-culture 3D invasion assay. OVCAR3-GFP cells were transfected with non-targeting (si-nt) or Rab25-targeting (si-Rab25) si-RNA. CAFs were labelled with Cell tracker™ Red CMTPX. Co-culture spheroids were generated with OVCAR3:CAF=2:1 and embedded in a matrix mix (3mg/mL of geltrex, 3mg/mL of collagen I and 25µg/mL of fibronectin). Media was refreshed on day 4. Spheroids were imaged live with a Nikon A1 confocal microscope, CFI Plan Fluor 10x objective (NA 0.3) on day 0, 4, 6 and 8, and analysed in ImageJ as described in section 2.2.11. **B.** The invasion area of OVCAR3 and CAFs was calculated by the total area - the initial area. The invasion area/initial area was normalised to si-nt on day 4 and plotted. Scale bar: 200µm. N=4 independent experiments. Box and whisker plots represent Min to Max, + represents the mean value. *p=0.0471, **p=0.0022, two-way ANOVA, Dunnett's multiple comparisons test. **C.** OVCAR3 cells were transfected as in A, lysed on day 4, 6 and 8 and Rab25 and GAPDH protein levels were measured by Western

Blotting. Membranes were imaged with a Licor Odyssey Sa system, and the band intensity was quantified by Image Studio Lite software. Rab25 signal was normalised to the GAPDH loading control, and the fold change of expression in si-Rab25 in comparison to si-nt was plotted. N=4 independent experiments. Data are presented as mean \pm SEM. * p=0.0286, Mann-Whitney test.

6.2.10 ADAMTS5 KD in OVCAR3 cells suppressed the invasion of OVCAR3 cells.

So far, my results have shown the importance of ADAMTS5 in promoting the invasion of both OC cells and CAFs in co-culture. Since the KD of Rab25, the upstream factor that mediates ADAMTS5 expression, in OVCAR3 cells reduced the invasion of both OVCAR3 and CAFs in co-culture, I investigated the effect of ADAMTS5 KD in OVCAR3 cells and CAFs invasion, by generating co-culture spheroids with CAFs and OVCAR3-GFP cells either control or ADAMTS5 KD ([Figure 6.11A](#)). The results of the invasion assay show that ADAMTS5 KD reduced the invasion of OVCAR3 cells, which is consistent with the results obtained with ADAMTS5 inhibitor ([Figure 6.7B](#)). As for the CAFs, the invasion ability was slightly reduced compared to the si-nt control, but this difference was not statistically significant. The KD efficiency of ADAMTS5 was tested by SYBR-green based qPCR ([Figure 6.11C](#)). Altogether, these results confirmed the role of ADAMTS5 in promoting OC cell invasion.

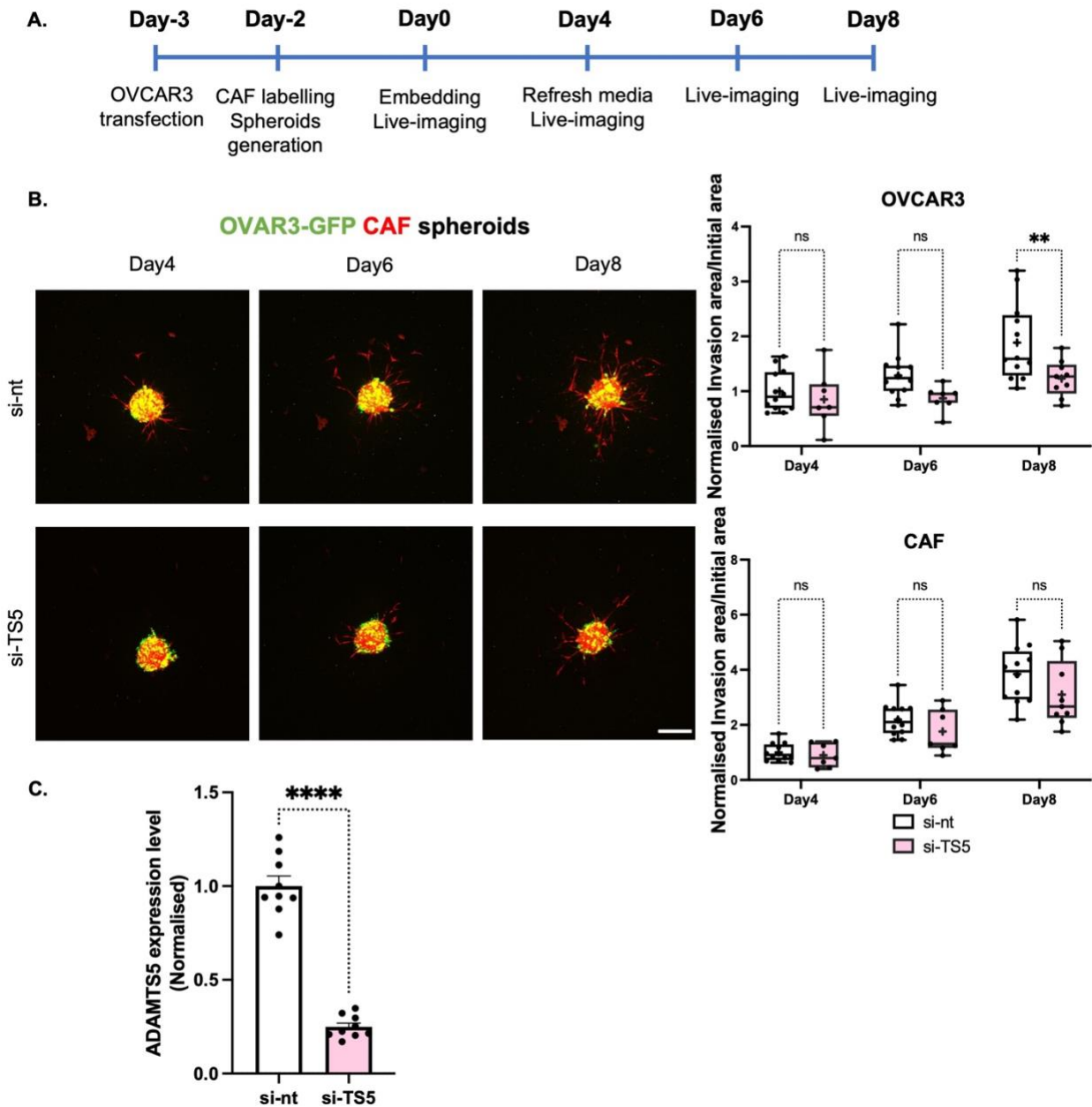
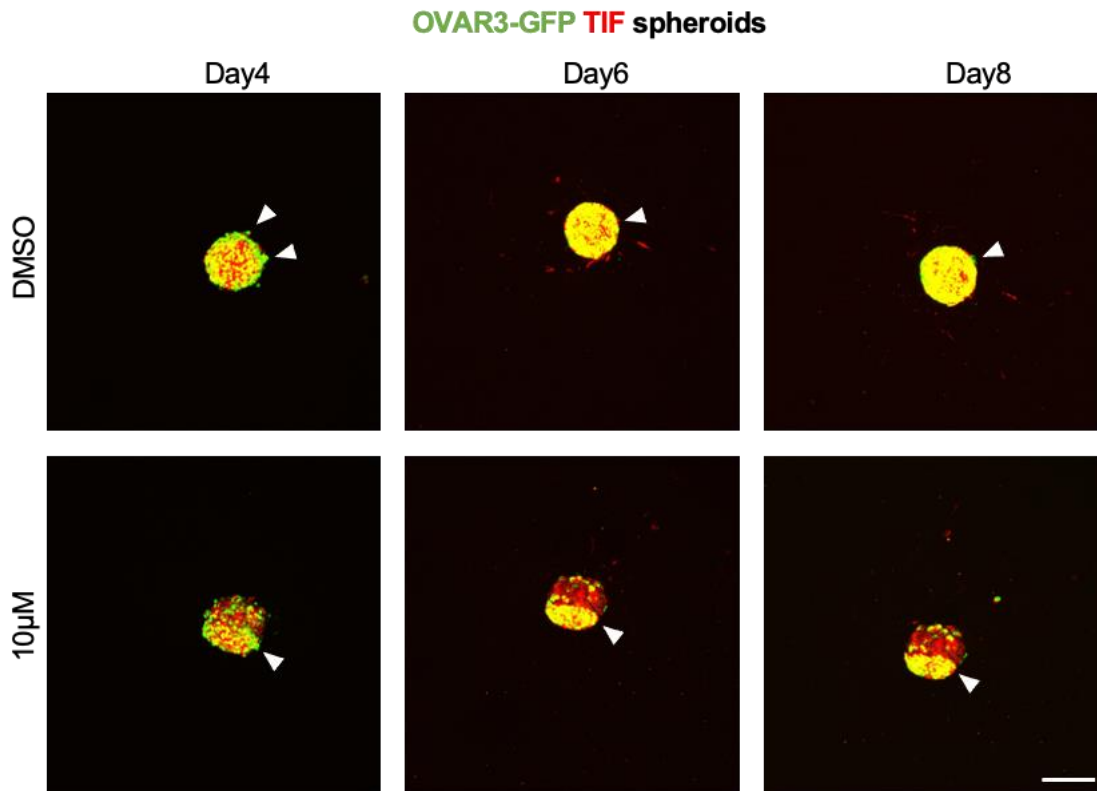


Figure 6.11. ADAMTS5 KD in OVCAR3 cells reduced the 3D invasion of OVCAR3 cells but not CAFs in co-culture. **A.** Schematic of co-culture 3D invasion assay. OVCAR3-GFP cells were transfected with non-targeting (si-nt) or ADAMTS5-targeting (si-TS5) si-RNA. CAFs were labelled with Cell tracker™ Red CMTPX. The co-culture spheroids were generated with OVCAR3:CAF=2:1 and embedded in a matrix mix (3mg/mL of geltrex, 3mg/mL of collagen I and 25µg/mL of fibronectin). Media was refreshed on day 4. The spheroids were imaged live with a Nikon A1 confocal microscope, CFI Plan Fluor 10x objective (NA 0.3) on day 0, 4, 6 and 8, and analysed in ImageJ as described in section 2.2.11. **B.** The invasion area of OVCAR3 and CAFs was calculated by the total area - the initial area. The invasion area/initial area was normalised to the mean of si-nt on day 4 and plotted. Scale bar: 200µm. N=4 independent experiments. Box and whisker plots represent Min to Max, + represents the mean value. **p=0.0075, two-way ANOVA, Dunnett's multiple comparisons test. **C.** OVCAR3-GFP cells were transfected as in A. 24hr after transfection the mRNA was extracted and ADAMTS5 and GAPDH mRNA levels were measured by SYBR-green based qPCR. GAPDH was used as the control housekeeping gene and the data was normalised to si-nt. Data are presented as mean ± SEM. N=3 independent experiments. **** p<0.0001, Mann-Whitney test.

6.2.11. TIFs failed to promote the invasion of OVCAR3 cells in co-culture spheroids.

In the previous chapters, I demonstrated that CAFs in co-culture with OVCAR3 promoted cancer cell proliferation, while TIFs on the other hand suppressed the proliferation of OVCAR3 cells. Here, I investigated in the role of TIFs in OVCAR3 cell 3D invasion. Co-culture spheroids of TIFs and OVCAR3-GFP cells were generated, embedded and imaged as described above (Figure 6.7A). DMSO or 10 μ M ADAMTS5 inhibitor was supplied in the culture media. As shown in Figure 6.12A, minimal invasion of TIFs or OVCAR3 cells was observed in co-culture spheroids. Although invading protrusions containing OVCAR3 cells can be detected at day 4, they disappeared at day 6 and day 8 (Figure 6.12A, white arrow heads). This suggested that TIFs failed to promote the invasion of OVCAR3 cells in co-culture. To investigate whether the different role of TIFs and CAFs in OC cell invasion was caused by differential ADAMTS5 levels, the expression of ADAMTS5 in two cell lines was measured by SYBR-green based qPCR. In comparison to CAFs, the expression level of ADAMTS5 in TIFs was highly variable between biological repeats (Figure 6.12B), but not significantly different. These data suggest that the inhibitory effect of TIFs on OC invasion was not due to reduced levels of ADAMTS5.

A.



B.

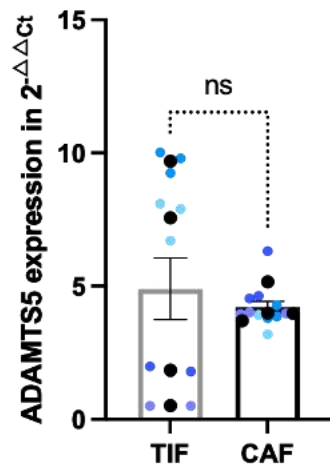


Figure 6.12. TIFs suppressed the invasion of OVCAR3 cells. A. The co-culture spheroids were generated with OVCAR3-GFP and TIFs labelled with Cell tracker™ Red (2:1), embedded in a matrix mix (3mg/mL of geltrex, 3mg/mL of collagen I and 25µg/mL of fibronectin) and cultured in media with DMSO or 10µM of ADAMTS5 inhibitor. Fresh media with inhibitor was replaced on day 4. The spheroids were imaged live with a Nikon A1 confocal microscope, CFI Plan Fluor 10x objective (NA 0.3) on day 0, 4, 6 and 8. White arrowheads point to invasive protrusion containing OVCAR3 cells. Scale bar: 200µm. B. mRNA was extracted from TIFs and CAFs and ADAMTS5 and GAPDH mRNA levels were assessed by SYBR-green based qPCR. GAPDH was used as the control housekeeping gene and the ADAMTS5 expression level was plotted in 2^{-ΔΔCt}. Data are presented as mean ± SEM. N=4 independent experiments, the black dots represent the mean of individual experiments. Kruskal-Wallis test.

6.3. Discussion

In this chapter, I demonstrated that ADAMTS5 is required for Rab25-dependent migration and invasion of OC cells. Previously, overexpressed Rab25 was shown to promote the directional migration of A2780 cells on CDM derived by human dermal fibroblasts or NIH 3T3 fibroblasts (Caswell et al., 2007), and consistent results were obtained on TIF-CDM in our lab. Additionally, enhanced pseudopod extension also indicated an increased migration capacity of A2780-Rab25 cells compared to A2780-DNA3 cells. A2780-Rab25 cells were also found to move slower than the A2780-DNA3 cells in Norman's lab. However, no significant change was obtained between the migration velocity of A2780-DNA3 and A2780-Rab25 cells in our lab. Rab25 was shown to promote OC cell migration by enhancing the delivery and recycling of $\alpha 5\beta 1$ integrin to the plasma membrane at the pseudopod tips. Here, my data showed that CM derived from Rab25 overexpressing cells promoted the migration of Rab25-non-expressing cells, which suggested an alternative mechanism through which Rab25 could promote OC cell migration. When inhibiting or knocking down ADAMTS5 in the CM, the promotion of cell migration by Rab25-CM was reduced back to the same level of DNA3-CM. Remarkably, reduced cell migration velocity was also observed in the cells treated with CM from ADAMTS5 KD cells or supplied with ADAMTS5 inhibitor, which was not identified when the inhibitor was added directly on the cells. This could be caused by nutrient starvation as the CM was harvested after 3 days from cell culture. Remarkably, this starvation is acceptable since the CM was supplied 1:1 with complete media. According to the proliferation results in Chapter 5, the proliferation of A2780 cells was only affected by the depletion of 50% of the nutrient until day 4, and in the random migration assays, the cells were only cultured in the CM overnight.

The 3D invasion of OC cells in either monoculture or co-culture with CAFs was found to depend on ADAMTS5. Interestingly, ADAMTS5 KD in OC cells and ADAMTS5 pharmacological inhibition suppressed the invasion of CAFs when in co-culture, while CAFs in monoculture were not affected by ADAMTS5 inhibition. This result indicated the potential role of ADAMTS5 in mediating the crosstalk between OC cells and CAFs. In the TME, TGF- β is one of the main cytokines that regulate the crosstalk between cancer cells and CAFs. Cancer cell-derived TGF- β stimulates the conversion of normal fibroblasts into CAFs and further maintains the status of CAFs in tumours (Wu et al., 2021). In glioblastoma cells, TGF- β was found to induce the expression of ADAMTS4 and 5 (Held-Feindt et

al., 2006). Furthermore, ADAMTS1 was found to enhance TGF- β expression in lung cancer cells, which further promoted EMT, migration and invasion of A549 cells (Hu et al., 2023). ADAMTS6 and 10 were shown to affect the extracellular availability of TGF- β (Cain et al., 2022). Therefore, it would be interesting to investigate the role of ADAMTS5 in the crosstalk between OC cells and CAFs. Additionally, CM from ovarian CAFs and normal fibroblasts upon TGF- β stimulation showed increased levels of secreted VCAN, a substrate of ADAMTS5, which promoted the invasion of OC cells (Yeung et al., 2013). Therefore, ADAMTS5 may promote the invasion of cancer cells and CAFs through the cleavage of CAF-derived VCAN in OC. Moreover, since CAFs also express ADAMTS5 at a considerable level, further research could investigate the role of CAF-derived ADAMTS5 in OC progression. Remarkably, the KD of Rab25 and ADAMTS5 in OC cells impacted CAF invasion, but the effect of ADAMTS5 KD was moderate in comparison to Rab25. This indicated that ADAMTS5 is one but not the only Rab25 downstream factor in mediating the crosstalk between OC cells and CAFs, which promotes cell invasiveness.

The EdU incorporation assay demonstrated that the proliferation of OVCAR3 cells was not affected by 10 μ M ADAMTS5 inhibitor, while the proliferation of OVCAR3 cells was reduced significantly when the cells were treated with ADAMTS5 inhibitor at the same concentration in 2D (Chapter 5). This result indicated that OC cells show less sensitivity in response to ADAMTS5 inhibitor in 3D than in the 2D model or ADAMTS5 is specifically involved in controlling cell proliferation in 2D environments. Consistently, cancer cells in 3D models showed a higher overall drug resistance, such as to chemotherapy drugs (Fontoura et al., 2020). Since the 3D models represent better cell-cell and cell-ECM interactions, which were previously shown to contribute to drug resistance of tumours, 3D models are considered to show more realistic effects in response to drugs and therefore are preferred for drug screening and characterisation both in the laboratory and industry (Atat et al., 2022). Therefore, the 2.5D migration assay combined with the 3D invasion assay in this project demonstrated a considerable role of ADAMTS5 in OC migration and invasion.

Consistent with the proliferation results, TIFs also suppressed the invasion of OVCAR3 cells in an ADAMTS5-independent manner. Again, since the TIFs were derived from skin, it would be important to validate this result with normal ovarian fibroblasts. Although A2780 cells behave normally on TIF-CDM, there is the possibility that TIF-CDM negatively affected the migration of A2780 cells.

Therefore, the results of the random migration assay might need to be confirmed on CAF-CDM. Another limitation of this research is that since OVCAR3 cells express nuclear GFP, the invasive pseudopods of OVCAR3 cells are not visible in the co-culture spheroids. Although OVCAR3 cells with cytoplasmic GFP were generated, the overall expression was too low to be captured by confocal microscopy. In our preliminary results, co-culture spheroids were generated with Cell tracker™ Red CMTPX labelled OVCAR3 cells and non-labelled CAFs, where thin and elongated OVCAR3 cells were observed (data not shown). This morphology change was only observed in the 3D co-culture model and not in the 2D co-culture. Therefore, it would also be interesting to further characterise the invasive pseudopods in OVCAR3 cells in our 3D models.

Altogether, this chapter demonstrated the important role of ADAMTS5 in promoting the migration and invasion of the OC cells and in mediating the crosstalk between OC cells and CAFs in the tumours. Targeting ADAMTS5 for therapy could therefore contribute to suppress invasion and metastasis of OC.

Chapter 7 – Discussion

7.1. Summary of key findings

The essential role of the TME in supporting cancer development has been widely reported in several types of cancers (Fidler, 2003). As a crucial non-cellular component of the TME, altered ECM composition and structure were also detected in solid tumours, including ovarian carcinoma (Cho et al., 2015). These changes in ECM were caused by the dysregulation of ECM-modifying enzymes, including MMPs, ADAMs and ADAMTSs (Cox, 2021). In OC, altered expression of ADAMTS5 was previously reported in tumour stroma and was correlated to poor overall survival of OC patients (Lima et al., 2016). In this study, I investigated the molecular mechanisms leading to ADAMTS5 upregulation in OC and demonstrated the tumour promoting role of ADAMTS5 in OC, which mainly contributed to OC cell migration and invasion in 3D models.

I found that Rab25 upregulated gene expression of ADAMTS5 in OC cells in an ECM-dependent manner (Chapter 3). In OC cells stably overexpressing Rab25, ADAMTS5 mRNA and protein levels were only increased when in contact with CDM. While in OC cells that endogenously overexpressed Rab25, KD of Rab25 reduced ADAMTS5 expression both on plastic and CDM. This indicated that overexpression of Rab25 and the presence of CDM are both required for the upregulation of ADAMTS5 in OC cell lines. To further investigate the mechanisms of Rab25-induced ADAMTS5 expression, I focused on TFs, including HIF-1 α and NF- κ B, that were previously found to bind to ADAMTS5 proximal promoter and induce ADAMTS5 expression in chondrogenic cells (Chapter 4). Surprisingly, inhibition of HIF-1 α induced ADAMTS5 expression and hypoxic conditions reduced ADAMTS5 expression, which suggests that instead of upregulating ADAMTS5, HIF-1 α suppressed the expression of ADAMTS5 in OC cells. Interestingly, OC cells with NF- κ B inhibition showed reduced ADAMTS5 expression levels. Furthermore, higher protein levels of NF- κ B were observed in both the cytosol and nucleus of the Rab25 overexpressing OC cells, and Rab25 KD reduced the level of NF- κ B. This suggested that Rab25 induces ADAMTS5 expression through upregulating NF- κ B. Indeed, Rab25 was previously reported to activate AKT, which is an upstream signalling factor of NF- κ B (Fan et al., 2015, Ghoneum and Said, 2019). However, the activation level of AKT was not affected by Rab25 expression in our model, which indicates that Rab25 upregulate NF- κ B activity in an AKT-independent way. Although the inhibition of PI3K with small molecule inhibitor LY294002 also

reduced the expression level of ADAMTS5, off-target effects of the inhibitor were previously reported. For example, it can also bind to and inhibit mTORC1 directly (Gharbi et al., 2007), which is also an upstream regulator of NF- κ B (Li et al., 2016, Dan et al., 2008). Therefore, detailed mechanisms of Rab25 in mediating NF- κ B upregulation remain unclear and need to be further investigated.

To characterise the role of ADAMTS5 in OC cell proliferation ([Chapter 5](#)), invasion and migration ([Chapter 6](#)), OC cells were either treated with a small molecule inhibitor that blocks the catalytic activity of ADAMTS5 or transfected with ADAMTS5 targeting si-RNA. The proliferation of OC cells was reduced when treated with 10 μ M ADAMTS5 inhibitor in the 2D but not the 3D model, indicating the limited effect of ADAMTS5 in OC cell proliferation. However, ADAMTS5 may play a role in controlling metabolic reprogramming under nutrient starvation, as a more apparent reduction of OC cell proliferation was identified when cells were placed under glucose and serum starvation and treated with the ADAMTS5 inhibitor ([Chapter 5](#)). The migration and invasion ability of Rab25 overexpressing OC cells were significantly reduced in response to ADAMTS5 inhibition or KD ([Chapter 6](#)), which suggested the tumour-promoting role of ADAMTS5 in OC. Additionally, the role of CAFs in promoting OC cell proliferation and invasion was also inhibited under ADAMTS5 inhibition or KD ([Chapters 5 and 6](#)). Furthermore, CAFs in co-culture with ADAMTS5 deficient OC cells also showed significantly reduced invasion ability, which indicated that the crosstalk between CAFs and OC cells was also affected by ADAMTS5 downregulation ([Chapter 6](#)).

Collectively, upregulated Rab25 in OC led to the upregulation of ADAMTS5 through NF- κ B, which further promoted OC cell migration and invasion into the ECM. The catalytic activity of ADAMTS5 is essential for these tumour-promoting functions, and the crosstalk between OC cells and CAFs is also mediated by ADAMTS5 ([Figure 7.1](#)). Further works investigating the detailed mechanism of how Rab25 upregulates NF- κ B and how ADAMTS5 promotes OC cell migration and invasion are still required.

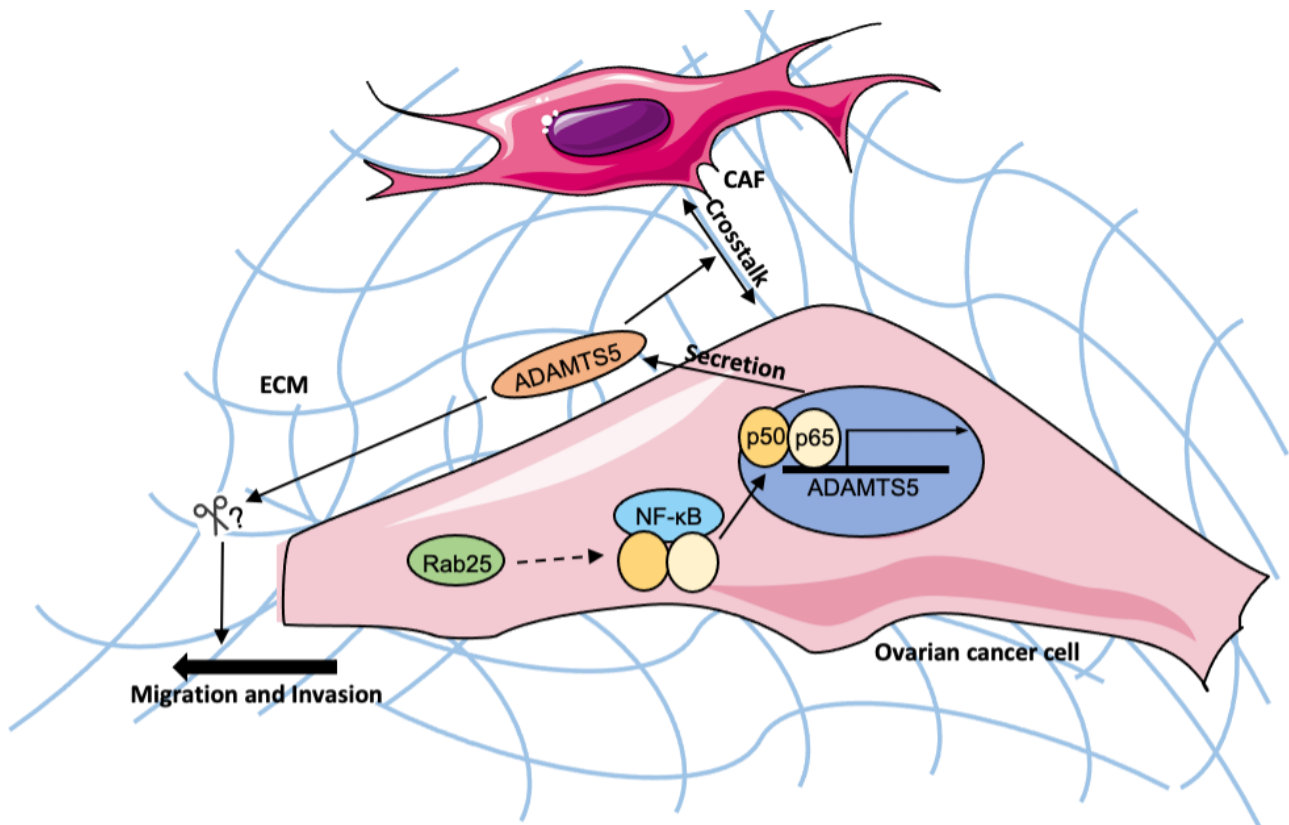


Figure 7.1. Schematic representation of the mechanisms of ADAMTS5 regulation and function. Upregulated Rab25 in OC cells induced ADAMTS5 expression through NF- κ B-related signalling pathways. OC cells secreted ADAMTS5 promoted OC cell migration and invasion into the ECM through its proteolytic activities. It can also mediate crosstalk between OC cells and CAFs in the TME. Image made with items adapted from Servier Medical Art

7.2. Rab25 regulated ADAMTS5 expression through NF- κ B-related signalling pathways.

Hyperactivation of NF- κ B was observed in multiple human malignancies, including OC (Dolcet et al., 2005, Concetti and Wilson, 2018). The activation of NF- κ B can be regulated by various signalling pathways that are triggered by cytokines and GFs. In OC, NF- κ B was shown to be activated via PI3K/AKT/mTOR signalling pathway (Figure 4.2) (Gharbi et al., 2007). However, the upregulation of NF- κ B by Rab25 in our model was found via an AKT-independent pathway (Chapter 4). Here, I will hypothesise other pathways that are potentially involved in the Rab25/NF- κ B/ADAMTS5 signalling cascade.

Apart from the PI3K/AKT pathway, ERK-mediated NF- κ B activation was also identified in multiple cancer types, including prostate, breast, ovarian carcinoma and melanoma (Kim et al., 2002, Wang

et al., 2020, Alberti et al., 2012, Dhawan and Richmond, 2002). Upon the stimulation of the small molecule tumour promoter 12-O-tetradecanoylphorbol-13-acetate (TPA), NF- κ B (p65/p50) activity and the expression of an NF- κ B-dependent gene, cyclooxygenase-2 (COX-2), were upregulated in mammary epithelial MCF10A cells (Kim et al., 2008). The activation of p38 MAPK and ERK1/2 was found essential in this pathway and the PD98059 (ERK inhibitor) and SB203580 (p38 MAPK inhibitor) significantly reduced NF- κ B activity and COX-2 expression. Similarly, inhibition of p38 MAPK in hepatocellular carcinoma also suppressed NF- κ B activation. Lenvatinib, a multi-kinase inhibitor that was used to treat hepatocellular carcinoma, was found to induce cell apoptosis and suppress metastasis both *in vitro* and *in vivo* by suppressing the p38 MAPK/NF- κ B axis (Wu et al., 2022). In prostate cancer cell lines 22Rv1, ERK was found to phosphorylate I κ B α under acidosis conditions, which further led to the activation of NF- κ B. Indeed, ERK inhibition or KD suppressed the acidosis-induced NF- κ B nuclear translocation (Chen et al., 2016a). MAPK/ERK pathway was also found involved in NF- κ B-inducing kinase (NIK)-induced NF- κ B activation in melanoma cells (Hs294T) (Dhawan and Richmond, 2002). Overexpression of NIK led to increased phosphorylation of ERK1/2, which can be suppressed by PD98059. PD98059 treatment resulted in the downregulation of NF- κ B (p50/p65) DNA binding activity, which also blocked the phosphorylation of I κ B α . In OC cells (IGROV1), EGF-induced EGFR activation led to the activation of NF- κ B and NF- κ B-dependent IL-6 and PAI-1 expression through both PI3K/AKT and MAPK/ERK pathways (Alberti et al., 2012). Cells treated with tyrosine kinase inhibitor AG1478, PI3K inhibitor LY294002, MAPK inhibitor UO126 or EGFR targeting si-RNA showed significantly reduced NF- κ B-dependent IL-6 expression.

EGFR is an important cell surface receptor that regulates MAPK/ERK signalling pathway in cancer cells through the EGFR/Ras/Raf signalling cascade (Martinelli et al., 2017). In EOC, EGF secreted by tumour-associated macrophages up-regulated the EGFR/ERK signalling pathway, which promoted OC cell migration and invasion (Zeng et al., 2019). The type I cGMP-dependent protein kinase (PKG I) was also identified as a tumour suppressor in EOC by inhibiting EGF-induced EGFR/MAPK/ERK pathway and suppressing EOC cell proliferation, migration and invasion (Lan et al., 2023). Interestingly, the association between Rab25 and EGFR activity was previously reported in multiple types of cancer. In radioresistant lung adenocarcinoma and nasopharyngeal carcinoma cells with Rab25 KD, significantly reduced levels of p-EGFR and downstream p-AKT and p-ERK were identified, indicating the role of Rab25 in mediating EGFR signalling pathways. Indeed, Rab25 was found to

mediate EGFR recycling from LE back to the cell surface in response to EGF stimulation in radioresistant nasopharyngeal carcinoma cells, and Rab25 silencing re-sensitised these cells to irradiation (Zhang et al., 2020). Alternatively, Rab25 can regulate EGFR activity through other cell surface receptors. Interactions between integrins and EGFR were previously identified in OC, which is mediated by Rab25 through integrin recycling and affects the downstream signalling pathways (Javadi et al., 2020, Cho and Lee, 2019). In breast cancer MCF-7 and OC SKOV3 cells expressing Rab25-containing vectors, increased $\beta 1$ integrin and p-EGFR levels were identified through western blotting. $\beta 1$ integrin KD in Rab25 overexpressing cells suppressed the activation of EGFR (Jeong et al., 2018). Similarly, silencing of $\beta 1$ integrin in lung cancer A549 cells reduced the activity of EGFR upon EGF stimulation, and the downstream signalling cascade was also affected (Morello et al., 2011). In a mouse model, tumours generated with $\beta 1$ integrin silenced cells were smaller compared to the control. The tumour lysate was analysed through western blotting: reduced, but not significant, p-AKT and significantly reduced p-EKR1/2 levels were detected (Morello et al., 2011). In OC A2780 cells, blocking of integrin $\alpha\beta 3$ promotes the recycling of integrin $\alpha 5\beta 1$ and enhances the interactions between integrin $\alpha 5\beta 1$ and Rab coupling protein (RCP). RCP can further interact with EGFR1 through the N terminus and mediate the recycling of integrin $\alpha 5\beta 1$ together with EGFR1 (Caswell et al., 2008). Inhibition of integrin $\alpha\beta 3$ was also found to promote EGF-induced EGFR activation and the association between EGFR, RCP and integrin $\alpha 5\beta 1$ is essential in this progress. Additionally, upregulation of downstream p-AKT but not p-ERK1/2 was observed.

Considering the association between Rab25 expression, $\beta 1$ integrin recycling, EGFR and the downstream signalling cascade activation, I hypothesise that in OC cells, upregulated Rab25 induces NF- κ B activation by promoting $\beta 1$ integrin recycling, which interacts and upregulates EGFR signalling pathways. The activated NF- κ B then mediate the expression of ADAMTS5 (Figure 7.2). As in the current research, I showed that NF- κ B activation was mediated by Rab25 in an AKT-independent pathway, it could be regulated by Rab25/EGFR/MAPK/ERK signalling pathway. Further research is required to investigate the role of the MAPK/ERK signalling pathway in Rab25 mediated NF- κ B activation in OC cells.

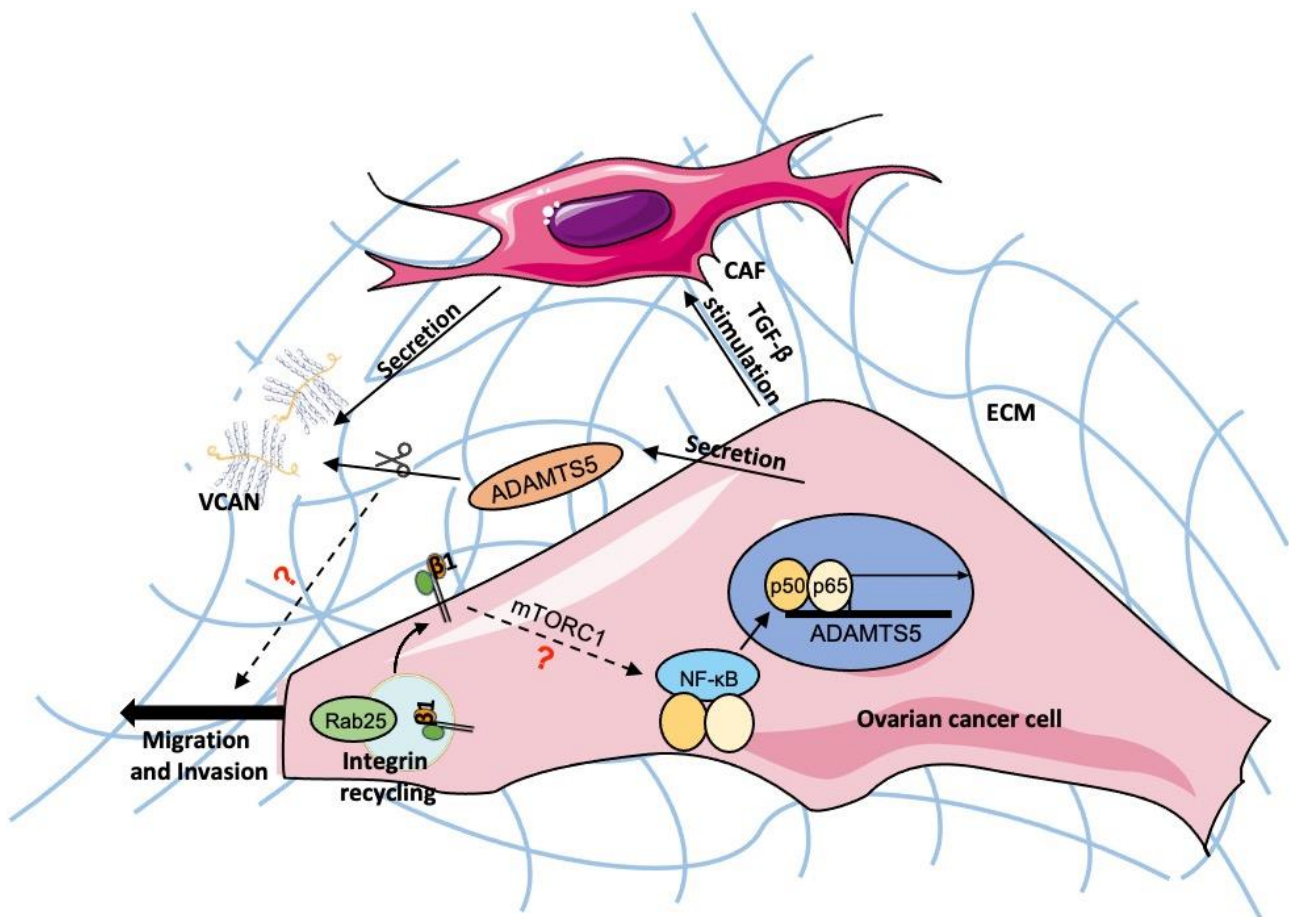


Figure 7.2. Hypothesised mechanism of Rab25 mediated NF-κB dependent ADAMTS5 upregulation and ADAMTS5 in promoting OC migration and invasion. Rab25 may upregulate NF-κB activation through $\beta 1$ integrin/EGFR/MAPK/ERK signalling cascade. Rab25 promotes $\beta 1$ integrin recycling, which associates and activates EGFR and further activates MAPK/ERK signalling pathway. Upregulated expression and enhanced secretion of ADAMTS5 by OC cells may promote cell migration and invasion by cleaving VCAN, which is derived by CAFs upon the stimulation of OC cell-secreted TGF- β .

7.3. ADAMTS5 might promote OC cell migration and invasion via VCAN cleavage.

In this project, I showed that the catalytic activity of ADAMTS5 is essential for OC cell migration and invasion. The substrates of ADAMTS5 include aggrecan, brevican, neurocan and VCAN, and the upregulation of VCAN in malignant EOC stroma has been previously observed in comparison with benign and borderline tumours (Lima et al., 2016). Furthermore, VCAN was also found to promote OC cell invasion and metastasis (Yeung et al., 2013, Ween et al., 2011), through interactions with HA and CD44, as described in [section 1.2.1.2](#). The overexpression of VCAN was mainly detected in the tumour stroma from OC patients in comparison to tumour epithelium and normal stroma, indicating that the main source of VCAN is tumour stoma cells instead of tumour cells (Ghosh et al., 2010). TGF- $\beta 3$ was found to activate primary omental CAF from HGSOC patients, which enhanced the deposition of VCAN (Delaine-Smith et al., 2021). Additionally, upon TGF- β stimulation, CAF-

secreted VCAN was found to promote OC migration and invasion (Yeung et al., 2013). ADAMTS5 can specifically cleave the V1 isoform of VCAN at the Glu⁴⁴¹-Ala⁴⁴² site and generate G1-DPEAAE versikine fragments (Longpre et al., 2009). Although the role of versikine in OC remains unclear, it has been previously reported to promote the migration and invasion of other tumour cells, such as glioma. In high-grade glioma cells, TGF- β 2 was found to upregulate the expression of VCAN isoforms V0 and V1. The level of ADAMTS5 cleaved versikine was also identified in glioma cells upon TGF- β 2 stimulation and found to contribute to the migration of glioma cells (Arslan et al., 2007). Therefore, it would be interesting to further investigate the role of ADAMTS5 cleaved VCAN in OC cell migration and invasion. The preliminary data from our lab suggested that ADAMTS5 is essential for the ECM uptake of OC cells. Since VCAN can interact with cell surface receptor CD44 which has been shown to mediate hyaluronic acid endocytosis (Ween et al., 2011), cleavage of VCAN may also be required for ECM internalisation.

A preliminary proteomic analysis was performed to compare the secretome from A2780-DNA3 and A2780-Rab25 cells when plated on plastic or TIF-CDM. Interestingly, increased TGF- β 1 level was identified in A2780-Rab25 on both plastic and CDM compared to A2780-DNA3 cells on plastic (data not shown), indicating that overexpression of Rab25 may promote the secretion of TGF- β 1 in OC cells. Similarly, the microarray data from Dozynkiewicz et al. (2012) showed that when cells were plated on CDM, TGF- β 1 expression in A2780-Rab25 cells was 1.5-fold higher in comparison with A2780-DNA3 cells. Therefore, I hypothesise that in the presence of CDM, OC cells overexpressing Rab25 might increase TGF- β secretion, which stimulates VCAN secretion from CAFs, in turn contributing to the progression of OC. ADAMTS5 secreted by OC cells then further promote the migration and invasion of OC by VCAN cleavage (Figure 7.2).

7.4. Conclusion and future directions.

The current study revealed the tumour-promotion role of ADAMTS5 in OC, which is regulated by Rab25 through an NF- κ B dependent pathway. Meanwhile, this study also raised several directions for further investigation:

- The detailed mechanism of Rab25 in regulating NF- κ B. Here, I hypothesised that Rab25 may upregulate NF- κ B activation through the EGFR/MAPK/ERK pathway instead of the PI3K/AKT

pathway. The activation level of MAPK and ERK could be tested in OC overexpressing Rab25, and the expression level of ADAMTS5 could also be tested in OC cells that were treated with MAPK/ERK pathway-specific inhibitors.

- The inhibitory role of HIF-1 in ADAMTS5 expression needs to be further characterised. In contrary with previous research, my data suggested an inhibitory role of HIF-1 in ADAMTS5 expression ([Chapter 4](#)). Under hypoxic conditions, downregulated ADAMTS5 and Rab25 expression was observed. It is not clear if the expression of any upstream regulating proteins of Rab25 and ADAMTS5 was altered under hypoxia conditions, which could be further investigated.
- Verify VCAN secretion by CAFs in co-culture with Rab25 overexpressing OC cells. Here, I hypothesised that OC cells stimulated the secretion of CAF-derived VCAN in our co-culture model by secreting TGF- β . Further experiments testing the effect of Rab25 expression in OC cells on mediating VCAN secretion by CAFs are needed.
- Verify the preliminary data of Rab25 overexpressing OC cells with enhanced TGF- β secretion when in contact with ECM, which could further explain the role of Rab25 in mediating crosstalk between OC cells and CAFs.
- ADAMTS5 may promote OC migration and invasion through VCAN cleavage. As a complement of the ADAMTS5 inhibition, antibody specifically targeting the VCAN cleavage site Glu⁴⁴¹-Ala⁴⁴² could be used to block the versican cleavage by ADAMTS5 (Foulcer et al., 2014). The migration and invasion ability of OC could be further investigated under the blocking VCAN cleavage.
- Investigate the role of ADAMTS5 cleaved versikine in promoting OC promotion. To assess this, ADAMTS5 knockdown cells will be incubated with recombinant versikine to see whether the cell migration and invasion are rescued.

Altogether, this study suggested that when in contact with ECM, the upregulation of Rab25 in OC further induced the overexpression of ADAMTS5, which was demonstrated as a promoter of OC. This study also revealed a novel function of NF- κ B in promoting OC progression through upregulating ADAMTS5 expression, which is regulated by Rab25 and potentially through the EGFR/MEPK/EKR signalling pathway. As the inhibition of ADAMTS5 catalytic activity significantly reduced the OC cell migration and invasion ability, ADMATS5 could be considered a potential therapy target for OC metastasis.

References

- AFRATIS, N. A., NIKITOVIC, D., MULTHAUPT, H. A., THEOCHARIS, A. D., COUCHMAN, J. R. & KARAMANOS, N. K. 2017. Syndecans - key regulators of cell signaling and biological functions. *FEBS J*, 284, 27-41.
- AGARWAL, R., JURISICA, I., MILLS, G. B. & CHENG, K. W. 2009. The emerging role of the RAB25 small GTPase in cancer. *Traffic*, 10, 1561-8.
- ALBERTI, C., PINCIROLI, P., VALERI, B., FERRI, R., DITTO, A., UMEZAWA, K., SENSI, M., CANEVARI, S. & TOMASSETTI, A. 2012. Ligand-dependent EGFR activation induces the co-expression of IL-6 and PAI-1 via the NFκB pathway in advanced-stage epithelial ovarian cancer. *Oncogene*, 31, 4139-49.
- AREF, S., GODA, T. & EL-SHERBINY, M. 2003. Syndecan-1 in multiple myeloma: relationship to conventional prognostic factors. *Hematology*, 8, 221-8.
- ARMSTRONG, T., PACKHAM, G., MURPHY, L. B., BATEMAN, A. C., CONTI, J. A., FINE, D. R., JOHNSON, C. D., BENYON, R. C. & IREDALE, J. P. 2004. Type I collagen promotes the malignant phenotype of pancreatic ductal adenocarcinoma. *Clinical Cancer Research*, 10, 7427-7437.
- ARSLAN, F., BOSSERHOFF, A. K., NICKL-JOCKSCHAT, T., DOERFELT, A., BOGDAHN, U. & HAU, P. 2007. The role of versican isoforms V0/V1 in glioma migration mediated by transforming growth factor-beta2. *Br J Cancer*, 96, 1560-8.
- ATACA, D., AOUAD, P., CONSTANTIN, C., LASZLO, C., BELEUT, M., SHAMSEDDIN, M., RAJARAM, R. D., JEITZNER, R., MEAD, T. J., CAIKOVSKI, M., BUCHER, P., AMBROSINI, G., APTE, S. S. & BRISKEN, C. 2020. The secreted protease Adamts18 links hormone action to activation of the mammary stem cell niche. *Nat Commun*, 11, 1571.
- ATAT, O. E., FARZANEH, Z., POURHAMZEH, M., TAKI, F., ABI-HABIB, R., VOSOUGH, M. & EL-SIBAI, M. 2022. 3D modeling in cancer studies. *Hum Cell*, 35, 23-36.
- AYHAN, A., MAO, T. L., SECKIN, T., WU, C. H., GUAN, B., OGAWA, H., FUTAGAMI, M., MIZUKAMI, H., YOKOYAMA, Y., KURMAN, R. J. & SHIH IE, M. 2012. Loss of ARID1A expression is an early molecular event in tumor progression from ovarian endometriotic cyst to clear cell and endometrioid carcinoma. *Int J Gynecol Cancer*, 22, 1310-5.
- BACCHETTI, R., YUAN, S. & RAINERO, E. 2024. ADAMTS Proteases: Their Multifaceted Role in the Regulation of Cancer Metastasis. *Diseases & Research*, 3, 1-13.
- BAGHBAN, R., ROSHANGAR, L., JAHANBAN-ESFAHLAN, R., SEIDI, K., EBRAHIMI-KALAN, A., JAYMAND, M., KOLAHIAN, S., JAVAHERI, T. & ZARE, P. 2020. Tumor microenvironment complexity and therapeutic implications at a glance. *Cell Commun Signal*, 18, 59.
- BAI, D., UENO, L. & VOGT, P. K. 2009. Akt-mediated regulation of NFκappaB and the essentialness of NFκappaB for the oncogenicity of PI3K and Akt. *Int J Cancer*, 125, 2863-70.
- BAST, R. C., JR., HENNESSY, B. & MILLS, G. B. 2009. The biology of ovarian cancer: new opportunities for translation. *Nat Rev Cancer*, 9, 415-28.
- BAYARMAGNAI, B., PERRIN, L., ESMAEILI POURFARHANGI, K., GRANA, X., TUZEL, E. & GLIGORIJEVIC, B. 2019. Invadopodia-mediated ECM degradation is enhanced in the G1 phase of the cell cycle. *J Cell Sci*, 132.
- BEAUVAIS, D. M., ELL, B. J., MCWHORTER, A. R. & RAPRAEGER, A. C. 2009. Syndecan-1 regulates alphavbeta3 and alphavbeta5 integrin activation during angiogenesis and is blocked by synstatin, a novel peptide inhibitor. *J Exp Med*, 206, 691-705.
- BEAUVAIS, D. M. & RAPRAEGER, A. C. 2010. Syndecan-1 couples the insulin-like growth factor-1 receptor to inside-out integrin activation. *J Cell Sci*, 123, 3796-807.

- BENTON, G., KLEINMAN, H. K., GEORGE, J. & ARNAOUTOVA, I. 2011. Multiple uses of basement membrane-like matrix (BME/Matrigel) in vitro and in vivo with cancer cells. *Int J Cancer*, 128, 1751-7.
- BHATLA, N. & JONES, A. 2018. THE WORLD OVARIAN CANCER COALITION ATLAS.
- BHOWMICK, N. A., NEILSON, E. G. & MOSES, H. L. 2004. Stromal fibroblasts in cancer initiation and progression. *Nature*, 432, 332-7.
- BINDER, M. J., MCCOOMBE, S., WILLIAMS, E. D., MCCULLOCH, D. R. & WARD, A. C. 2020. ADAMTS-15 Has a Tumor Suppressor Role in Prostate Cancer. *Biomolecules*, 10.
- BLOBEL, C. P. 2005. ADAMs: key components in EGFR signalling and development. *Nat Rev Mol Cell Biol*, 6, 32-43.
- BONADIO, R. R. C. C., FOGACE, R. N., MIRANDA, V. C. & DIZ, M. 2018. Homologous recombination deficiency in ovarian cancer: a review of its epidemiology and management. *Clinics (Sao Paulo)*, 73, e450s.
- BONNANS, C., CHOU, J. & WERB, Z. 2014. Remodelling the extracellular matrix in development and disease. *Nat Rev Mol Cell Biol*, 15, 786-801.
- BOS, J. L., REHMANN, H. & WITTINGHOFER, A. 2007. GEFs and GAPs: critical elements in the control of small G proteins. *Cell*, 129, 865-77.
- BOURGUIGNON, L. Y., ZHU, H., SHAO, L. & CHEN, Y. W. 2001. CD44 interaction with c-Src kinase promotes cortactin-mediated cytoskeleton function and hyaluronic acid-dependent ovarian tumor cell migration. *J Biol Chem*, 276, 7327-36.
- BOWTELL, D. D., BOHM, S., AHMED, A. A., ASPURIA, P. J., BAST, R. C., JR., BERAL, V., BEREK, J. S., BIRRER, M. J., BLAGDEN, S., BOOKMAN, M. A., BRENTON, J. D., CHIAPPINELLI, K. B., MARTINS, F. C., COUKOS, G., DRAPKIN, R., EDMONDSON, R., FOTOPOULOU, C., GABRA, H., GALON, J., GOURLEY, C., HEONG, V., HUNTSMAN, D. G., IWANICKI, M., KARLAN, B. Y., KAYE, A., LENGYEL, E., LEVINE, D. A., LU, K. H., MCNEISH, I. A., MENON, U., NAROD, S. A., NELSON, B. H., NEPHEW, K. P., PHAROAH, P., POWELL, D. J., JR., RAMOS, P., ROMERO, I. L., SCOTT, C. L., SOOD, A. K., STRONACH, E. A. & BALKWILL, F. R. 2015. Rethinking ovarian cancer II: reducing mortality from high-grade serous ovarian cancer. *Nat Rev Cancer*, 15, 668-79.
- BRACHOVA, P., THIEL, K. W. & LESLIE, K. K. 2013. The consequence of oncomorphic TP53 mutations in ovarian cancer. *Int J Mol Sci*, 14, 19257-75.
- BREBION, F., GOSMINI, R., DEPRez, P., VARIN, M., PEIXOTO, C., ALVEY, L., JARY, H., BIENVENU, N., TRIBALLEAU, N., BLANQUE, R., COTTEREAUX, C., CHRISTOPHE, T., VANDERVOORT, N., MOLLAT, P., TOUITOU, R., LEONARD, P., DE CEUNINCK, F., BOTEZ, I., MONJARDET, A., VAN DER AAR, E. & AMANTINI, D. 2021. Discovery of GLPG1972/S201086, a Potent, Selective, and Orally Bioavailable ADAMTS-5 Inhibitor for the Treatment of Osteoarthritis. *J Med Chem*, 64, 2937-2952.
- BROWNING, L., PATEL, M. R., HORVATH, E. B., TAWARA, K. & JORCYK, C. L. 2018. IL-6 and ovarian cancer: inflammatory cytokines in promotion of metastasis. *Cancer Manag Res*, 10, 6685-6693.
- BURLESON, K. M., CASEY, R. C., SKUBITZ, K. M., PAMBUCCIAN, S. E., OEGEMA, T. R., JR. & SKUBITZ, A. P. 2004. Ovarian carcinoma ascites spheroids adhere to extracellular matrix components and mesothelial cell monolayers. *Gynecol Oncol*, 93, 170-81.
- BUSHWELLER, J. H. 2019. Targeting transcription factors in cancer - from undruggable to reality. *Nat Rev Cancer*, 19, 611-624.
- CABRAL-PACHECO, G. A., GARZA-VELOZ, I., CASTRUITA-DE LA ROSA, C., RAMIREZ-ACUNA, J. M., PEREZ-ROMERO, B. A., GUERRERO-RODRIGUEZ, J. F., MARTINEZ-AVILA, N. & MARTINEZ-

- FIERRO, M. L. 2020. The Roles of Matrix Metalloproteinases and Their Inhibitors in Human Diseases. *Int J Mol Sci*, 21.
- CAI, X., WANG, K. C. & MENG, Z. 2021. Mechanoregulation of YAP and TAZ in Cellular Homeostasis and Disease Progression. *Front Cell Dev Biol*, 9, 673599.
- CAIN, S. A., WOODS, S., SINGH, M., KIMBER, S. J. & BALDOCK, C. 2022. ADAMTS6 cleaves the large latent TGFbeta complex and increases the mechanotension of cells to activate TGFbeta. *Matrix Biol*, 114, 18-34.
- CAO, C., LU, C., XU, J., ZHANG, J., ZHANG, J. & LI, M. 2013. Expression of Rab25 correlates with the invasion and metastasis of gastric cancer. *Chin J Cancer Res*, 25, 192-9.
- CARDUNER, L., AGNIEL, R., KELLOUCHE, S., PICOT, C. R., BLANC-FOURNIER, C., LEROY-DUDAL, J. & CARREIRAS, F. 2013. Ovarian cancer ascites-derived vitronectin and fibronectin: combined purification, molecular features and effects on cell response. *Biochim Biophys Acta*, 1830, 4885-97.
- CASANOVA, J. E., WANG, X., KUMAR, R., BHARTUR, S. G., NAVARRE, J., WOODRUM, J. E., ALTSCHULER, Y., RAY, G. S. & GOLDENRING, J. R. 1999. Association of Rab25 and Rab11a with the apical recycling system of polarized Madin–Darby canine kidney cells. *Molecular biology of the cell*, 10, 47-61.
- CASWELL, P. T., CHAN, M., LINDSAY, A. J., MCCAFFREY, M. W., BOETTIGER, D. & NORMAN, J. C. 2008. Rab-coupling protein coordinates recycling of alpha5beta1 integrin and EGFR1 to promote cell migration in 3D microenvironments. *J Cell Biol*, 183, 143-55.
- CASWELL, P. T., SPENCE, H. J., PARSONS, M., WHITE, D. P., CLARK, K., CHENG, K. W., MILLS, G. B., HUMPHRIES, M. J., MESSENT, A. J., ANDERSON, K. I., MCCAFFREY, M. W., OZANNE, B. W. & NORMAN, J. C. 2007. Rab25 associates with alpha5beta1 integrin to promote invasive migration in 3D microenvironments. *Dev Cell*, 13, 496-510.
- CATHCART, J., PULKOSKI-GROSS, A. & CAO, J. 2015. Targeting Matrix Metalloproteinases in Cancer: Bringing New Life to Old Ideas. *Genes Dis*, 2, 26-34.
- CHAUSSADE, C., REWCASTLE, G. W., KENDALL, J. D., DENNY, W. A., CHO, K., GRONNING, L. M., CHONG, M. L., ANAGNOSTOU, S. H., JACKSON, S. P., DANIELE, N. & SHEPHERD, P. R. 2007. Evidence for functional redundancy of class IA PI3K isoforms in insulin signalling. *Biochem J*, 404, 449-58.
- CHEAIB, B., AUGUSTE, A. & LEARY, A. 2015. The PI3K/Akt/mTOR pathway in ovarian cancer: therapeutic opportunities and challenges. *Chin J Cancer*, 34, 4-16.
- CHEN, B., LIU, J., HO, T. T., DING, X. & MO, Y. Y. 2016a. ERK-mediated NF-kappaB activation through ASIC1 in response to acidosis. *Oncogenesis*, 5, e279.
- CHEN, S., CAVAZZA, E., BARLIER, C., SALLERON, J., FILHINE-TRESARRIEU, P., GAVOILLES, C., MERLIN, J. L. & HARLE, A. 2016b. Beside P53 and PTEN: Identification of molecular alterations of the RAS/MAPK and PI3K/AKT signaling pathways in high-grade serous ovarian carcinomas to determine potential novel therapeutic targets. *Oncol Lett*, 12, 3264-3272.
- CHENG, K. W., LAHAD, J. P., KUO, W. L., LAPUK, A., YAMADA, K., AUERSPERG, N., LIU, J., SMITH-MCCUNE, K., LU, K. H., FISHMAN, D., GRAY, J. W. & MILLS, G. B. 2004. The RAB25 small GTPase determines aggressiveness of ovarian and breast cancers. *Nat Med*, 10, 1251-6.
- CHENG, N., CHYTLIL, A., SHYR, Y., JOLY, A. & MOSES, H. L. 2008. Transforming growth factor-beta signaling-deficient fibroblasts enhance hepatocyte growth factor signaling in mammary carcinoma cells to promote scattering and invasion. *Mol Cancer Res*, 6, 1521-33.

- CHEUNG, A., SHAH, S., PARKER, J., SOOR, P., LIMBU, A., SHERIFF, M. & BOUSSIOS, S. 2022. Non-Epithelial Ovarian Cancers: How Much Do We Really Know? *Int J Environ Res Public Health*, 19.
- CHO, A., HOWELL, V. M. & COLVIN, E. K. 2015. The Extracellular Matrix in Epithelial Ovarian Cancer - A Piece of a Puzzle. *Front Oncol*, 5, 245.
- CHO, K. H. & LEE, H. Y. 2019. Rab25 and RCP in cancer progression. *Arch Pharm Res*, 42, 101-112.
- CHO, K. R. & SHIH, L. 2009. Ovarian cancer. *Annu Rev Pathol*, 4, 287-313.
- CHO, S. J., JEONG, B. Y., YOON, S. H., PARK, C. G. & LEE, H. Y. 2024. Rab25 suppresses colon cancer cell invasion through upregulating claudin-7 expression. *Oncol Rep*, 51.
- CLAUSEN, M. J., MELCHERS, L. J., MASTIK, M. F., SLAGTER-MENKEMA, L., GROEN, H. J., LAAN, B. F., VAN CRIEKINGE, W., DE MEYER, T., DENIL, S., VAN DER VEGT, B., WISMAN, G. B., ROODENBURG, J. L. & SCHUURING, E. 2016. RAB25 expression is epigenetically downregulated in oral and oropharyngeal squamous cell carcinoma with lymph node metastasis. *Epigenetics*, 11, 653-663.
- COLICELLI, J. 2004. Human RAS superfamily proteins and related GTPases. *Sci STKE*, 2004, RE13.
- CONCETTI, J. & WILSON, C. L. 2018. NFKB1 and Cancer: Friend or Foe? *Cells*, 7.
- CONRAD, C., GOTTE, M., SCHLOMANN, U., ROESSLER, M., PAGENSTECHE, A., ANDERSON, P., PRESTON, J., PRUESSMEYER, J., LUDWIG, A., LI, R., KAMM, R. D., RITZ, R., CARL, B., NIMSKY, C. & BARTSCH, J. W. 2018. ADAM8 expression in breast cancer derived brain metastases: Functional implications on MMP-9 expression and transendothelial migration in breast cancer cells. *Int J Cancer*, 142, 779-791.
- CORDELIÈRES, F. P. 2005. Manual tracking. *Institut Curie, Orsay (France)*.
- COSTA, A., KIEFFER, Y., SCHOLER-DAHIREL, A., PELON, F., BOURACHOT, B., CARDON, M., SIRVEN, P., MAGAGNA, I., FUHRMANN, L., BERNARD, C., BONNEAU, C., KONDRATOVA, M., KUPERSTEIN, I., ZINOVYEV, A., GIVEL, A. M., PARRINI, M. C., SOUMELIS, V., VINCENT-SALOMON, A. & MECHTA-GRIGORIOU, F. 2018. Fibroblast Heterogeneity and Immunosuppressive Environment in Human Breast Cancer. *Cancer Cell*, 33, 463-479 e10.
- COWARD, J., KULBE, H., CHAKRAVARTY, P., LEADER, D., VASSILEVA, V., LEINSTER, D. A., THOMPSON, R., SCHIOPPA, T., NEMETH, J., VERMEULEN, J., SINGH, N., AVRIL, N., CUMMINGS, J., REXHEPAJ, E., JIRSTROM, K., GALLAGHER, W. M., BRENNAN, D. J., MCNEISH, I. A. & BALKWILL, F. R. 2011. Interleukin-6 as a therapeutic target in human ovarian cancer. *Clin Cancer Res*, 17, 6083-96.
- COX, T. R. 2021. The matrix in cancer. *Nat Rev Cancer*, 21, 217-238.
- CROSS, N. A., CHANDRASEKHARAN, S., JOKONYA, N., FOWLES, A., HAMDY, F. C., BUTTLE, D. J. & EATON, C. L. 2005. The expression and regulation of ADAMTS-1, -4, -5, -9, and -15, and TIMP-3 by TGFbeta1 in prostate cells: relevance to the accumulation of versican. *Prostate*, 63, 269-75.
- DAN, H. C., COOPER, M. J., COGSWELL, P. C., DUNCAN, J. A., TING, J. P. & BALDWIN, A. S. 2008. Akt-dependent regulation of NF-kappaB is controlled by mTOR and Raptor in association with IKK. *Genes Dev*, 22, 1490-500.
- DELAINE-SMITH, R. M., MANIATI, E., MALACRIDA, B., NICHOLS, S., ROOZITALAB, R., JONES, R. R., LECKER, L. S. M., PEARCE, O. M. T., KNIGHT, M. M. & BALKWILL, F. R. 2021. Modelling TGFbetaR and Hh pathway regulation of prognostic matrix molecules in ovarian cancer. *iScience*, 24, 102674.
- DELINASSIOS, J. G. & HOFFMAN, R. M. 2022. The cancer-inhibitory effects of proliferating tumor-residing fibroblasts. *Biochim Biophys Acta Rev Cancer*, 1877, 188673.

- DEMIRCAN, K., GUNDUZ, E., GUNDUZ, M., BEDER, L. B., HIROHATA, S., NAGATSUKA, H., CENGIZ, B., CILEK, M. Z., YAMANAKA, N., SHIMIZU, K. & NINOMIYA, Y. 2009. Increased mRNA expression of ADAMTS metalloproteinases in metastatic foci of head and neck cancer. *Head Neck*, 31, 793-801.
- DERYUGINA, E. I., SOROCEANU, L. & STRONGIN, A. Y. 2002. Up-regulation of vascular endothelial growth factor by membrane-type 1 matrix metalloproteinase stimulates human glioma xenograft growth and angiogenesis. *Cancer research*, 62, 580-588.
- DESAI, B., ROGERS, M. J. & CHELLAIAH, M. A. 2007. Mechanisms of osteopontin and CD44 as metastatic principles in prostate cancer cells. *Mol Cancer*, 6, 18.
- DEYING, W., FENG, G., SHUMEI, L., HUI, Z., MING, L. & HONGQING, W. 2017. CAF-derived HGF promotes cell proliferation and drug resistance by up-regulating the c-Met/PI3K/Akt and GRP78 signalling in ovarian cancer cells. *Biosci Rep*, 37.
- DHAWAN, P. & RICHMOND, A. 2002. A novel NF-kappa B-inducing kinase-MAPK signaling pathway up-regulates NF-kappa B activity in melanoma cells. *J Biol Chem*, 277, 7920-8.
- DING, B., CUI, B., GAO, M., LI, Z., XU, C., FAN, S. & HE, W. 2017. Knockdown of Ras-Related Protein 25 (Rab25) Inhibits the In Vitro Cytotoxicity and In Vivo Antitumor Activity of Human Glioblastoma Multiforme Cells. *Oncol Res*, 25, 331-340.
- DING, B., YE, Z., YIN, H., HONG, X. Y., FENG, S. W., XU, J. Y. & SHEN, Y. 2023. Exosomes derived from ovarian cancer cells regulate proliferation and migration of cancer-associated fibroblasts. *Genomics*, 115, 110703.
- DOLCET, X., LLOBET, D., PALLARES, J. & MATIAS-GUIU, X. 2005. NF-kB in development and progression of human cancer. *Virchows Arch*, 446, 475-82.
- DOMCKE, S., SINHA, R., LEVINE, D. A., SANDER, C. & SCHULTZ, N. 2013. Evaluating cell lines as tumour models by comparison of genomic profiles. *Nat Commun*, 4, 2126.
- DOŻYNKIEWICZ, M., A. 2011. *The role of the Chloride Intracellular Channel-3 (CLIC3) in integrin trafficking and tumour progression*. Doctor of Philosophy, University of Glasgow.
- DOZYNKIEWICZ, M. A., JAMIESON, N. B., MACPHERSON, I., GRINDLAY, J., VAN DEN BERGHE, P. V., VON THUN, A., MORTON, J. P., GOURLEY, C., TIMPSON, P., NIXON, C., MCKAY, C. J., CARTER, R., STRACHAN, D., ANDERSON, K., SANSOM, O. J., CASWELL, P. T. & NORMAN, J. C. 2012. Rab25 and CLIC3 collaborate to promote integrin recycling from late endosomes/lysosomes and drive cancer progression. *Dev Cell*, 22, 131-45.
- EBERHARDY, S. R. & FARNHAM, P. J. 2002. Myc recruits P-TEFb to mediate the final step in the transcriptional activation of the cad promoter. *J Biol Chem*, 277, 40156-62.
- EDWARDS, D. R., HANDSLEY, M. M. & PENNINGTON, C. J. 2008. The ADAM metalloproteinases. *Mol Aspects Med*, 29, 258-89.
- EFEYAN, A., ZONCU, R. & SABATINI, D. M. 2012. Amino acids and mTORC1: from lysosomes to disease. *Trends Mol Med*, 18, 524-33.
- EOH, K. J., KIM, H. M., LEE, J. Y., KIM, S., KIM, S. W., KIM, Y. T. & NAM, E. J. 2020. Mutation landscape of germline and somatic BRCA1/2 in patients with high-grade serous ovarian cancer. *BMC Cancer*, 20, 204.
- EREZ, N., GLANZ, S., RAZ, Y., AVIVI, C. & BARSHACK, I. 2013. Cancer associated fibroblasts express pro-inflammatory factors in human breast and ovarian tumors. *Biochem Biophys Res Commun*, 437, 397-402.
- FAN, Y., WANG, L., HAN, X., LIU, X. & MA, H. 2015. Rab25 is responsible for phosphoinositide 3-kinase/AKT-mediated cisplatin resistance in human epithelial ovarian cancer cells. *Mol Med Rep*, 11, 2173-8.

- FIDLER, I. J. 2003. The pathogenesis of cancer metastasis: the 'seed and soil' hypothesis revisited. *Nature reviews cancer*, 3, 453-458.
- FLORIO, T. J., LOKAREDDY, R. K., YEGGONI, D. P., SANKHALA, R. S., OTT, C. A., GILLILAN, R. E. & CINGOLANI, G. 2022. Differential recognition of canonical NF-kappaB dimers by Importin alpha3. *Nat Commun*, 13, 1207.
- FONTANIL, T., ÁLVAREZ-TEIJEIRO, S., VILLARONGA, M. Á., MOHAMEDI, Y., SOLARES, L., MONCADA-PAZOS, A., VEGA, J. A., GARCÍA-SUÁREZ, O., PÉREZ-BASTERRECHEA, M. & GARCÍA-PEDRERO, J. M. 2017. Cleavage of Fibulin-2 by the aggrecanases ADAMTS-4 and ADAMTS-5 contributes to the tumorigenic potential of breast cancer cells. *Oncotarget*, 8, 13716.
- FONTANIL, T., MOHAMEDI, Y., MONCADA-PAZOS, A., COBO, T., VEGA, J. A., COBO, J. L., GARCIA-SUAREZ, O., COBO, J., OBAYA, A. J. & CAL, S. 2019. Neurocan is a New Substrate for the ADAMTS12 Metalloprotease: Potential Implications in Neuropathies. *Cell Physiol Biochem*, 52, 1003-1016.
- FONTANIL, T., RÚA, S., LLAMAZARES, M., MONCADA-PAZOS, A., QUIRÓS, P. M., GARCÍA-SUÓREZ, O., VEGA, J. A., SASAKI, T., MOHAMEDI, Y. & ESTEBAN, M. M. 2014. Interaction between the ADAMTS-12 metalloprotease and fibulin-2 induces tumor-suppressive effects in breast cancer cells. *Oncotarget*, 5, 1253.
- FONTOURA, J. C., VIEZZER, C., DOS SANTOS, F. G., LIGABUE, R. A., WEINLICH, R., PUGA, R. D., ANTONOW, D., SEVERINO, P. & BONORINO, C. 2020. Comparison of 2D and 3D cell culture models for cell growth, gene expression and drug resistance. *Mater Sci Eng C Mater Biol Appl*, 107, 110264.
- FOTOPOULOU, C., HALL, M., CRUICKSHANK, D., GABRA, H., GANESAN, R., HUGHES, C., KEHOE, S., LEDERMANN, J., MORRISON, J., NAIK, R., ROLLAND, P. & SUNDAR, S. 2017. British Gynaecological Cancer Society (BGCS) epithelial ovarian/fallopian tube/primary peritoneal cancer guidelines: recommendations for practice. *Eur J Obstet Gynecol Reprod Biol*, 213, 123-139.
- FOULCER, S. J., NELSON, C. M., QUINTERO, M. V., KUBERAN, B., LARKIN, J., DOURS-ZIMMERMANN, M. T., ZIMMERMANN, D. R. & APTE, S. S. 2014. Determinants of versican-V1 proteoglycan processing by the metalloproteinase ADAMTS5. *J Biol Chem*, 289, 27859-73.
- FRANTZ, C., STEWART, K. M. & WEAVER, V. M. 2010. The extracellular matrix at a glance. *J Cell Sci*, 123, 4195-200.
- FRIETZE, S. & FARNHAM, P. J. 2011. Transcription factor effector domains. *Subcell Biochem*, 52, 261-77.
- FUJIKAWA, K., SUZUKI, H., MCMULLEN, B. & CHUNG, D. 2001. Purification of human von Willebrand factor-cleaving protease and its identification as a new member of the metalloproteinase family. *Blood, The Journal of the American Society of Hematology*, 98, 1662-1666.
- GAGGIOLI, C., HOOPER, S., HIDALGO-CARCEDO, C., GROSSE, R., MARSHALL, J. F., HARRINGTON, K. & SAHAI, E. 2007. Fibroblast-led collective invasion of carcinoma cells with differing roles for RhoGTPases in leading and following cells. *Nat Cell Biol*, 9, 1392-400.
- GAO, Q., YANG, Z., XU, S., LI, X., YANG, X., JIN, P., LIU, Y., ZHOU, X., ZHANG, T., GONG, C., WEI, X., LIU, D., SUN, C., CHEN, G., HU, J., MENG, L., ZHOU, J., SAWADA, K., FRUSCIO, R., GRUNT, T. W., WISCHHUSEN, J., VARGAS-HERNANDEZ, V. M., POTHURI, B. & COLEMAN, R. L. 2019. Heterotypic CAF-tumor spheroids promote early peritoneal metastasis of ovarian cancer. *J Exp Med*, 216, 688-703.
- GEERTZ, M., SHORE, D. & MAERKL, S. J. 2012. Massively parallel measurements of molecular interaction kinetics on a microfluidic platform. *Proc Natl Acad Sci U S A*, 109, 16540-5.

- GHARBI, S. I., ZVELEBIL, M. J., SHUTTLEWORTH, S. J., HANCOX, T., SAGHIR, N., TIMMS, J. F. & WATERFIELD, M. D. 2007. Exploring the specificity of the PI3K family inhibitor LY294002. *Biochem J*, 404, 15-21.
- GHONEUM, A. & SAID, N. 2019. PI3K-AKT-mTOR and NFkappaB Pathways in Ovarian Cancer: Implications for Targeted Therapeutics. *Cancers (Basel)*, 11.
- GHOSH, S., ALBITAR, L., LEBARON, R., WELCH, W. R., SAMIMI, G., BIRRER, M. J., BERKOWITZ, R. S. & MOK, S. C. 2010. Up-regulation of stromal versican expression in advanced stage serous ovarian cancer. *Gynecologic oncology*, 119, 114-120.
- GIBNEY, E. R. & NOLAN, C. M. 2010. Epigenetics and gene expression. *Heredity (Edinb)*, 105, 4-13.
- GIBSON, S. V., MADZHAROVA, E., TAN, A. C., ALLEN, M. D., KELLER, U. A. D., LOUISE JONES, J., CARTER, E. P. & GROSE, R. P. 2023. ADAMTS3 restricts cancer invasion in models of early breast cancer progression through enhanced fibronectin degradation. *Matrix Biol*, 121, 74-89.
- GIEBELER, N. & ZIGRINO, P. 2016. A Disintegrin and Metalloprotease (ADAM): Historical Overview of Their Functions. *Toxins (Basel)*, 8, 122.
- GILBERT, A. M., BURSAVICH, M. G., LOMBARDI, S., GEORGIADIS, K. E., REIFENBERG, E., FLANNERY, C. R. & MORRIS, E. A. 2007. 5-((1H-pyrazol-4-yl)methylene)-2-thioxothiazolidin-4-one inhibitors of ADAMTS-5. *Bioorg Med Chem Lett*, 17, 1189-92.
- GIOPANO, I., BRAVOU, V., PAPANASTASOPOULOS, P., LILIS, I., AROUKATOS, P., PAPACHRISTOU, D., KOUNELIS, S. & PAPADAKI, H. 2014. Metadherin, p50, and p65 expression in epithelial ovarian neoplasms: an immunohistochemical study. *Biomed Res Int*, 2014, 178410.
- GOLDENRING, J. R. & NAM, K. T. 2011. Rab25 as a tumour suppressor in colon carcinogenesis. *Br J Cancer*, 104, 33-6.
- GOMEZ-ROMAN, N., MCGREGOR, F., WHEATE, N. J. & PLUMB, J. A. 2015. Cucurbit [7] uril encapsulated cisplatin overcomes resistance to cisplatin induced by Rab25 overexpression in an intraperitoneal ovarian cancer model. *J Ovarian Res*, 8, 62.
- GOMEZ-ROMAN, N., SAHASRABUDHE, N. M., MCGREGOR, F., CHALMERS, A. J., CASSIDY, J. & PLUMB, J. 2016. Hypoxia-inducible factor 1 alpha is required for the tumourigenic and aggressive phenotype associated with Rab25 expression in ovarian cancer. *Oncotarget*, 7, 22650.
- GOODISON, S., URQUIDI, V. & TARIN, D. 1999. CD44 cell adhesion molecules. *Molecular pathology*, 52, 189.
- GU, J., CHEN, J., FENG, J., LIU, Y., XUE, Q., MAO, G., GAI, L., LU, X., ZHANG, R., CHENG, J., HU, Y., SHAO, M., SHEN, H. & HUANG, J. 2016. Overexpression of ADAMTS5 can regulate the migration and invasion of non-small cell lung cancer. *Tumour Biol*, 37, 8681-9.
- GUO, D. & DONNER, D. B. 1996. Tumor necrosis factor promotes phosphorylation and binding of insulin receptor substrate 1 to phosphatidylinositol 3-kinase in 3T3-L1 adipocytes. *J Biol Chem*, 271, 615-8.
- GUO, H., HA, C., DONG, H., YANG, Z., MA, Y. & DING, Y. 2019. Cancer-associated fibroblast-derived exosomal microRNA-98-5p promotes cisplatin resistance in ovarian cancer by targeting CDKN1A. *Cancer Cell Int*, 19, 347.
- GUPTA, A., CAO, W. & CHELLAIAH, M. A. 2012. Integrin $\alpha\beta3$ and CD44 pathways in metastatic prostate cancer cells support osteoclastogenesis via a Runx2/Smad 5/receptor activator of NF- κ B ligand signaling axis. *Molecular cancer*, 11, 1-17.
- GYORFFY, B., LANCZKY, A. & SZALLASI, Z. 2012. Implementing an online tool for genome-wide validation of survival-associated biomarkers in ovarian-cancer using microarray data from 1287 patients. *Endocr Relat Cancer*, 19, 197-208.

- HAN, Q., TAN, S., GONG, L., LI, G., WU, Q., CHEN, L., DU, S., LI, W., LIU, X., CAI, J. & WANG, Z. 2023. Omental cancer-associated fibroblast-derived exosomes with low microRNA-29c-3p promote ovarian cancer peritoneal metastasis. *Cancer Sci*, 114, 1929-1942.
- HANAHAH, D. & WEINBERG, R. A. 2011. Hallmarks of cancer: the next generation. *Cell*, 144, 646-74.
- HARAGUCHI, N., OHARA, N., KOSEKI, J., TAKAHASHI, H., NISHIMURA, J., HATA, T., MIZUSHIMA, T., YAMAMOTO, H., ISHII, H., DOKI, Y. & MORI, M. 2017. High expression of ADAMTS5 is a potent marker for lymphatic invasion and lymph node metastasis in colorectal cancer. *Mol Clin Oncol*, 6, 130-134.
- HARRIS, A. L. 2002. Hypoxia--a key regulatory factor in tumour growth. *Nat Rev Cancer*, 2, 38-47.
- HE, H., DAI, F., YU, L., SHE, X., ZHAO, Y., JIANG, J., CHEN, X. & ZHAO, S. 2002. Identification and characterization of nine novel human small GTPases showing variable expressions in liver cancer tissues. *Gene Expression The Journal of Liver Research*, 10, 231-242.
- HE, S., HUANG, Q., HU, J., LI, L., XIAO, Y., YU, H., HAN, Z., WANG, T., ZHOU, W., WEI, H. & XIAO, J. 2019. EWS-FLI1-mediated tenascin-C expression promotes tumour progression by targeting MALAT1 through integrin alpha5beta1-mediated YAP activation in Ewing sarcoma. *Br J Cancer*, 121, 922-933.
- HELD-FEINDT, J., PAREDES, E. B., BLOMER, U., SEIDENBECHER, C., STARK, A. M., MEHDORN, H. M. & MENTLEIN, R. 2006. Matrix-degrading proteases ADAMTS4 and ADAMTS5 (disintegrins and metalloproteinases with thrombospondin motifs 4 and 5) are expressed in human glioblastomas. *Int J Cancer*, 118, 55-61.
- HERNANDEZ, L., KIM, M. K., LYLE, L. T., BUNCH, K. P., HOUSE, C. D., NING, F., NOONAN, A. M. & ANNUNZIATA, C. M. 2016. Characterization of ovarian cancer cell lines as in vivo models for preclinical studies. *Gynecol Oncol*, 142, 332-40.
- HERNANDEZ-BARRANTES, S., SHIMURA, Y., SOLOWAY, P. D., SANG, Q. A. & FRIDMAN, R. 2001. Differential roles of TIMP-4 and TIMP-2 in pro-MMP-2 activation by MT1-MMP. *Biochem Biophys Res Commun*, 281, 126-30.
- HERNANDEZ-FERNAUD, J. R., RUENGLER, E., CASAZZA, A., NEILSON, L. J., PULLEINE, E., SANTI, A., ISMAIL, S., LILLA, S., DHAYADE, S., MACPHERSON, I. R., MCNEISH, I., ENNIS, D., ALI, H., KUGERATSKI, F. G., AL KHAMICI, H., VAN DEN BIGGELAAR, M., VAN DEN BERGHE, P. V., CLOIX, C., MCDONALD, L., MILLAN, D., HOYLE, A., KUCHNIO, A., CARMELIET, P., VALENZUELA, S. M., BLYTH, K., YIN, H., MAZZONE, M., NORMAN, J. C. & ZANIVAN, S. 2017. Secreted CLIC3 drives cancer progression through its glutathione-dependent oxidoreductase activity. *Nat Commun*, 8, 14206.
- HILLEMAYER, L., ESPINOZA-SANCHEZ, N. A., GREVE, B., HASSAN, N., CHELARIU-RAICU, A., KIESEL, L. & GOTTE, M. 2022. The Cell Surface Heparan Sulfate Proteoglycan Syndecan-3 Promotes Ovarian Cancer Pathogenesis. *Int J Mol Sci*, 23.
- HOESEL, B. & SCHMID, J. A. 2013. The complexity of NF- κ B signaling in inflammation and cancer. *Molecular cancer*, 12, 1-15.
- HOLLIS, R. L., THOMSON, J. P., VAN BAAL, J., ILENKOVAN, N., CHURCHMAN, M., VAN DE VIJVER, K., DIJK, F., MEYNERT, A. M., BARTOS, C., RYE, T., CROY, I., DIANA, P., VAN GENT, M., CREEDON, H., NIRSIMLOO, R., LOK, C., GOURLEY, C. & HERRINGTON, C. S. 2023. Distinct histopathological features are associated with molecular subtypes and outcome in low grade serous ovarian carcinoma. *Sci Rep*, 13, 7681.
- HOU, J., YAN, D., LIU, Y., HUANG, P. & CUI, H. 2020. The Roles of Integrin alpha5beta1 in Human Cancer. *Onco Targets Ther*, 13, 13329-13344.

- HU, C., CHEN, B., ZHOU, Y. & SHAN, Y. 2017. High expression of Rab25 contributes to malignant phenotypes and biochemical recurrence in patients with prostate cancer after radical prostatectomy. *Cancer Cell Int*, 17, 45.
- HU, X., JIANG, C., HU, N. & HONG, S. 2023. ADAMTS1 induces epithelial-mesenchymal transition pathway in non-small cell lung cancer by regulating TGF- β . *Aging (Albany NY)*, 15, 2097.
- HUANG, H., WANG, Z., ZHANG, Y., PRADHAN, R. N., GANGULY, D., CHANDRA, R., MURIMWA, G., WRIGHT, S., GU, X., MADDIPATI, R., MULLER, S., TURLEY, S. J. & BREKKEN, R. A. 2022a. Mesothelial cell-derived antigen-presenting cancer-associated fibroblasts induce expansion of regulatory T cells in pancreatic cancer. *Cancer Cell*, 40, 656-673 e7.
- HUANG, J., CHAN, W. C., NGAI, C. H., LOK, V., ZHANG, L., LUCERO-PRISNO, D. E., 3RD, XU, W., ZHENG, Z. J., ELCARTE, E., WITHERS, M., WONG, M. C. S. & ON BEHALF OF NCD GLOBAL HEALTH RESEARCH GROUP OF ASSOCIATION OF PACIFIC RIM UNIVERSITIES, A. 2022b. Worldwide Burden, Risk Factors, and Temporal Trends of Ovarian Cancer: A Global Study. *Cancers (Basel)*, 14.
- HUANG, J., SUN, Y., CHEN, H., LIAO, Y., LI, S., CHEN, C. & YANG, Z. 2019. ADAMTS5 acts as a tumor suppressor by inhibiting migration, invasion and angiogenesis in human gastric cancer. *Gastric Cancer*, 22, 287-301.
- HUANG, J., ZHANG, L., WAN, D., ZHOU, L., ZHENG, S., LIN, S. & QIAO, Y. 2021. Extracellular matrix and its therapeutic potential for cancer treatment. *Signal Transduct Target Ther*, 6, 153.
- HUVENEERS, S., TRUONG, H., FASSLER, R., SONNENBERG, A. & DANEN, E. H. 2008. Binding of soluble fibronectin to integrin alpha5 beta1 - link to focal adhesion redistribution and contractile shape. *J Cell Sci*, 121, 2452-62.
- HYNES, R. O. 1987. Integrins: a family of cell surface receptors. *cell*, 48, 549-554.
- HYNES, R. O. 2002. Integrins: bidirectional, allosteric signaling machines. *cell*, 110, 673-687.
- HYNES, R. O. & YAMADA, K. M. 1982. Fibronectins: multifunctional modular glycoproteins. *The Journal of cell biology*, 95, 369-377.
- IOZZO, R. V. & SCHAEFER, L. 2015. Proteoglycan form and function: A comprehensive nomenclature of proteoglycans. *Matrix Biol*, 42, 11-55.
- JAVADI, S., ZHIANI, M., MOUSAVI, M. A. & FATHI, M. 2020. Crosstalk between Epidermal Growth Factor Receptors (EGFR) and integrins in resistance to EGFR tyrosine kinase inhibitors (TKIs) in solid tumors. *Eur J Cell Biol*, 99, 151083.
- JEONG, B. Y., CHO, K. H., JEONG, K. J., PARK, Y. Y., KIM, J. M., RHA, S. Y., PARK, C. G., MILLS, G. B., CHEONG, J. H. & LEE, H. Y. 2018. Rab25 augments cancer cell invasiveness through a beta1 integrin/EGFR/VEGF-A/Snail signaling axis and expression of fascin. *Exp Mol Med*, 50, e435.
- JI, Q., XU, X., ZHANG, Q., KANG, L., XU, Y., ZHANG, K., LI, L., LIANG, Y., HONG, T., YE, Q. & WANG, Y. 2016. The IL-1beta/AP-1/miR-30a/ADAMTS-5 axis regulates cartilage matrix degradation in human osteoarthritis. *J Mol Med (Berl)*, 94, 771-85.
- JIANG, L., LIN, J., ZHAO, S., WU, J., JIN, Y., YU, L., WU, N., WU, Z., WANG, Y. & LIN, M. 2021. ADAMTS5 in Osteoarthritis: Biological Functions, Regulatory Network, and Potential Targeting Therapies. *Front Mol Biosci*, 8, 703110.
- JUBELIN, C., MUNOZ-GARCIA, J., GRISCOM, L., COCHONNEAU, D., OLLIVIER, E., HEYMANN, M. F., VALLETTE, F. M., OLIVER, L. & HEYMANN, D. 2022. Three-dimensional in vitro culture models in oncology research. *Cell Biosci*, 12, 155.
- KALLURI, R. 2016. The biology and function of fibroblasts in cancer. *Nat Rev Cancer*, 16, 582-98.
- KARIN, M. & BEN-NERIAH, Y. 2000. Phosphorylation meets ubiquitination: the control of NF- κ B activity. *Annual review of immunology*, 18, 621-663.

- KAUKONEN, R., MAI, A., GEORGIADOU, M., SAARI, M., DE FRANCESCHI, N., BETZ, T., SIHTO, H., VENTELA, S., ELO, L., JOKITALO, E., WESTERMARCK, J., KELLOKUMPU-LEHTINEN, P. L., JOENSUU, H., GRENNAN, R. & IVASKA, J. 2016. Normal stroma suppresses cancer cell proliferation via mechanosensitive regulation of JMJD1a-mediated transcription. *Nat Commun*, 7, 12237.
- KAWASHIMA, H., HIROSE, M., HIROSE, J., NAGAKUBO, D., PLAAS, A. H. & MIYASAKA, M. 2000. Binding of a large chondroitin sulfate/dermatan sulfate proteoglycan, versican, to L-selectin, P-selectin, and CD44. *J Biol Chem*, 275, 35448-56.
- KELWICK, R., DESANLIS, I., WHEELER, G. N. & EDWARDS, D. R. 2015. The ADAMTS (A Disintegrin and Metalloproteinase with Thrombospondin motifs) family. *Genome Biol*, 16, 113.
- KENNY, H. A., CHIANG, C. Y., WHITE, E. A., SCHRYVER, E. M., HABIS, M., ROMERO, I. L., LADANYI, A., PENICKA, C. V., GEORGE, J., MATLIN, K., MONTAG, A., WROBLEWSKI, K., YAMADA, S. D., MAZAR, A. P., BOWTELL, D. & LENGYEL, E. 2014. Mesothelial cells promote early ovarian cancer metastasis through fibronectin secretion. *J Clin Invest*, 124, 4614-28.
- KENNY, H. A., KAUR, S., COUSSENS, L. M. & LENGYEL, E. 2008. The initial steps of ovarian cancer cell metastasis are mediated by MMP-2 cleavage of vitronectin and fibronectin. *J Clin Invest*, 118, 1367-79.
- KERDIDANI, D., AERAKIS, E., VERROU, K. M., ANGELIDIS, I., DOUKA, K., MANIOU, M. A., STAMOULIS, P., GOUDEVENOU, K., PRADOS, A., TZAFERIS, C., NTAFIS, V., VAMVAKARIS, I., KANIARIS, E., VACHLAS, K., SEPSAS, E., KOUTSOPOULOS, A., POTARIS, K. & TSOUMAKIDOU, M. 2022. Lung tumor MHCII immunity depends on in situ antigen presentation by fibroblasts. *J Exp Med*, 219.
- KIM, B.-Y., GAYNOR, R. B., SONG, K., DRITSCHILO, A. & JUNG, M. 2002. Constitutive activation of NF- κ B in Ki-ras-transformed prostate epithelial cells. *Oncogene*, 21, 4490-4497.
- KIM, J. H., NA, H. K., PAK, Y. K., LEE, Y. S., LEE, S. J., MOON, A. & SURH, Y. J. 2008. Roles of ERK and p38 mitogen-activated protein kinases in phorbol ester-induced NF-kappaB activation and COX-2 expression in human breast epithelial cells. *Chem Biol Interact*, 171, 133-41.
- KIM, K. S., SENGUPTA, S., BERK, M., KWAK, Y. G., ESCOBAR, P. F., BELINSON, J., MOK, S. C. & XU, Y. 2006. Hypoxia enhances lysophosphatidic acid responsiveness in ovarian cancer cells and lysophosphatidic acid induces ovarian tumor metastasis in vivo. *Cancer Res*, 66, 7983-90.
- KIM, S. H., LEE, H. Y., JUNG, S. P., KIM, S., LEE, J. E., NAM, S. J. & BAE, J. W. 2014. Role of secreted type I collagen derived from stromal cells in two breast cancer cell lines. *Oncol Lett*, 8, 507-512.
- KINBARA, K., GOLDFINGER, L. E., HANSEN, M., CHOU, F. L. & GINSBERG, M. H. 2003. Ras GTPases: integrins' friends or foes? *Nat Rev Mol Cell Biol*, 4, 767-76.
- KLEMBBA, A., BODNAR, L., WAS, H., BRODACZEWSKA, K. K., WCISLO, G., SZCZYLIK, C. A. & KIEDA, C. 2020. Hypoxia-Mediated Decrease of Ovarian Cancer Cells Reaction to Treatment: Significance for Chemo- and Immunotherapies. *Int J Mol Sci*, 21.
- KOBAYASHI, H., HIRATA, M., SAITO, T., ITOH, S., CHUNG, U. I. & KAWAGUCHI, H. 2013. Transcriptional induction of ADAMTS5 protein by nuclear factor-kappaB (NF-kappaB) family member RelA/p65 in chondrocytes during osteoarthritis development. *J Biol Chem*, 288, 28620-9.
- KONG, D., PARK, E. J., STEPHEN, A. G., CALVANI, M., CARDELLINA, J. H., MONKS, A., FISHER, R. J., SHOEMAKER, R. H. & MELILLO, G. 2005. Echinomycin, a small-molecule inhibitor of hypoxia-inducible factor-1 DNA-binding activity. *Cancer Res*, 65, 9047-55.

- KONSTANTINOPOULOS, P. A., KARAMOUZIS, M. V., PAPATSORIS, A. G. & PAPAVALASSILIOU, A. G. 2008. Matrix metalloproteinase inhibitors as anticancer agents. *Int J Biochem Cell Biol*, 40, 1156-68.
- KOSHIYAMA, M., MATSUMURA, N. & KONISHI, I. 2017. Subtypes of Ovarian Cancer and Ovarian Cancer Screening. *Diagnostics (Basel)*, 7.
- KOUL, D., YAO, Y., ABBRUZZESE, J. L., YUNG, W. K. & REDDY, S. A. 2001. Tumor suppressor MMAC/PTEN inhibits cytokine-induced NFkappaB activation without interfering with the IkappaB degradation pathway. *J Biol Chem*, 276, 11402-8.
- KUJAWA, K. A., ZEMBALA-NOZYNSKA, E., CORTEZ, A. J., KUJAWA, T., KUPRYJANCZYK, J. & LISOWSKA, K. M. 2020. Fibronectin and Periostin as Prognostic Markers in Ovarian Cancer. *Cells*, 9.
- KUMAR, S., SHARGHI-NAMINI, S., RAO, N. & GE, R. 2012. ADAMTS5 functions as an anti-angiogenic and anti-tumorigenic protein independent of its proteoglycanase activity. *Am J Pathol*, 181, 1056-68.
- KUTZ, W. E., WANG, L. W., BADER, H. L., MAJORS, A. K., IWATA, K., TRABOULSI, E. I., SAKAI, L. Y., KEENE, D. R. & APTE, S. S. 2011. ADAMTS10 protein interacts with fibrillin-1 and promotes its deposition in extracellular matrix of cultured fibroblasts. *J Biol Chem*, 286, 17156-67.
- LAMBERT, S. A., JOLMA, A., CAMPITELLI, L. F., DAS, P. K., YIN, Y., ALBU, M., CHEN, X., TAIPALE, J., HUGHES, T. R. & WEIRAUCH, M. T. 2018. The Human Transcription Factors. *Cell*, 172, 650-665.
- LAN, T., LI, Y., WANG, Y., WANG, Z. C., MU, C. Y., TAO, A. B., GONG, J. L., ZHOU, Y., XU, H., LI, S. B., GU, B., MA, P. & LUO, L. 2023. Increased endogenous PKG I activity attenuates EGF-induced proliferation and migration of epithelial ovarian cancer via the MAPK/ERK pathway. *Cell Death Dis*, 14, 39.
- LATCHMAN, D. S. 1997. Transcription factors: an overview. *The international journal of biochemistry & cell biology*, 29, 1305-1312.
- LATOURTE, A., CHERIFI, C., MAILLET, J., EA, H. K., BOUAZIZ, W., FUNCK-BRENTANO, T., COHEN-SOLAL, M., HAY, E. & RICHELLE, P. 2017. Systemic inhibition of IL-6/Stat3 signalling protects against experimental osteoarthritis. *Ann Rheum Dis*, 76, 748-755.
- LEBLANC, R., SAHAY, D., HOUSSIN, A., MACHUCA-GAYET, I. & PEYRUCHAUD, O. 2018. Autotaxin- β interaction with the cell surface via syndecan-4 impacts on cancer cell proliferation and metastasis. *Oncotarget*, 9, 33170.
- LEE, T. I. & YOUNG, R. A. 2013. Transcriptional regulation and its misregulation in disease. *Cell*, 152, 1237-51.
- LEITAO, M. M., SOSLOW, R. A., BAERGEN, R. N., OLVERA, N., ARROYO, C. & BOYD, J. 2004. Mutation and expression of the TP53 gene in early stage epithelial ovarian carcinoma. *Gynecol Oncol*, 93, 301-6.
- LENGYEL, E. 2010. Ovarian cancer development and metastasis. *Am J Pathol*, 177, 1053-64.
- LI, C., XIONG, Y., YANG, X., WANG, L., ZHANG, S., DAI, N., LI, M., REN, T., YANG, Y., ZHOU, S. F., GAN, L. & WANG, D. 2015a. Lost expression of ADAMTS5 protein associates with progression and poor prognosis of hepatocellular carcinoma. *Drug Des Devel Ther*, 9, 1773-83.
- LI, H., ZENG, J. & SHEN, K. 2014. PI3K/AKT/mTOR signaling pathway as a therapeutic target for ovarian cancer. *Arch Gynecol Obstet*, 290, 1067-78.
- LI, J., LIAO, Y., HUANG, J., SUN, Y., CHEN, H., CHEN, C., LI, S. & YANG, Z. 2018. Epigenetic silencing of ADAMTS5 is associated with increased invasiveness and poor survival in patients with colorectal cancer. *J Cancer Res Clin Oncol*, 144, 215-227.

- LI, M., WANG, J., WANG, C., XIA, L., XU, J., XIE, X. & LU, W. 2020. Microenvironment remodeled by tumor and stromal cells elevates fibroblast-derived COL1A1 and facilitates ovarian cancer metastasis. *Exp Cell Res*, 394, 112153.
- LI, Y., JIA, Q., ZHANG, Q. & WAN, Y. 2015b. Rab25 upregulation correlates with the proliferation, migration, and invasion of renal cell carcinoma. *Biochem Biophys Res Commun*, 458, 745-50.
- LI, Z., YANG, Z., PASSANITI, A., LAPIDUS, R. G., LIU, X., CULLEN, K. J. & DAN, H. C. 2016. A positive feedback loop involving EGFR/Akt/mTORC1 and IKK/NF- κ B regulates head and neck squamous cell carcinoma proliferation. *Oncotarget*, 7, 31892.
- LIM, H. C. & COUCHMAN, J. R. 2014. Syndecan-2 regulation of morphology in breast carcinoma cells is dependent on RhoGTPases. *Biochim Biophys Acta*, 1840, 2482-90.
- LIMA, M. A., DOS SANTOS, L., TURRI, J. A., NONOGAKI, S., BUIM, M., LIMA, J. F., DE JESUS VIANA PINHEIRO, J., BUENO DE TOLEDO OSORIO, C. A., SOARES, F. A. & FREITAS, V. M. 2016. Prognostic Value of ADAMTS Proteases and Their Substrates in Epithelial Ovarian Cancer. *Pathobiology*, 83, 316-26.
- LIN, Y., LIANG, X., ZHANG, X., NI, Y., ZHOU, X. & ZHAO, X. 2022. Metabolic cross-talk between ovarian cancer and the tumor microenvironment-providing potential targets for cancer therapy. *Front Biosci (Landmark Ed)*, 27, 139.
- LIU, Y., TAO, X., JIA, L., CHENG, K. W., LU, Y., YU, Y. & FENG, Y. 2012. Knockdown of RAB25 promotes autophagy and inhibits cell growth in ovarian cancer cells. *Molecular medicine reports*, 6, 1006-1012.
- LIU, Y. J., XU, Y. & YU, Q. 2006. Full-length ADAMTS-1 and the ADAMTS-1 fragments display pro- and antimetastatic activity, respectively. *Oncogene*, 25, 2452-67.
- LONGPRE, J. M., MCCULLOCH, D. R., KOO, B. H., ALEXANDER, J. P., APTE, S. S. & LEDUC, R. 2009. Characterization of proADAMTS5 processing by proprotein convertases. *Int J Biochem Cell Biol*, 41, 1116-26.
- LORD, S. J., VELLE, K. B., MULLINS, R. D. & FRITZ-LAYLIN, L. K. 2020. SuperPlots: Communicating reproducibility and variability in cell biology. *J Cell Biol*, 219.
- LU, J., ZHOU, S., SIECH, M., HABISCH, H., SEUFFERLEIN, T. & BACHEM, M. G. 2014. Pancreatic stellate cells promote hapto-migration of cancer cells through collagen I-mediated signalling pathway. *Br J Cancer*, 110, 409-20.
- MA, B. & YU, R. 2023. Pan-cancer analysis of ADAMs: A promising biomarker for prognosis and response to chemotherapy and immunotherapy. *Front Genet*, 14, 1105900.
- MABUCHI, S., OHMICHU, M., NISHIO, Y., HAYASAKA, T., KIMURA, A., OHTA, T., SAITO, M., KAWAGOE, J., TAKAHASHI, K., YADA-HASHIMOTO, N., SAKATA, M., MOTOYAMA, T., KURACHI, H., TASAKA, K. & MURATA, Y. 2004. Inhibition of NFkappaB increases the efficacy of cisplatin in in vitro and in vivo ovarian cancer models. *J Biol Chem*, 279, 23477-85.
- MAINGONNAT, C., COUREL, M. N., BERTRAND, P., VINCENT, J. C., SESBOUE, R. & DELPECH, B. 2003. Hyaluronidase in sera of tumour-bearing nude mice. *Biomarkers*, 8, 333-8.
- MANNING-GEIST, B., GORDHANDAS, S., LIU, Y. L., ZHOU, Q., IASONOS, A., DA CRUZ PAULA, A., MANDELKER, D., LONG ROCHE, K., ZIVANOVIC, O., MAIO, A., KEMEL, Y., CHI, D. S., O'CEARBHAILL, R. E., AGHAJANIAN, C., WEIGELT, B., CHUI, M. H. & GRISHAM, R. N. 2022. MAPK Pathway Genetic Alterations Are Associated with Prolonged Overall Survival in Low-Grade Serous Ovarian Carcinoma. *Clin Cancer Res*, 28, 4456-4465.
- MARITSCHNEGG, E., WANG, Y., PECHA, N., HORVAT, R., VAN NIEUWENHUYSEN, E., VERGOTE, I., HEITZ, F., SEHOULI, J., KINDE, I., DIAZ, L. A., JR., PAPADOPOULOS, N., KINZLER, K. W., VOGELSTEIN, B., SPEISER, P. & ZEILLINGER, R. 2015. Lavage of the Uterine Cavity for

- Molecular Detection of Mullerian Duct Carcinomas: A Proof-of-Concept Study. *J Clin Oncol*, 33, 4293-300.
- MARTINCUKS, A., LI, P. C., ZHAO, Q., ZHANG, C., LI, Y. J., YU, H. & RODRIGUEZ-RODRIGUEZ, L. 2020. CD44 in Ovarian Cancer Progression and Therapy Resistance-A Critical Role for STAT3. *Front Oncol*, 10, 589601.
- MARTINELLI, E., MORGILLO, F., TROIANI, T. & CIARDIELLO, F. 2017. Cancer resistance to therapies against the EGFR-RAS-RAF pathway: The role of MEK. *Cancer Treat Rev*, 53, 61-69.
- MARTINO-ECHARRI, E., FERNANDEZ-RODRIGUEZ, R., RODRIGUEZ-BAENA, F. J., BARRIENTOS-DURAN, A., TORRES-COLLADO, A. X., PLAZA-CALONGE MDEL, C., AMADOR-CUBERO, S., CORTES, J., REYNOLDS, L. E., HODIVALA-DILKE, K. M. & RODRIGUEZ-MANZANEQUE, J. C. 2013. Contribution of ADAMTS1 as a tumor suppressor gene in human breast carcinoma. Linking its tumor inhibitory properties to its proteolytic activity on nidogen-1 and nidogen-2. *Int J Cancer*, 133, 2315-24.
- MASUI, T., HOSOTANI, R., TSUJI, S., MIYAMOTO, Y., YASUDA, S., IDA, J., NAKAJIMA, S., KAWAGUCHI, M., KOBAYASHI, H. & KOIZUMI, M. 2001. Expression of METH-1 and METH-2 in pancreatic cancer. *Clinical Cancer Research*, 7, 3437-3443.
- MCFARLANE, S., COULTER, J. A., TIBBITS, P., O'GRADY, A., MCFARLANE, C., MONTGOMERY, N., HILL, A., MCCARTHY, H. O., YOUNG, L. S. & KAY, E. W. 2015. CD44 increases the efficiency of distant metastasis of breast cancer. *Oncotarget*, 6, 11465.
- MEIER-SOELCH, J., MAYR-BURO, C., JULI, J., LEIB, L., LINNE, U., DREUTE, J., PAPANTONIS, A., SCHMITZ, M. L. & KRACHT, M. 2021. Monitoring the Levels of Cellular NF-kappaB Activation States. *Cancers (Basel)*, 13.
- MEMMOTT, R. M. & DENNIS, P. A. 2009. Akt-dependent and -independent mechanisms of mTOR regulation in cancer. *Cell Signal*, 21, 656-64.
- MIERKE, C. T. 2023. The versatile roles of ADAM8 in cancer cell migration, mechanics, and extracellular matrix remodeling. *Front Cell Dev Biol*, 11, 1130823.
- MOLIERE, S., JAULIN, A., TOMASETTO, C. L. & DALI-YOUCHEF, N. 2023. Roles of Matrix Metalloproteinases and Their Natural Inhibitors in Metabolism: Insights into Health and Disease. *Int J Mol Sci*, 24.
- MONTEL, V., KLEEMAN, J., AGARWAL, D., SPINELLA, D., KAWAI, K. & TARIN, D. 2004. Altered metastatic behavior of human breast cancer cells after experimental manipulation of matrix metalloproteinase 8 gene expression. *Cancer Research*, 64, 1687-1694.
- MOORE, A. R., ROSENBERG, S. C., MCCORMICK, F. & MALEK, S. 2020. RAS-targeted therapies: is the undruggable drugged? *Nat Rev Drug Discov*, 19, 533-552.
- MORELLO, V., CABODI, S., SIGISMUND, S., CAMACHO-LEAL, M. P., REPETTO, D., VOLANTE, M., PAPOTTI, M., TURCO, E. & DEFILIPPI, P. 2011. beta1 integrin controls EGFR signaling and tumorigenic properties of lung cancer cells. *Oncogene*, 30, 4087-96.
- MORENO-LAYSECA, P., ICHA, J., HAMIDI, H. & IVASKA, J. 2019. Integrin trafficking in cells and tissues. *Nat Cell Biol*, 21, 122-132.
- MORGAN, M. R., HUMPHRIES, M. J. & BASS, M. D. 2007. Synergistic control of cell adhesion by integrins and syndecans. *Nat Rev Mol Cell Biol*, 8, 957-69.
- MOSS, N. M., BARBOLINA, M. V., LIU, Y., SUN, L., MUNSHI, H. G. & STACK, M. S. 2009. Ovarian cancer cell detachment and multicellular aggregate formation are regulated by membrane type 1 matrix metalloproteinase: a potential role in l.p. metastatic dissemination. *Cancer Res*, 69, 7121-9.

- MOSTAFAVI-POUR, Z., ASKARI, J. A., PARKINSON, S. J., PARKER, P. J., NG, T. T. & HUMPHRIES, M. J. 2003. Integrin-specific signaling pathways controlling focal adhesion formation and cell migration. *J Cell Biol*, 161, 155-67.
- MOUW, J. K., OU, G. & WEAVER, V. M. 2014. Extracellular matrix assembly: a multiscale deconstruction. *Nat Rev Mol Cell Biol*, 15, 771-85.
- MULLOOLY, M., MCGOWAN, P. M., CROWN, J. & DUFFY, M. J. 2016. The ADAMs family of proteases as targets for the treatment of cancer. *Cancer Biol Ther*, 17, 870-80.
- MURAKAMI, T., NISHIYAMA, T., SHIROTANI, T., SHINOHARA, Y., KAN, M., ISHII, K., KANAI, F., NAKAZURU, S. & EBINA, Y. 1992. Identification of two enhancer elements in the gene encoding the type 1 glucose transporter from the mouse which are responsive to serum, growth factor, and oncogenes. *Journal of Biological Chemistry*, 267, 9300-9306.
- MURANEN, T., IWANICKI, M. P., CURRY, N. L., HWANG, J., DUBOIS, C. D., COLOFF, J. L., HITCHCOCK, D. S., CLISH, C. B., BRUGGE, J. S. & KALAANY, N. Y. 2017. Starved epithelial cells uptake extracellular matrix for survival. *Nat Commun*, 8, 13989.
- NABA, A., CLAUSER, K. R., HOERSCH, S., LIU, H., CARR, S. A. & HYNES, R. O. 2012. The matrisome: in silico definition and in vivo characterization by proteomics of normal and tumor extracellular matrices. *Mol Cell Proteomics*, 11, M111 014647.
- NAM, K. T., LEE, H. J., SMITH, J. J., LAPIERRE, L. A., KAMATH, V. P., CHEN, X., ARONOW, B. J., YEATMAN, T. J., BHARTUR, S. G., CALHOUN, B. C., CONDIE, B., MANLEY, N. R., BEAUCHAMP, R. D., COFFEY, R. J. & GOLDENRING, J. R. 2010. Loss of Rab25 promotes the development of intestinal neoplasia in mice and is associated with human colorectal adenocarcinomas. *J Clin Invest*, 120, 840-9.
- NAMEKI, R., CHANG, H., REDDY, J., CORONA, R. I. & LAWRENSON, K. 2021. Transcription factors in epithelial ovarian cancer: histotype-specific drivers and novel therapeutic targets. *Pharmacol Ther*, 220, 107722.
- NAZEMI, M. 2021. *ECM internalisation as a novel modulator of cancer cell growth/survival*. Doctor of Philosophy, The University of Sheffield.
- NAZEMI, M., YANES, B., MARTINEZ, M. L., WALKER, H. J., PHAM, K., COLLINS, M. O., BARD, F. & RAINERO, E. 2024. The extracellular matrix supports breast cancer cell growth under amino acid starvation by promoting tyrosine catabolism. *PLoS Biol*, 22, e3002406.
- NILAND, S. & EBLE, J. A. 2020. Hold on or Cut? Integrin- and MMP-Mediated Cell-Matrix Interactions in the Tumor Microenvironment. *Int J Mol Sci*, 22.
- NISSEN, N. I., KARSDAL, M. & WILLUMSEN, N. 2019. Collagens and Cancer associated fibroblasts in the reactive stroma and its relation to Cancer biology. *J Exp Clin Cancer Res*, 38, 115.
- NORTHCUTT, L. A., QUESTELL, A. M., RHOADES, J. & RAFAT, M. 2023. Development of an alginate-Matrigel hydrogel system to evaluate cancer cell behavior in the stiffness range of the bone marrow. *Front Biomater Sci*, 2.
- NYANTE, S. J., WANG, T., TAN, X., OZDOWSKI, E. F. & LAWTON, T. J. 2019. Quantitative expression of MMPs 2, 9, 14, and collagen IV in LCIS and paired normal breast tissue. *Sci Rep*, 9, 13432.
- PANG, X., HE, X., QIU, Z., ZHANG, H., XIE, R., LIU, Z., GU, Y., ZHAO, N., XIANG, Q. & CUI, Y. 2023. Targeting integrin pathways: mechanisms and advances in therapy. *Signal Transduct Target Ther*, 8, 1.
- PANKOV, R., CUKIERMAN, E., KATZ, B.-Z., MATSUMOTO, K., LIN, D. C., LIN, S., HAHN, C. & YAMADA, K. M. 2000. Integrin dynamics and matrix assembly: tensin-dependent translocation of $\alpha 5 \beta 1$ integrins promotes early fibronectin fibrillogenesis. *The Journal of cell biology*, 148, 1075-1090.

- PAPADAS, A. & ASIMAKOPOULOS, F. 2020. Versican in the Tumor Microenvironment. *Adv Exp Med Biol*, 1272, 55-72.
- PARIS, S., SESBOUE, R., CHAUZY, C., MAINGONNAT, C. & DELPECH, B. 2006. Hyaluronectin modulation of lung metastasis in nude mice. *Eur J Cancer*, 42, 3253-9.
- PATEL, A. G., SARKARIA, J. N. & KAUFMANN, S. H. 2011. Nonhomologous end joining drives poly(ADP-ribose) polymerase (PARP) inhibitor lethality in homologous recombination-deficient cells. *Proc Natl Acad Sci U S A*, 108, 3406-11.
- PEARCE, O. M. T., DELAINE-SMITH, R. M., MANIATI, E., NICHOLS, S., WANG, J., BOHM, S., RAJEEVE, V., ULLAH, D., CHAKRAVARTY, P., JONES, R. R., MONTFORT, A., DOWE, T., GRIBBEN, J., JONES, J. L., KOCHER, H. M., SERODY, J. S., VINCENT, B. G., CONNELLY, J., BRENTON, J. D., CHELALA, C., CUTILLAS, P. R., LOCKLEY, M., BESSANT, C., KNIGHT, M. M. & BALKWILL, F. R. 2018. Deconstruction of a Metastatic Tumor Microenvironment Reveals a Common Matrix Response in Human Cancers. *Cancer Discov*, 8, 304-319.
- PFEIFFER, T., SCHUSTER, S. & BONHOEFFER, S. 2001. Cooperation and competition in the evolution of ATP-producing pathways. *Science*, 292, 504-507.
- PIERCE, J. W., SCHOENLEBER, R., JESMOK, G., BEST, J., MOORE, S. A., COLLINS, T. & GERRITSEN, M. E. 1997. Novel inhibitors of cytokine-induced I κ B α phosphorylation and endothelial cell adhesion molecule expression show anti-inflammatory effects in vivo. *Journal of Biological Chemistry*, 272, 21096-21103.
- POLANSKA, U. M., ACAR, A. & ORIMO, A. 2011. Experimental generation of carcinoma-associated fibroblasts (CAFs) from human mammary fibroblasts. *J Vis Exp*, e3201.
- PRADEEP, S., KIM, S. W., WU, S. Y., NISHIMURA, M., CHALUVALLY-RAGHAVAN, P., MIYAKE, T., PECOT, C. V., KIM, S. J., CHOI, H. J., BISCHOFF, F. Z., MAYER, J. A., HUANG, L., NICK, A. M., HALL, C. S., RODRIGUEZ-AGUAYO, C., ZAND, B., DALTON, H. J., ARUMUGAM, T., LEE, H. J., HAN, H. D., CHO, M. S., RUPAIMOOLE, R., MANGALA, L. S., SEHGAL, V., OH, S. C., LIU, J., LEE, J. S., COLEMAN, R. L., RAM, P., LOPEZ-BERESTEIN, G., FIDLER, I. J. & SOOD, A. K. 2014. Hematogenous metastasis of ovarian cancer: rethinking mode of spread. *Cancer Cell*, 26, 77-91.
- PRAT, J. 2014. Staging classification for cancer of the ovary, fallopian tube, and peritoneum. *Int J Gynaecol Obstet*, 124, 1-5.
- QUAIL, D. F. & JOYCE, J. A. 2013. Microenvironmental regulation of tumor progression and metastasis. *Nat Med*, 19, 1423-37.
- RA, H. J. & PARKS, W. C. 2007. Control of matrix metalloproteinase catalytic activity. *Matrix Biol*, 26, 587-96.
- RAINERO, E., HOWE, J. D., CASWELL, P. T., JAMIESON, N. B., ANDERSON, K., CRITCHLEY, D. R., MACHESKY, L. & NORMAN, J. C. 2015. Ligand-Occupied Integrin Internalization Links Nutrient Signaling to Invasive Migration. *Cell Rep*, 10, 398-413.
- REDDY, S. A., HUANG, J. H. & LIAO, W. S. 1997. Phosphatidylinositol 3-kinase in interleukin 1 signaling. Physical interaction with the interleukin 1 receptor and requirement in NF κ B and AP-1 activation. *J Biol Chem*, 272, 29167-73.
- REDMAN, C., DUFFY, S., BROMHAM, N., FRANCIS, K. & GUIDELINE DEVELOPMENT, G. 2011. Recognition and initial management of ovarian cancer: summary of NICE guidance. *BMJ*, 342, d2073.
- REITER, F., WIENERROITHER, S. & STARK, A. 2017. Combinatorial function of transcription factors and cofactors. *Curr Opin Genet Dev*, 43, 73-81.
- RICARD-BLUM, S. 2011. The collagen family. *Cold Spring Harb Perspect Biol*, 3, a004978.

- RODRIGUEZ-MANZANEQUE, J. C., CARPIZO, D., PLAZA-CALONGE MDEL, C., TORRES-COLLADO, A. X., THAI, S. N., SIMONS, M., HOROWITZ, A. & IRUELA-ARISPE, M. L. 2009. Cleavage of syndecan-4 by ADAMTS1 provokes defects in adhesion. *Int J Biochem Cell Biol*, 41, 800-10.
- ROSE, K. W. J., TAYE, N., KAROULIAS, S. Z. & HUBMACHER, D. 2021. Regulation of ADAMTS Proteases. *Front Mol Biosci*, 8, 701959.
- RUBI-SANS, G., NYGA, A., REBOLLO, E., PEREZ-AMODIO, S., OTERO, J., NAVAJAS, D., MATEOS-TIMONEDA, M. A. & ENGEL, E. 2021. Development of Cell-Derived Matrices for Three-Dimensional In Vitro Cancer Cell Models. *ACS Appl Mater Interfaces*, 13, 44108-44123.
- SACCANI, S., PANTANO, S. & NATOLI, G. 2003. Modulation of NF-kappaB activity by exchange of dimers. *Mol Cell*, 11, 1563-74.
- SAHAI, E., ASTSATUROV, I., CUKIERMAN, E., DENARDO, D. G., EGEBLAD, M., EVANS, R. M., FEARON, D., GRETEN, F. R., HINGORANI, S. R., HUNTER, T., HYNES, R. O., JAIN, R. K., JANOWITZ, T., JORGENSEN, C., KIMMELMAN, A. C., KOLONIN, M. G., MAKI, R. G., POWERS, R. S., PURE, E., RAMIREZ, D. C., SCHERZ-SHOVAL, R., SHERMAN, M. H., STEWART, S., TLSTY, T. D., TUVESON, D. A., WATT, F. M., WEAVER, V., WEERARATNA, A. T. & WERB, Z. 2020. A framework for advancing our understanding of cancer-associated fibroblasts. *Nat Rev Cancer*, 20, 174-186.
- SALEHI, F., DUNFIELD, L., PHILLIPS, K. P., KREWSKI, D. & VANDERHYDEN, B. C. 2008. Risk factors for ovarian cancer: an overview with emphasis on hormonal factors. *J Toxicol Environ Health B Crit Rev*, 11, 301-21.
- SALMIVIRTA, M. & JALKANEN, M. 1995. Syndecan family of cell surface proteoglycans: developmentally regulated receptors for extracellular effector molecules. *Experientia*, 51, 863-872.
- SANTAMARIA, S. 2020. ADAMTS-5: A difficult teenager turning 20. *Int J Exp Pathol*, 101, 4-20.
- SARWAR, M., SYKES, P. H., CHITCHOLTAN, K. & EVANS, J. J. 2022. Collagen I dysregulation is pivotal for ovarian cancer progression. *Tissue Cell*, 74, 101704.
- SCHINDELIN, J., ARGANDA-CARRERAS, I., FRISE, E., KAYNIG, V., LONGAIR, M., PIETZSCH, T., PREIBISCH, S., RUEDEN, C., SAALFELD, S., SCHMID, B., TINEVEZ, J. Y., WHITE, D. J., HARTENSTEIN, V., ELICEIRI, K., TOMANCAK, P. & CARDONA, A. 2012. Fiji: an open-source platform for biological-image analysis. *Nat Methods*, 9, 676-82.
- SCHLOMANN, U., KOLLER, G., CONRAD, C., FERDOUS, T., GOLFI, P., GARCIA, A. M., HOFLING, S., PARSONS, M., COSTA, P., SOPER, R., BOSSARD, M., HAGEMANN, T., ROSHANI, R., SEWALD, N., KETCHEM, R. R., MOSS, M. L., RASMUSSEN, F. H., MILLER, M. A., LAUFFENBURGER, D. A., TUVESON, D. A., NIMSKY, C. & BARTSCH, J. W. 2015. ADAM8 as a drug target in pancreatic cancer. *Nat Commun*, 6, 6175.
- SCHMALFELDT, B., PRECHTEL, D., HÄRTING, K., SPÄTHE, K., RUTKE, S., KONIK, E., FRIDMAN, R., BERGER, U., SCHMITT, M. & KUHN, W. 2001. Increased expression of matrix metalloproteinases (MMP)-2, MMP-9, and the urokinase-type plasminogen activator is associated with progression from benign to advanced ovarian cancer. *Clinical Cancer Research*, 7, 2396-2404.
- SCHNELLMANN, R., SACK, R., HESS, D., ANNIS, D. S., MOSHER, D. F., APTE, S. S. & CHIQUET-EHRISMANN, R. 2018. A Selective Extracellular Matrix Proteomics Approach Identifies Fibronectin Proteolysis by A Disintegrin-like and Metalloprotease Domain with Thrombospondin Type 1 Motifs (ADAMTS16) and Its Impact on Spheroid Morphogenesis. *Mol Cell Proteomics*, 17, 1410-1425.
- SCHNITZER, T., PUEYO, M., DECKX, H., VAN DER AAR, E., BERNARD, K., HATCH, S., VAN DER STOEP, M., GRANKOV, S., PHUNG, D., IMBERT, O., CHIMITS, D., MULLER, K., HOCHBERG, M. C.,

- BLIDDAL, H., WIRTH, W., ECKSTEIN, F. & CONAGHAN, P. G. 2023. Evaluation of S201086/GLPG1972, an ADAMTS-5 inhibitor, for the treatment of knee osteoarthritis in ROCCELLA: a phase 2 randomized clinical trial. *Osteoarthritis Cartilage*, 31, 985-994.
- SENBANJO, L. T. & CHELLAIAH, M. A. 2017. CD44: A Multifunctional Cell Surface Adhesion Receptor Is a Regulator of Progression and Metastasis of Cancer Cells. *Front Cell Dev Biol*, 5, 18.
- SEVEN, D., DOGAN, S., KILIC, E., KARAMAN, E., KOSEOGLU, H. & BUYRU, N. 2015. Downregulation of Rab25 activates Akt1 in head and neck squamous cell carcinoma. *Oncol Lett*, 10, 1927-1931.
- SHAHABI, A., NAGHILI, B., ANSARIN, K., MONTAZERI, M., DADASHPOUR, M. & ZARGHAMI, N. 2021. Let-7d and miR-185 Impede Epithelial-Mesenchymal Transition by Downregulating Rab25 in Breast Cancer. *Asian Pac J Cancer Prev*, 22, 305-313.
- SHENDER, V. O., PAVLYUKOV, M. S., ZIGANSHIN, R. H., ARAPIDI, G. P., KOVALCHUK, S. I., ANIKANOV, N. A., ALTUKHOV, I. A., ALEXEEV, D. G., BUTENKO, I. O., SHAVARDA, A. L., KHOMYAKOVA, E. B., EVTUSHENKO, E., ASHRAFYAN, L. A., ANTONOVA, I. B., KUZNETCOV, I. N., GORBACHEV, A. Y., SHAKHPARONOV, M. I. & GOVORUN, V. M. 2014. Proteome-metabolome profiling of ovarian cancer ascites reveals novel components involved in intercellular communication. *Mol Cell Proteomics*, 13, 3558-71.
- SHI, R., ZHANG, Z., ZHU, A., XIONG, X., ZHANG, J., XU, J., SY, M. S. & LI, C. 2022. Targeting type I collagen for cancer treatment. *Int J Cancer*, 151, 665-683.
- SHIN, J., KIM, G., KABIR, M. H., PARK, S. J., LEE, S. T. & LEE, C. 2015. Use of composite protein database including search result sequences for mass spectrometric analysis of cell secretome. *PLoS One*, 10, e0121692.
- SHIN, J., RHIM, J., KWON, Y., CHOI, S. Y., SHIN, S., HA, C. W. & LEE, C. 2019. Comparative analysis of differentially secreted proteins in serum-free and serum-containing media by using BONCAT and pulsed SILAC. *Sci Rep*, 9, 3096.
- SIZEMORE, N., LEUNG, S. & STARK, G. R. 1999. Activation of phosphatidylinositol 3-kinase in response to interleukin-1 leads to phosphorylation and activation of the NF- κ B p65/RelA subunit. *Molecular and cellular biology*, 19, 4798-4805.
- SNOEK-VAN BEURDEN, P. A. & VON DEN HOFF, J. W. 2005. Zymographic techniques for the analysis of matrix metalloproteinases and their inhibitors. *Biotechniques*, 38, 73-83.
- SORENSEN, E. W., GERBER, S. A., SEDLACEK, A. L., RYBALKO, V. Y., CHAN, W. M. & LORD, E. M. 2009. Omental immune aggregates and tumor metastasis within the peritoneal cavity. *Immunologic research*, 45, 185-194.
- SOUNNI, N. E., ROGHI, C., CHABOTTAUX, V., JANSSEN, M., MUNAUT, C., MAQUOI, E., GALVEZ, B. G., GILLES, C., FRANKENNE, F., MURPHY, G., FOIDART, J. M. & NOEL, A. 2004. Up-regulation of vascular endothelial growth factor-A by active membrane-type 1 matrix metalloproteinase through activation of Src-tyrosine kinases. *J Biol Chem*, 279, 13564-74.
- STANTON, H., MELROSE, J., LITTLE, C. B. & FOSANG, A. J. 2011. Proteoglycan degradation by the ADAMTS family of proteinases. *Biochim Biophys Acta*, 1812, 1616-29.
- STUELTEN, C. H., DACOSTA BYFIELD, S., ARANY, P. R., KARPOVA, T. S., STETLER-STEVENSON, W. G. & ROBERTS, A. B. 2005. Breast cancer cells induce stromal fibroblasts to express MMP-9 via secretion of TNF- α and TGF- β . *J Cell Sci*, 118, 2143-53.
- SUH, J., KIM, D. H. & SURH, Y. J. 2018. Resveratrol suppresses migration, invasion and stemness of human breast cancer cells by interfering with tumor-stromal cross-talk. *Arch Biochem Biophys*, 643, 62-71.

- SUNDAR, S. S., ZHANG, H., BROWN, P., MANEK, S., HAN, C., KAUR, K., CHARNOCK, M. F., JACKSON, D. & GANESAN, T. S. 2006. Role of lymphangiogenesis in epithelial ovarian cancer. *Br J Cancer*, 94, 1650-7.
- SUNG, H., FERLAY, J., SIEGEL, R. L., LAVERSANNE, M., SOERJOMATARAM, I., JEMAL, A. & BRAY, F. 2021. Global Cancer Statistics 2020: GLOBOCAN Estimates of Incidence and Mortality Worldwide for 36 Cancers in 185 Countries. *CA Cancer J Clin*, 71, 209-249.
- TALMADGE, J. E. & FIDLER, I. J. 2010. AACR centennial series: the biology of cancer metastasis: historical perspective. *Cancer Res*, 70, 5649-69.
- TEMEL, S. G., GIRAY, A., KARAKAS, B., GUL, O., KOZANOGLU, I., CELIK, H., BASAGA, H., ACIKBAS, U., SUCULARLI, C., OZTOP, S., AKA, Y. & KUTUK, O. 2020. RAB25 confers resistance to chemotherapy by altering mitochondrial apoptosis signaling in ovarian cancer cells. *Apoptosis*, 25, 799-816.
- THODETI, C. K., ALBRECHTSEN, R., GRAUSLUND, M., ASMAR, M., LARSSON, C., TAKADA, Y., MERCURIO, A. M., COUCHMAN, J. R. & WEWER, U. M. 2003. ADAM12/syndecan-4 signaling promotes beta 1 integrin-dependent cell spreading through protein kinase Calpha and RhoA. *J Biol Chem*, 278, 9576-84.
- THOMPSON, C. B. & BIELSKA, A. A. 2019. Growth factors stimulate anabolic metabolism by directing nutrient uptake. *J Biol Chem*, 294, 17883-17888.
- TIMMS, K. P. & MAURICE, S. B. 2020. Context-dependent bioactivity of versican fragments. *Glycobiology*, 30, 365-373.
- TONG, M., CHAN, K. W., BAO, J. Y., WONG, K. Y., CHEN, J. N., KWAN, P. S., TANG, K. H., FU, L., QIN, Y. R., LOK, S., GUAN, X. Y. & MA, S. 2012. Rab25 is a tumor suppressor gene with antiangiogenic and anti-invasive activities in esophageal squamous cell carcinoma. *Cancer Res*, 72, 6024-35.
- TORRE, L. A., TRABERT, B., DESANTIS, C. E., MILLER, K. D., SAMIMI, G., RUNOWICZ, C. D., GAUDET, M. M., JEMAL, A. & SIEGEL, R. L. 2018. Ovarian cancer statistics, 2018. *CA Cancer J Clin*, 68, 284-296.
- TORTORELLA, M. D., MALFAIT, F., BARVE, R. A., SHIEH, H. S. & MALFAIT, A. M. 2009. A review of the ADAMTS family, pharmaceutical targets of the future. *Curr Pharm Des*, 15, 2359-74.
- VAN DER AAR, E., DECKX, H., DUPONT, S., FIEUW, A., DELAGE, S., LARSSON, S., STRUGLICS, A., LOHMANDER, L. S., LALANDE, A., LEROUX, E., AMANTINI, D. & PASSIER, P. 2022. Safety, Pharmacokinetics, and Pharmacodynamics of the ADAMTS-5 Inhibitor GLPG1972/S201086 in Healthy Volunteers and Participants With Osteoarthritis of the Knee or Hip. *Clin Pharmacol Drug Dev*, 11, 112-122.
- VAUGHAN, S., COWARD, J. I., BAST, R. C., JR., BERCHUCK, A., BEREK, J. S., BRENTON, J. D., COUKOS, G., CRUM, C. C., DRAPKIN, R., ETEMADMOGHADAM, D., FRIEDLANDER, M., GABRA, H., KAYE, S. B., LORD, C. J., LENGYEL, E., LEVINE, D. A., MCNEISH, I. A., MENON, U., MILLS, G. B., NEPHEW, K. P., OZA, A. M., SOOD, A. K., STRONACH, E. A., WALCZAK, H., BOWTELL, D. D. & BALKWILL, F. R. 2011. Rethinking ovarian cancer: recommendations for improving outcomes. *Nat Rev Cancer*, 11, 719-25.
- VETTER, M. H. & HAYS, J. L. 2018. Use of Targeted Therapeutics in Epithelial Ovarian Cancer: A Review of Current Literature and Future Directions. *Clin Ther*, 40, 361-371.
- VOUSDEN, K. H. & LANE, D. P. 2007. p53 in health and disease. *Nat Rev Mol Cell Biol*, 8, 275-83.
- VU, T. H. & WERB, Z. 2000. Matrix metalloproteinases: effectors of development and normal physiology. *Genes & development*, 14, 2123-2133.

- WANG, D. & LIPPARD, S. J. 2005. Cellular processing of platinum anticancer drugs. *Nat Rev Drug Discov*, 4, 307-20.
- WANG, F. T., SUN, W., ZHANG, J. T. & FAN, Y. Z. 2019a. Cancer-associated fibroblast regulation of tumor neo-angiogenesis as a therapeutic target in cancer. *Oncol Lett*, 17, 3055-3065.
- WANG, J., ZHOU, P., WANG, X., YU, Y., ZHU, G., ZHENG, L., XU, Z., LI, F., YOU, Q., YANG, Q., ZHUO, W., SUN, J. & CHEN, Z. 2019b. Rab25 promotes erlotinib resistance by activating the beta1 integrin/AKT/beta-catenin pathway in NSCLC. *Cell Prolif*, 52, e12592.
- WANG, S., HU, C., WU, F. & HE, S. 2017. Rab25 GTPase: Functional roles in cancer. *Oncotarget*, 8, 64591.
- WANG, X., DU, Z. W., XU, T. M., WANG, X. J., LI, W., GAO, J. L., LI, J. & ZHU, H. 2021. HIF-1alpha Is a Rational Target for Future Ovarian Cancer Therapies. *Front Oncol*, 11, 785111.
- WANG, X., FANG, Y., SUN, W., XU, Z., ZHANG, Y., WEI, X., DING, X. & XU, Y. 2020. Endocrinotherapy resistance of prostate and breast cancer: Importance of the NF-kappaB pathway (Review). *Int J Oncol*, 56, 1064-1074.
- WANG, Y., LIU, Y., MALEK, S. N., ZHENG, P. & LIU, Y. 2011. Targeting HIF1alpha eliminates cancer stem cells in hematological malignancies. *Cell Stem Cell*, 8, 399-411.
- WARBURG, O., WIND, F. & NEGELEIN, E. 1927. The metabolism of tumors in the body. *The Journal of general physiology*, 8, 519.
- WEEN, M. P., HUMMITZSCH, K., RODGERS, R. J., OEHLER, M. K. & RICCIARDELLI, C. 2011. Versican induces a pro-metastatic ovarian cancer cell behavior which can be inhibited by small hyaluronan oligosaccharides. *Clin Exp Metastasis*, 28, 113-25.
- WIEMAN, H. L., WOFFORD, J. A. & RATHMELL, J. C. 2007. Cytokine stimulation promotes glucose uptake via phosphatidylinositol-3 kinase/Akt regulation of Glut1 activity and trafficking. *Molecular biology of the cell*, 18, 1437-1446.
- WINKLER, J., ABISOYE-OGUNNIYAN, A., METCALF, K. J. & WERB, Z. 2020. Concepts of extracellular matrix remodelling in tumour progression and metastasis. *Nat Commun*, 11, 5120.
- WU, C. H., HSU, F. T., CHAO, T. L., LEE, Y. H. & KUO, Y. C. 2022. Revealing the suppressive role of protein kinase C delta and p38 mitogen-activated protein kinase (MAPK)/NF-kappaB axis associates with lenvatinib-inhibited progression in hepatocellular carcinoma in vitro and in vivo. *Biomed Pharmacother*, 145, 112437.
- WU, F., YANG, J., LIU, J., WANG, Y., MU, J., ZENG, Q., DENG, S. & ZHOU, H. 2021. Signaling pathways in cancer-associated fibroblasts and targeted therapy for cancer. *Signal Transduct Target Ther*, 6, 218.
- WU, Y., CHEN, L., ZHENG, P.-S. & YANG, B. B. 2002. β 1-Integrin-mediated glioma cell adhesion and free radical-induced apoptosis are regulated by binding to a C-terminal domain of PG-M/versican. *Journal of Biological Chemistry*, 277, 12294-12301.
- XIAO, C. W., YAN, X., LI, Y., REDDY, S. A. & TSANG, B. K. 2003. Resistance of human ovarian cancer cells to tumor necrosis factor alpha is a consequence of nuclear factor kappaB-mediated induction of Fas-associated death domain-like interleukin-1beta-converting enzyme-like inhibitory protein. *Endocrinology*, 144, 623-30.
- XIE, Y., GOU, Q., XIE, K., WANG, Z., WANG, Y. & ZHENG, H. 2016. ADAMTS6 suppresses tumor progression via the ERK signaling pathway and serves as a prognostic marker in human breast cancer. *Oncotarget*, 7, 61273.
- YANAGISHITA, M. 1993. Function of proteoglycans in the extracellular matrix. *Acta Pathologica Japonica*, 43, 283-293.

- YANG, D., LIU, J., QIAN, H. & ZHUANG, Q. 2023. Cancer-associated fibroblasts: from basic science to anticancer therapy. *Exp Mol Med*, 55, 1322-1332.
- YAO, J., ZHANG, L. L., HUANG, X. M., LI, W. Y. & GAO, S. G. 2017. Pleiotrophin and N-syndecan promote perineural invasion and tumor progression in an orthotopic mouse model of pancreatic cancer. *World J Gastroenterol*, 23, 3907-3914.
- YEUNG, T. L., LEUNG, C. S., WONG, K. K., SAMIMI, G., THOMPSON, M. S., LIU, J., ZAID, T. M., GHOSH, S., BIRRER, M. J. & MOK, S. C. 2013. TGF-beta modulates ovarian cancer invasion by upregulating CAF-derived versican in the tumor microenvironment. *Cancer Res*, 73, 5016-28.
- YEUNG, T. L., LEUNG, C. S., YIP, K. P., AU YEUNG, C. L., WONG, S. T. & MOK, S. C. 2015. Cellular and molecular processes in ovarian cancer metastasis. A Review in the Theme: Cell and Molecular Processes in Cancer Metastasis. *Am J Physiol Cell Physiol*, 309, C444-56.
- YIN, C., MOU, Q., PAN, X., ZHANG, G., LI, H. & SUN, Y. 2018. MiR-577 suppresses epithelial-mesenchymal transition and metastasis of breast cancer by targeting Rab25. *Thorac Cancer*, 9, 472-479.
- YIN, Y. X., SHEN, F., PEI, H., DING, Y., ZHAO, H., ZHAO, M. & CHEN, Q. 2012. Increased expression of Rab25 in breast cancer correlates with lymphatic metastasis. *Tumour Biol*, 33, 1581-7.
- YOUNESI, F. S., MILLER, A. E., BARKER, T. H., ROSSI, F. M. V. & HINZ, B. 2024. Fibroblast and myofibroblast activation in normal tissue repair and fibrosis. *Nat Rev Mol Cell Biol*.
- YOUSIF, N. G. 2014. Fibronectin promotes migration and invasion of ovarian cancer cells through up-regulation of FAK-PI3K/Akt pathway. *Cell Biol Int*, 38, 85-91.
- ZENG, X. Y., XIE, H., YUAN, J., JIANG, X. Y., YONG, J. H., ZENG, D., DOU, Y. Y. & XIAO, S. S. 2019. M2-like tumor-associated macrophages-secreted EGF promotes epithelial ovarian cancer metastasis via activating EGFR-ERK signaling and suppressing lncRNA LIMT expression. *Cancer Biol Ther*, 20, 956-966.
- ZENG, Z.-S., COHEN, A. M. & GUILLEM, J. G. 1999. Loss of basement membrane type IV collagen is associated with increased expression of metalloproteinases 2 and 9 (MMP-2 and MMP-9) during human colorectal tumorigenesis. *Carcinogenesis*, 20, 749-755.
- ZERIAL, M. & MCBRIDE, H. 2001. Rab proteins as membrane organizers. *Nature reviews Molecular cell biology*, 2, 107-117.
- ZHANG, L., XIE, B., QIU, Y., JING, D., ZHANG, J., DUAN, Y., LI, Z., FAN, M., HE, J., QIU, Y., TAN, R., LI, J. J. & SUN, L. Q. 2020. Rab25-Mediated EGFR Recycling Causes Tumor Acquired Radioresistance. *iScience*, 23, 100997.
- ZHANG, M., CHEN, Z., WANG, Y., ZHAO, H. & DU, Y. 2022a. The Role of Cancer-Associated Fibroblasts in Ovarian Cancer. *Cancers (Basel)*, 14.
- ZHANG, M., CHENG, S., JIN, Y., ZHAO, Y. & WANG, Y. 2021. Roles of CA125 in diagnosis, prediction, and oncogenesis of ovarian cancer. *Biochim Biophys Acta Rev Cancer*, 1875, 188503.
- ZHANG, R., SIU, M. K. Y., NGAN, H. Y. S. & CHAN, K. K. L. 2022b. Molecular Biomarkers for the Early Detection of Ovarian Cancer. *Int J Mol Sci*, 23.
- ZHANG, Y., XU, H., MU, J., GUO, S., YE, L., LI, D., PENG, W., HE, X. & XIANG, T. 2019. Inactivation of ADAMTS18 by aberrant promoter hypermethylation contribute to lung cancer progression. *J Cell Physiol*, 234, 6965-6975.
- ZHU, Z., XU, J., WU, X., LIN, S., LI, L., YE, W. & HUANG, Z. 2021. In Silico Identification of Contradictory Role of ADAMTS5 in Hepatocellular Carcinoma. *Technol Cancer Res Treat*, 20, 1533033820986826.
- ZHUANG, X., ZHANG, H. & HU, G. 2019. Cancer and Microenvironment Plasticity: Double-Edged Swords in Metastasis. *Trends Pharmacol Sci*, 40, 419-429.

ZONG, X. & NEPHEW, K. P. 2019. Ovarian Cancer Stem Cells: Role in Metastasis and Opportunity for Therapeutic Targeting. *Cancers (Basel)*, 11.